Structural Studies of Integrin Activation

Nicholas Jay Anthis

Lincoln College
University of Oxford

Thesis submitted in partial fulfilment of the requirements
for the degree of Doctor of Philosophy

Trinity Term 2009

ABSTRACT

Structural Studies of Integrin Activation

Nicholas Jay Anthis
Submitted for the degree of Doctor of Philosophy
Lincoln College, Trinity Term 2009

Fundamental to cell adhesion and migration, integrins are large heterodimeric membrane proteins that link the extracellular matrix to the actin cytoskeleton. Uniquely, these adhesion receptors mediate inside-out signal transduction, whereby extracellular adhesion is activated from within the cell by talin, a large cytoskeletal protein that binds to the cytoplasmic tail of the β integrin subunit via its PTB-like F3 domain. Features of the interface between talin1 and small β3 fragments only have been described previously.

Through NMR studies of full-length integrin β tails, we have found that β tails differ widely in their interactions with different talin isoforms. The muscle-specific β1D/talin2 complex exhibited particularly high affinity, leading to the X-ray crystal structure of the β1D tail/talin2 F2-F3 complex. Further NMR and biological experiments demonstrated that integrin activation is induced by a concerted series of interactions between the talin F3 domain and the β tail and between the talin F2 domain and the cell membrane. Additional studies revealed the structural determinants of tight talin2/β1D binding and the basis of more general differences between β1 and β3 talin binding.

NMR studies were also performed on tyrosine-phosphorylated integrin tails binding to the PTB domains of talin1 and Dok1, an inhibitor of integrin activation; these revealed that phosphorylation can inhibit integrin activation by increasing the affinity of the β tail for talin competitors. Key residues governing this switch were identified, and proteins were engineered with reversed affinities, offering potentially useful biological tools. Taken together, these results reveal the remarkable complexity of structural features that enable talin and its competitors to mediate this important form of transmembrane signalling.

ACKNOWLEDGEMENTS

I would like to thank Iain Campbell for his wide-ranging contributions to this thesis as my supervisor—particularly for allowing me to pursue my DPhil in his lab, for securing the funding for us to undertake this work, for funding the fourth year of my DPhil, for providing so many interesting ideas and suggestions along the way, and for critically reading my thesis. I would also like to thank Kate Wegener for the additional supervisory role she played and her contributions to the science presented in this thesis.

I would like to thank my many collaborators from outside of Oxford, whose contributions have added substantially to the quality and reach of the work presented here. David Critchley (University of Leicester) has been a constant source of ideas and advice, and he contributed to the crafting of Chapters III and IV. Likewise, Mark Ginsberg (University of California San Diego) has contributed significantly to the intellectual framework of this thesis, particularly to the text of Chapter III, and he provided several DNA constructs. Feng Ye and Chungho Kim (University of California San Diego) performed the integrin activation studies presented in Chapter III, Ben Goult (University of Leicester) performed the vesicle cosedimentation assays presented in Chapter III, and Jacob Haling (University of California San Diego) performed the cell biology experiments presented in Chapter V. I greatly appreciate all of these valuable contributions and the willingness of these contributors for me to reproduce their work here. I also thank Neil Bate (University of Leicester) for producing many of the talin constructs used in this study, John Kuriyan and Markus Seeliger (University of California Berkeley) for providing Src and YopH constructs, David Calderwood (Yale University) for providing cDNA for β1A, β1D, and β7, and Tobias Ulmer (University of Southern California) for providing the coordinates of the αIIbβ3 transmembrane structure before they were published.

Many others at Oxford have contributed to this thesis, and I owe all of them a debt of gratitude. John Vakonakis was helpful on a variety of fronts, and without his friendly and always willing assistance this thesis would not have been possible in its current form. In addition, I thank Ed Lowe for offering his helpful expertise with the X-ray crystallography work. I would also like to thank the following for their assistance: Nick Soffe (NMR), Jonathan Boyd (NMR), Christina Redfield (NMR), David Staunton (isothermal titration calorimetry, protein production), Max Soegaard (phosphorylation), Camilla Oxley (Dok1), Paul Emsley (X-ray crystallography), Charlie Taylor (NMR), and Sonja Lorenz (protein production). I would like to thank everyone else in the IDC group and in the LMB, particularly Maria Hoellerer, Pengju Jiang, Chris Millard, and Amanda Pagett. Also, I would like to thank the students I supervised—notably Massimiliano Memo, whose work on β7 appears in this thesis—but also Ben Oestringer, Alison Takemura, and Misty Watson. I also appreciate Mary Gregoriou's assistance in navigating the Oxford thesis process.

I would like to thank the Rhodes Trust for funding my first three years in Oxford, and I would like to acknowledge the following additional funding sources: the Wellcome Trust, the BBSRC, the National Institutes of Health, and Lincoln College, Oxford.

I am indebted to the good people at Texas A&M University who made it possible for me to come to Oxford in the first place—particularly Martyn Gunn, Ed Funkhouser, George Davis, and Marcella Ellis. Finally, I am grateful for the loving encouragement of Meredith Clancy; this would have been a much more difficult process without the constant support of her, my family, and my friends.

CONTENTS

ABBREVIATIONS

ATP	adenosine triphosphate
FERM	band four-point-one, ezrin, radixin, moesin [domain]
BSA	bovine serum albumin
c-Src	cellular Src
δ	chemical shift
CHO	Chinese hamster ovary [cell]
CD	circular dichroism
DSS	2,2-dimethyl-2-silapentane-5-sulfonate
DTT	dithiothreitol
Dok1	docking protein 1, downstream of tyrosine kinase 1
EM	electron microscopy
EDTA	ethylenediaminetetraacetic acid
EGTA	ethylene glycol tetraacetic acid
ECM	extracellular matrix
fMD	far membrane-distal
FACS	fluorescence-activated cell sorting
GPCR	G protein-coupled receptor
GST	glutathione S-transferase
GFP	green fluorescent protein
GTP	guanosine triphosphate
HSQC	heteronuclear single quantum coherence [spectroscopy]
HPLC	high performance liquid chromatography
I-EGF	integrin epidermal growth factor-like [domain]
ICAM	intercellular adhesion molecule

IPTG	isopropyl β-D-1-thiogalactopyranoside
ITC	isothermal titration calorimetry
LB	lysogeny broth
MFI	mean fluorescence intensity
MD	membrane-distal
MOP	membrane orientation patch
MP	membrane-proximal
MME	monomethyl ether
MEF	mouse embryonic fibroblast
nMD	near membrane-distal
NMR	nuclear magnetic resonance
NOE	nuclear Overhauser effect
NOESY	nuclear Overhauser enhancement spectroscopy
PRE	paramagnetic relaxation enhancement
ppm	parts per million
PSI	plexin, semaphoring, integrin [domain]
PBS	phosphate-buffered saline
PC	phosphatidylcholine
PS	phosphatidylserine
PIP2	phosphatidylinositol-4,5-bisphosphate
PIPK1γ	phosphatidylinositol phosphate kinase type 1γ
pY	phosphotyrosine
PTB	phosphotyrosine-binding [domain]
PH	pleckstrin homology [domain]
PEG	polyethylene glycol

PCR	polymerase chain reaction
PI	propidium iodide
RIAM	Rap1-interacting adaptor molecule
RMSD	root mean square deviation
SDS-PAGE	sodium dodecyl sulphate polyacrylamide gel electrophoresis
SYF	Src, Yes, and Fyn-deficient
TEV	tobacco etch virus [protease]
TOCSY	total correlation spectroscopy
TM	transmembrane
TROSY	transverse relaxation optimized spectroscopy
TFA	trifluoroacetic acid
Tris	tris(hydroxymethyl)aminomethane
v-Src	viral Src
Δ(H,N)	weighted combined change in ^{1}H and ^{15}N amide chemical shifts
WT	wild type

CHAPTER I: INTRODUCTION

1.1 Integrins in Cell Adhesion

Most cells in the body of a multicellular organism adhere to the extracellular matrix (ECM) and/or other cells. Even cells that circulate through the body must sometimes undergo cell adhesion during certain biological processes—such as platelets during thrombosis or leukocytes during the immune response. In either case, cell adhesion is dynamically regulated, as adherent cells must also grasp and disengage from their surroundings when undergoing cell migration, which plays a key role in a variety of biological processes including growth, development, and wound healing.

Thus, cell adhesion and migration figure centrally in normal physiology, but they are also involved in a wide range of pathologies—notably cancer. The correct functioning of adherent cells—including survival and proper response to signalling molecules—depends on cell adhesion, and if such cells become detached they undergo apoptosis (anoikis). Cancer cells, however, evolve mechanisms to evade this constraint, allowing metastasis to proceed. Their subsequent invasion into new tissues also involves cell adhesion and migration (Assoian, 1997; Chiarugi & Giannoni, 2008; Danen & Yamada, 2001; Douma *et al.*, 2004; Frisch & Francis, 1994; Frisch & Screaton, 2001). These pathological cell adhesion and migration processes, like their physiological counterparts, are mediated by the integrins.

Effectively serving as the "hands" of the cell, the primary receptors for the ECM are the integrins. These proteins span the cell membrane and connect the ECM to the actin cytoskeleton—by a direct interaction with ECM proteins on the exterior of the cell and via adapter proteins inside. Each integrin heterodimer consists of one α subunit and one β subunit, each made up of several linked globular extracellular domains, a single

transmembrane (TM) helix, and a generally short C-terminal cytoplasmic tail. Integrins exist in all metazoa; mammals express 18 different α subunits and 8 different β subunits, which combine to form 24 unique noncovalently-linked αβ heterodimers—not including additional splice variants (Fig. 1.1). These integrins occupy overlapping but nonredundant biological niches, as evidenced by the markedly diverse phenotypes exhibited by mice with different integrin subunits knocked out (Hynes, 2002a). Simpler metazoa express a more limited set of integrins. The nematode *Caenorhabditis elegans*, for example, expresses just two integrins (one β subunit capable of partnering with two different α subunits) (Brown, 2000).

Integrin function is closely tied to structure. The extracellular portion of the β integrin subunit is about 700 residues in length and consists of (starting at the N-terminus) a PSI domain, a hybrid domain (with an inserted I/A domain), four I-EGF domains, and a tail domain—which should not be confused with the cytoplasmic tail (Fig. 1.2). The extracellular portion of the α subunit is slightly larger, from about 940 to 1,120 residues in length. It consists of a propeller domain (with an inserted I/A domain in half of the α subunits), a thigh domain, and two calf domains. In integrins with the inserted α I/A domain, this is the main site of ligand binding. The β subunit I/A domain and α subunit propeller domain also participate in ligand binding. The cytoplasmic domains, on the other hand, are much smaller. With one exception, the cytoplasmic tails of the β subunits in humans vary from 46 to 70 residues in length; these tails are mostly unstructured, as demonstrated by NMR-based evidence presented in this thesis and in previous studies (Bhunia *et al.*, 2009; Li *et al.*, 2002; Ulmer *et al.*, 2001; Vinogradova *et al.*, 2002). The β4 cytoplasmic portion, on the other hand, is large (about 1,100 residues) and consists of multiple globular domains. Of the seven shorter β tails, all but one (β8)

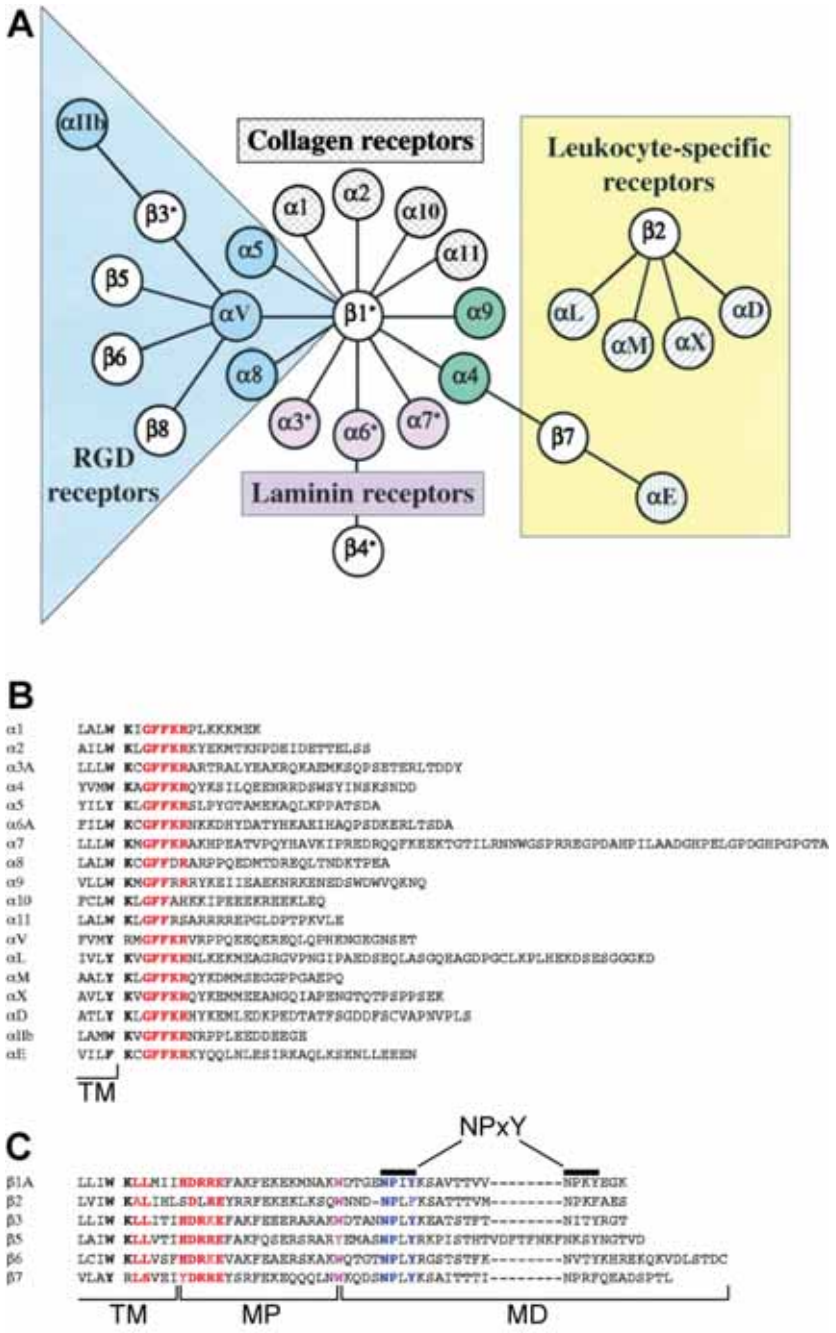

Figure 1.1 The α and β integrin subunits in humans. (A) This panel, reproduced from Hynes, 2002, shows the 18 α and 8 β integrin subunits found in mammals, as well as the 24 unique integrin αβ heterodimers they form. Tissue or extracellular ligand specificity is indicated. Subunits with an asterisk are alternatively spliced in their cytoplasmic domains, and the α subunits highlighted with a hatching or stippling pattern contain an I/A domain inserted in the propeller domain. (B) This panel, modified from Calderwood, 2004, shows an alignment of the cytoplasmic tails of all 18 integrin α subunits found in humans. The highly-conserved GFFKR motif is highlighted. (C) This panel, also modified from Calderwood, 2004, shows an alignment of the 6 (out of 8 total) β integrin cytoplasmic tails that exhibit significant sequence homology to one another. Conserved sequences are highlighted. Three regions have been denoted on the figure: the C-terminal portion of the transmembrane (TM) region and the membrane-proximal (MP) and membrane-distal (MD) portions of the cytoplasmic tail. The two NPxY/NPxY-motifs sites have also been indicated.

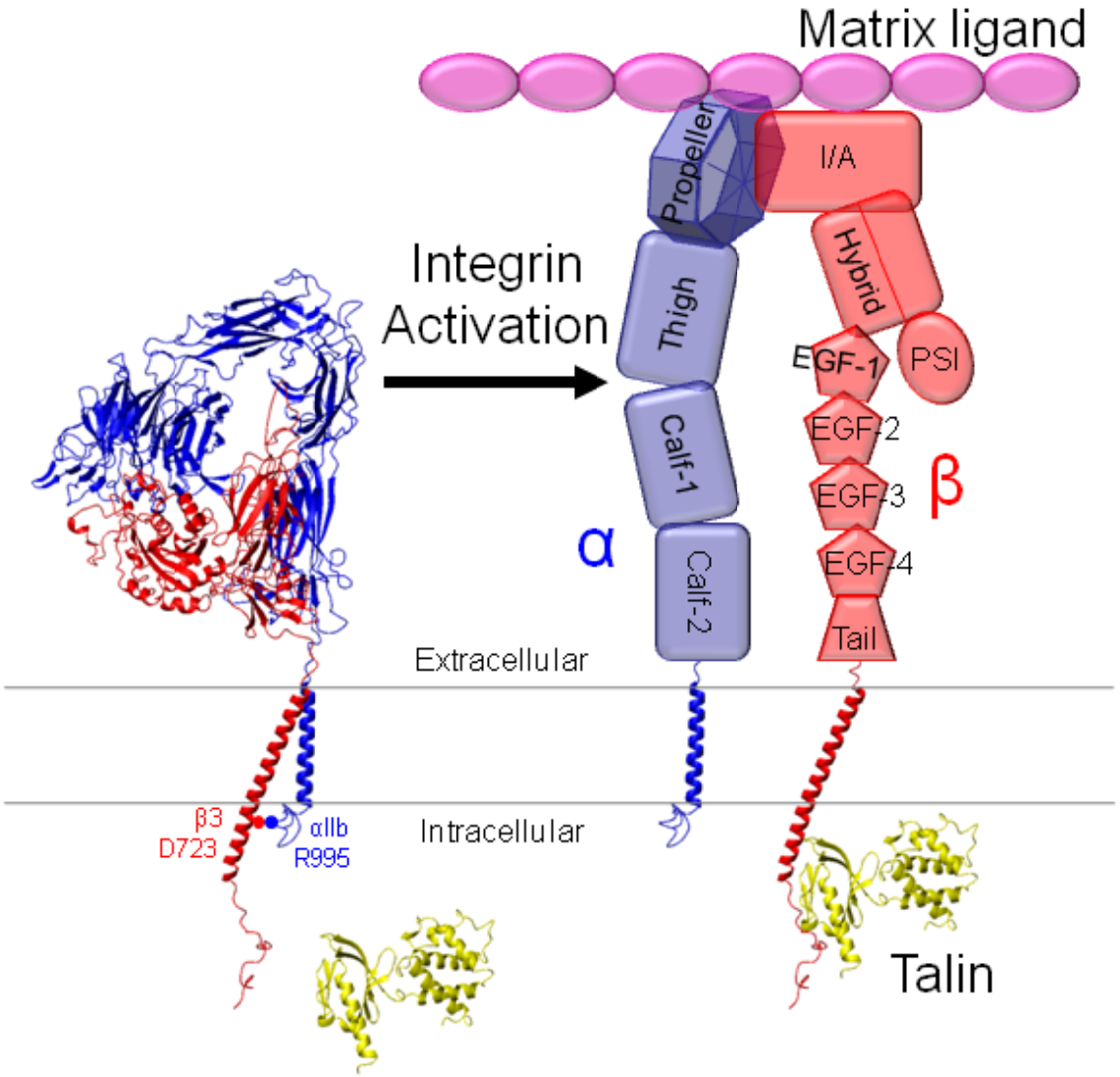

Figure 1.2 The switchblade mechanism of integrin activation. The integrin is held in a bent inactive state by an interaction between the transmembrane domains and cytoplasmic tails of the α and β subunits. Talin disrupts this interaction, causing the tails to separate, inducing a more open extracellular domain conformation with higher affinity for matrix ligands. The membrane-proximal integrin tail salt bridge that holds the integrin in the inactive conformation is labelled on the inactive structure on the left. The integrin extracellular domains are labelled on the active structure on the right. The structure of the inactive transmembrane domain comes from PDB 2K9J (Lau *et al.*, 2009), and the structure of the inactive extracellular domain comes from PDB 1JV2 (Xiong *et al.*, 2001).

share a great deal of sequence similarity. These integrin tails consist of a membrane-proximal (MP) helix and a membrane-distal (MD) unstructured region. The MD region consists of two NPxY or NPxY-like motifs (Fig. 1.1C). The α tails are much more heterogeneous, and although in humans they vary from 15 to 78 residues in length, they are generally shorter than the β tails (Fig. 1.1B). The MP portion of these tails contains a highly-conserved GFFKR motif (Calderwood, 2004; Hynes, 2002a). The vast majority of integrin interactions with cytoplasmic proteins are mediated by the β tail, which serves as a hub for protein-protein interactions and integrin-related signalling pathways (Liu *et al.*, 2000). Alternatively, to an approximation at least, the α subunit is the major determinant of extracellular binding specificity (Hynes, 2002a).

Integrins play a key structural role in the body, serving as the link between the ECM and the cytoskeleton (Delon & Brown, 2007). Beyond this, however, integrins are dynamic signalling molecules, transmitting signals in both directions across the cell membrane through allosteric means. The binding of an integrin to an extracellular ligand triggers a variety of signalling events, some due to allosteric structural changes and some due to integrin clustering (Cluzel *et al.*, 2005; Hynes, 2002a; Miyamoto *et al.*, 1995). Central to such outside-in signalling events are the recruitment and activation of the tyrosine kinases Src and focal adhesion kinase (Burridge & Chrzanowska-Wodnicka, 1996; Shattil, 2005). Alternatively, integrin adhesiveness for extracellular matrix ligands can be activated from within the cell by inside-out signalling (Fig. 1.2). Inside-out integrin activation is uniquely induced by the cytoskeletal protein talin, which binds to the β integrin subunit, disrupting connections between the TM and cytoplasmic portions of the α and β subunits, leading to structural changes outside of the cell that increase integrin affinity for ECM ligands (Calderwood, 2004; Campbell & Ginsberg, 2004; Ginsberg *et al.*, 2005; Hynes, 2002a). In another bidirectional signalling process,

integrins also sense mechanical force. Specifically, ECM-integrin-cytoskeleton connections are strengthened in response to the application of such force (Choquet *et al.*, 1997; Galbraith *et al.*, 2002). Thus, in their capacity as outside-in signalling molecules, integrins behave analogously to cell surface receptors for soluble growth factors (just binding to a different sort of ligand). However, integrin inside-out activation is a unique process, and mechanistically it does not closely resemble any other known biological process.

Members of the integrin family were discovered independently during the 1980s in three different capacities: as receptors for the ECM, as the platelet glycoprotein IIb/IIIa (integrin αIIbβ3), and as a surface antigen on leukocytes (Hynes, 2004). By 1987, though, the name "integrin" and the α/β terminology had been applied to the entire family (Hynes, 1987). It is now recognized that the integrins play a central role in a variety of physiological processes, from growth and development to haemostasis and leukocyte trafficking. In adherent cells, integrins serve as receptors for ECM proteins—including collagen, laminin, and RGD motif-containing proteins such as fibronectin and vitronectin. With one exception, they anchor the ECM to the actin cytoskeleton in large transient complexes, called focal contacts or focal adhesions, consisting of many clustered integrins (Burridge & Chrzanowska-Wodnicka, 1996; Geiger *et al.*, 2001). Epithelial cells, however, can adhere to the ECM via hemidesmosomes, where the integrin α6β4 links basement membrane laminin to keratin intermediate filaments (Litjens *et al.*, 2006). This unique connectivity correlates with the unusual structure of the β4 cytoplasmic domain.

Specialized integrins also exist in myeloid and lymphoid cells. Platelets uniquely express the integrin αIIbβ3, which exists in a default inactive state. Upon platelet activation, αIIbβ3 is activated from within the platelet, causing it to bind fibrinogen and

allowing thrombosis to occur. This pathway can be initiated by various extracellular signals, several acting on G protein-coupled receptors (GPCRs), but one being the binding of collagen to α2β1 (Hynes, 2002b; Schwartz & Ginsberg, 2002). In humans, genetic disruption of αIIbβ3 leads to Glanzmann's thrombasthenia, characterized by defective clotting and excessive bleeding (Kato, 1997), and mice in which the β3 gene has been knocked out replicate this phenotype (Hodivala-Dilke *et al.*, 1999). Although the αIIb subunit is unique to platelets, the β3 subunit occurs in other physiological contexts. Leukocytes, however, express two unique β subunits: β2 and β7 (Fig. 1.1A). Uniquely, the β2 integrins mediate cell-cell adhesion, by binding to ICAM molecules expressed on target cells. As with αIIbβ3, β2 integrins remain inactive in circulating cells but are activated as part of the immune response to allow adhesion to the vascular wall and subsequent invasion into surrounding tissues (Hynes, 2002a). Crosstalk between integrins also occurs in leukocytes, as the binding of α4β7 to extracellular ligands can trigger activation of αLβ2 (Arthos *et al.*, 2008; Bargatze *et al.*, 1995; Chan *et al.*, 2000). Human patients with a genetic defect in the β2 integrin suffer from leukocyte adhesion deficiency, characterized by recurrent infections, impaired wound healing, and leukocytosis (Etzioni *et al.*, 1999). Thus, leukocyte integrins are a potential target for clinical therapies against inflammation and autoimmune diseases (Cantor *et al.*, 2008; Gottlieb *et al.*, 2000; Jackson, 2002), and αIIbβ3 is already a target of effective antithrombotic drugs (Coller, 1997; Scarborough & Gretler, 2000).

Although these specialized integrins play key roles in circulating cells, the vast majority of integrins in the body exist in adherent cells. And, unlike myeloid and lymphoid integrins that exist in default off states, only to be activated at specific biological moments, the integrins of adherent cells are much more dynamically regulated and often exist in a more constitutively active state. This applies to the majority of

integrins, including those with the most ubiquitously-expressed integrin subunit, β1. In these cells, integrin adhesion is intricately regulated in time and space (Hynes, 2002a). Such integrins are capable of forming a variety of types of adhesions, from weak, transient focal complexes, to more stable focal adhesions. Integrins participate in particularly strong semi-permanent adhesions in the case of striated muscle, such as in costameres or the myotendinous junction (Burridge & Chrzanowska-Wodnicka, 1996; Geiger & Bershadsky, 2001). These different types of integrin adhesions differ in morphology and function.

Integrin adhesions are large, heterogeneous structures consisting of a variety of different protein components. They do not have a defined three-dimensional structure, but are instead characterized by specific—but often transient—protein-protein interactions. One model of the "integrin adhesome", for example, in which experimental results were used to construct a protein-protein interaction network, included 151 proteins and 690 interactions (Zaidel-Bar *et al.*, 2007). The adhesome includes many scaffold proteins—such as talin, vinculin, actinin, filamin, and paxillin—that play a role in linking the integrin to the actin cytoskeleton. When a cell migrates, small focal complexes form at the leading edge. These relatively small integrin-based adhesions (less than 1 μm in length) are associated with actin-based membrane ruffles (lamellipodia) and their formation is induced by the activity of the small GTPase Rac (Geiger *et al.*, 2001). These nascent focal complexes act as mechanosensors; when they become established with firm connections to the cytoskeleton and the ECM with the application of force, they are further reinforced, growing in size and strength (Choquet *et al.*, 1997; Galbraith *et al.*, 2002; Lauffenburger & Horwitz, 1996; Riveline *et al.*, 2001). These larger adhesions (up to 10 μm in length) are called focal adhesions and provide a firm connection between the cytoskeleton and the ECM. They are anchored to thick actin bundles called stress fibres,

and their formation is induced by the activity of the small GTPase Rho (Burridge & Chrzanowska-Wodnicka, 1996; Geiger & Bershadsky, 2001). Such a site remains fixed in one position in space, as contraction of the cytoskeleton pulls the body of the cell past it (Hu *et al.*, 2007; Ponti *et al.*, 2004). Both the ECM and the cytoskeleton provide complementary scaffolds upon which to apply this force. The cytoskeleton and ECM are closely linked; the presence of one affects the assembly and orientation of the other (Ali & Hynes, 1977; Ali *et al.*, 1977). Then, at the trailing end of the cell, the focal adhesion must be dissembled (Wehrle-Haller & Imhof, 2002), and the integrins must then be recycled for the formation of new adhesions at the leading edge (Sheetz *et al.*, 1999). Thus, integrin adhesions can anchor the cell to the ECM firmly, but they must be dynamically regulated for proper cell function. Central to these biological functions is the process of inside-out integrin activation.

Inside-out integrin activation—the modulation of integrin extracellular affinity from within the cell—is a process of considerable interest, and it is the primary subject of this thesis. It is discussed in detail later in this chapter, but it will be introduced briefly here. An interaction between the α and β TM and cytoplasmic domains (Fig. 1.3A) maintains the integrin in the inactive state, characterized by a bent, closed conformation on the cell surface (Luo *et al.*, 2007). The cytoskeletal protein talin activates the integrin (Tadokoro *et al.*, 2003) through a direct interaction between its F3 domain and the β integrin tail (Calderwood *et al.*, 2002; Wegener *et al.*, 2007) (Fig. 1.3B). This disrupts the α/β interaction, causing tail separation (Kim *et al.*, 2009), leading to the integrin adopting a more open and extended extracellular conformation, which binds extracellular ligands much more tightly (Luo *et al.*, 2007). This is known as the "switchblade" model of integrin activation (Fig. 1.2). A competing "deadbolt" model has also been advanced (Xiong *et al.*, 2003a), and these will be compared in greater detail later in the chapter.

Regardless of the model, though, talin plays a key role in this process, as the primary protein capable of directly activating integrins.

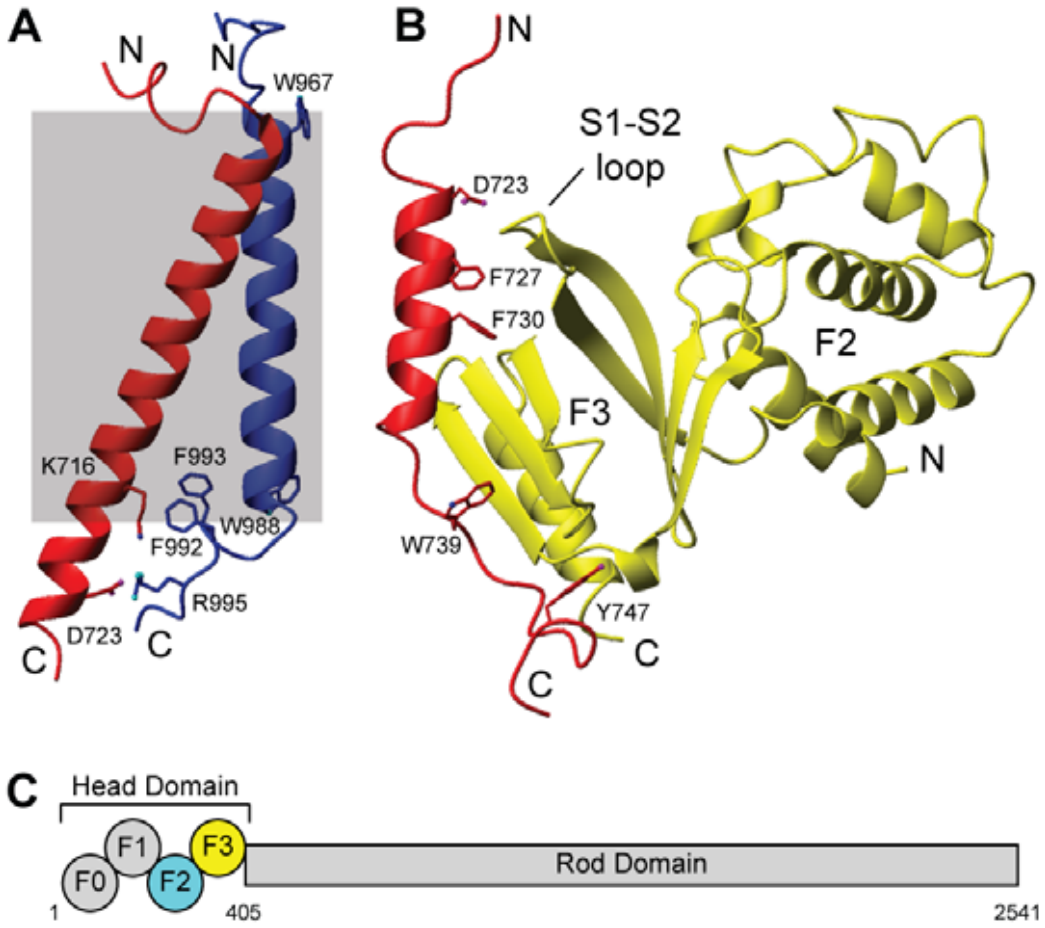

Figure 1.3 Key integrin structures for the active and inactive states. (A) The structure of the transmembrane region of the αIIbβ3 complex (PDB 2K9J), corresponding to the inactive state of the integrin (Lau *et al.*, 2009). The shaded area roughly corresponds to the portion of the integrin that is buried in the membrane. Key residues are highlighted, including the αIIb interfacial tryptophan residues, certain residues in the αIIb GFFKR motif, β3 K716, and the salt bridge-forming residues in the membrane-proximal portion of both tails. (B) The structure of the β3 tail bound to talin1, corresponding to the active state of the integrin. To produce this illustration, two structures have been merged: 1MK9, which includes a short membrane-distal portion of β3 bound to the talin1 F2-F3 domain pair (Garcia-Alvarez *et al.*, 2003), and 2H7E, which includes the membrane-proximal portion of β3 bound to the talin1 F3 domain (Wegener *et al.*, 2007). The boundary between the two β3 structures is at W739. Other key β3 residues have been highlighted. The talin1 F3 S1-S2 activation loop (highlighted) comes from 2H7E, and the rest of the talin molecule comes from 1MK9. (C) A schematic of the domain structure of talin1. Talin homodimerization (not shown) occurs at the C-terminus.

1.2 Talin: The Integrin Activator

Integrins are activated by a direct interaction between the β integrin tail and talin (Calderwood *et al.*, 2002; Tadokoro *et al.*, 2003; Wegener *et al.*, 2007). Talin is a large cytoskeletal protein that can form a noncovalent homodimer, each chain about 2,500 residues in length. The N-terminal roughly 400 residues constitute a head domain made up of four subdomains: F0, F1, F2, and F3, with F1-3 constituting a FERM (band four-point-one, ezrin, radixin, moesin) domain (Fig. 1.3C). Integrin binding occurs in the phosphotyrosine-binding (PTB)-like F3 domain. The F2 domain is a helical bundle, and the F0 and F1 domains adopt ubiquitin-like folds. The majority of the talin molecule is made up of the rod domain, which contains a series of helical bundles that include binding sites for actin and vinculin. Homodimerization occurs at the most C-terminal helix (Critchley & Gingras, 2008). Some evidence exists for a second integrin binding site located in the talin rod domain, with a role distinct from that of the primary site located in the F3 domain (Gingras *et al.*, 2009; Moes *et al.*, 2007; Rodius *et al.*, 2008; Tanentzapf & Brown, 2006). Atomic resolution structures have been published for many of the domains of talin, but no atomic resolution—or even low resolution—structure exists for the entire molecule; the largest published structures consist of only two domains (Garcia-Alvarez *et al.*, 2003; Gingras *et al.*, 2009; Goult *et al.*, 2009; Papagrigoriou *et al.*, 2004).

Talin provides a direct link between the integrin and the actin cytoskeleton (Critchley, 2004; Nayal *et al.*, 2004) that is capable of sustaining a significant amount of force (Jiang *et al.*, 2003). The binding of talin to integrins triggers the formation of focal adhesions, and such structures will not form in the absence of talin (Critchley, 2004; Legate *et al.*, 2009). Talin is necessary for the force-dependent strengthening of integrin adhesions in general (Critchley & Gingras, 2008). Although the talin head is sufficient to

cause integrin activation, the full molecule is required for focal adhesion formation, connection of the integrin to actin, and cell spreading (Calderwood *et al.*, 2000; Turner & Burridge, 1991; Zhang *et al.*, 2008). Talin was originally discovered as a component of focal adhesions (Burridge & Connell, 1983), and it was soon purified and demonstrated to form a direct interaction with integrins (Horwitz *et al.*, 1986). As such, it was the first cytoplasmic integrin binding partner discovered, although since then it has become clear that the β integrin tail participates in many interactions in its capacity as a signalling hub (Liu *et al.*, 2000).

Vertebrates express two isoforms of talin. Talin1 is widely expressed; talin2 is found primarily in striated muscles and in the brain, although it is expressed elsewhere (Senetar *et al.*, 2007). The knockout of talin1 in mice is embryonic lethal (Monkley *et al.*, 2000), and conditional knockouts have demonstrated that talin is essential for integrin activation in platelets; such mice are characterized by spontaneous bleeding. (Nieswandt *et al.*, 2007; Petrich *et al.*, 2007). Talin1 is also essential for leukocyte integrin function (Lim *et al.*, 2007; Manevich *et al.*, 2007; Simonson *et al.*, 2006). Talin function is highly conserved, and talin is essential for integrin function in *Drosophila melanogaster* (Brown *et al.*, 2002) and *C. elegans* (Cram *et al.*, 2003) as well. Talin1 and talin2 exhibit 74% amino acid sequence identity; they have some overlap in function (Zhang *et al.*, 2008), and mice in which talin1 has been depleted only in muscle display only a mild phenotype (Zhang *et al.*, 2008). Talin2 is not as well characterized as talin1, but its most well-understood function is in forming strong, stable integrin adhesions in the costameres and myotendinous junctions of striated muscle cells (Monkley *et al.*, 2001; Senetar & McCann, 2005; Senetar *et al.*, 2007). Striated muscle cells also express a unique integrin subunit, β1D, which is a splice variant of β1 that differs from the more common β1A variant only in the C-terminal portion of its cytoplasmic tail (Belkin *et al.*, 1996). Along

with talin2, β1D is targeted to costameres and myotendinous junctions, where it forms more stable connections with the actin cytoskeleton (Belkin *et al.*, 1997) due to tighter binding to talin (Pfaff *et al.*, 1998).

Talin is unique in that it is immediately responsible for integrin activation through a direct interaction with the β integrin tail (Tadokoro *et al.*, 2003). This activation activity has been narrowed down to the talin F3 domain, which adopts a PTB-like fold (Calderwood *et al.*, 2002), although additional head domains contribute to activation (Bouaouina *et al.*, 2008). Many other PTB domains bind to β integrin tails, which generally have two NPxY or NPxY-like motifs—the canonical binding sites for PTB domains (Calderwood *et al.*, 2003); however, only talin activates. An early crystal structure demonstrated that the talin1 F3 domain does in fact bind to the more membrane-proximal NPxY motif of the β3 integrin tail in canonical PTB domain fashion (Garcia-Alvarez *et al.*, 2003). However, a later NMR structure demonstrated that talin also binds to the MP helix of the β3 tail, and this unique interaction is responsible for integrin activation (Wegener *et al.*, 2007) (Fig. 1.3B), which results from talin disrupting an interaction between the α and β integrin tails and TM domains (Kim *et al.*, 2003). Recently, a novel family of proteins, the kindlins, have been demonstrated to also participate in integrin activation through an interaction with the C-terminus of the integrin tail (Ma *et al.*, 2008; Montanez *et al.*, 2008; Moser *et al.*, 2009a; Moser *et al.*, 2008; Ussar *et al.*, 2008). Their activation activity is dependent on talin, however, and although the mechanism of kindlin activation enhancement is unknown, it probably involves an interplay with the talin molecule. Also, most kindlin integrin activation studies have focused on β3 integrins, and kindlin has actually been demonstrated to decrease β1 activation (Harburger *et al.*, 2009), making it unclear how relevant or widespread the role of kindlin in integrin activation actually is.

Talin activation of the integrin must be induced within the cell, and talin is maintained in an inactive conformation by an intermolecular interaction between its head and rod domains (Goksoy *et al.*, 2008; Goult *et al.*, 2009). Specifically, a helical bundle in the rod domain binds to the F3 domain, partially masking the integrin binding site (Goult *et al.*, 2009). This explains why the talin head domain alone is more effective at activating integrins than the full molecule (Goksoy *et al.*, 2008; Yan *et al.*, 2001). Several mechanisms have been proposed for talin activation, and all of them probably play a role under some biological conditions. One of these is proteolysis. Talin can be cleaved in a flexible linker between the head and rod domain (Beckerle *et al.*, 1986; O'Halloran *et al.*, 1985) by calpain (Franco *et al.*, 2004), and this cleavage contributes to activity presumably by releasing the rod/head inhibitory interaction—thus increasing talin affinity for the integrin tail (Yan *et al.*, 2001). However, talin proteolysis is not a necessary event for activation to occur (Franco *et al.*, 2004), indicating that other mechanisms may play a more central role in activation. A second mechanism involves the second messenger molecule phosphatidylinositol-4,5-bisphosphate (PIP2). PIP2 increases talin binding to integrin tails (Martel *et al.*, 2001) by releasing the inhibitory head/rod interaction (Goksoy *et al.*, 2008). Additionally, the talin F3 domain binds to phosphatidylinositol phosphate kinase type 1γ (PIPK1γ) (Barsukov *et al.*, 2003; de Pereda *et al.*, 2005), and this targets talin to focal adhesions (Di Paolo *et al.*, 2002; Ling *et al.*, 2002). Thus, PIPK1γ both targets talin to the membrane and further activates it through generation of PIP2. The findings of our current study—that integrin activation depends upon a direct interaction between the talin F2 domain and the membrane—offer an additional explanation for the sensitivity of talin-induced integrin activation to negatively-charged moieties (i.e. PIP2) in the membrane.

A third mechanism of talin activation involves the small GTPase Rap1. This pathway has been studied particularly extensively in platelets. Removal of Rap1 from platelets decreases activation of αIIbβ3 (Chrzanowska-Wodnicka *et al.*, 2005). In CHO cells expressing αIIbβ3, knockdown of Rap1 decreases integrin activation, and introduction of a constitutively active mutant leads to an increase in activation (Han *et al.*, 2006). These effects are dependent on the presence of talin, and Rap1 has been shown to act by inducing the formation of a complex that includes the integrin, talin, and RIAM (Rap1-interacting adaptor molecule) (Han *et al.*, 2006). Furthermore, it has been demonstrated that RIAM is necessary for αIIbβ3 activation in CHO Cells (Watanabe *et al.*, 2008). Constitutively active Rap1 also induces integrin activation in T cells (Sebzda *et al.*, 2002), and RIAM is necessary for integrin activation there as well (Krause *et al.*, 2004; Lafuente *et al.*, 2004). Evidence also exists that such mechanisms are more general in nature, operating outside of hematopoietic cells (Moser *et al.*, 2009b). For example, talin interacts with lamellipodin—a protein related to RIAM—and this interaction leads to integrin activation (Lee *et al.*, 2009). More directly, unpublished studies by Ben Goult and David Critchley at the University of Leicester have indicated that Rap1 interacts directly with the F0 domain of talin. Such an interaction could explain why the N-terminal domains of talin (particularly F0) contribute to integrin activation (Bouaouina *et al.*, 2008), despite not interacting directly with the integrin. Either way, the bulk of the evidence indicates that Rap1 and RIAM act in concert to activate talin—possibly by targeting it to the integrin—in order to induce integrin activation. Such a pathway could act alone or in concert with the other talin activation mechanisms discussed above.

1.3 Structural Biology of Integrins

Despite the large number of atomic resolution structural studies performed on integrins, the only integrin for which atomic resolution structures exist covering the entire molecule is αIIbβ3. It is one of only two integrins for which the entire extracellular domain structure is known (Zhu *et al.*, 2008). The other is αVβ3 (Xiong *et al.*, 2001). It is the only integrin for which the TM domain structures are known (separately (Lau *et al.*, 2008a; Lau *et al.*, 2008b) and in complex with one another (Lau *et al.*, 2009) (Fig. 1.3A)). Likewise, αIIbβ3 is the only integrin for which the full cytoplasmic tail structures are known (Hwang & Vogel, 2000; Vinogradova *et al.*, 2000; Vinogradova *et al.*, 2002), although these domains are largely unstructured, and the recent TM structure has indicated that the previous structure of the full-length αIIbβ3 tails in complex (Vinogradova *et al.*, 2002) is either incorrect or not physiologically relevant (Lau *et al.*, 2009; Zhu *et al.*, 2009). The structure of the relatively long αL tail has also been solved, and a complex of it with β2 has been modelled, although only by chemical shift perturbation mapping (Bhunia *et al.*, 2009). Many additional studies have been conducted on smaller fragments of the extracellular or cytoplasmic domains. Unlike the integrin extracellular domains—where almost all of the structures have been solved by X-ray crystallography—most structures of the TM and cytoplasmic domains have been solved by NMR, due to greater flexibility in the tails and the difficulties of conducting structural work in a membrane environment. Although not exclusively, these structural studies have focused largely on β3 integrins. In the current study, however, we present the structure of the β1D cytoplasmic tail bound to talin—the first atomic resolution structure of a full-length β integrin tail other than β3.

Various lower resolution structural studies of integrins have also been conducted. Full-length αIIbβ3 has been studied extensively by electron microscopy (EM) (Adair &

Yeager, 2002; Carrell *et al.*, 1985; Du *et al.*, 1993; Erb *et al.*, 1997; Hantgan *et al.*, 1999; Iwasaki *et al.*, 2005; Parise & Phillips, 1985; Weisel *et al.*, 1992; Ye *et al.*, 2008), and some early studies were conducted on β1 integrins (Kelly *et al.*, 1987; Nermut *et al.*, 1988). The extracellular domains of αIIbβ3 (Zhu *et al.*, 2008), αVβ3 (Adair *et al.*, 2005; Takagi *et al.*, 2002), and α5β1 (Takagi *et al.*, 2001) have also been studied by EM, as well as a smaller fragment of α5β1 (Takagi *et al.*, 2003). These studies have been particularly valuable in identifying large structural rearrangements in the extracellular domains upon integrin activation, and they will be discussed in greater detail later in the section on integrin activation.

The first integrin-related atomic resolution structure was an X-ray crystal structure of the I/A domain of the αM integrin, published in 1995 by Lee *et al*. of Robert Liddington's research group (Lee *et al.*, 1995b). This was followed by additional structures of this domain and the I/A domains from other α integrins. In fact, the majority of integrin atomic resolution structural studies have involved crystal structures of just the I/A domain from various α integrins (αM, αL, α2, α1, and αX) alone or bound to various ligands. Although only a handful of these studies have related to integrin activation (many of the more recent, especially, involved the characterization of small molecule integrin antagonists), some of the earlier ones shed significant light on the mechanism of integrin binding to extracellular ligands, and provided some insight into the process of integrin activation. For example, later in 1995, Lee *et al*. published a second structure of the αM I/A domain. Whereas in the first structure the integrin domain was bound to Mg^{2+}, in this second structure it was bound to Mn^{2+} (Lee *et al.*, 1995a). The authors observed a significant change in conformation between these two states, particularly in the C-terminal helix of the domain. Contrary to what later studies would indicate, the authors attributed the Mg^{2+}-bound state to the active integrin and the Mn^{2+}-bound state to the

inactive integrin. Two subsequent studies, however, found no major structural rearrangements upon metal binding in the I/A domains of αL (Qu & Leahy, 1996) and α1 (Nolte *et al.*, 1999). Despite that, in support of allosteric regulation of integrin activation, two later studies found major structural rearrangements in the α2 I/A domain upon collagen binding (Emsley *et al.*, 2000) and in the αM I/A domain upon an inactivating N-terminal deletion and an activating C-terminal mutation (Xiong *et al.*, 2000). Some later crystallographic studies on isolated I/A domains also explored conformational differences—and also yielded mixed results—but in 2001 structural studies on integrin activation began to advance significantly with structures of much larger integrin fragments.

In 2001, Xiong *et al*. of Amin Arnaout's group published an X-ray crystal structure of the full extracellular domain of αVβ3 (Xiong *et al.*, 2001). Up to this point, all structural work involving full integrin extracellular domain had been low-resolution, using EM, and all had shown some form of an extended and/or open structure (Carrell *et al.*, 1985; Du *et al.*, 1993; Erb *et al.*, 1997; Hantgan *et al.*, 1999; Kelly *et al.*, 1987; Nermut *et al.*, 1988; Parise & Phillips, 1985; Weisel *et al.*, 1992). The crystal structure, however, exhibits a bent, closed conformation, with the ligand binding site facing where the membrane would presumably sit *in vivo*. In this structure, the integrin consists of a head domain at the end of two bent legs. The head domain contains the α subunit propeller domain and the β subunit I/A and hybrid domains. The remaining domains in the α and β subunits make up the two legs. The α leg is bent at a knee (or "genu") between the thigh domain and first calf domain (Xiong *et al.*, 2001). The knee region of the β subunit was not well-resolved in this crystal structure, but later work indicated that it sits between the first two I-EGF domains (Shi *et al.*, 2007). This first structure was followed up by a second study by the same group, in which the extracellular domain of

αVβ3 was crystallized with and without a ligand-mimetic cyclic RGD peptide (Xiong *et al.*, 2002). Binding to the ligand was associated with small structural rearrangements. However, even when ligand-bound, the integrin still adopts a bent and largely closed overall shape.

In 2004, additional structural work involving smaller portions of integrin extracellular domains (but more than just the I/A domain) shed additional light on the process of integrin activation. Xiao *et al*. from Timothy Springer's group published a series of structures of a collection of extracellular domains of αIIbβ3 they termed the integrin "headpiece" (Xiao *et al.*, 2004). The headpiece corresponds to the domains in the α and β subunits that would be located furthest from the cell membrane in an extended structure. They found these structures consistent with an open, extended integrin conformation, and they described a mechanism for allosterically transmitting structural changes through the integrin extracellular domain based on these structures. Later, Shi *et al*. (with Julien Lescar and Alex Law) published two structures consisting of mid-extracellular fragments of the β2 integrin. One crystallized in a bent conformation, and the addition of a C-terminal EGF domain produced a construct that crystallized in an open conformation. Based on these structures, they were able to produce an αLβ2 integrin that was constrained in the closed state (Shi *et al.*, 2007). Soon after that, Springer *et al*. published another series of αIIbβ3 headpiece structures, in various ligand-bound states, also in an open conformation (Springer *et al.*, 2008). That same year, Zhu *et al*, also from Timothy Springer's group, published the structure of the αIIbβ3 extracellular domain in the closed, bent state (Zhu *et al.*, 2008). In the same paper, they published an αIIbβ3 headpiece structure that is consistent with an open conformation. Through additional studies, they demonstrated that it would be possible for lateral force to stabilize an open, extended integrin conformation (Zhu *et al.*, 2008).

Structural work on the cytoplasmic portions of the integrins has been more limited—partly because of the generally much smaller size of the tails and their intrinsic flexibility. The only integrin cytoplasmic domain that does not fit that description is that of β4, which is over 1,000 residues long, and is made up of a series of globular domains. Structures of some of these domains (solved by X-ray crystallography) have been published (de Pereda *et al.*, 2009; de Pereda *et al.*, 1999), and no more will be said about them here. Otherwise, almost all integrin structural biology on the cytoplasmic side of the membrane has involved αIIb and/or β3. In 2000, two groups published NMR structures of the cytoplasmic tail of αIIb. Hwang *et al*. (Hans Vogel's lab) solved the structure in 45% TFE (Hwang & Vogel, 2000), and Vinogradova *et al*. (Jun Qin's lab) solved it in detergent micelles (Vinogradova *et al.*, 2000). This revealed a structure that was largely flexible, although the C-terminal fragment folded back on the tail to make contact with the MP helix. Then, in 2001, Ulmer *et al*. (in Iain Campbell's lab) studied the αIIb and β3 tails by NMR (Ulmer *et al.*, 2001). They did not solve an atomic-resolution structure, but they did characterize the general structure and dynamics of the tails, finding them both largely unstructured, but with some helical character in the MP region of β3 (Ulmer *et al.*, 2001). This was consistent with earlier studies performed by circular dichroism (CD) indicating that these tails are largely unstructured (Haas & Plow, 1996; Haas & Plow, 1997; Muir *et al.*, 1994). The Ulmer *et al*. studies were carried out using a coiled-coil construct in order to place the tails in an environment similar to what would be found *in vivo*. One of the goals of these studies was to characterize the αIIbβ3 cytoplasmic domain complex. However, Ulmer *et al*. detected no interaction between the tails, despite such an interaction being expected from other studies (Haas & Plow, 1996; Vallar *et al.*, 1999). At the time, these results were mysterious, but now that the TM αIIbβ3 complex structure has been solved, it is clear that very little of the interaction between these two integrins

takes place in the cytoplasmic region (Lau *et al.*, 2009). Also, the arrangement in the earlier Ulmer *et al*. study would not have placed the tails together as they would be *in vivo*, because the junction between the TM domain and tail of αIIb forms an unusual non-helical structure, and—whereas the TM domains in reality form a right-handed crossing angle—the coiled-coil employed by Ulmer *et al*. was left-handed. While the Ulmer *et al*. study was correct in finding that there is not an extensive cytoplasmic interaction between the two integrin tails, it was able to say little else about the αIIbβ3 complex. Its value, then, was in characterizing integrin tail dynamics. Soon after that, another study that looked at a β3 construct that included the TM domain and tail by NMR—this time in detergent micelles—also found it largely unstructured, although with more helical character than reported previously (in particular this involved a second MD helix) (Li *et al.*, 2002). The results presented in this thesis confirm that the β3 tail is largely unstructured and show that the same applies to other integrin tails as well. This intrinsic flexibility is key to the activity of β tails as signalling hubs.

β integrin tails act as hubs for protein-protein interactions. More than 20 unique interactions have been identified by various methods (Liu *et al.*, 2000), although only a small fraction have been validated and further studied by structural biological methods. These protein-protein interactions involving the β integrin tail mediate both inside-out and outside-in integrin signalling, and how such interactions are regulated in time and space and how these various binding partners function both cooperatively and antagonistically are questions of great interest. One of these methods—integrin phosphorylation (Oxley *et al.*, 2008)—is explored in depth in Chapter V of this thesis. Acting as a hub for protein-protein interactions is a characteristic of many intrinsically unstructured proteins. Such interactions can be enthalpically favourable due to specific hydrogen bond or electrostatic contacts (or entropically favourable if hydrophobic

interfaces are involved), but there is a large entropic cost to binding since this involves the ordering of what was previously a disordered peptide. As such, this allows interactions to still be highly specific, but also weak and transient (Kriwacki *et al.*, 1996). This is particularly relevant in integrin signalling, where the activation state of the integrin needs to be regulated rapidly by switching binding partners. In an environment such as a focal adhesion, the various interacting proteins are highly crosslinked through multiple interactions, making such weak interactions essential—otherwise they would become permanent. Protein disorder is common throughout biology. Depending on how it is measured, it has been estimated that 33% of eukaryotic proteins contain disordered regions of 30 or more residues (Ward *et al.*, 2004), and the amount of disorder found in the proteome increases with the complexity of the organism (Dunker *et al.*, 2005; Uversky *et al.*, 2005). Despite their importance, such disordered regions are underrepresented in the Protein Data Bank and general biophysical characterization of such regions has only recently become common. NMR is particularly well-suited for studying such interactions, however, and it already has and will continue to play an important role in the study of intrinsically unstructured proteins—including the integrin tails—and their protein-protein interactions.

Despite the unstructured nature of the tails, some additional atomic resolution work has still been carried out on them. In 2002, two groups solved NMR structures of the cytoplasmic complex of αIIbβ3. Vinogradova *et al*. solved the structure of the complex involving the full cytoplasmic tails using peptides fused to maltose binding protein (Vinogradova *et al.*, 2002). They found that the MP portions of the two tails form weakly interacting helices, stabilized by a salt bridge between αIIb R995 and β3 D723—which had been previously demonstrated by mutagenesis and integrin activation studies (Hughes *et al.*, 1996). This was an unlikely structure, though, because as discussed above

there is a large entropic cost to binding by unstructured peptides, and interactions involving two unstructured peptides are uncommon. Also, Vinogradova *et al*. reported chemical shift perturbations of a very small magnitude in the tails caused by this interaction—shifts that Ulmer *et al*. attributed to non-specific effects (Ulmer *et al.*, 2001). Also, various lines of evidence indicate that most of the residues found interacting by Vinogradova *et al*. are actually buried in the membrane *in vivo* (Armulik *et al.*, 1999; Lau *et al.*, 2008a; Lau *et al.*, 2009; Lau *et al.*, 2008b; Li *et al.*, 2001; Stefansson *et al.*, 2004; Vinogradova *et al.*, 2004). Earlier that same year, Weljie *et al*. from the lab of Hans Vogel reported an NMR structure of a complex of short synthetic peptides corresponding to the MP portion of αIIbβ3 tails (Weljie *et al.*, 2002). Unusually, Weljie *et al*. were able to solve two distinct complex structures, one of them compatible with the MP salt bridge. The existence of two distinct structures, while not impossible, seems unlikely to be detected for such a weak interaction involving two highly flexible peptides, and no other study has reproduced such a finding. The Weljie *et al*. structures were vaguely similar to the Vinogradova *et al*. structure, in that they involved two weakly interacting helices. However, the atomic details of the two were quite different, indicating that the two approaches either produced different actual structures due to differences in methods, that the two approaches did not generate enough structural restraints to precisely determine the structure, that the two approaches were not measuring the actual complex but instead nonspecific effects, or a combination of these. Regardless, now that a structure of the αIIbβ3 TM domain complex is available (Lau *et al.*, 2009), along with a similar model produced from disulfide restraints acquired on the full integrin (Zhu *et al.*, 2009), it has become clear that neither of these structures is compatible with the actual arrangement of the integrin TM and tail segments *in vivo*.

A few additional studies have been carried out on pairs of α and β integrin tails since then. Vinogradova *et al*. performed a later structural study on the αIIbβ3 cytoplasmic domains, but this time in detergent micelles (Vinogradova *et al.*, 2004). Under these conditions, however, they did not detect an interaction between the tails. Also, in line with the previous study of β3 in detergent, they detected a second MD helix in the β3 tail. More recently, Bhunia *et al*. solved a solution NMR structure of the αL cytoplasmic domain (Bhunia *et al.*, 2009). They found that the αL tail, which is 38 residues longer than αIIb, forms a globular structure consisting of three packed helices. NMR studies indicated that the β2 tail bound between two of these helices. They also found the β2 tail to be largely unstructured, so they did not solve an atomic resolution structure of β2 or the complex. However, they did model the αLβ2 complex based on the chemical shift perturbation data. This produced a structure characterized by helix-helix interactions—including the MP salt bridge—with some similarities to the Vinogradova *et al*. structure, but with a more extensive interface. Therefore, it is unclear whether this structure reflects the actual structure *in vivo*—making αLβ2 significantly different in structure from αIIbβ3—or whether studies of the αLβ2 TM domains would reveal a structure similar to αIIbβ3. Based on sequence conservation, it is unlikely that these structures would be significantly different, casting doubt on the relevance of this αLβ2 cytoplasmic domain structural model.

In addition to these structures involving integrin tails alone or bound to one another, studies have also been carried out on integrin tails interacting with other proteins. Until the current study, these had only involved small fragments of the tail, and studies with talin had only involved small fragments of β3 specifically. Such structural studies of integrin activation by talin have been limited by the fact that talin only interacts with integrins weakly in the systems studied; also, poor solubility and chemical shift exchange

broadening have limited NMR-based analysis specifically. Various strategies have been employed to overcome this problem. In 2003, Garcia-Alvarez *et al*. in the lab of Robert Liddington published a crystal structure of a short membrane-distal fragment of the β3 tail covalently tethered to the N-terminus of the talin1 F2-F3 domain pair (Garcia-Alvarez *et al.*, 2003). This showed that the F3 domain interacts with the NPxY motif of the β3 tail in canonical PTB domain fashion (Calderwood *et al.*, 2003), but this gave no information about the membrane-proximal region of the β3 tail, a region known to be essential for activation (Hughes *et al.*, 1995; Ulmer *et al.*, 2003; Vinogradova *et al.*, 2004; Vinogradova *et al.*, 2002). However, in 2007, Wegener *et al*. in Iain Campbell's group published a second structure, solved by NMR, which elucidated the interface between the F3 domain and the β3 membrane-proximal helix (Wegener *et al.*, 2007). This was made possible by constructing a chimeric peptide of the β3 helix attached to a sequence from PIPK1γ that binds tightly to the talin NPxY binding pocket (Barsukov *et al.*, 2003; de Pereda *et al.*, 2005). This structure demonstrated that talin forms a novel interaction with the MP portion of the helix, particularly with β3 residues F727 and F730 (Fig. 1.3B). This interaction involves a flexible loop between strands S1 and S2, which is unique to talin. In their study, Wegener *et al*. demonstrated that this interaction is necessary for integrin activation. Together, these studies offered some insight into the β3/talin1 complex and the structural basis of integrin activation, but they did not answer questions about how general this process is among different integrins and how much it differs—questions addressed in the current study.

Structural studies on the TM segments of the integrin tails are much fewer in number, due to the difficulties of working in a membrane environment. The TM portion of the integrin α/β integrin complex has been extensively subjected to modelling studies (Gottschalk, 2005; Gottschalk *et al.*, 2002; Gottschalk & Kessler, 2004; Li *et al.*, 2005;

Luo *et al.*, 2004; Partridge *et al.*, 2005; Zhu *et al.*, 2009), but the only atomic-resolution structural data to date has come from a series of recent NMR structures from Tobias Ulmer's group. As with all of the previously published TM modelling studies, these structures specifically involved αIIbβ3. In 2008, Lau *et al*. published structures of the αIIb (Lau *et al.*, 2008a) and β3 (Lau *et al.*, 2008b) TM segments in lipid bicelles. Each turned out to be more interesting than one might expect for a TM helix, and each contributed to our understanding of integrin activation. The αIIb TM segment forms a 24-residue membrane-spanning helix that sits vertically in the lipid bilayer, constrained by tryptophan residues at each membrane interface (Lau *et al.*, 2008a), a role often played by such residues (Yau *et al.*, 1998). Interestingly, the C-terminus of the TM segment consists of a GFFKR motif (residues 991-995), which is highly conserved among α integrins (Fig. 1.1B). Uniquely, these two phenylalanine residues are packed against the TM helix in the membrane (Lau *et al.*, 2008a)—an arrangement not predicted by any of the previous modelling studies. The β3 TM segment, on the other hand, forms a longer 29-residue helix that Lau *et al*. determined to be tilted by about 20-30° from a vertical orientation within the membrane. There could be more flexibility in this arrangement, though, because the β3 TM domain is not as constrained by interfacial tryptophan residues as αIIb is. The β3 TM domain also exhibits interesting features at its C-terminus. It is buried through I721, and this segment includes the charged residue K716, but due to the helical tilt the charged side chain is able to snorkel through the membrane to the more polar environment at the interface with the cytoplasm (Lau *et al.*, 2008b). Although these specific aspects of the structure were novel, the span of buried residues is in line with what had been suggested by earlier glycosylation mapping experiments (Armulik *et al.*, 1999; Stefansson *et al.*, 2004). This is an important distinction, though, because the residue K716 has often been treated as the beginning of the cytoplasmic domain.

Following up on the structures of the individual TM domains, Lau *et al*. subsequently solved the NMR structure of the αIIbβ3 TM complex in lipid bicelles (Lau *et al.*, 2009). This revealed a TM dimer of unique structure, with the individual segments exhibiting similar structures to what has been found individually and crossing at an angle of about 30° (Fig. 1.3A). The dimer is stabilized by two interactions: an outer membrane clasp that involves glycine-mediated TM helix packing and an inner membrane clasp that includes the D723/R995 cytoplasmic salt bridge and packing between αIIb F992/F993 and the two TM helices (Lau *et al.*, 2009). Of particular interest is the cytoplasmic salt bridge, which was originally identified by mutagenesis (Hughes *et al.*, 1996) and figures centrally into the mechanism of integrin activation presented in this thesis. The Lau *et al*. structure advanced our understanding of integrin structure and function considerably, and it explains to an extent why previous results involving just cytoplasmic fragments had given such inconsistent results. It is also now clear that the various modelling studies performed on this complex gave incorrect results—predicting standard coiled-coil structures with none of the unique features identified in these NMR studies. Interestingly, though, the one TM modelling study that has been published since these NMR structures became available generated a complex very similar to that of Lau *et al*. In that study, Zhu *et al*. from the laboratory of Timothy Springer used disulfide crosslinking to generate restraints to model the structure of the αIIbβ3 TM segment (Zhu *et al.*, 2009). Although the Lau *et al*. atomic resolution structure of the complex was published first, this model is still of interest because the crosslinking studies were performed on an intact integrin, lending additional validity to the Lau *et al*. structure, which was performed on isolated TM domains. Thus, in the case of the TM domains—as with the rest of the integrin heterodimer—atomic resolution structural data has greatly advanced our understanding of

integrin function. Together with additional studies, this has enabled the formulation of a largely accepted model of integrin activation.

1.4 Inside-Out Integrin Activation

Since integrins signal in both directions across the cell membrane, dissecting and deconvoluting these different signalling events can be difficult. Because of that, it is essential that consistent and meaningful terminology is used. In this thesis, the term integrin "activation" should be read as "inside-out activation". Although the term "activation" is sometimes used to refer to outside-in signalling, these are two unique processes with different mechanisms. Confusion of and disagreement about terminology may be responsible for some of the current controversy over integrin activation mechanisms. Inside-out integrin activation *in viv*o is always initiated by binding of talin to the β integrin tail (Tadokoro *et al.*, 2003). This binding causes separation of the α and β TM and cytoplasmic regions, and these changes are propagated to the extracellular domains, causing the integrin to adopt a conformation with higher affinity for the extracellular matrix (Hynes, 2002a; Wegener & Campbell, 2008). The exact nature of these extracellular changes in conformation is a subject of some controversy, but most lines of evidence indicate that activation involves the integrin adopting a more extended and/or more open conformation (Luo *et al.*, 2007). Broadly speaking, though, there are two prevalent models for how integrin activation proceeds. The switchblade model (Fig. 1.2), advanced largely by Timothy Springer and colleagues, postulates that large structural rearrangements (particularly integrin extension) directly modulate integrin affinity (Luo *et al.*, 2007). Alternatively, the deadbolt model, advanced largely by Amin Arnaout and colleagues, postulates that only moderate conformational changes are

necessary for integrin activation to occur, and although more dramatic structural rearrangements may occur, they are not essential (Xiong *et al.*, 2003b).

In contrast to inside-out activation, outside-in signalling refers to what may be a more heterogeneous collection of processes initiated by binding of the integrin to an extracellular ligand, generally an ECM protein. Outside-in signalling then proceeds through integrin conformational changes (which may or may not resemble those associated with inside-out activation) (Zhu *et al.*, 2007b), integrin clustering (Cluzel *et al.*, 2005; Miyamoto *et al.*, 1995), mechanical force (Choquet *et al.*, 1997; Galbraith *et al.*, 2002), or some combination of these. This can lead to the activation of various intracellular signalling pathways, although primarily those involving the tyrosine kinases Src and focal adhesion kinase (Burridge & Chrzanowska-Wodnicka, 1996; Shattil, 2005). Often in experimental work, divalent cations—particularly Mn^{2+}—are employed to study integrin "activation", because they cause an increase in integrin affinity for extracellular ligands (Ye *et al.*, 2008). Although this may with some accuracy be called an outside-in or an inside-out effect, depending on perspective, it does not fully replicate either physiological process. Although these cations bind to the extracellular portion of the integrin, this is not technically an outside-in process, since it causes increased affinity on the extracellular portion and does not otherwise resemble the complex nature of outside-in signalling. Likewise, this is not technically an inside-out process since it does not initiate inside the cell. There are also very distinct differences between Mn^{2+}-initiated activation and talin-induced inside-out activation (Kim *et al.*, 2003; Lu *et al.*, 2001; Luo *et al.*, 2004). The use of divalent cations has certainly been instrumental in advancing our understanding of integrin signalling processes, but the over-extrapolation of such results could be a factor in perpetuating controversy and confusion (Arnaout *et al.*, 2007; Askari *et al.*, 2009; Luo *et al.*, 2007; Wegener & Campbell, 2008; Ye *et al.*, 2008) over the true

nature of integrin inside-out activation. Regardless, outside-in signalling appears to be a more complex process that is much more difficult to study outside of the context of a live cell. With those distinctions in mind, the remainder of this thesis will focus primarily on inside-out activation, which much of the evidence indicates follows a switchblade mechanism.

Unlike some other aspects of integrin activation, it is well-accepted that inside-out activation involves separation of the C-terminal portions of the integrin (i.e. the TM domains and tails). Early studies indicated that deletion of the α or β integrin tail could lead to integrin activation (Crowe *et al.*, 1994; Hughes *et al.*, 1995; O'Toole *et al.*, 1994; O'Toole *et al.*, 1991), and dissection of the tails indicated that it was just the MP portion of each that was essential for maintaining the inactive state, specifically the highly conserved GFFKR motif in the α tail (Hughes *et al.*, 1996; Lu & Springer, 1997; O'Toole *et al.*, 1994) and the slightly less conserved KLLvxiHD motif in the β tail (Crowe *et al.*, 1994; Hughes *et al.*, 1995). It was later shown that a lipid-modified (i.e. membrane-targeted) KVGFFKR peptide could cause integrin activation in platelets (Stephens *et al.*, 1998) and mice with a knock-in GFFKR deletion in αL display persistent αLβ2 activation, resulting in an impaired immune response (Semmrich *et al.*, 2005). With the exception of the lysine residue, the mutation of any of these GFFKR residues to alanine induces activation, indicating that each residue plays an important role (Hughes *et al.*, 1996; Lu & Springer, 1997).

Of particular interest in this region is a salt bridge formed between the α and β MP tail regions. This was first demonstrated by Hughes *et al*. in Mark Ginsberg's lab. They found that mutation of αIIb R995 or β3 D723 to an oppositely-charged residue causes constitutive αIIbβ3 activation. Satisfyingly, simultaneous mutation of both tails reverts the integrin to its natural default inactive state. Interestingly, these mutations also cause

constitutive outside-in signalling (Hughes *et al.*, 1996). Such a salt bridge has been detected by or is at least compatible with every atomic-resolution structural study of αIIbβ3 to date (Lau *et al.*, 2009; Vinogradova *et al.*, 2002; Weljie *et al.*, 2002), as well as the one NMR-based model of αLβ2 (Bhunia *et al.*, 2009). Overall, studies have indicated that mutation of these salt bridge-forming residues leads to inside-out activation of αIIbβ3 (Hughes *et al.*, 1996; Kim *et al.*, 2009; Lau *et al.*, 2009; Partridge *et al.*, 2005; Tadokoro *et al.*, 2003; Vallar *et al.*, 1999; Vinogradova *et al.*, 2002; Wegener *et al.*, 2007), αLβ2 (Li *et al.*, 2007; Lu & Springer, 1997; Tang *et al.*, 2008), α4β1 and α4β7 (Imai *et al.*, 2008), and α5β1 (Millon-Fremillon *et al.*, 2008; Sakai *et al.*, 1998). Surprisingly, when Czuchra *et al*. of Reinhard Fassler's group produced a mouse with the knock-in D759A mutation in β1, they found no pronounced phenotype (Czuchra *et al.*, 2006). This stands in contrast to experiments demonstrating that such a mutation causes β1 integrin activation in cell culture (Millon-Fremillon *et al.*, 2008; Sakai *et al.*, 1998), and explanations are offered for this in Chapters III and IV of this thesis. Alternatively, mice with a knock-in mutation in the corresponding residue in α4 display disrupted leukocyte homing to the gut associated lymphoid tissue due to persistent integrin activation (Imai *et al.*, 2008), and in humans the mutation D723H in β3 causes an inherited macrothrombocytopenia due to spontaneous integrin activation in platelet precursors (Ghevaert *et al.*, 2008). Thus, this salt bridge forms an integral part of the MP α/β interface responsible for maintaining the integrin in the inactive form (Fig. 1.2, 1.3A).

Making this model of activation controversial for some time, though, were the inconsistent results of biophysical experiments used to directly identify a direct interaction between the integrin tails. A couple of early studies found an interaction between the αIIb and β3 tails by CD (Haas & Plow, 1996) and surface plasmon resonance (Vallar *et al.*, 1999). However, the first attempt to observe this interaction directly by

NMR failed to detect one (Ulmer *et al.*, 2001). Two subsequent NMR studies did detect an interaction, leading to structures of the complex (Vinogradova *et al.*, 2002; Weljie *et al.*, 2002), but then another study found no interaction in the presence of detergent micelles (Vinogradova *et al.*, 2004). It has subsequently become clear, however, that these studies were fundamentally flawed, because they did not include the TM domains of the integrin, which form a much larger interface than the tails (Lau *et al.*, 2009).

After these initial studies on the integrin tails, our understanding of the process of integrin activation was advanced considerably by several elegant studies that either artificially restrained the integrin or explored the α/β TM interface. Many of these studies came from the laboratory of Timothy Springer, including two studies published in May 2001. Lu *et al*., similar to earlier studies, found that deletion of the β2 tail causes constitutive αLβ2 and αMβ2 activation. Taking things one step further, though, they found that if they then replaced both the αL and β2 tails with a strongly-interacting coiled coil motif, this restores the inactive state of the integrin (Lu *et al.*, 2001). Taking a slightly different approach, Takagi *et al*. pursued experiments with just the extracellular fragments of α5β1 but with an artificial C-terminal clasp where the TM domains would begin. Such an integrin was inactive, but release of the clasp activated it, increasing its affinity for fibronectin, and causing the two extracellular legs to separate by about 14 nm (Takagi *et al.*, 2001). Takagi *et al*. also demonstrated a similar effect in αVβ3 (Takagi *et al.*, 2002). In 2003, the Springer group provided more direct evidence for the tail separation mechanism of integrin activation, this time using FRET. Kim *et al*. attached fluorophores to the C-termini of αL and β2 and detected a large FRET signal consistent with the integrin tails sitting in close proximity. Activation of the integrin, either by stimulating activating signalling pathways, mutating the αL GFFKR motif, or by adding talin, caused a decrease in FRET signal consistent with a major tail separation. In support

of tail separation in response to outside-in signalling as well, the addition of Mn^{2+} and the extracellular ligand ICAM together also caused a decrease in FRET signal (Kim *et al.*, 2003). The next year, Luo *et al*. published a cysteine scanning study to map the αIIbβ3 TM interface. In the default inactive state, they detected a disulfide bonding pattern consistent with a helix-helix interface. If the integrin was activated, though, by mutating the MP region of αIIb, they then detected decreased disulfide bonding, reminiscent of a nonspecific interaction. Tellingly, when they did allow this mutant integrin to form disulfide bonds, it no longer exhibited constitutive activity (Luo *et al.*, 2004). As a whole, these studies provide convincing evidence that an interaction between the C-terminal portions of the integrin maintains it in the inactive state, and activation is achieved by separation of the C-termini.

Over the past five years, this model of activation and the structure of the integrin TM complex have been further refined. A couple of studies showed that various mutations in the TM domain and MP tail are capable of activating αIIbβ3, and these studies further defined the interface between these subunits (Li *et al.*, 2005; Luo *et al.*, 2005; Partridge *et al.*, 2005). The Springer lab has also more recently conducted additional disulfide crosslinking experiments on αIIbβ3. In 2007, Zhu *et al*. provided evidence that tail separation plays an important role in outside-in signalling in this integrin, as αIIbβ3 with disulfide-linked TM domains was deficient in several outside-in signalling activities (Zhu *et al.*, 2007b). In 2009, Zhu *et al*. conducted a detailed disulfide-linking study and used these data as structural restraints to model the structure of the αIIbβ3 TM structure. The results showed an interesting structure, characterized by a significant β3 tilt and an unusual turn at the C-terminus of the αIIb helix that placed part of the two phenylalanines of the GFFKR motif back in the membrane (Zhu *et al.*, 2009). However, by that point, this was basically a moot point, as Lau *et al*. in Tobias Ulmer's

group had already published the atomic-resolution NMR structure of the complex in lipid bicelles (Lau *et al.*, 2009). The fact that the two complexes were so similar, though, and the fact that the Zhu *et al*. model was based on restraints derived on the intact integrin, offer good evidence that these structures represent the true form of the integrin *in vivo*. Also in 2009, Kim *et al*. from Mark Ginsberg's group published a study using "miniature integrins" consisting of just the TM and tail domains of αIIbβ3. Using a pull-down system, they demonstrated a direct interaction between αIIb and β3 in cell membranes, an interaction that could be disrupted by adding talin or breaking the MP salt bridge (Kim *et al.*, 2009). Thus, the separation of integrin tails as the mechanism for inside-out activation has become well-established.

It was identified early-on that integrins undergo conformational change in conjunction with signalling events. An early study using a variety of indirect methods found evidence for a change in conformation of αIIbβ3 upon binding to an RGD ligand (Parise *et al.*, 1987). Later, another study used FRET to identify a conformational change in αIIbβ3 in response to thrombin-induced inside-out activation (Sims *et al.*, 1991). Many other studies offered evidence for conformational changes during integrin signalling processes, but these generally used more indirect methods, particularly antibodies that recognize activated conformations (Frelinger *et al.*, 1988), so the nature of these conformational changes remained unknown. Starting in 1995, a series of structures of I/A domains from integrin α subunits were solved, and these showed evidence of structural rearrangements in response to ligand or cation binding (Emsley *et al.*, 1997; Emsley *et al.*, 2000; Lee *et al.*, 1995a; Lee *et al.*, 1995b; Qu & Leahy, 1995; Qu & Leahy, 1996). By this time, it had also become clear that the MP portions of the α and β tails interact with one another to maintain the integrin in the inactive state, and it would soon become clear that this is part of a larger interface including the TM domains, and that the release of this

interaction was responsible for inside-out integrin activation; however, a mechanism coupling tail separation to extracellular ligand affinity remained elusive.

Despite the importance of these early functional studies and later atomic resolution structural studies, our understanding of integrin extracellular conformational change has come largely from lower resolution EM studies. However, all early EM studies showed the integrin in an extended and/or open conformation—generally with a globular head domain and two flexible legs (Carrell *et al.*, 1985; Du *et al.*, 1993; Erb *et al.*, 1997; Hantgan *et al.*, 1999; Kelly *et al.*, 1987; Nermut *et al.*, 1988; Parise & Phillips, 1985; Weisel *et al.*, 1992). This commonly observed open/extended structure was thought to represent the active state of the integrin. However, these early studies were for the most part conducted on detergent-solubilised integrins, and these non-physiological experimental conditions may have influenced the results. Regardless, the most recent of these early EM studies found that, although the (detergent-solubilised) integrin was always seen in an extended form, binding of an RGD peptide caused it adopt a slightly more open conformation, with additional separation between the α and β subunits (Hantgan *et al.*, 1999). Thus, allosteric regulation of integrin activity appeared to be a distinct possibility, but there was not yet a plausible mechanism for how a signal could be transmitted from the C-terminus to the N-terminus (or vice versa) of the integrin.

Starting in 2001, a series of structural and mechanistic studies began to shine light on the mechanism of inside-out integrin activation as it takes place on the exterior of the cell, but these studies led to two competing schools of thought. In May 2001, Takagi *et al*. of the Springer group published an EM-based study using the extracellular domains of α5β1. They found that when they restrained the C-termini of the integrin with an artificial clasp (mimicking a TM/TM interaction), the integrin existed in a closed, bent shape (as observed by EM) and did not bind fibronectin. However, when this clasp was released,

the integrin adopted an open, extended shape and became capable of binding fibronectin. Thus was born the switchblade model of activation (Takagi *et al.*, 2001). However, later that year, Xiong *et al*. of the Arnaout group published the crystal structure of the intact extracellular domain of αVβ3. Although this integrin would be expected to be active—lacking its C-termini—it was found in a closed bent shape. Its bent knees placed the ligand-binding portion of the integrin in close proximity to where the membrane surface would be *in vivo* (Xiong *et al.*, 2001). The next year, Xiong *et al*. published additional structures of the αVβ3 extracellular domain bound to Mn^{2+} and an RGD ligand. Only small conformational adjustments were observed between these structures, thus giving rise to the deadbolt model of integrin activation (Xiong *et al.*, 2002).

Since then, a variety of studies have provided evidence for both models; however, the weight of the evidence favours a switchblade mechanism, at least as far as inside-out activation is concerned. The most compelling evidence for the deadbolt model comes from EM studies that do not offer evidence for a change in integrin height upon activation (Adair *et al.*, 2005; Ye *et al.*, 2008). However, these studies used the addition of Mn^{2+} to induce "activation", a practice that is of debatable relevance, as discussed above. Additional evidence for the deadbolt model comes from a study—using αIIbβ3 bound by two fluorescent antibodies—that found only a modest change in FRET signal upon platelet activation (Coutinho *et al.*, 2007). Other studies also offered more indirect evidence for such a model (Gupta *et al.*, 2007; Wei *et al.*, 2005), although they did not always distinguish between inside-out and outside-in signalling. However, the deadbolt model of integrin activation fails to provide a plausible mechanism for inside-out activation; one study found that mutating residues that should disrupt the deadbolt region of the integrin did not affect integrin activation, but inserting disulfide bonds to make the integrin incapable of extension prevented integrin activation (Zhu *et al.*, 2007a).

Over this same period of time, additional evidence has built up in favour of the switchblade mechanism. The first single-particle EM reconstruction of a full-length integrin was published by Adair *et al*. of Mark Yeager's group in 2002. In contrast to earlier studies, they found detergent-solubilised αIIbβ3 to be in a compact, inactive conformation, although it was unique from the more bent conformation seen in the crystal structures. Using additional methods, they found that the addition of an extracellular ligand caused the integrin to adopt a more open and/or extended state (Adair & Yeager, 2002). The Springer lab has published several additional studies in favour of a switchblade mechanism. In 2003, Takagi *et al*. published an EM study on the α5β1 headpiece, finding it in a closed conformation in the inactive unbound state. The addition of fibronectin, however, induced a major structural rearrangement, leading to a more open conformation (Takagi *et al.*, 2003). More relevant to inside-out activation, though, the Springer group has also replicated in other integrins their key experiments originally conducted on C-terminally-clasped α5β1 extracellular domain (Takagi *et al.*, 2001). They have since demonstrated in αVβ3 (Takagi *et al.*, 2002) and αIIbβ3 (Zhu *et al.*, 2008) that clasped integrins adopt a bent, closed conformation (as observed by EM), with low extracellular ligand affinity. Release of this clasp induces an open, extended conformation, with a much higher affinity for extracellular ligands, thus directly demonstrating the switchblade mechanism by EM using C-terminally clasped integrin extracellular domains—a system that is particularly relevant for studying inside-out activation. These studies offer the most direct evidence for the role of major conformational changes in integrin inside-out activation, and additional studies have provided further support for this model (Chigaev *et al.*, 2003; Shi *et al.*, 2007).

Overall, although bidirectional integrin signalling is a complex and somewhat heterogeneous process, good evidence exists for a switchblade mechanism of inside-out

integrin activation. Thus, tail and TM separation induces major structural rearrangements in the extracellular domain, leading to a higher affinity for extracellular ligands. To some approximation, the integrin exists in an allosteric equilibrium between these two states: a closed low affinity state and an open high affinity state. Thus, the high affinity state is stabilized by either by binding of extracellular ligands or the separation of the cytoplasmic tails. This is true insofar as there is some evidence that outside-in activation involves integrin opening and tail separation (Zhu *et al.*, 2007b). However, inside-out and outside-in signalling events are otherwise fundamentally different, as outside-in signalling can take on a variety of forms unrelated to inside-out activation (Choquet *et al.*, 1997; Cluzel *et al.*, 2005; Galbraith *et al.*, 2002; Miyamoto *et al.*, 1995). Thus, some aspects of outside-in signalling may be consistent with a deadbolt model and others with a switchblade. Inside-out activation, however, appears to strictly follow a switchblade mechanism, and studies of integrin activation by talin have further clarified the molecular details of this process.

Based on these studies on extracellular conformational changes, TM separation, and additional studies on integrin activation by talin, a general model of inside-out integrin activation can be constructed. It has been demonstrated that talin is essential for inside-out integrin activation to occur (Tadokoro *et al.*, 2003) and that this activation involves the PTB-like talin F3 domain interacting directly with the β integrin tail (Calderwood *et al.*, 2002). A variety of studies have indicated that talin interacts with the MP portion of the β integrin tail (Hughes *et al.*, 1995; Ulmer *et al.*, 2003; Vinogradova *et al.*, 2004; Vinogradova *et al.*, 2002), thus disrupting the α/β interaction that maintains the integrin inactive state. This was elucidated in detail by a later NMR structure that showed that the talin1 F3 domain forms an extended interface with the MP β3 helix (Wegener *et al.*, 2007). When compared with the best relevant structure of the inactive integrin

available at the time—the 2002 full-length αIIbβ3 tail structure (Vinogradova *et al.*, 2002)—limited steric clashes were observed between talin and the αIIb subunit. The result is the same if the Wegener *et al*. structure is compared with the more recent and more reliable αIIbβ3 TM structure (Lau *et al.*, 2009). Wegener *et al*. also provided some evidence that an interaction between talin and the cell membrane may also play a role in targeting talin to the membrane for activation. However, the N-terminus of the β3 integrin tail peptide was unstructured in their complex, and a more complete picture of the activating complex oriented with respect to the membrane could not be generated. This was problematic, because the only steric clashes between the talin F3 domain and the αIIb tail were located around α/β MP salt bridge. This alone would not be sufficient for integrin activation, because it has been demonstrated that although mutations that break the integrin salt bridge activate the integrin, full activation only occurs in the presence of talin (Tadokoro *et al.*, 2003; Wegener *et al.*, 2007). Therefore, another effect must also be at play. Also, this structure only involved a small fragment of the β3 integrin tail in a chimeric construct, and the applicability of these findings to a native integrin tail and to other integrins besides β3 remained to be determined. The results presented in this thesis will address these issues; our new structural, biophysical, and biological data allow us to define a more complete model of integrin activation, and we can now apply these findings to integrins other than β3.

1.5 Aims of the Thesis

Despite what is currently known about inside-out integrin activation, myriad details remain elusive; how integrin activation is regulated in time and space remains an even more open area. And, although studies of integrin activation have been conducted on a wide variety of integrins, a large number of them—particularly those involving talin—

have focused just on β3 integrins. How does this mechanism translate to other integrins, and in what ways does it differ? This thesis addresses a subset of these broader questions, focusing on the mechanism of talin activation of integrins, as it occurs on the cytoplasmic face of the plasma membrane.

Chapter III of this thesis proposes a new more comprehensive model of integrin activation by talin. We explain how the talin F3 domain binds to the β integrin tail, and through an interaction with the MP portion of the tail disrupts a salt bridge between the α and β subunits. We also demonstrate that the F2 domain forms a direct interaction with the plasma membrane and that this interaction may precisely orient the talin/integrin complex to disrupt the interactions between the α and β TM domains. We show that this model is—to an extent—generalizable across different types of integrins.

Chapter IV of this thesis expands on the results presented in Chapter III. Whereas Chapter III presents a general model of integrin activation by talin, Chapter IV explains how this model may differ in subtle ways between different integrins. In particular, this study explores differences between β3, β1A, and β1D. The data presented here indicate that the MD portions of the integrin play a key role in modulating the affinity of the integrin for talin, but that subtle differences in the dynamics of the MP portions can have significant and biologically-relevant effects on the ability of talin to activate the integrin. We also present additional evidence that the integrin tail, like many other intrinsically disordered proteins, is able to act as a protein-protein interaction hub by forming enthalpically-favourable but entropically-unfavourable weak and transient interactions.

Finally, Chapter V addresses the question of how integrin activation is regulated in the cell. Specifically, this chapter covers the role of tyrosine phosphorylation in modulating the activation state of the integrin. We demonstrate that phosphorylation of the more MP NPxY motif tyrosine in β3, β1A, and β7 decreases talin affinity for integrins

while also greatly increasing the affinity of the integrin for Dok1, an integrin inactivator—showing that this is a conserved mechanism of activation control. Based on structural data, we have designed mutations to reverse this switch, producing a talin mutant that behaves significantly differently in live cells—validating some aspects of these structures and our general hypothesis of how integrin activation is regulated by tyrosine phosphorylation.

To conduct these studies, a multidisciplinary approach has been undertaken. The primary method in this thesis is NMR, and it has been complemented by X-ray crystallography and isothermal titration calorimetry. To increase the power and breadth of our findings—and to present as comprehensive a picture of integrin activation as possible—additional experiments were undertaken by collaborators. In particular, Feng Ye and Chungho Kim performed integrin activation assays in live cells in Mark Ginsberg's lab at the University of California San Diego. Also, Ben Goult in David Critchley's lab at the University of Leicester conducted vesicle binding studies.

The foundation of this thesis is an NMR-based system for studying integrin protein-protein interactions. The cytoplasmic portions of the β3, β1A, β1D, and β7 integrins were produced in *E. coli*. This system was advantageous because isotopic labelling (^{15}N specifically) was inexpensive and straightforward. Also, integrin modifications could be made in a straightforward manner by site-directed mutagenesis. Protein-protein interactions were monitored by acquiring HSQC spectra of ^{15}N-labelled integrin tails. The addition of an unlabelled protein, if it interacts with the integrin tail, perturbs the HSQC spectrum of the tail in a specific manner. By assigning the ^{1}H and ^{15}N resonances of the tail, the interaction site can then be mapped. This process is called chemical shift perturbation mapping and is a well-established mechanism for identifying protein-protein interaction sites (Clarkson & Campbell, 2003). If these perturbations are

monitored over several concentrations of unlabelled protein, the K_d of the interaction can be determined. NMR is unique in being able to provide both atomic resolution data (or at least amino acid resolution in this case) across the entire molecule as well as affinity data from a single experiment.

These NMR studies revealed significant heterogeneity in how different integrins interact with signalling proteins. Of particular interest is the unusually high affinity of the β1D/talin2 interaction, which allowed this protein to be crystallized. The resulting 2.2 Å structure offers novel insights into the mechanism of integrin activation (Chapter III) and how this mechanism differs between different integrins (Chapter IV). Based on this structure and on our initial NMR experiments, additional biophysical and biological experiments were performed. The results of these studies have expanded our understanding of integrin activation—a process that is structurally interesting and is of fundamental biological importance.

1.6 References

Adair B.D., Xiong J.P., Maddock C., Goodman S.L., Arnaout M.A., Yeager M. (2005) Three-dimensional EM structure of the ectodomain of integrin {alpha}V{beta}3 in a complex with fibronectin. *J Cell Biol* **168:** 1109-1118

Adair B.D., Yeager M. (2002) Three-dimensional model of the human platelet integrin alpha IIbbeta 3 based on electron cryomicroscopy and x-ray crystallography. *Proc Natl Acad Sci U S A* **99:** 14059-14064

Ali I.U., Hynes R.O. (1977) Effects of cytochalasin B and colchicine on attachment of a major surface protein of fibroblasts. *Biochim Biophys Acta* **471:** 16-24

Ali I.U., Mautner V., Lanza R., Hynes R.O. (1977) Restoration of normal morphology, adhesion and cytoskeleton in transformed cells by addition of a transformation-sensitive surface protein. *Cell* **11:** 115-126

Armulik A., Nilsson I., von Heijne G., Johansson S. (1999) Determination of the border between the transmembrane and cytoplasmic domains of human integrin subunits. *J Biol Chem* **274:** 37030-37034

Arnaout M.A., Goodman S.L., Xiong J.P. (2007) Structure and mechanics of integrin-based cell adhesion. *Curr Opin Cell Biol* **19:** 495-507

Arthos J., Cicala C., Martinelli E., Macleod K., Van Ryk D., Wei D., Xiao Z., Veenstra T.D., Conrad T.P., Lempicki R.A., McLaughlin S., Pascuccio M., Gopaul R., McNally J., Cruz C.C., Censoplano N., Chung E., Reitano K.N., Kottilil S., Goode D.J., Fauci A.S. (2008) HIV-1 envelope protein binds to and signals

through integrin alpha4beta7, the gut mucosal homing receptor for peripheral T cells. *Nat Immunol* **9:** 301-309

Askari J.A., Buckley P.A., Mould A.P., Humphries M.J. (2009) Linking integrin conformation to function. *J Cell Sci* **122:** 165-170

Assoian R.K. (1997) Anchorage-dependent cell cycle progression. *J Cell Biol* **136:** 1-4

Bargatze R.F., Jutila M.A., Butcher E.C. (1995) Distinct roles of L-selectin and integrins alpha 4 beta 7 and LFA-1 in lymphocyte homing to Peyer's patch-HEV in situ: the multistep model confirmed and refined. *Immunity* **3:** 99-108

Barsukov I.L., Prescot A., Bate N., Patel B., Floyd D.N., Bhanji N., Bagshaw C.R., Letinic K., Di Paolo G., De Camilli P., Roberts G.C., Critchley D.R. (2003) Phosphatidylinositol phosphate kinase type 1gamma and beta1-integrin cytoplasmic domain bind to the same region in the talin FERM domain. *J Biol Chem* **278:** 31202-31209

Beckerle M.C., O'Halloran T., Burridge K. (1986) Demonstration of a relationship between talin and P235, a major substrate of the calcium-dependent protease in platelets. *J Cell Biochem* **30:** 259-270

Belkin A.M., Retta S.F., Pletjushkina O.Y., Balzac F., Silengo L., Fassler R., Koteliansky V.E., Burridge K., Tarone G. (1997) Muscle beta1D integrin reinforces the cytoskeleton-matrix link: modulation of integrin adhesive function by alternative splicing. *J Cell Biol* **139:** 1583-1595

Belkin A.M., Zhidkova N.I., Balzac F., Altruda F., Tomatis D., Maier A., Tarone G., Koteliansky V.E., Burridge K. (1996) Beta 1D integrin displaces the beta 1A isoform in striated muscles: localization at junctional structures and signaling potential in nonmuscle cells. *J Cell Biol* **132:** 211-226

Bhunia A., Tang X.Y., Mohanram H., Tan S.M., Bhattacharjya S. (2009) NMR solution conformations and interactions of integrin alphaLbeta2 cytoplasmic tails. *J Biol Chem* **284:** 3873-3884

Bouaouina M., Lad Y., Calderwood D.A. (2008) The N-terminal domains of talin cooperate with the phosphotyrosine binding-like domain to activate beta1 and beta3 integrins. *J Biol Chem* **283:** 6118-6125

Brown N.H. (2000) Cell-cell adhesion via the ECM: integrin genetics in fly and worm. *Matrix Biol* **19:** 191-201

Brown N.H., Gregory S.L., Rickoll W.L., Fessler L.I., Prout M., White R.A., Fristrom J.W. (2002) Talin is essential for integrin function in Drosophila. *Dev Cell* **3:** 569-579

Burridge K., Chrzanowska-Wodnicka M. (1996) Focal adhesions, contractility, and signaling. *Annu Rev Cell Dev Biol* **12:** 463-518

Burridge K., Connell L. (1983) A new protein of adhesion plaques and ruffling membranes. *J Cell Biol* **97:** 359-367

Calderwood D.A. (2004) Integrin activation. *J Cell Sci* **117:** 657-666

Calderwood D.A., Fujioka Y., de Pereda J.M., Garcia-Alvarez B., Nakamoto T., Margolis B., McGlade C.J., Liddington R.C., Ginsberg M.H. (2003) Integrin beta cytoplasmic domain interactions with phosphotyrosine-binding domains: a structural prototype for diversity in integrin signaling. *Proc Natl Acad Sci U S A* **100:** 2272-2277

Calderwood D.A., Shattil S.J., Ginsberg M.H. (2000) Integrins and actin filaments: reciprocal regulation of cell adhesion and signaling. *J Biol Chem* **275:** 22607-22610

Calderwood D.A., Yan B., de Pereda J.M., Alvarez B.G., Fujioka Y., Liddington R.C., Ginsberg M.H. (2002) The phosphotyrosine binding-like domain of talin activates integrins. *J Biol Chem* **277:** 21749-21758

Campbell I.D., Ginsberg M.H. (2004) The talin-tail interaction places integrin activation on FERM ground. *Trends Biochem Sci* **29:** 429-435

Cantor J.M., Ginsberg M.H., Rose D.M. (2008) Integrin-associated proteins as potential therapeutic targets. *Immunol Rev* **223:** 236-251

Carrell N.A., Fitzgerald L.A., Steiner B., Erickson H.P., Phillips D.R. (1985) Structure of human platelet membrane glycoproteins IIb and IIIa as determined by electron microscopy. *J Biol Chem* **260:** 1743-1749

Chan J.R., Hyduk S.J., Cybulsky M.I. (2000) Alpha 4 beta 1 integrin/VCAM-1 interaction activates alpha L beta 2 integrin-mediated adhesion to ICAM-1 in human T cells. *J Immunol* **164:** 746-753

Chiarugi P., Giannoni E. (2008) Anoikis: a necessary death program for anchorage-dependent cells. *Biochem Pharmacol* **76:** 1352-1364

Chigaev A., Buranda T., Dwyer D.C., Prossnitz E.R., Sklar L.A. (2003) FRET detection of cellular alpha4-integrin conformational activation. *Biophys J* **85:** 3951-3962

Choquet D., Felsenfeld D.P., Sheetz M.P. (1997) Extracellular matrix rigidity causes strengthening of integrin-cytoskeleton linkages. *Cell* **88:** 39-48

Chrzanowska-Wodnicka M., Smyth S.S., Schoenwaelder S.M., Fischer T.H., White G.C., 2nd (2005) Rap1b is required for normal platelet function and hemostasis in mice. *J Clin Invest* **115:** 680-687

Clarkson J., Campbell I.D. (2003) Studies of protein-ligand interactions by NMR. *Biochem Soc Trans* **31:** 1006-1009

Cluzel C., Saltel F., Lussi J., Paulhe F., Imhof B.A., Wehrle-Haller B. (2005) The mechanisms and dynamics of (alpha)v(beta)3 integrin clustering in living cells. *J Cell Biol* **171:** 383-392

Coller B.S. (1997) Platelet GPIIb/IIIa antagonists: the first anti-integrin receptor therapeutics. *J Clin Invest* **99:** 1467-1471

Coutinho A., Garcia C., Gonzalez-Rodriguez J., Lillo M.P. (2007) Conformational changes in human integrin alphaIIbbeta3 after platelet activation, monitored by FRET. *Biophys Chem* **130:** 76-87

Cram E.J., Clark S.G., Schwarzbauer J.E. (2003) Talin loss-of-function uncovers roles in cell contractility and migration in C. elegans. *J Cell Sci* **116:** 3871-3878

Critchley D.R. (2004) Cytoskeletal proteins talin and vinculin in integrin-mediated adhesion. *Biochem Soc Trans* **32:** 831-836

Critchley D.R., Gingras A.R. (2008) Talin at a glance. *J Cell Sci* **121:** 1345-1347

Crowe D.T., Chiu H., Fong S., Weissman I.L. (1994) Regulation of the avidity of integrin alpha 4 beta 7 by the beta 7 cytoplasmic domain. *J Biol Chem* **269:** 14411-14418

Czuchra A., Meyer H., Legate K.R., Brakebusch C., Fassler R. (2006) Genetic analysis of beta1 integrin "activation motifs" in mice. *J Cell Biol* **174:** 889-899

Danen E.H., Yamada K.M. (2001) Fibronectin, integrins, and growth control. *J Cell Physiol* **189:** 1-13

de Pereda J.M., Lillo M.P., Sonnenberg A. (2009) Structural basis of the interaction between integrin alpha6beta4 and plectin at the hemidesmosomes. *EMBO J* **28:** 1180-1190

de Pereda J.M., Wegener K.L., Santelli E., Bate N., Ginsberg M.H., Critchley D.R., Campbell I.D., Liddington R.C. (2005) Structural basis for phosphatidylinositol phosphate kinase type Igamma binding to talin at focal adhesions. *J Biol Chem* **280:** 8381-8386

de Pereda J.M., Wiche G., Liddington R.C. (1999) Crystal structure of a tandem pair of fibronectin type III domains from the cytoplasmic tail of integrin alpha6beta4. *EMBO J* **18:** 4087-4095

Delon I., Brown N.H. (2007) Integrins and the actin cytoskeleton. *Curr Opin Cell Biol* **19:** 43-50

Di Paolo G., Pellegrini L., Letinic K., Cestra G., Zoncu R., Voronov S., Chang S., Guo J., Wenk M.R., De Camilli P. (2002) Recruitment and regulation of phosphatidylinositol phosphate kinase type 1 gamma by the FERM domain of talin. *Nature* **420:** 85-89

Douma S., Van Laar T., Zevenhoven J., Meuwissen R., Van Garderen E., Peeper D.S. (2004) Suppression of anoikis and induction of metastasis by the neurotrophic receptor TrkB. *Nature* **430:** 1034-1039

Du X., Gu M., Weisel J.W., Nagaswami C., Bennett J.S., Bowditch R., Ginsberg M.H. (1993) Long range propagation of conformational changes in integrin alpha IIb beta 3. *J Biol Chem* **268:** 23087-23092

Dunker A.K., Cortese M.S., Romero P., Iakoucheva L.M., Uversky V.N. (2005) Flexible nets. The roles of intrinsic disorder in protein interaction networks. *FEBS J* **272:** 5129-5148

Emsley J., King S.L., Bergelson J.M., Liddington R.C. (1997) Crystal structure of the I domain from integrin alpha2beta1. *J Biol Chem* **272:** 28512-28517

Emsley J., Knight C.G., Farndale R.W., Barnes M.J., Liddington R.C. (2000) Structural basis of collagen recognition by integrin alpha2beta1. *Cell* **101:** 47-56

Erb E.M., Tangemann K., Bohrmann B., Muller B., Engel J. (1997) Integrin alphaIIb beta3 reconstituted into lipid bilayers is nonclustered in its activated state but clusters after fibrinogen binding. *Biochemistry* **36:** 7395-7402

Etzioni A., Doerschuk C.M., Harlan J.M. (1999) Of man and mouse: leukocyte and endothelial adhesion molecule deficiencies. *Blood* **94:** 3281-3288

Franco S.J., Rodgers M.A., Perrin B.J., Han J., Bennin D.A., Critchley D.R., Huttenlocher A. (2004) Calpain-mediated proteolysis of talin regulates adhesion dynamics. *Nat Cell Biol* **6:** 977-983

Frelinger A.L., 3rd, Lam S.C., Plow E.F., Smith M.A., Loftus J.C., Ginsberg M.H. (1988) Occupancy of an adhesive glycoprotein receptor modulates expression of an antigenic site involved in cell adhesion. *J Biol Chem* **263:** 12397-12402

Frisch S.M., Francis H. (1994) Disruption of epithelial cell-matrix interactions induces apoptosis. *J Cell Biol* **124:** 619-626

Frisch S.M., Screaton R.A. (2001) Anoikis mechanisms. *Curr Opin Cell Biol* **13:** 555-562

Galbraith C.G., Yamada K.M., Sheetz M.P. (2002) The relationship between force and focal complex development. *J Cell Biol* **159:** 695-705

Garcia-Alvarez B., de Pereda J.M., Calderwood D.A., Ulmer T.S., Critchley D., Campbell I.D., Ginsberg M.H., Liddington R.C. (2003) Structural determinants of integrin recognition by talin. *Mol Cell* **11:** 49-58

Geiger B., Bershadsky A. (2001) Assembly and mechanosensory function of focal contacts. *Curr Opin Cell Biol* **13:** 584-592

Geiger B., Bershadsky A., Pankov R., Yamada K.M. (2001) Transmembrane crosstalk between the extracellular matrix--cytoskeleton crosstalk. *Nat Rev Mol Cell Biol* **2:** 793-805

Ghevaert C., Salsmann A., Watkins N.A., Schaffner-Reckinger E., Rankin A., Garner S.F., Stephens J., Smith G.A., Debili N., Vainchenker W., de Groot P.G., Huntington J.A., Laffan M., Kieffer N., Ouwehand W.H. (2008) A nonsynonymous SNP in the ITGB3 gene disrupts the conserved membrane-proximal cytoplasmic salt bridge in the alphaIIbbeta3 integrin and cosegregates dominantly with abnormal proplatelet formation and macrothrombocytopenia. *Blood* **111:** 3407-3414

Gingras A.R., Ziegler W.H., Bobkov A.A., Joyce M.G., Fasci D., Himmel M., Rothemund S., Ritter A., Grossmann J.G., Patel B., Bate N., Goult B.T., Emsley J., Barsukov I.L., Roberts G.C., Liddington R.C., Ginsberg M.H., Critchley D.R. (2009) Structural determinants of integrin binding to the talin rod. *J Biol Chem* **284:** 8866-8876

Ginsberg M.H., Partridge A., Shattil S.J. (2005) Integrin regulation. *Curr Opin Cell Biol* **17:** 509-516

Goksoy E., Ma Y.Q., Wang X., Kong X., Perera D., Plow E.F., Qin J. (2008) Structural basis for the autoinhibition of talin in regulating integrin activation. *Mol Cell* **31:** 124-133

Gottlieb A., Krueger J.G., Bright R., Ling M., Lebwohl M., Kang S., Feldman S., Spellman M., Wittkowski K., Ochs H.D., Jardieu P., Bauer R., White M., Dedrick R., Garovoy M. (2000) Effects of administration of a single dose of a humanized monoclonal antibody to CD11a on the immunobiology and clinical activity of psoriasis. *J Am Acad Dermatol* **42:** 428-435

Gottschalk K.E. (2005) A coiled-coil structure of the alphaIIbbeta3 integrin transmembrane and cytoplasmic domains in its resting state. *Structure* **13:** 703-712

Gottschalk K.E., Adams P.D., Brunger A.T., Kessler H. (2002) Transmembrane signal transduction of the alpha(IIb)beta(3) integrin. *Protein Sci* **11:** 1800-1812

Gottschalk K.E., Kessler H. (2004) Evidence for hetero-association of transmembrane helices of integrins. *FEBS Lett* **557:** 253-258

Goult B.T., Bate N., Anthis N.J., Wegener K.L., Gingras A.R., Patel B., Barsukov I.L., Campbell I.D., Roberts G.C., Critchley D.R. (2009) The structure of an interdomain complex that regulates talin activity. *J Biol Chem* **284:** 15097-15106

Gupta V., Gylling A., Alonso J.L., Sugimori T., Ianakiev P., Xiong J.P., Arnaout M.A. (2007) The beta-tail domain (betaTD) regulates physiologic ligand binding to integrin CD11b/CD18. *Blood* **109:** 3513-3520

Haas T.A., Plow E.F. (1996) The cytoplasmic domain of alphaIIb beta3. A ternary complex of the integrin alpha and beta subunits and a divalent cation. *J Biol Chem* **271:** 6017-6026

Haas T.A., Plow E.F. (1997) Development of a structural model for the cytoplasmic domain of an integrin. *Protein Eng* **10:** 1395-1405

Han J., Lim C.J., Watanabe N., Soriani A., Ratnikov B., Calderwood D.A., Puzon-McLaughlin W., Lafuente E.M., Boussiotis V.A., Shattil S.J., Ginsberg M.H. (2006) Reconstructing and deconstructing agonist-induced activation of integrin alphaIIbbeta3. *Curr Biol* **16:** 1796-1806

Hantgan R.R., Paumi C., Rocco M., Weisel J.W. (1999) Effects of ligand-mimetic peptides Arg-Gly-Asp-X (X = Phe, Trp, Ser) on alphaIIbbeta3 integrin conformation and oligomerization. *Biochemistry* **38:** 14461-14474

Harburger D.S., Bouaouina M., Calderwood D.A. (2009) Kindlin-1 and -2 directly bind the C-terminal region of beta integrin cytoplasmic tails and exert integrin-specific activation effects. *J Biol Chem* **284:** 11485-11497

Hodivala-Dilke K.M., McHugh K.P., Tsakiris D.A., Rayburn H., Crowley D., Ullman-Cullere M., Ross F.P., Coller B.S., Teitelbaum S., Hynes R.O. (1999) Beta3-integrin-deficient mice are a model for Glanzmann thrombasthenia showing placental defects and reduced survival. *J Clin Invest* **103:** 229-238

Horwitz A., Duggan K., Buck C., Beckerle M.C., Burridge K. (1986) Interaction of plasma membrane fibronectin receptor with talin--a transmembrane linkage. *Nature* **320:** 531-533

Hu K., Ji L., Applegate K.T., Danuser G., Waterman-Storer C.M. (2007) Differential transmission of actin motion within focal adhesions. *Science* **315:** 111-115

Hughes P.E., Diaz-Gonzalez F., Leong L., Wu C., McDonald J.A., Shattil S.J., Ginsberg M.H. (1996) Breaking the integrin hinge. A defined structural constraint regulates integrin signaling. *J Biol Chem* **271:** 6571-6574

Hughes P.E., O'Toole T.E., Ylanne J., Shattil S.J., Ginsberg M.H. (1995) The conserved membrane-proximal region of an integrin cytoplasmic domain specifies ligand binding affinity. *J Biol Chem* **270:** 12411-12417

Hwang P.M., Vogel H.J. (2000) Structures of the platelet calcium- and integrin-binding protein and the alphaIIb-integrin cytoplasmic domain suggest a mechanism for calcium-regulated recognition; homology modelling and NMR studies. *J Mol Recognit* **13:** 83-92

Hynes R.O. (1987) Integrins: a family of cell surface receptors. *Cell* **48:** 549-554

Hynes R.O. (2002a) Integrins: bidirectional, allosteric signaling machines. *Cell* **110:** 673-687

Hynes R.O. (2002b) A reevaluation of integrins as regulators of angiogenesis. *Nat Med* **8:** 918-921

Hynes R.O. (2004) The emergence of integrins: a personal and historical perspective. *Matrix Biol* **23:** 333-340

Imai Y., Park E.J., Peer D., Peixoto A., Cheng G., von Andrian U.H., Carman C.V., Shimaoka M. (2008) Genetic perturbation of the putative cytoplasmic membrane-proximal salt bridge aberrantly activates alpha(4) integrins. *Blood* **112:** 5007-5015

Iwasaki K., Mitsuoka K., Fujiyoshi Y., Fujisawa Y., Kikuchi M., Sekiguchi K., Yamada T. (2005) Electron tomography reveals diverse conformations of integrin alphaIIbbeta3 in the active state. *J Struct Biol* **150:** 259-267

Jackson D.Y. (2002) Alpha 4 integrin antagonists. *Curr Pharm Des* **8:** 1229-1253

Jiang G., Giannone G., Critchley D.R., Fukumoto E., Sheetz M.P. (2003) Two-piconewton slip bond between fibronectin and the cytoskeleton depends on talin. *Nature* **424:** 334-337

Kato A. (1997) The biologic and clinical spectrum of Glanzmann's thrombasthenia: implications of integrin alpha IIb beta 3 for its pathogenesis. *Crit Rev Oncol Hematol* **26:** 1-23

Kelly T., Molony L., Burridge K. (1987) Purification of two smooth muscle glycoproteins related to integrin. Distribution in cultured chicken embryo fibroblasts. *J Biol Chem* **262:** 17189-17199

Kim C., Lau T.L., Ulmer T.S., Ginsberg M.H. (2009) Interactions of platelet integrin alphaIIb and beta3 transmembrane domains in mammalian cell membranes and their role in integrin activation. *Blood* **113:** 4747-4753

Kim M., Carman C.V., Springer T.A. (2003) Bidirectional transmembrane signaling by cytoplasmic domain separation in integrins. *Science* **301:** 1720-1725

Krause M., Leslie J.D., Stewart M., Lafuente E.M., Valderrama F., Jagannathan R., Strasser G.A., Rubinson D.A., Liu H., Way M., Yaffe M.B., Boussiotis V.A., Gertler F.B. (2004) Lamellipodin, an Ena/VASP ligand, is implicated in the regulation of lamellipodial dynamics. *Dev Cell* **7:** 571-583

Kriwacki R.W., Hengst L., Tennant L., Reed S.I., Wright P.E. (1996) Structural studies of p21Waf1/Cip1/Sdi1 in the free and Cdk2-bound state: conformational disorder mediates binding diversity. *Proc Natl Acad Sci U S A* **93:** 11504-11509

Lafuente E.M., van Puijenbroek A.A., Krause M., Carman C.V., Freeman G.J., Berezovskaya A., Constantine E., Springer T.A., Gertler F.B., Boussiotis V.A. (2004) RIAM, an Ena/VASP and Profilin ligand, interacts with Rap1-GTP and mediates Rap1-induced adhesion. *Dev Cell* **7:** 585-595

Lau T.L., Dua V., Ulmer T.S. (2008a) Structure of the integrin alphaIIb transmembrane segment. *J Biol Chem* **283:** 16162-16168

Lau T.L., Kim C., Ginsberg M.H., Ulmer T.S. (2009) The structure of the integrin alphaIIbbeta3 transmembrane complex explains integrin transmembrane signalling. *EMBO J* **28:** 1351-1361

Lau T.L., Partridge A.W., Ginsberg M.H., Ulmer T.S. (2008b) Structure of the integrin beta3 transmembrane segment in phospholipid bicelles and detergent micelles. *Biochemistry* **47:** 4008-4016

Lauffenburger D.A., Horwitz A.F. (1996) Cell migration: a physically integrated molecular process. *Cell* **84:** 359-369

Lee H.S., Lim C.J., Puzon-McLaughlin W., Shattil S.J., Ginsberg M.H. (2009) RIAM activates integrins by linking talin to ras GTPase membrane-targeting sequences. *J Biol Chem* **284:** 5119-5127

Lee J.O., Bankston L.A., Arnaout M.A., Liddington R.C. (1995a) Two conformations of the integrin A-domain (I-domain): a pathway for activation? *Structure* **3:** 1333-1340

Lee J.O., Rieu P., Arnaout M.A., Liddington R. (1995b) Crystal structure of the A domain from the alpha subunit of integrin CR3 (CD11b/CD18). *Cell* **80:** 631-638

Legate K.R., Wickstrom S.A., Fassler R. (2009) Genetic and cell biological analysis of integrin outside-in signaling. *Genes Dev* **23:** 397-418

Li R., Babu C.R., Lear J.D., Wand A.J., Bennett J.S., DeGrado W.F. (2001) Oligomerization of the integrin alphaIIbbeta3: roles of the transmembrane and cytoplasmic domains. *Proc Natl Acad Sci U S A* **98:** 12462-12467

Li R., Babu C.R., Valentine K., Lear J.D., Wand A.J., Bennett J.S., DeGrado W.F. (2002) Characterization of the monomeric form of the transmembrane and cytoplasmic domains of the integrin beta 3 subunit by NMR spectroscopy. *Biochemistry* **41:** 15618-15624

Li W., Metcalf D.G., Gorelik R., Li R., Mitra N., Nanda V., Law P.B., Lear J.D., Degrado W.F., Bennett J.S. (2005) A push-pull mechanism for regulating integrin function. *Proc Natl Acad Sci U S A* **102:** 1424-1429

Li Y.F., Tang R.H., Puan K.J., Law S.K., Tan S.M. (2007) The cytosolic protein talin induces an intermediate affinity integrin alphaLbeta2. *J Biol Chem* **282:** 24310-24319

Lim J., Wiedemann A., Tzircotis G., Monkley S.J., Critchley D.R., Caron E. (2007) An essential role for talin during alpha(M)beta(2)-mediated phagocytosis. *Mol Biol Cell* **18:** 976-985

Ling K., Doughman R.L., Firestone A.J., Bunce M.W., Anderson R.A. (2002) Type I gamma phosphatidylinositol phosphate kinase targets and regulates focal adhesions. *Nature* **420:** 89-93

Litjens S.H., de Pereda J.M., Sonnenberg A. (2006) Current insights into the formation and breakdown of hemidesmosomes. *Trends Cell Biol* **16:** 376-383

Liu S., Calderwood D.A., Ginsberg M.H. (2000) Integrin cytoplasmic domain-binding proteins. *J Cell Sci* **113 (Pt 20):** 3563-3571

Lu C., Takagi J., Springer T.A. (2001) Association of the membrane proximal regions of the alpha and beta subunit cytoplasmic domains constrains an integrin in the inactive state. *J Biol Chem* **276:** 14642-14648

Lu C.F., Springer T.A. (1997) The alpha subunit cytoplasmic domain regulates the assembly and adhesiveness of integrin lymphocyte function-associated antigen-1. *J Immunol* **159:** 268-278

Luo B.H., Carman C.V., Springer T.A. (2007) Structural basis of integrin regulation and signaling. *Annu Rev Immunol* **25:** 619-647

Luo B.H., Carman C.V., Takagi J., Springer T.A. (2005) Disrupting integrin transmembrane domain heterodimerization increases ligand binding affinity, not valency or clustering. *Proc Natl Acad Sci U S A* **102:** 3679-3684

Luo B.H., Springer T.A., Takagi J. (2004) A specific interface between integrin transmembrane helices and affinity for ligand. *PLoS Biol* **2:** e153

Ma Y.Q., Qin J., Wu C., Plow E.F. (2008) Kindlin-2 (Mig-2): a co-activator of beta3 integrins. *J Cell Biol* **181:** 439-446

Manevich E., Grabovsky V., Feigelson S.W., Alon R. (2007) Talin 1 and paxillin facilitate distinct steps in rapid VLA-4-mediated adhesion strengthening to vascular cell adhesion molecule 1. *J Biol Chem* **282:** 25338-25348

Martel V., Racaud-Sultan C., Dupe S., Marie C., Paulhe F., Galmiche A., Block M.R., Albiges-Rizo C. (2001) Conformation, localization, and integrin binding of talin depend on its interaction with phosphoinositides. *J Biol Chem* **276:** 21217-21227

Millon-Fremillon A., Bouvard D., Grichine A., Manet-Dupe S., Block M.R., Albiges-Rizo C. (2008) Cell adaptive response to extracellular matrix density is controlled by ICAP-1-dependent beta1-integrin affinity. *J Cell Biol* **180:** 427-441

Miyamoto S., Akiyama S.K., Yamada K.M. (1995) Synergistic roles for receptor occupancy and aggregation in integrin transmembrane function. *Science* **267:** 883-885

Moes M., Rodius S., Coleman S.J., Monkley S.J., Goormaghtigh E., Tremuth L., Kox C., van der Holst P.P., Critchley D.R., Kieffer N. (2007) The integrin binding site 2 (IBS2) in the talin rod domain is essential for linking integrin beta subunits to the cytoskeleton. *J Biol Chem* **282:** 17280-17288

Monkley S.J., Pritchard C.A., Critchley D.R. (2001) Analysis of the mammalian talin2 gene TLN2. *Biochem Biophys Res Commun* **286:** 880-885

Monkley S.J., Zhou X.H., Kinston S.J., Giblett S.M., Hemmings L., Priddle H., Brown J.E., Pritchard C.A., Critchley D.R., Fassler R. (2000) Disruption of the talin gene arrests mouse development at the gastrulation stage. *Dev Dyn* **219:** 560-574

Montanez E., Ussar S., Schifferer M., Bosl M., Zent R., Moser M., Fassler R. (2008) Kindlin-2 controls bidirectional signaling of integrins. *Genes Dev* **22:** 1325-1330

Moser M., Bauer M., Schmid S., Ruppert R., Schmidt S., Sixt M., Wang H.V., Sperandio M., Fassler R. (2009a) Kindlin-3 is required for beta2 integrin-mediated leukocyte adhesion to endothelial cells. *Nat Med* **15:** 300-305

Moser M., Legate K.R., Zent R., Fassler R. (2009b) The tail of integrins, talin, and kindlins. *Science* **324:** 895-899

Moser M., Nieswandt B., Ussar S., Pozgajova M., Fassler R. (2008) Kindlin-3 is essential for integrin activation and platelet aggregation. *Nat Med* **14:** 325-330

Muir T.W., Williams M.J., Ginsberg M.H., Kent S.B. (1994) Design and chemical synthesis of a neoprotein structural model for the cytoplasmic domain of a multisubunit cell-surface receptor: integrin alpha IIb beta 3 (platelet GPIIb-IIIa). *Biochemistry* **33:** 7701-7708

Nayal A., Webb D.J., Horwitz A.F. (2004) Talin: an emerging focal point of adhesion dynamics. *Curr Opin Cell Biol* **16:** 94-98

Nermut M.V., Green N.M., Eason P., Yamada S.S., Yamada K.M. (1988) Electron microscopy and structural model of human fibronectin receptor. *EMBO J* **7:** 4093-4099

Nieswandt B., Moser M., Pleines I., Varga-Szabo D., Monkley S., Critchley D., Fassler R. (2007) Loss of talin1 in platelets abrogates integrin activation, platelet aggregation, and thrombus formation in vitro and in vivo. *J Exp Med* **204:** 3113-3118

Nolte M., Pepinsky R.B., Venyaminov S., Koteliansky V., Gotwals P.J., Karpusas M. (1999) Crystal structure of the alpha1beta1 integrin I-domain: insights into integrin I-domain function. *FEBS Lett* **452:** 379-385

O'Halloran T., Beckerle M.C., Burridge K. (1985) Identification of talin as a major cytoplasmic protein implicated in platelet activation. *Nature* **317:** 449-451

O'Toole T.E., Katagiri Y., Faull R.J., Peter K., Tamura R., Quaranta V., Loftus J.C., Shattil S.J., Ginsberg M.H. (1994) Integrin cytoplasmic domains mediate inside-out signal transduction. *J Cell Biol* **124:** 1047-1059

O'Toole T.E., Mandelman D., Forsyth J., Shattil S.J., Plow E.F., Ginsberg M.H. (1991) Modulation of the affinity of integrin alpha IIb beta 3 (GPIIb-IIIa) by the cytoplasmic domain of alpha IIb. *Science* **254:** 845-847

Oxley C.L., Anthis N.J., Lowe E.D., Vakonakis I., Campbell I.D., Wegener K.L. (2008) An integrin phosphorylation switch: the effect of beta3 integrin tail phosphorylation on Dok1 and talin binding. *J Biol Chem* **283:** 5420-5426

Papagrigoriou E., Gingras A.R., Barsukov I.L., Bate N., Fillingham I.J., Patel B., Frank R., Ziegler W.H., Roberts G.C., Critchley D.R., Emsley J. (2004) Activation of a vinculin-binding site in the talin rod involves rearrangement of a five-helix bundle. *EMBO J* **23:** 2942-2951

Parise L.V., Helgerson S.L., Steiner B., Nannizzi L., Phillips D.R. (1987) Synthetic peptides derived from fibrinogen and fibronectin change the conformation of purified platelet glycoprotein IIb-IIIa. *J Biol Chem* **262:** 12597-12602

Parise L.V., Phillips D.R. (1985) Platelet membrane glycoprotein IIb-IIIa complex incorporated into phospholipid vesicles. Preparation and morphology. *J Biol Chem* **260:** 1750-1756

Partridge A.W., Liu S., Kim S., Bowie J.U., Ginsberg M.H. (2005) Transmembrane domain helix packing stabilizes integrin alphaIIbbeta3 in the low affinity state. *J Biol Chem* **280:** 7294-7300

Petrich B.G., Marchese P., Ruggeri Z.M., Spiess S., Weichert R.A., Ye F., Tiedt R., Skoda R.C., Monkley S.J., Critchley D.R., Ginsberg M.H. (2007) Talin is required for integrin-mediated platelet function in hemostasis and thrombosis. *J Exp Med* **204:** 3103-3111

Pfaff M., Liu S., Erle D.J., Ginsberg M.H. (1998) Integrin beta cytoplasmic domains differentially bind to cytoskeletal proteins. *J Biol Chem* **273:** 6104-6109

Ponti A., Machacek M., Gupton S.L., Waterman-Storer C.M., Danuser G. (2004) Two distinct actin networks drive the protrusion of migrating cells. *Science* **305:** 1782-1786

Qu A., Leahy D.J. (1995) Crystal structure of the I-domain from the CD11a/CD18 (LFA-1, alpha L beta 2) integrin. *Proc Natl Acad Sci U S A* **92:** 10277-10281

Qu A., Leahy D.J. (1996) The role of the divalent cation in the structure of the I domain from the CD11a/CD18 integrin. *Structure* **4:** 931-942

Riveline D., Zamir E., Balaban N.Q., Schwarz U.S., Ishizaki T., Narumiya S., Kam Z., Geiger B., Bershadsky A.D. (2001) Focal contacts as mechanosensors: externally applied local mechanical force induces growth of focal contacts by an mDia1-dependent and ROCK-independent mechanism. *J Cell Biol* **153:** 1175-1186

Rodius S., Chaloin O., Moes M., Schaffner-Reckinger E., Landrieu I., Lippens G., Lin M., Zhang J., Kieffer N. (2008) The talin rod IBS2 alpha-helix interacts with the beta3 integrin cytoplasmic tail

membrane-proximal helix by establishing charge complementary salt bridges. *J Biol Chem* **283:** 24212-24223

Sakai T., Zhang Q., Fassler R., Mosher D.F. (1998) Modulation of beta1A integrin functions by tyrosine residues in the beta1 cytoplasmic domain. *J Cell Biol* **141:** 527-538

Scarborough R.M., Gretler D.D. (2000) Platelet glycoprotein IIb-IIIa antagonists as prototypical integrin blockers: novel parenteral and potential oral antithrombotic agents. *J Med Chem* **43:** 3453-3473

Schwartz M.A., Ginsberg M.H. (2002) Networks and crosstalk: integrin signalling spreads. *Nat Cell Biol* **4:** E65-68

Sebzda E., Bracke M., Tugal T., Hogg N., Cantrell D.A. (2002) Rap1A positively regulates T cells via integrin activation rather than inhibiting lymphocyte signaling. *Nat Immunol* **3:** 251-258

Semmrich M., Smith A., Feterowski C., Beer S., Engelhardt B., Busch D.H., Bartsch B., Laschinger M., Hogg N., Pfeffer K., Holzmann B. (2005) Importance of integrin LFA-1 deactivation for the generation of immune responses. *J Exp Med* **201:** 1987-1998

Senetar M.A., McCann R.O. (2005) Gene duplication and functional divergence during evolution of the cytoskeletal linker protein talin. *Gene* **362:** 141-152

Senetar M.A., Moncman C.L., McCann R.O. (2007) Talin2 is induced during striated muscle differentiation and is targeted to stable adhesion complexes in mature muscle. *Cell Motil Cytoskeleton* **64:** 157-173

Shattil S.J. (2005) Integrins and Src: dynamic duo of adhesion signaling. *Trends Cell Biol* **15:** 399-403

Sheetz M.P., Felsenfeld D., Galbraith C.G., Choquet D. (1999) Cell migration as a five-step cycle. *Biochem Soc Symp* **65:** 233-243

Shi M., Foo S.Y., Tan S.M., Mitchell E.P., Law S.K., Lescar J. (2007) A structural hypothesis for the transition between bent and extended conformations of the leukocyte beta2 integrins. *J Biol Chem* **282:** 30198-30206

Simonson W.T., Franco S.J., Huttenlocher A. (2006) Talin1 regulates TCR-mediated LFA-1 function. *J Immunol* **177:** 7707-7714

Sims P.J., Ginsberg M.H., Plow E.F., Shattil S.J. (1991) Effect of platelet activation on the conformation of the plasma membrane glycoprotein IIb-IIIa complex. *J Biol Chem* **266:** 7345-7352

Springer T.A., Zhu J., Xiao T. (2008) Structural basis for distinctive recognition of fibrinogen gammaC peptide by the platelet integrin alphaIIbbeta3. *J Cell Biol* **182:** 791-800

Stefansson A., Armulik A., Nilsson I., von Heijne G., Johansson S. (2004) Determination of N- and C-terminal borders of the transmembrane domain of integrin subunits. *J Biol Chem* **279:** 21200-21205

Stephens G., O'Luanaigh N., Reilly D., Harriott P., Walker B., Fitzgerald D., Moran N. (1998) A sequence within the cytoplasmic tail of GpIIb independently activates platelet aggregation and thromboxane synthesis. *J Biol Chem* **273:** 20317-20322

Tadokoro S., Shattil S.J., Eto K., Tai V., Liddington R.C., de Pereda J.M., Ginsberg M.H., Calderwood D.A. (2003) Talin binding to integrin beta tails: a final common step in integrin activation. *Science* **302:** 103-106

Takagi J., Erickson H.P., Springer T.A. (2001) C-terminal opening mimics 'inside-out' activation of integrin alpha5beta1. *Nat Struct Biol* **8:** 412-416

Takagi J., Petre B.M., Walz T., Springer T.A. (2002) Global conformational rearrangements in integrin extracellular domains in outside-in and inside-out signaling. *Cell* **110:** 599-511

Takagi J., Strokovich K., Springer T.A., Walz T. (2003) Structure of integrin alpha5beta1 in complex with fibronectin. *EMBO J* **22:** 4607-4615

Tanentzapf G., Brown N.H. (2006) An interaction between integrin and the talin FERM domain mediates integrin activation but not linkage to the cytoskeleton. *Nat Cell Biol* **8:** 601-606

Tang X.Y., Li Y.F., Tan S.M. (2008) Intercellular adhesion molecule-3 binding of integrin alphaL beta2 requires both extension and opening of the integrin headpiece. *J Immunol* **180:** 4793-4804

Turner C.E., Burridge K. (1991) Transmembrane molecular assemblies in cell-extracellular matrix interactions. *Curr Opin Cell Biol* **3:** 849-853

Ulmer T.S., Calderwood D.A., Ginsberg M.H., Campbell I.D. (2003) Domain-specific interactions of talin with the membrane-proximal region of the integrin beta3 subunit. *Biochemistry* **42:** 8307-8312

Ulmer T.S., Yaspan B., Ginsberg M.H., Campbell I.D. (2001) NMR analysis of structure and dynamics of the cytosolic tails of integrin alpha IIb beta 3 in aqueous solution. *Biochemistry* **40:** 7498-7508

Ussar S., Moser M., Widmaier M., Rognoni E., Harrer C., Genzel-Boroviczeny O., Fassler R. (2008) Loss of Kindlin-1 causes skin atrophy and lethal neonatal intestinal epithelial dysfunction. *PLoS Genet* **4:** e1000289

Uversky V.N., Oldfield C.J., Dunker A.K. (2005) Showing your ID: intrinsic disorder as an ID for recognition, regulation and cell signaling. *J Mol Recognit* **18:** 343-384

Vallar L., Melchior C., Plancon S., Drobecq H., Lippens G., Regnault V., Kieffer N. (1999) Divalent cations differentially regulate integrin alphaIIb cytoplasmic tail binding to beta3 and to calcium- and integrin-binding protein. *J Biol Chem* **274:** 17257-17266

Vinogradova O., Haas T., Plow E.F., Qin J. (2000) A structural basis for integrin activation by the cytoplasmic tail of the alpha IIb-subunit. *Proc Natl Acad Sci U S A* **97:** 1450-1455

Vinogradova O., Vaynberg J., Kong X., Haas T.A., Plow E.F., Qin J. (2004) Membrane-mediated structural transitions at the cytoplasmic face during integrin activation. *Proc Natl Acad Sci U S A* **101:** 4094-4099

Vinogradova O., Velyvis A., Velyviene A., Hu B., Haas T., Plow E., Qin J. (2002) A structural mechanism of integrin alpha(IIb)beta(3) "inside-out" activation as regulated by its cytoplasmic face. *Cell* **110:** 587-597

Ward J.J., Sodhi J.S., McGuffin L.J., Buxton B.F., Jones D.T. (2004) Prediction and functional analysis of native disorder in proteins from the three kingdoms of life. *J Mol Biol* **337:** 635-645

Watanabe N., Bodin L., Pandey M., Krause M., Coughlin S., Boussiotis V.A., Ginsberg M.H., Shattil S.J. (2008) Mechanisms and consequences of agonist-induced talin recruitment to platelet integrin alphaIIbbeta3. *J Cell Biol* **181:** 1211-1222

Wegener K.L., Campbell I.D. (2008) Transmembrane and cytoplasmic domains in integrin activation and protein-protein interactions (review). *Mol Membr Biol* **25:** 376-387

Wegener K.L., Partridge A.W., Han J., Pickford A.R., Liddington R.C., Ginsberg M.H., Campbell I.D. (2007) Structural basis of integrin activation by talin. *Cell* **128:** 171-182

Wehrle-Haller B., Imhof B. (2002) The inner lives of focal adhesions. *Trends Cell Biol* **12:** 382-389

Wei Y., Czekay R.P., Robillard L., Kugler M.C., Zhang F., Kim K.K., Xiong J.P., Humphries M.J., Chapman H.A. (2005) Regulation of alpha5beta1 integrin conformation and function by urokinase receptor binding. *J Cell Biol* **168:** 501-511

Weisel J.W., Nagaswami C., Vilaire G., Bennett J.S. (1992) Examination of the platelet membrane glycoprotein IIb-IIIa complex and its interaction with fibrinogen and other ligands by electron microscopy. *J Biol Chem* **267:** 16637-16643

Weljie A.M., Hwang P.M., Vogel H.J. (2002) Solution structures of the cytoplasmic tail complex from platelet integrin alpha IIb- and beta 3-subunits. *Proc Natl Acad Sci U S A* **99:** 5878-5883

Xiao T., Takagi J., Coller B.S., Wang J.H., Springer T.A. (2004) Structural basis for allostery in integrins and binding to fibrinogen-mimetic therapeutics. *Nature* **432:** 59-67

Xiong J.P., Li R., Essafi M., Stehle T., Arnaout M.A. (2000) An isoleucine-based allosteric switch controls affinity and shape shifting in integrin CD11b A-domain. *J Biol Chem* **275:** 38762-38767

Xiong J.P., Stehle T., Diefenbach B., Zhang R., Dunker R., Scott D.L., Joachimiak A., Goodman S.L., Arnaout M.A. (2001) Crystal structure of the extracellular segment of integrin alpha Vbeta3. *Science* **294:** 339-345

Xiong J.P., Stehle T., Goodman S.L., Arnaout M.A. (2003a) New insights into the structural basis of integrin activation. *Blood* **102:** 1155-1159

Xiong J.P., Stehle T., Zhang R., Joachimiak A., Frech M., Goodman S.L., Arnaout M.A. (2002) Crystal structure of the extracellular segment of integrin alpha Vbeta3 in complex with an Arg-Gly-Asp ligand. *Science* **296:** 151-155

Xiong Y.M., Chen J., Zhang L. (2003b) Modulation of CD11b/CD18 adhesive activity by its extracellular, membrane-proximal regions. *J Immunol* **171:** 1042-1050

Yan B., Calderwood D.A., Yaspan B., Ginsberg M.H. (2001) Calpain cleavage promotes talin binding to the beta 3 integrin cytoplasmic domain. *J Biol Chem* **276:** 28164-28170

Yau W.M., Wimley W.C., Gawrisch K., White S.H. (1998) The preference of tryptophan for membrane interfaces. *Biochemistry* **37:** 14713-14718

Ye F., Liu J., Winkler H., Taylor K.A. (2008) Integrin alpha IIb beta 3 in a membrane environment remains the same height after Mn2+ activation when observed by cryoelectron tomography. *J Mol Biol* **378:** 976-986

Zaidel-Bar R., Itzkovitz S., Ma'ayan A., Iyengar R., Geiger B. (2007) Functional atlas of the integrin adhesome. *Nat Cell Biol* **9:** 858-867

Zhang X., Jiang G., Cai Y., Monkley S.J., Critchley D.R., Sheetz M.P. (2008) Talin depletion reveals independence of initial cell spreading from integrin activation and traction. *Nat Cell Biol* **10:** 1062-1068

Zhu J., Boylan B., Luo B.H., Newman P.J., Springer T.A. (2007a) Tests of the extension and deadbolt models of integrin activation. *J Biol Chem* **282:** 11914-11920

Zhu J., Carman C.V., Kim M., Shimaoka M., Springer T.A., Luo B.H. (2007b) Requirement of alpha and beta subunit transmembrane helix separation for integrin outside-in signaling. *Blood* **110:** 2475-2483

Zhu J., Luo B.H., Barth P., Schonbrun J., Baker D., Springer T.A. (2009) The structure of a receptor with two associating transmembrane domains on the cell surface: integrin alphaIIbbeta3. *Mol Cell* **34:** 234-249

Zhu J., Luo B.H., Xiao T., Zhang C., Nishida N., Springer T.A. (2008) Structure of a complete integrin ectodomain in a physiologic resting state and activation and deactivation by applied forces. *Mol Cell* **32:** 849-861

CHAPTER II: METHODS

2.1 Protein Production

2.1.1 DNA cloning and mutagenesis

Constructs for expressing β integrin tails were generated using the Clontech In-Fusion System (Takara Bio). PCR was performed using primers made up of a 21-nucleotide sequence, identical to the region of the vector immediately flanking the site of the insert, and a sequence identical to the gene being amplified. The vector was then digested at a site within 30 base pairs of the desired insertion site. The PCR product and vector were mixed at an insert:vector molar ratio of 10:1—with a final vector concentration of 100 ng per 10 μL reaction—added to a tube of In-Fusion Dry-Down Reaction Mix (Takara Bio), and incubated at 42°C for 30 minutes. The product was then transformed into *E. coli* Gold competent cells (Stratagene). Clones containing the correct insert were identified by colony PCR and verified by DNA sequencing (Geneservice Oxford Department of Biochemistry DNA Sequencing Facility).

Using the above method, β3 K716-T762, β1A K752-K798, β1D K752-L801, and β7 R747-L798 were cloned into a pET16b vector that had been previously modified with a 3C protease cleavage site inserted between the N-terminal polyhistidine tag and the multiple cloning site. An additional construct of β1D K752-L801 was cloned into pET30b to produce the β1D integrin tail with a C-terminal polyhistidine tag (β1D-His_6). All β integrin constructs contained the DNA sequence from *Homo sapiens* (although the corresponding amino acid sequence was identical to *Mus musculus* for all except β7).

All other DNA constructs used in this study were generated by colleagues at Oxford or collaborators elsewhere, using traditional digest/ligation cloning methods. The talin1 F2 (K196-G309) and talin2 F3 (G311-S408) domains were cloned into pGEX-6P-2

by Neil Bate (David Critchley's group, University of Leicester) using the *Mus musculus* DNA sequence (amino acid sequences identical to those in *Homo sapiens*; see Chapter III for an alignment of talin head domain sequences from different organisms). The talin1 F3 domain (G309-S405) was cloned into pGEX-6P-2 by Kate Wegener using the DNA sequence from *Gallus gallus* (amino acid sequence identical to that from *Mus musculus* and differs from that of *Homo sapiens* by only one residue). The Dok1 PTB domain (Q154–G256) was cloned into pGEX-6P-2 by Camilla Oxley using the DNA sequence from *Homo sapiens*. The talin1 (K196-S405) and talin2 (K198-S408) F2-F3 domains were cloned into pET151 by Neil Bate using the DNA sequence from *Mus musculus* (amino acid sequences identical to those of *Homo sapiens* except for a single amino acid substitution in the talin2 F2 domain and one in the talin1 F3 domain).

Mutations in the β integrin tails and other constructs were introduced using the QuikChange kit (Stratagene). The manufacturer's protocol was used, and mutants were verified by DNA sequencing.

2.1.2 Expression and purification of proteins

DNA plasmids carrying the correct sequence were transformed into *E. coli* CodonPlus cells (Stratagene), using RIPL (DE3) strains for constructs in pET16b, pET30b, or pET151 and RIL (non-DE3) strains for constructs in pGEX-6P-2.

The β integrin tails were expressed (from pET16b or pET30b) into inclusion bodies and purified under denaturing conditions. *E. coli* was grown at 37°C in M9 minimal media (enriched with $^{15}NH_4Cl$ for production of ^{15}N-labelled tails). When cultures reached an optical density of OD_{600} = 0.5, cultures were induced with 1 mM IPTG and allowed to continue growing overnight. Cultures were then centrifuged at 10,000 g for 10 minutes, and the pellet was resuspended in 25 mL (per 1L original culture

volume) of buffer HDA (50 mL sodium phosphate, 8 M urea, 300 mM NaCl, 0.035% β-mercaptoethanol, pH 7.0). After three freeze/thaw cycles in liquid nitrogen, lysates were centrifuged at 35,000 g for 45 minutes. The supernatant was then sonicated and added to 5 mL (per initial 1 L of culture volume) of Talon resin (Takara Bio). The resin was then washed with 100 mL of buffer HDA and then 100 mL of buffer HDB (50 mL sodium phosphate, 8 M urea, 300 mM NaCl, 0.035% β-mercaptoethanol, 5 mM imidazole, pH 7.0). The integrin tail was then eluted in buffer HDC (50 mL sodium phosphate, 8 M urea, 300 mM NaCl, 0.035% β-mercaptoethanol, 200 mM imidazole, pH 7.0). The progress of the purification process was tracked by SDS-PAGE, using NuPAGE 10% acrylamide Bis-Tris gels in MES buffer (Invitrogen). Gels were stained in 0.2% Coomassie brilliant blue R for 15 minutes, destained in 10% acetic acid and 40% methanol and dried in 5% glycerol and 30% ethanol. Fractions containing the integrin tail were then further purified by reverse phase HPLC in a gradient of increasing acetonitrile concentration (in 0.1 % TFA), using a Varian ProStar with a C_4 column (Phenomenex), and then freeze-dried overnight. For constructs produced from pET16b, the freeze-dried material was then resuspended in 3C cleavage buffer (50 mM sodium acetate, 100 mM NaCl, 0.035% β-mercaptoethanol, pH 6.0) and cleaved overnight (without agitation) with 3C protease at 4°C. After cleavage, HPLC was performed to remove the polyhistidine tag and uncleaved fusion protein, and then the integrin tail was freeze-dried again.

All other proteins were produced under native conditions. For expression of proteins from pGEX-6P-2, transformed *E. coli* was first grown at 37°C in lysogeny broth (LB). When cultures reached an optical density of OD_{600} = 0.5, the temperature was lowered to 25°C, and cultures were induced with 0.2 mM IPTG overnight. Cultures were then centrifuged at 10,000 g for 10 minutes, and the pellet was resuspended in 25 mL (per 1L culture volume) of buffer GNA (75 mM Tris, 200 mM NaCl, 0.035% β-

mercaptoethanol, 0.4% Triton-X, 1 Complete Protease Inhibitor tablet (Roche) per 50 mL, pH 7.0). After adding 1 mg/mL hen egg lysozyme, 10 mL $MgCl_2$, and 20 μg/mL DNase I, three freeze/thaw cycles were conducted in liquid nitrogen, and lysates were centrifuged at 35,000 g for 30 minutes. The supernatant was mixed for 1 hour at 4°C with 5 mL (per 1 L of initial culture volume) glutathione sepharose beads (GE Healthcare). The resin was then washed with 100 mL buffer GNC (50 mM Tris, 1 M NaCl, 0.035% β-mercaptoethanol, 1 Complete Protease Inhibitor tablet (Roche) per 500 mL, pH 7.0) and then 200 mL of buffer GN3C (50 mM Tris, 150 mM NaCl, 1 mM EDTA, 1 mM DTT, pH 7.0). The protein of interest was then eluted in buffer GN3C (plus 30 mM reduced glutathione). The GST fusion tag was removed by cleavage with 3C protease (overnight, 4°C). The protein was then further purified and separated from the fusion tag by gel filtration chromatography in pH 7.0 NMR buffer (50 mM sodium phosphate, 100 mM NaCl, 1 mM DTT), using a HiLoad 26/60 Superdex 75 prep grade column (GE Healthcare) on an AKTA FPLC system. Finally, the protein was concentrated with an Amicon Ultra Centrifugal Filter Device (Millipore).

Protein constructs in pET151 were produced similarly to those in pGEX-6P-2, but with a few key differences. When cultures reached an optical density of OD_{600} = 0.5, the temperature was lowered to 18°C, and cultures were induced with 1 mM IPTG overnight. After centrifugation, the pellet was resuspended in 25 mL (per 1L initial culture volume) of buffer HNA (50 mL sodium phosphate, 300 mM NaCl, 0.035% β-mercaptoethanol, 1 Complete Protease Inhibitor tablet (Roche) per 50 mL, pH 7.0). After lysis and further centrifugation, the supernatant was added to 5 mL (per 1 L initial culture volume) Talon resin. The resin was then washed with 100 mL buffer HNA and then 100 mL buffer HNB (50 mL sodium phosphate, 300 mM NaCl, 0.035% β-mercaptoethanol, 5 mM imidazole, pH 7.0). The protein of interest was then eluted in buffer HNC (50 mL sodium phosphate,

300 mM NaCl, 0.035% β-mercaptoethanol, 200 mM imidazole, pH 7.0). The polyhistidine tag was removed by cleavage with TEV protease (overnight, room temperature), and the protein was then further purified by gel filtration chromatography and concentrated.

2.1.3 Tyrosine phosphorylation of integrin tails

The kinase domain of *Gallus gallus* c-Src (Q251-L533) in pET28 was co-expressed with *Yersinia pseudotuberculosis* YopH in pCDFDuet-1 and purified by immobilized metal affinity chromatography as previously reported (Seeliger *et al.*, 2005). Tyrosine phosphorylation was performed overnight at 30°C with 20 μM integrin tail and 0.015 mg/mL Src in 50 mM Tris, 20 mM $MgCl_2$, 10 mM $MnCl_2$, 1 mM ATP, 1 mM DTT, pH 7.0. Phosphorylated tails were separated from unphosphorylated tails by C_4 reverse phase HPLC and were identified by mass spectrometry and NMR. This protocol and the unsuccessful attempts at integrin tyrosine phosphorylation that preceded it are further expounded upon in Chapter V.

2.2 Structural and Biophysical Methods

2.2.1 NMR spectroscopy

All NMR experiments were performed on spectrometers equipped with Oxford Instruments superconducting magnets (500, 600, 750, and 950 MHz ^1H operating frequencies) and GE/Omega computers. Unless otherwise indicated, samples were prepared in NMR buffer (50 mM sodium phosphate, 100 mM NaCl, 1 mM DTT, pH 6.1) with 5% D_2O and Complete protease inhibitors (Roche). Experiments were performed at 25°C. Spectra were referenced in the direct dimension to DSS at 0 ppm, with indirect referencing in the ^{15}N dimension using a $^{15}N/^1H$ frequency ratio of 0.101329118 (Wishart

et al., 1995). Data were processed using NMRPipe (Delaglio *et al.*, 1995) and spectra were visualized using the program SPARKY (www.cgl.ucsf.edu/home/sparky) or CCPN Analysis (Vranken *et al.*, 2005). The ^{1}H and ^{15}N resonances of ^{15}N-labelled β integrin tails were assigned using 3D NOESY-HSQC and 3D TOCSY-HSQC spectra recorded in 20 mM sodium acetate, 5% D_2O, and 0.02% sodium azide. The β1A and β1D tails were assigned using 1 mM samples at pH 5.0, the β3 tail was assigned using a 1 mM sample at pH 4.0, and the β7 was assigned (by Massimiliano Memo, under my guidance) using a 0.2 mM sample at pH 4.5. Resonance assignments were then transferred to pH 6.1 through pH titrations. Resonance assignments for β1D were first performed on β1D-His_6, due to higher expression levels, and assignments were transferred to untagged β1D.

Heteronuclear steady-state $\{^{1}H\}$-^{15}N NOE experiments (Kay *et al.*, 1989) were conducted at a 600 MHz ^{1}H operating frequency on samples containing 0.2-0.25 mM integrin tail. The heteronuclear NOE value was calculated for each peak as I_s/I_0, where I_s is peak intensity with saturation and I_0 is intensity without saturation.

2.2.2 NMR protein-protein interaction studies

^{1}H-^{15}N HSQC titrations were performed with 0.05 mM U-^{15}N-labelled integrin tail and increasing amounts of unlabelled protein, from 0 to 1 mM. Weighted combined ^{1}H and ^{15}N amide shifts (Δ(H,N)) were calculated using the equation:

$$\Delta(H,N) = \sqrt{(\Delta_H W_H)^2 + (\Delta_N W_N)^2},$$

where W_H and W_N are weighting factors for the ^{1}H and ^{15}N amide shifts, respectively ($W_H = 1$, $W_N = 0.154$) (Ayed *et al.*, 2001) and $\Delta = \delta_{bound} - \delta_{free}$. Dissociation constants were determined by fitting changes in backbone chemical shifts upon increasing protein concentration to the following equation:

$$\Delta(H,N) = \Delta(H,N)_{\max} \frac{[L]+[U]+K_d - \sqrt{([L]+[U]+K_d)^2 - 4[L][U]}}{2[L]}$$

where K_d is the dissociation constant, Δ(H,N) is the weighted shift change, $\Delta(H,N)_{max}$ is the shift change at saturation, and [L] and [U] are the concentrations of the labelled and unlabelled proteins, respectively. Data from peaks that were well-resolved, had a significant change in position, and were discernable throughout the titration were fitted simultaneously to this equation with the program OriginPro 8 (OriginLab Corporation), extracting a single K_d and multiple $\Delta(H,N)_{max}$ values. Values for ΔG were calculated from K_d.

Data are presented throughout the paper as the K_d value ± standard error. This error only takes into account the error from the fitting procedure. The other major source of error in these experiments is concentration error, but it is not reported due to difficulty estimating such an error. However, experience indicates that these errors in K_d stemming from talin or Dok1 concentration inaccuracies would at most be about 10% (corresponding to a maximum error in ΔG of 0.25 kJ/mol). For interactions with K_d values less than about 100 μM, this would be compounded by β integrin concentration determination errors, leading to a maximum total K_d error due to concentration errors of about 20% (corresponding to a maximum error in ΔG of 0.5 kJ/mol).

Some K_d values are reported as approximate because binding was too weak for the generation of a binding curve at the concentrations available. In these cases, the value of $\Delta(H,N)_{max}$ was estimated by comparing maximum Δ(H,N) values for peaks unaffected by the given mutation to Δ(H,N) of peaks in the corresponding wt titration. The fitting procedure was then carried out as before, but with the value of $\Delta(H,N)_{max}$ restrained. No errors are reported for these values, as they are only estimates.

All K_d values were determined by tracing HSQC peak positions through titration points. However, the interaction of talin2 with β1D (D776/T777Q778)V exhibited slow

exchange kinetics (see Chapter IV). For this titration, peak intensities were measured instead of peak positions (although the interaction was still too tight for the K_d value to be reliably determined by this method; it was instead determined by ITC). For each concentration of talin, an HSQC spectrum was acquired, and the intensity of each peak was recorded. Only peaks that began with an appreciable signal/noise ratio, were not overlapped, and corresponded to residues within the binding site were used to plot the normalized average signal/noise ratio ± standard error.

2.2.3 X-ray crystallography

Samples for crystallization contained 6 mg/mL (250 μM) talin2 F2-F3 and 3 mg/mL (500 μM) β1D integrin tail in crystallization buffer (10 mM tris, 100 mM NaCl, pH 7.0). Crystals were grown by the sitting drop method at 4°C in 0.1 M ammonium acetate, 0.02 M magnesium chloride, 0.05 M HEPES (pH 7.0), and 5% PEG 8k. For data collection, crystals were soaked in the same buffer plus 30% glycerol and then flash-frozen in liquid nitrogen.

Data were collected at the ESRF on beamline ID23.EH2 at a wavelength of 0.8726 Å. The crystal diffracted to 2.17 Å resolution. Data were indexed and integrated using MOSFLM, and scaled and merged using SCALA from the CCP4 program suite (CCP4, 1994). The structure was phased by molecular replacement using the talin1 F2-F3 domains from PDB entries 1MIX, 1MK7, and 1MK9 (Garcia-Alvarez *et al.*, 2003) as search models and using the program Phaser (Read, 2001). The crystal indexed to the space group $P2_12_12_1$ and contained 2 molecules in the asymmetric unit. Model building was performed in Coot (Emsley & Cowtan, 2004), and refinement in Refmac (Winn *et al.*, 2003) and PHENIX Refine (Adams *et al.*, 2002). The integrin tail was not included in the original molecular replacement model, but it could be built into electron density early

in the refinement process. The structure refined to R_{work} = 21.30% and R_{free} = 24.85%. In a Ramachandran plot, 91.2% of residues lie in favoured regions, 8.6% in allowed regions, 0.2% in generously allowed regions, and 0.0% in disallowed regions.

2.2.4 Isothermal titration calorimetry

ITC was performed on a MicroCal iTC_{200} calorimeter with integrin β tail peptide in the instrument cell (200 μL) and talin in the injection syringe (40 μL). Experiments were carried out at 25°C in pH 6.1 NMR buffer. For the titration of β1D wt with talin2 F3, the cell contained 149 μM integrin, the syringe contained 1.873 μM talin, and 16 2.5-μL injections were performed (5 seconds each, separated by 180-second intervals). For the titration of β1D (D776/T777/Q778)V with talin2 F3, the cell contained 5 μM integrin, the syringe contained 50 μM talin, and 20 2-μL injections were performed (4 seconds each, separated by 180-second intervals). Experimental data were analyzed using MicroCal Origin software. K_d values ± standard error were calculated from affinity constants.

2.2.5 Accession codes

Atomic coordinates of the talin2/β1D complex have been deposited in the Protein Data Bank under the accession number 3G9W. Chemical shift resonance assignments have been deposited in the Biological Magnetic Resonance Bank (BMRB) under the following accession numbers: 16159 (β1A), 16158 (β1D), 16162 (β1D-His_6), 15552 (β3), and 16259 (β7).

2.3 Studies Performed by Collaborators

2.3.1 Phospholipid cosedimentation assays

These studies were performed by Ben Goult (David Critchley's group, University of Leicester), who contributed to writing this subsection. Large multilamellar vesicles were prepared essentially as described previously (Niggli *et al.*, 1994). Briefly, films of dried phospholipids (Sigma) were swollen at 5 mg/ml in 20 mM Hepes (pH 7.4), 0.2 mM EGTA for 3 hours at 42°C. The vesicles were then centrifuged (20,000 g for 20 minutes at 4°C), and the pellet was resuspended in the same buffer at 5 mg/ml. Protein samples were diluted into 20 mM Tris/HCl (pH 7.4), 0.1 mM EDTA, 15 mM β-mercaptoethanol. After centrifugation (20,000 g for 20 minutes at 4°C) proteins (0.15 mg/ml) were incubated (30 minutes, 25°C) in the absence or presence of phospholipid vesicles (0.5 mg/ml), 200 µL total volume, followed by centrifugation (25,000 g for 20 minutes at 4°C). Pellet and supernatant fractions were subjected to SDS-PAGE. The percentage of protein bound (protein in pellet / total protein) was calculated by measuring band density in ImageJ (Abramoff *et al.*, 1994).

2.3.2 Integrin activation assays

These studies were performed by Feng Ye and Chungho Kim (Mark Ginsberg's group, University of California San Diego), who each contributed to writing this subsection. PAC1 binding was measured by two-colour flow cytometry as described previously (Han *et al.*, 2006). In brief, A5 cells (CHO cells expressing integrin αIIbβ3) were transfected with N-terminal GFP-fused talin1 F3 or F1-F2-F3 constructs, or co-transfected with GFP and Talin F0-F1-F2-F3 constructs. Experiments were similarly performed on CHO cells expressing a chimeric integrin consisting of the extracellular and TM domains of αIIbβ3 and the intracellular domains of α5β1A, which has been described previously (O'Toole *et*

al., 1994). Twenty-four hours after talin transfection, cells were harvested, incubated with activation-specific anti-αIIbβ3 antibody PAC1 (Shattil *et al.*, 1985), and then stained by R-phycoerythrin-conjugated anti-IgM antibody. Five minutes prior to analysis, propidium iodide (PI) was added, and PAC1 binding was measured with FACSCalibur (BD Bioscience). Only GFP-positive and PI-negative cells (live cells) were analyzed to calculate the level of integrin activation. The ability of talin constructs containing various mutations to activate integrins is presented as percent of maximal integrin activation, and was calculated as (Fo - Fr) / (Fmax - Fr), where Fo is the mean fluorescence intensity (MFI) of PAC1 binding of various mutant transfected cell, Fr is the MFI of PAC1 binding in the presence of competitive inhibitor eptifibatide (Scarborough *et al.*, 1993), and Fmax is the MFI of PAC1 binding of wt F1-F2-F3 or F0-F1-F2-F3 transfected cells.

2.3.3 Immunofluorescence imaging

These studies were performed by Jacob Haling (Mark Ginsberg's group, University of California San Diego), who contributed to writing this subsection. SYF cells (mouse embryonic fibroblasts (MEFs) deficient in c-Src, c-Fyn, and c-Yes) and SYF + Src cells (SYF MEFs reconstituted with c-Src) (Klinghoffer *et al.*, 1999) were obtained from the American Type Culture Collection. Cells were maintained in Dulbecco's modified Eagle's medium supplemented with 10% foetal bovine serum, L-glutamine, and antibiotics at 37°C with 6% CO_2. Transient transfections were carried out with Lipofectamine Plus (Invitrogen) as described by the manufacturer. For experiments in mammalian cells, the cDNA encoding full-length mouse talin1 was amplified by PCR and subcloned into pEGFP-C1. Mutations in pEGFP-C1 were introduced with the QuikChange II XL kit (Stratagene). Anti-green fluorescent protein (GFP) rabbit polyclonal antibody was obtained from Clontech. Anti-vinculin mouse monoclonal

antibody was purchased from Sigma. Anti-phospho-tyrosine (pY100) mouse monoclonal antibody was purchased from Cell Signaling Technology. Anti-paxillin rabbit polyclonal antibody (RB4536) was developed in house.

After transfection, MEF cells were plated on 7.5 μg/ml fibronectin-coated coverslips, allowed to adhere for 90 minutes in Dulbecco's modified Eagle's medium, rinsed once in phosphate-buffered saline (PBS), and fixed with 3.7% formaldehyde in PBS. After fixation, cells were permeabilized in 0.1% Triton X-100 for 5 minutes, blocked with 3% BSA, 2% normal goat serum for 1 hour, and then incubated with the appropriate primary antibody in blocking solution overnight at 4°C. Bound antibodies were detected by the corresponding fluorescein isothiocyanate-conjugated goat secondary antibodies (Santa Cruz Biotechnology). Coverslips were subsequently mounted in Prolong Gold antifade reagent (Invitrogen) on slides. Epifluorescent images of cells were acquired with a 60x oil immersion objective on a Nikon Eclipse TE2000-U microscope equipped with the appropriate excitation and emission filter sets (Semrock). Additional post-acquisition processing of images was performed using ImageJ (rsb.info.nih.gov/ij) and Adobe Photoshop.

2.4 References

Abramoff M.D., Magelhaes P.J., Ram S.J. (1994) Image Processing with ImageJ. *Biophoton Int* **11:** 36-42

Adams P.D., Grosse-Kunstleve R.W., Hung L.W., Ioerger T.R., McCoy A.J., Moriarty N.W., Read R.J., Sacchettini J.C., Sauter N.K., Terwilliger T.C. (2002) PHENIX: building new software for automated crystallographic structure determination. *Acta Crystallogr D Biol Crystallogr* **58:** 1948-1954

Ayed A., Mulder F.A., Yi G.S., Lu Y., Kay L.E., Arrowsmith C.H. (2001) Latent and active p53 are identical in conformation. *Nat Struct Biol* **8:** 756-760

CCP4 (1994) The CCP4 suite: programs for protein crystallography. *Acta Crystallogr D Biol Crystallogr* **50:** 760-763

Delaglio F., Grzesiek S., Vuister G.W., Zhu G., Pfeifer J., Bax A. (1995) NMRPipe: a multidimensional spectral processing system based on UNIX pipes. *J Biomol NMR* **6:** 277-293

Emsley P., Cowtan K. (2004) Coot: model-building tools for molecular graphics. *Acta Crystallogr D Biol Crystallogr* **60:** 2126-2132

Garcia-Alvarez B., de Pereda J.M., Calderwood D.A., Ulmer T.S., Critchley D., Campbell I.D., Ginsberg M.H., Liddington R.C. (2003) Structural determinants of integrin recognition by talin. *Mol Cell* **11:** 49-58

Han J., Lim C.J., Watanabe N., Soriani A., Ratnikov B., Calderwood D.A., Puzon-McLaughlin W., Lafuente E.M., Boussiotis V.A., Shattil S.J., Ginsberg M.H. (2006) Reconstructing and deconstructing agonist-induced activation of integrin alphaIIbbeta3. *Curr Biol* **16:** 1796-1806

Kay L.E., Torchia D.A., Bax A. (1989) Backbone dynamics of proteins as studied by 15N inverse detected heteronuclear NMR spectroscopy: application to staphylococcal nuclease. *Biochemistry* **28:** 8972-8979

Klinghoffer R.A., Sachsenmaier C., Cooper J.A., Soriano P. (1999) Src family kinases are required for integrin but not PDGFR signal transduction. *EMBO J* **18:** 2459-2471

Niggli V., Kaufmann S., Goldmann W.H., Weber T., Isenberg G. (1994) Identification of functional domains in the cytoskeletal protein talin. *Eur J Biochem* **224:** 951-957

O'Toole T.E., Katagiri Y., Faull R.J., Peter K., Tamura R., Quaranta V., Loftus J.C., Shattil S.J., Ginsberg M.H. (1994) Integrin cytoplasmic domains mediate inside-out signal transduction. *J Cell Biol* **124:** 1047-1059

Read R.J. (2001) Pushing the boundaries of molecular replacement with maximum likelihood. *Acta Crystallogr D Biol Crystallogr* **57:** 1373-1382

Scarborough R.M., Naughton M.A., Teng W., Rose J.W., Phillips D.R., Nannizzi L., Arfsten A., Campbell A.M., Charo I.F. (1993) Design of potent and specific integrin antagonists. Peptide antagonists with high specificity for glycoprotein IIb-IIIa. *J Biol Chem* **268:** 1066-1073

Seeliger M.A., Young M., Henderson M.N., Pellicena P., King D.S., Falick A.M., Kuriyan J. (2005) High yield bacterial expression of active c-Abl and c-Src tyrosine kinases. *Protein Sci* **14:** 3135-3139

Shattil S.J., Hoxie J.A., Cunningham M., Brass L.F. (1985) Changes in the platelet membrane glycoprotein IIb.IIIa complex during platelet activation. *J Biol Chem* **260:** 11107-11114

Vranken W.F., Boucher W., Stevens T.J., Fogh R.H., Pajon A., Llinas M., Ulrich E.L., Markley J.L., Ionides J., Laue E.D. (2005) The CCPN data model for NMR spectroscopy: development of a software pipeline. *Proteins* **59:** 687-696

Winn M.D., Murshudov G.N., Papiz M.Z. (2003) Macromolecular TLS refinement in REFMAC at moderate resolutions. *Methods Enzymol* **374:** 300-321

Wishart D.S., Bigam C.G., Yao J., Abildgaard F., Dyson H.J., Oldfield E., Markley J.L., Sykes B.D. (1995) 1H, 13C and 15N chemical shift referencing in biomolecular NMR. *J Biomol NMR* **6:** 135-140

CHAPTER III: THE MECHANISM OF INTEGRIN ACTIVATION BY TALIN

3.1 Introduction

Integrins can be activated from within the cell by a direct interaction with the cytoskeletal protein talin (Tadokoro *et al.*, 2003), causing the integrin to adopt a conformation with higher affinity for extracellular matrix proteins (Luo *et al.*, 2007). However, structural studies of integrin activation have been hampered by the weak nature of the talin/integrin interaction and unfavourable solution characteristics. Various strategies have been employed to overcome this problem, beginning with a crystal structure of a short membrane-distal (MD) fragment of the β3 tail covalently tethered to the talin1 F2-F3 fragment (Garcia-Alvarez *et al.*, 2003). This showed that the F3 domain interacts with the NPxY motif of the β3 tail in canonical PTB domain fashion (Calderwood *et al.*, 2003). However, despite illuminating this MD binding interface, this study gave no information about the membrane-proximal (MP) region of the β3 tail, a region known to be essential for activation (Hughes *et al.*, 1995; Ulmer *et al.*, 2003; Vinogradova *et al.*, 2002).

Instead, our most detailed structural information about talin-induced integrin activation to date has come from a more recent NMR structure that elucidated the interface between the talin1 F3 domain and the β3 MP helix (Wegener *et al.*, 2007). This structure was made possible by constructing a chimeric peptide that included the β3 helix attached to a sequence from PIPK1γ that binds tightly to the talin NPxY binding pocket (Barsukov *et al.*, 2003; de Pereda *et al.*, 2005). This structure revealed that the MP helix of the β3 tail forms an extensive binding surface with the S1, S2, S6, and S7 strands of the talin1 F3 domain. Of particular significance are two β3 phenylalanine residues (F727 and F730) that fit into a hydrophobic pocket formed in part by the talin S1-S2 loop—which is flexible in the unbound state, but becomes ordered upon binding. This flexible

loop is unique to talin (compared to other PTB domains), and Wegener *et al*. demonstrated that these interactions are required for integrin activation by talin. Although it was apparent from this structure that talin may cause activation by sterically disrupting the interaction between the α and β tails that helps maintain the integrin inactive state, the scope of this study was limited in part because the N-terminus of the β3 tail remained unstructured in solution. Thus, neither the structural details of the most MP part of the interface nor the precise orientation of the overall talin/integrin complex with respect to the membrane could be defined. Although the Wegener *et al*. study provided exceptional insight into the process of integrin activation by talin, it left many questions unanswered.

Additional insight has come from structural studies on the transmembrane (TM) segments of αIIb (Lau *et al.*, 2008a), β3 (Lau *et al.*, 2008b), and the αIIbβ3 complex (Lau *et al.*, 2009). These structures—which were solved by NMR in lipid bicelles—are discussed in some detail in Chapter I, and the structure of the αIIbβ3 complex is discussed below in Section 3.3. Of particular significance here, though, is the structure of the β3 TM domain, which Lau *et al*. found to form a relatively long 29-residue helix. Although they could not precisely determine the angle of the helix within the membrane, they estimated it to be tilted by about 20-30° from a vertical orientation (Lau *et al.*, 2008b). The β3 helix extends to H722 and is buried in the membrane through I721, indicating that the N-terminal residues that were unstructured in the Wegener *et al*. structure remain helical in a more physiological environment. The more recent structure of the αIIbβ3 TM complex also reveals a similar β3 structure and orientation (Lau *et al.*, 2009), and the availability of these structures significantly enhances the conclusions we can draw from our current studies.

Prior structural studies of integrin activation by talin have involved a single integrin and talin isoform. However, mammals express two isoforms of talin (Fig. 3.1B)

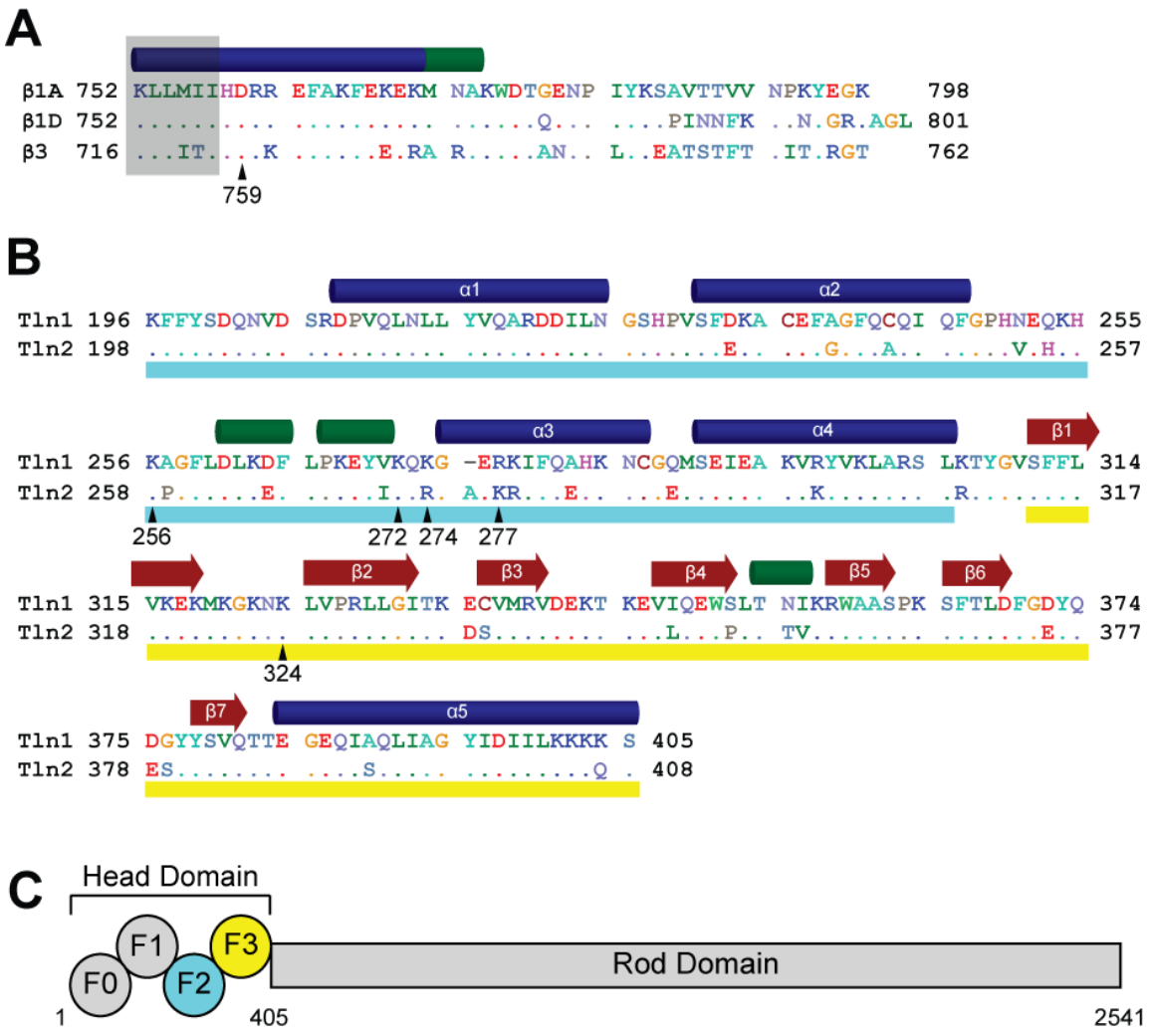

Figure 3.1 Integrin and talin sequence comparisons. (A) Sequence of the cytoplasmic tails of the β1A, β1D, and β3 integrins. Residues in β1D and β3 that differ from β1A are highlighted, and a key membrane-proximal aspartate residue is indicated with β1 numbering. Secondary structure (α helices in blue, 3_{10} helices in green) is based on the β1D/talin2 complex structure. Residues embedded in the membrane (Lau *et al.*, 2008b) are shaded in grey. (B) Sequence of the F2-F3 domains of talin1 and talin2. Residues in talin2 that differ from talin1 are highlighted, and secondary structure was determined as in (A). The F2 domain is underlined in cyan and the F3 in yellow. (C) A schematic of the domain structure of talin. Talin homodimerization (not shown) occurs at the C-terminus.

and eight different β integrins, some of which exhibit additional splice variants (Fig. 3.1A). In this chapter, we explore a wider range of talin/integrin interactions in order to identify a pair more suitable for structure determination. The resulting crystal structure, along with a multi-technique experimental approach, reveals a concerted series of evolutionarily-conserved interactions that initiate inside-out signalling.

3.2 Results

3.2.1 The structure of the talin2/β1D complex

In Chapter II we present an NMR-based system for studying protein-protein interactions involving the cytoplasmic tails or β integrins. Using ^{15}N-labelled integrin tails produced in *E. coli*, we have explored the interactions of the β1A, β1D, and β3 tails with the talin1 and talin2 F3 domains by chemical shift perturbation mapping. HSQC spectra of labelled tails were acquired with increasing concentrations of unlabelled talin F3 domain, and the change in position of each peak (i.e. perturbation in chemical shift) was measured (Fig. 3.2). These measurements can be used to construct a chemical shift map for each interaction in order to identify and study binding sites; such an approach is carried out in detail in Chapter IV. The change in peak position versus talin concentration can also be fit to a function to determine the affinity (i.e. K_d) of the interaction, as described in Chapter II (Fig. 3.2C, Table 3.1).

Through these NMR studies of β tail/talin complexes, we have found that integrin β tails differ widely in their affinity for different isoforms of talin, and that β1D binds to talin2 with a much higher affinity than any integrin/talin pair we have previously studied (Table 3.1, Fig. 3.2C). This higher affinity interaction also exhibits slower kinetics; whereas the talin1/β3 interaction is primarily in the fast chemical exchange regime (Fig. 3.2A), the talin2/β1D interaction is largely in the intermediate exchange regime,

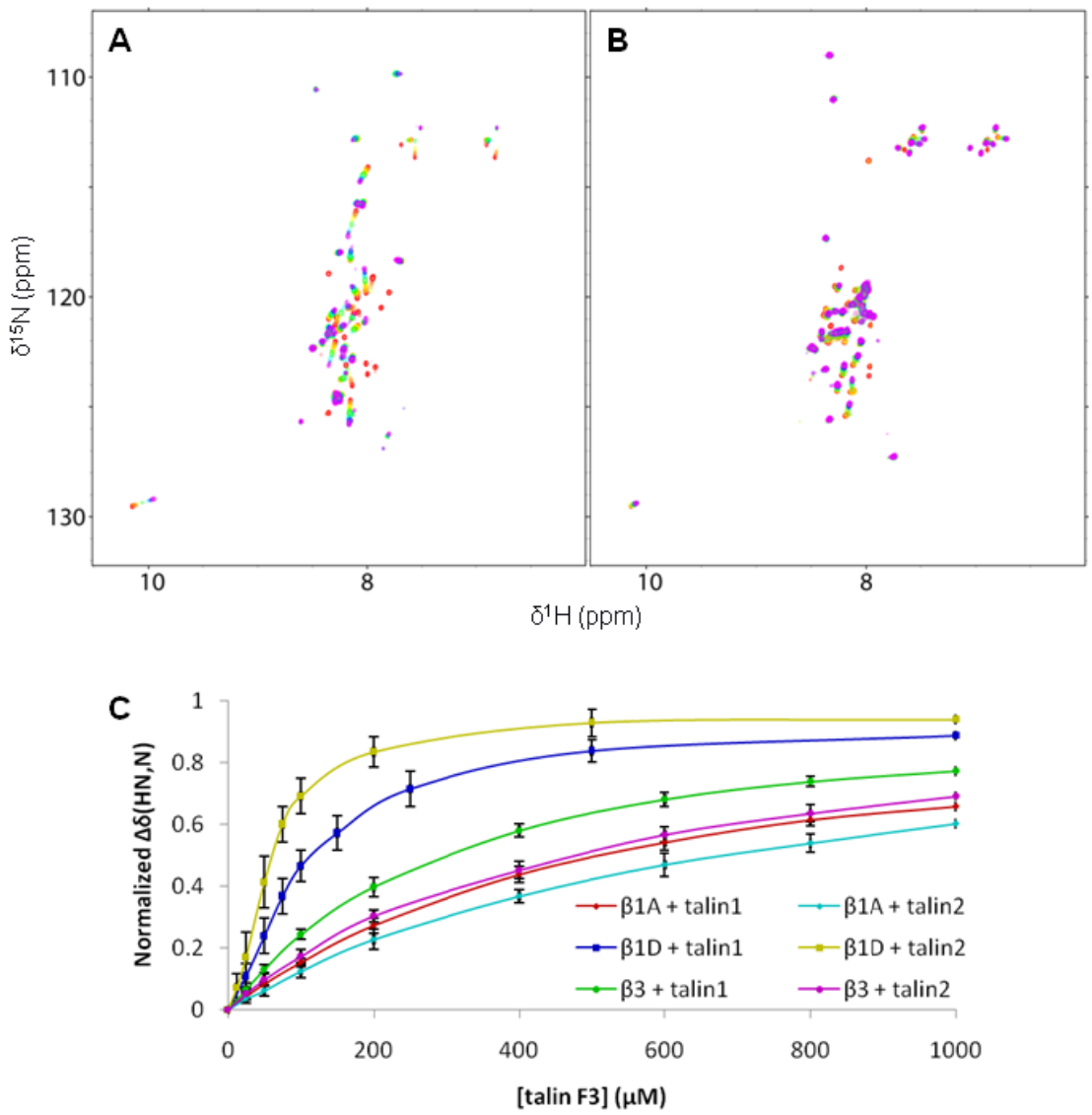

Figure 3.2 Chemical shift perturbation experiments with integrin tails. (A) ^{1}H-^{15}N HSQC spectra of 0.05 mM ^{15}N-labelled β3 tail with increasing concentrations of talin1 F3 domain: 0 mM (red), 0.025 mM (tomato), 0.05 mM (orange), 0.1 mM (yellow), 0.2 mM (green), 0.4 mM (cyan), 0.6 mM (blue), 0.8 mM (purple), 1 mM (magenta). (B) ^{1}H-^{15}N HSQC spectra of 0.05 mM ^{15}N-labelled β1D tail with increasing concentrations of talin2 F3 domain: 0 mM (red), 0.0125 mM (tomato), 0.025 mM (orange), 0.05 mM (yellow), 0.075 mM (green), 0.1 mM (cyan), 0.2 mM (blue), 0.5 mM (purple), 1 mM (magenta). Several of the peaks broaden out due to intermediate exchange, but many of these can still be traced when the contour levels are taken lower. (C) Binding curves used for K_d calculation. Peaks were tracked through HSQC spectra of ^{15}N-labelled β tail acquired with increasing concentrations of talin F3 domain. For each trackable peak, the change in chemical shift was normalized to the change at 1 mM talin. Note that while K_d values were determined by fitting several curves simultaneously, for clarity each value plotted here shows the average of several peaks ± standard error.

characterised by extensive broadening and disappearance of β1D peaks at intermediate talin concentrations (Fig. 3.2B). Talin2 and β1D, a splice variant of β1 differing from β1A only in its C-terminus (Fig. 3.1A), are the major isoforms found in striated muscle (Belkin *et al.*, 1996; Conti *et al.*, 2008; Senetar *et al.*, 2007), and the formation of this higher affinity complex is consistent with the high forces that this talin/integrin complex is subjected to in myotendinous junctions (Belkin *et al.*, 1996; Conti *et al.*, 2008).

In addition to being biologically relevant, this high affinity complex presented a promising structural target. Solving the structure of the complex by NMR would have been a daunting prospect because the talin2/β1D interaction exists largely in the intermediate exchange regime (Fig. 3.2B), so protein crystallography was attempted. Initial trials were conducted with a solution of the talin2 F3 domain and the β1D integrin tail. Although these yielded some initial crystals in conditions containing PEG 2k MME or PEG 5k MME (Fig. 3.3A), they gave a poor X-ray diffraction pattern (Fig. 3.3E). Additional trials were then conducted with a longer talin2 fragment containing the F2-F3 domain pair. This construct, in combination with the β1D tail, gave needle-like crystals in a wide variety of conditions. Further optimization yielded three-dimensional crystals in conditions containing PEG 8k and Mg^{2+} (Fig. 3.3B-D). These diffracted to a higher resolution and gave a much more optimal diffraction pattern (Fig. 3.3F).

Thus, we were able to solve the structure of the β1D integrin tail/talin2 F2-F3 complex at 2.2 Å resolution (Fig. 3.4A, Table 3.2). This is the first structure of talin bound to an authentic β integrin tail and the first involving either of these two striated muscle-specific isoforms. Each asymmetric unit in the crystal contained two integrin/talin heterodimers (Fig. 3.5A) with distinct electron density visible for the N-terminal 37 residues of the integrin tail (Fig. 3.6). The last 13 residues were not observed, suggesting that they remain unstructured. The talin2 F2-F3 domains exhibit similar folds and relative

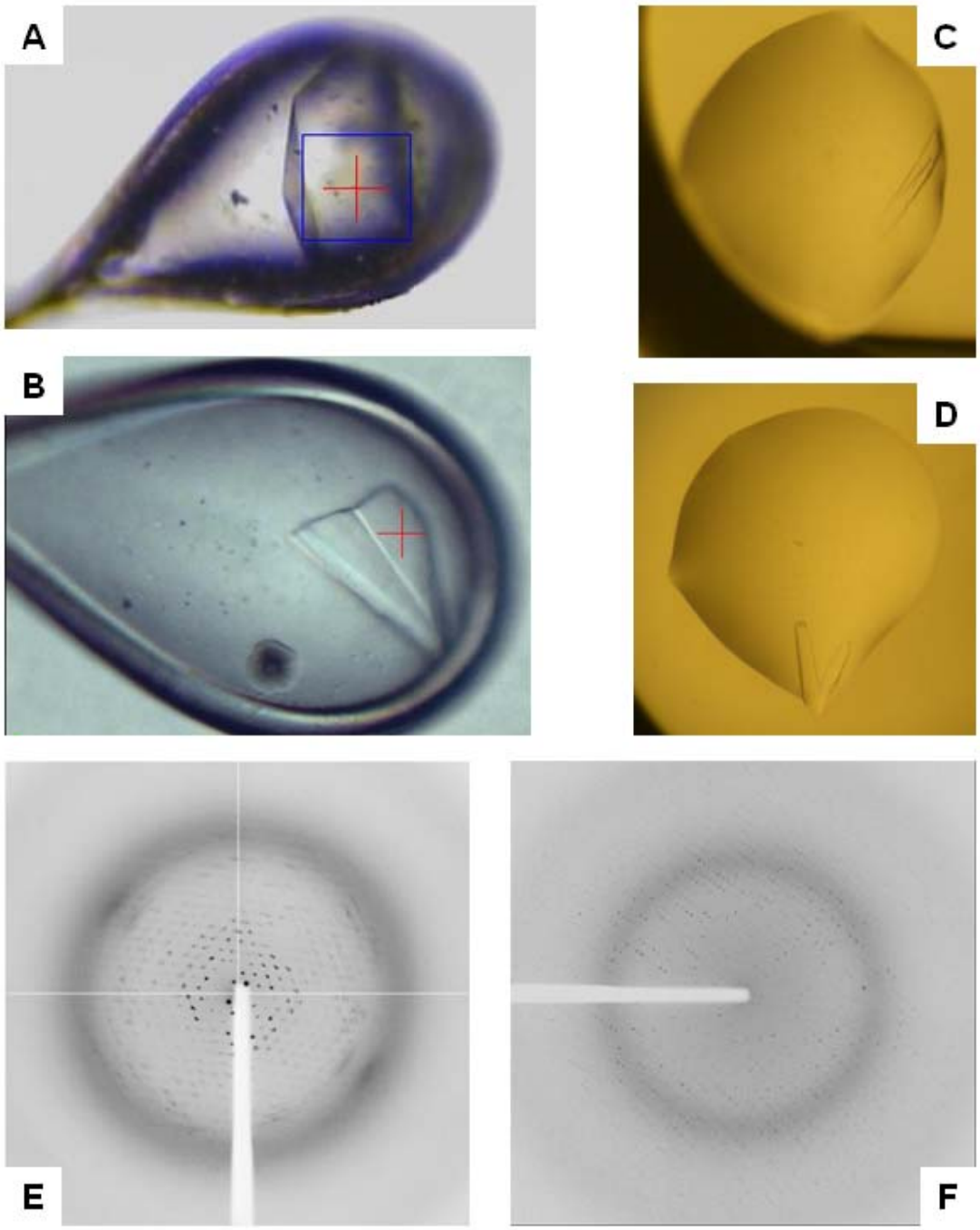

Figure 3.3 X-ray crystallography of the talin2/β1D complex. (A) Crystal of the talin2 F3 domain with the β1D tail in 100 mM sodium acetate (pH 4.5) and 24% PEG 5k MME. This crystal gave the diffraction pattern seen in panel E. (B) Crystal of the talin2 F2-F3 domain pair with the β1D tail in 50 mM HEPES (pH 7.0), 100 mM ammonium acetate, 20 mM magnesium chloride, and 5% PEG 8k. This crystal gave the diffraction pattern seen in panel F. (C & D) Additional talin2 F2-F3/β1D tail crystals in similar conditions to panel B. (E) X-ray diffraction pattern of the crystal shown in panel A (talin2 F3/β1D tail). Note that the crystal only diffracts to a relatively low resolution and gives a pattern of diffuse, indistinct, and irregular spots. (F) X-ray diffraction pattern of the crystal shown in panel B (talin2 F2-F3/β1D tail). This diffraction pattern was of high enough resolution and sufficient quality to solve the structure of the complex.

Table 3.1 K_d values of talin F3/β integrin tail interactions

K_d (μM)	talin1	talin2
β1A	490 ± 10	652 ± 20
β1D	95 ± 4	36 ± 2
β3	273 ± 6	438 ± 15

K_d values are given in μM ± standard error.

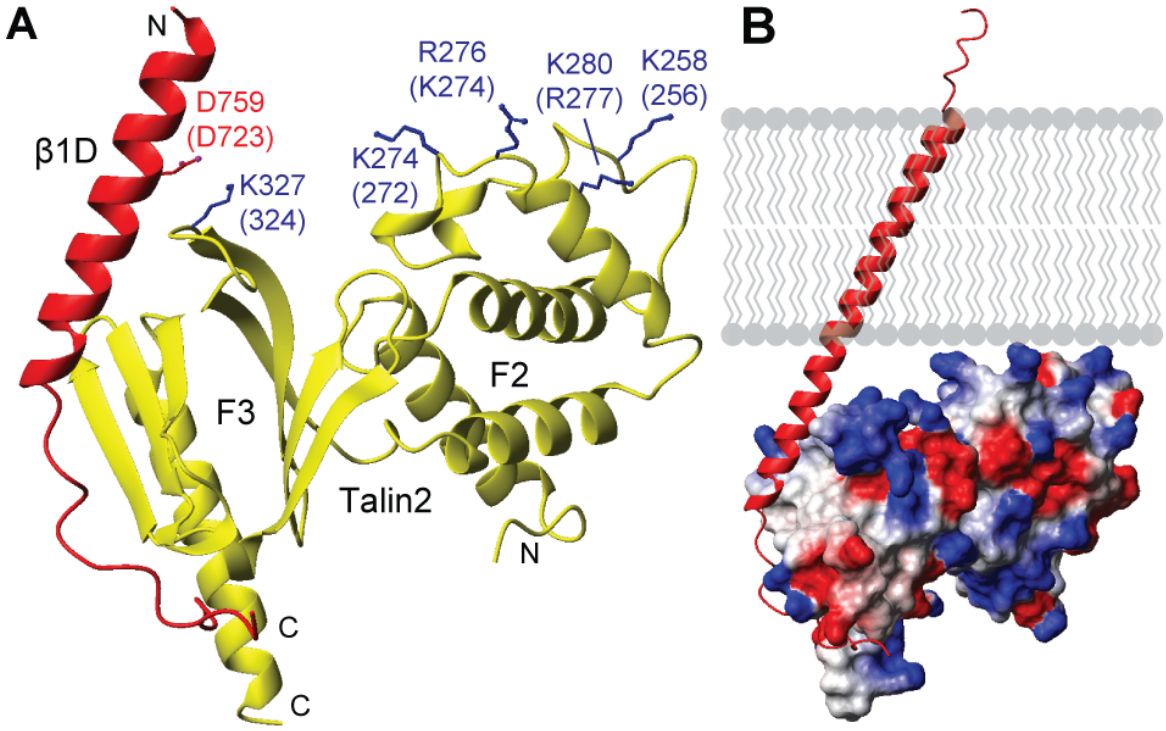

Figure 3.4 The talin2/β1D structure. (A) One heterodimer from the crystal structure of talin2 F2-F3 bound to the β1D integrin tail. Labelling is for talin2/β1D with talin1/β3 numbering in parentheses. Highlighted residues interact with the membrane or form a key integrin/talin salt bridge. All structure images were generated with MOLMOL (Koradi *et al.*, 1996). (B) The talin2/β1D structure was merged with the β3 transmembrane segment (PDB 2RMZ) (Lau *et al.*, 2008b) and aligned to the calculated membrane tilt angle of 25°. The electrostatic potential is mapped on talin (positive charges in blue, negative in red), illustrating the juxtaposition of several positively-charged residues next to the membrane surface.

Table 3.2 Data collection and refinement statistics

Data collection	
Beam line	ESRF ID23.EH2
Space group	$P2_12_12_1$
Cell parameters	a = 53.26 Å, b = 108.72 Å, c = 131.85 Å
	$\alpha = \beta = \gamma = 90°$
Wavelength (Å)	0.8726
Resolution (Å)	41.95 – 2.17 (2.28 – 2.17)*
Total reflections	154133 (21979)
Unique reflections	41362 (5982)
R_{Merge}	0.114 (0.338)
Completeness (%)	99.6 (99.9)
Multiplicity	3.7 (3.7)
I/σ(I)	8.3 (3.5)
Refinement	
R_{work}	0.2130
R_{free}	0.2485
Overall mean *B* values (Å^2)	32.26
No. of amino acid residues per asymmetric unit	500
No. of water molecules	382
Matthews coefficient	3.05 (water content, 59.72%)
RMSD from ideal values	
Bonds / angles (Å/°)	0.005 / 0.874
Estimated error based on maximum likelihood	
Coordinate / phase (Å/°)	0.32 / 25.114

The structure was solved from one crystal
*Highest resolution shell is shown in parenthesis.

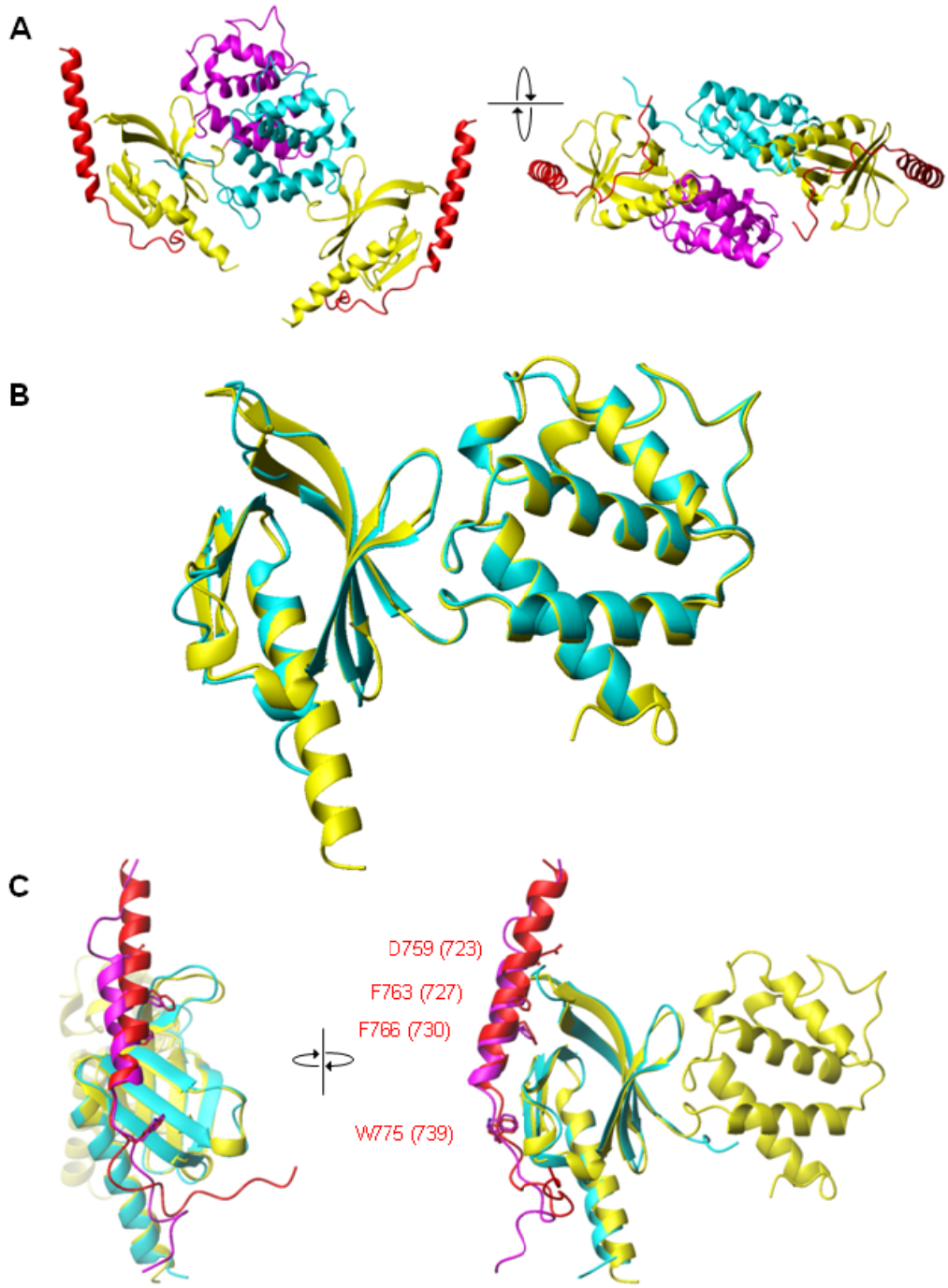

Figure 3.5 Comparisons of the talin2 and talin1 structures. (A) Asymmetric unit of the crystal structure of talin2 F2-F3 bound to the β1D integrin tail, shown in two orthogonal orientations. The integrin tail is shown in red, the talin2 F3 domain in yellow, and the talin2 F2 domain in cyan or magenta. (B) Structure of talin2 F2-F3 (yellow) aligned with the F2-F3 domains of talin1 from PDB 1MK9 (cyan) (Garcia-Alvarez *et al.*, 2003). (C) Structure of β1D (red) bound to talin2 F2-F3 (yellow) aligned to the structure of the β3/PIPK1γ peptide (magenta) bound to talin1 F3 (cyan) from PDB 2H7E (Wegener *et al.*, 2007). The alignment used the backbone of the talin1 F3 domain. It is shown in two orthogonal views, and key residues are highlighted.

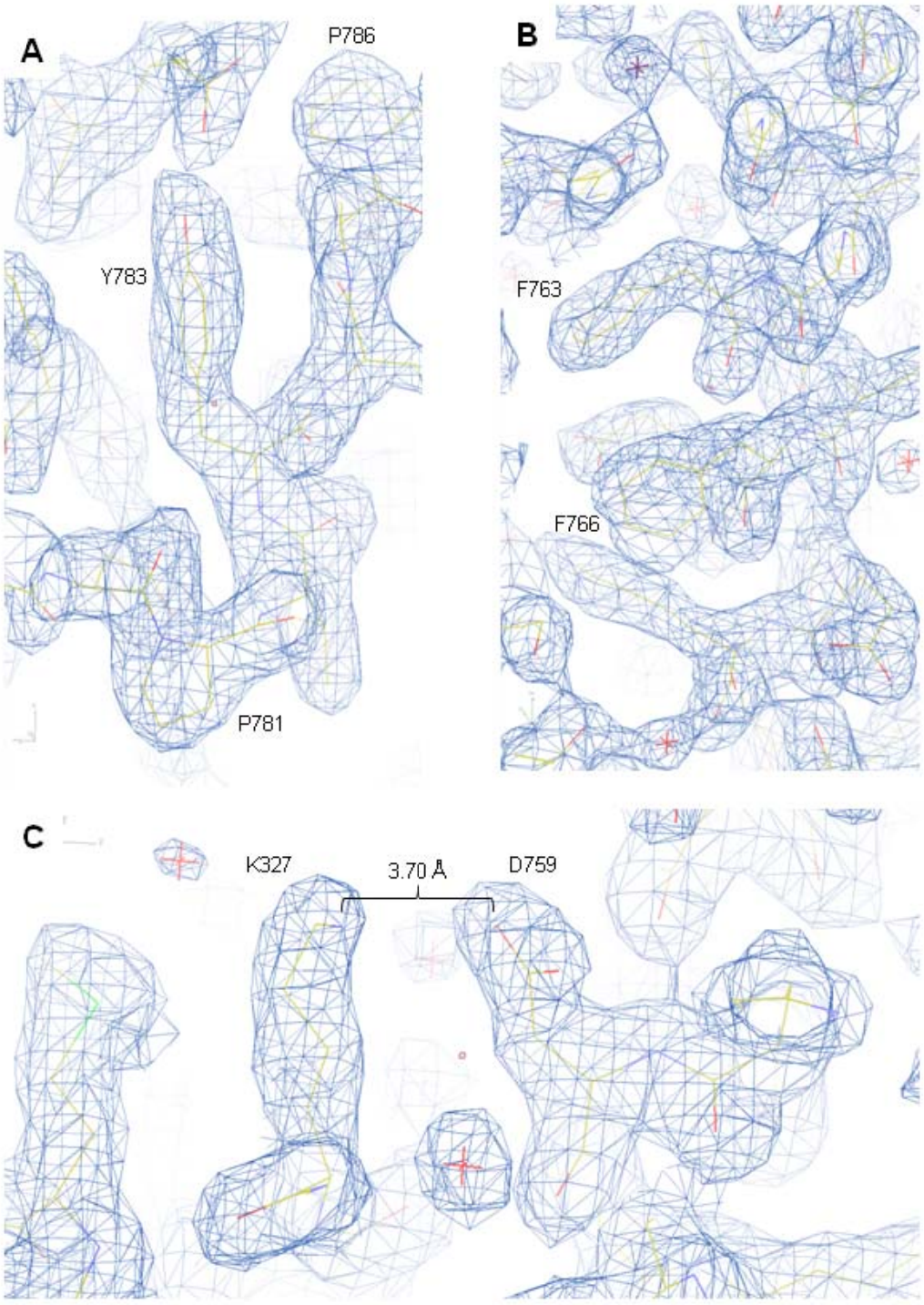

Figure 3.6 Electron density maps from the β1D/talin2 crystal structure. (A) The NPxY motif of β1D, showing distinct electron density (sigma 1.2). (B) A portion of the β1D membrane-proximal helix, showing distinct electron density (sigma 1.2). (C) The membrane-proximal salt bridge, showing distinct electron density (sigma 1.2). The side chain nitrogen of talin2 K327 and the side chain oxygen of β1D D759 are separated by 3.70 Å. Electron density map images were generated in Coot (Emsley & Cowtan, 2004).

orientations to those seen in previous talin1 F2-F3 structures (Fig. 3.5B, Table 3.3), and the interface of the MP integrin helix with the talin F3 activation loop is similar to that observed for the β3/PIPK1γ chimera (Fig. 3.5C). However, this new structure allows detailed comparisons of the complexes formed between different talin and integrin isoforms (see Chapter IV) and also reveals several novel features that permit the formulation of a new comprehensive structural model of integrin activation.

3.2.2 A positively-charged patch on talin binds to the cell membrane

The talin2/β1D structure exhibits a well-defined N-terminal β tail helix extending from K752 to A773 (corresponding to K716-A737 in β3). This helix overlaps with the recent NMR structure of the β3 TM domain, which exhibits a membrane-embedded helix extending to I721 and tilted by about 20-30° to the membrane bilayer (Lau *et al.*, 2008b). Thus, β1D residues K752-I757 can be overlaid and merged with the membrane-embedded residues K716-I721 of the β3 TM structure; such a procedure could not be performed using the β3/PIPK1γ model because the integrin N-terminus did not exhibit a defined structure in solution. The predicted orientation of the talin2/β1D structure with respect to the membrane (Fig. 3.4B) results in the striking juxtaposition of a positively-charged patch in the F2 domain (residues K258, K274, R276, and K280 in talin2; K256, K272, K274, and R277 in talin1) with the membrane (Fig. 3.4A). These residues are conserved across species (Fig. 3.7), and we thus hypothesized that the residues forming this membrane orientation patch (MOP) play a key role in integrin activation.

This hypothesis was tested using a well-established αIIbβ3 integrin activation assay in CHO cells (Han *et al.*, 2006). The integrin activation experiments described in this paragraph were performed by Feng Ye (Mark Ginsberg's group, University of California San Diego). Expression of wild type (WT) talin1 F3 slightly increased integrin

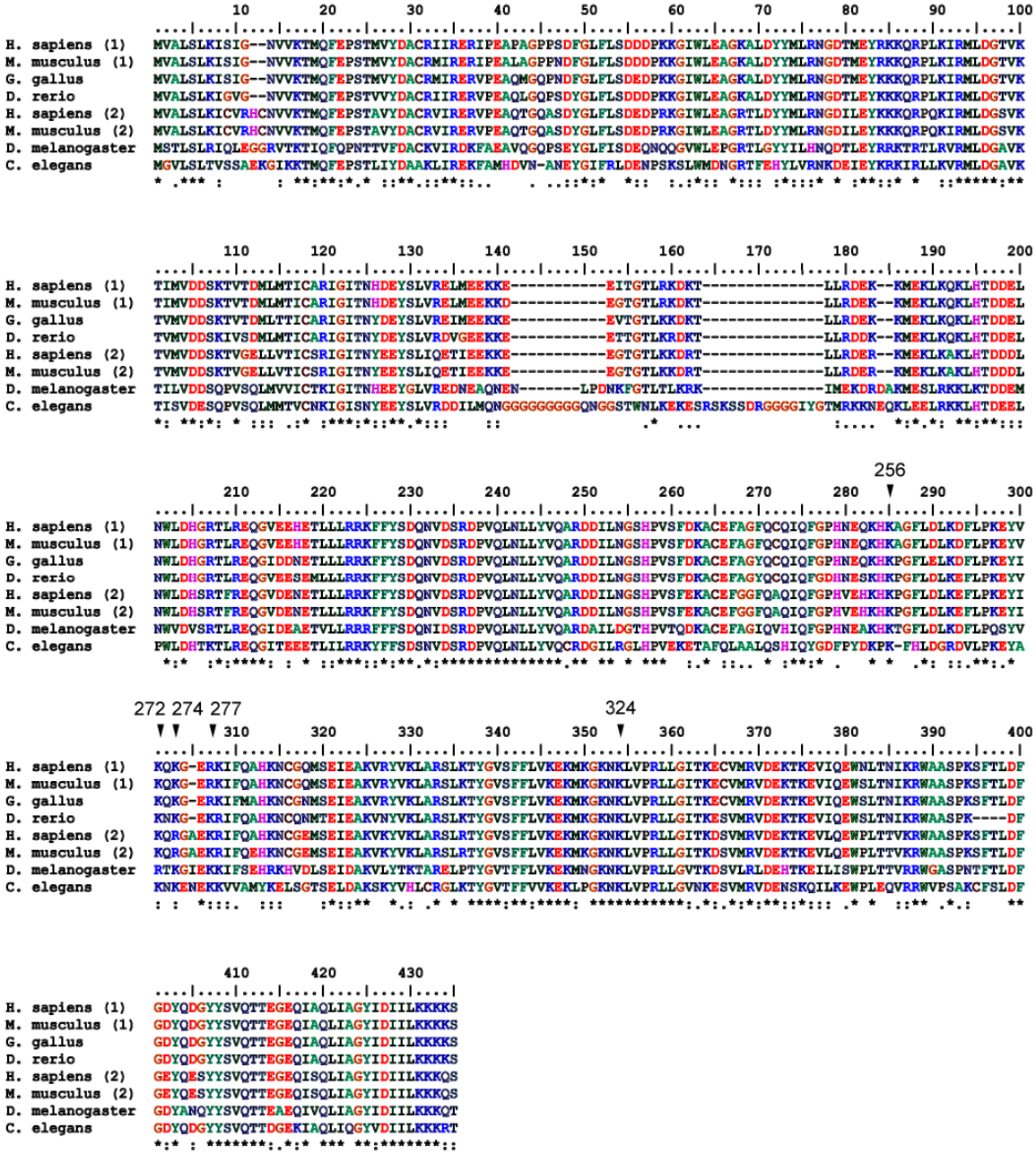

Figure 3.7 Alignment of talin head domain sequences from different organisms. The amino acid sequence of talin isoforms from various organisms were aligned using ClustalW (Larkin *et al.*, 2007). Only the sequence of the N-terminal head domain is shown. Residues located in the membrane orientation patch (MOP) in the F2 domain or involved in a key talin/integrin salt bridge are highlighted and labelled with vertebrate talin1 numbering. These residues are conserved in all talin sequences tested.

activation, but expression of a longer talin1 construct with additional N-terminal domains (F1-F2-F3) caused a much more pronounced increase in integrin activation (Fig. 3.8B). This activation was partially or fully abrogated by mutating the four MOP residues singly, doubly, or quadruply (4E) to glutamate (Fig. 3.8A). To ensure that the observed effects were not due to protein instability, decreased integrin binding, or major structural changes, NMR studies were conducted on the 4E mutant. The mutations did not significantly affect integrin binding or the NMR spectrum of talin1 F2-F3, indicating that the 4E construct was folded and stable (Fig. 3.9). To test the generalizability of these findings, these experiments were repeated in CHO cells expressing a chimeric integrin consisting of the extracellular and TM domains of αIIbβ3 and the intracellular domains of α5β1A (O'Toole *et al.*, 1994) (Fig. 3.8C). Consistent with previous findings (Bouaouina *et al.*, 2008; Hato *et al.*, 2008; O'Toole *et al.*, 1994), the effect of talin on this integrin was reduced in comparison to αIIbβ3, due to both higher basal activation and decreased maximal activation in response to talin. However, talin1 F1-F2-F3 did increase activation of this integrin, and this increase was abrogated by mutating MOP residues.

To demonstrate a direct interaction between the talin MOP and the membrane, vesicle cosedimentation assays (Fig. 3.10) were performed by Ben Goult (David Critchley's group, University of Leicester). A solution containing protein and vesicles was separated by centrifugation into a pellet consisting of the vesicles plus bound protein and a supernatant containing unbound material. In the presence of neutral phosphatidylcholine (PC) vesicles, talin1 F2-F3 remained in the unbound supernatant fraction. However, addition of 20% negatively-charged phosphatidylserine (PS) to these vesicles caused 40% of talin1 F2-F3 to precipitate with the vesicles, and this binding was fully abrogated by the 4E mutation. Increasing the negatively-charged content of the vesicles to 100% PS caused WT talin1 F2-F3 to become fully bound; the 4E mutation

Table 3.3 Backbone RMSD values for alignment of talin2 with various talin1 structures

Talin1 structure	F2-F3 (209-398)	F2 (209-304)	F3 (311-398)
1MK9	1.002	0.520	1.125
1MK7	1.110	0.697	1.194
1MIX	1.396	0.638	1.858
2H7E	-	-	1.056

RMSD values are given in Å and were calculated with MOLMOL (Koradi *et al.*, 1996).

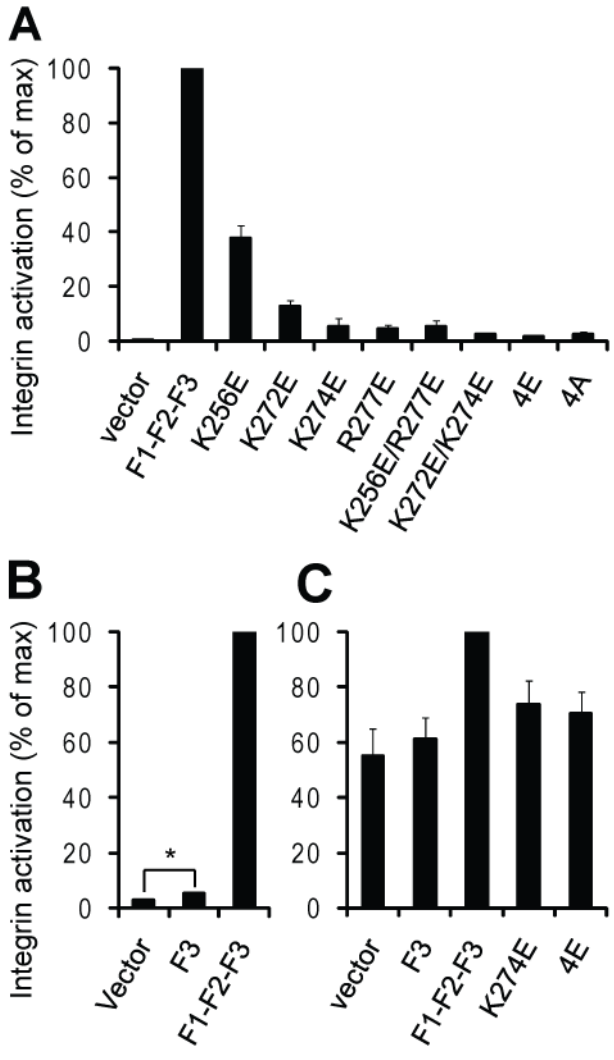

Figure 3.8 A key role for a talin/membrane interaction in integrin activation. (A) GFP-talin1 F1-F2-F3 wild type (F1-F2-F3) or F1-F2-F3 with various mutations in the F2 domain were transfected into αIIbβ3-expressing CHO cells. Activated integrins were detected with PAC1 antibody and analyzed by FACS 24 hours after transfection. Integrin activity was normalized against GFP-F1-F2-F3 WT transfected cells. Error bars represent standard errors of three independent experiments. 4E corresponds to all four membrane orientation patch (MOP) residues mutated to glutamate, and 4A corresponds to all four mutated to alanine. (B) As in panel A, but with GFP-talin1 F3 WT or F1-F2-F3 WT. Error bars (barely visible due to small size) represent standard errors of two independent experiments. F3 caused a statistically significant increase in integrin activation (*) of P = 0.0388 by one tail test. (C) As in panels A and B, but GFP-talin1 F3 wild type, F1-F2-F3 wild type, or F1-F2-F3 mutants were transfected into CHO cells expressing a chimeric integrin containing the intracellular domains of α5β1A. Error bars represent standard errors of four independent experiments. These experiments were performed by Feng Ye (Mark Ginsberg's group, University of California San Diego).

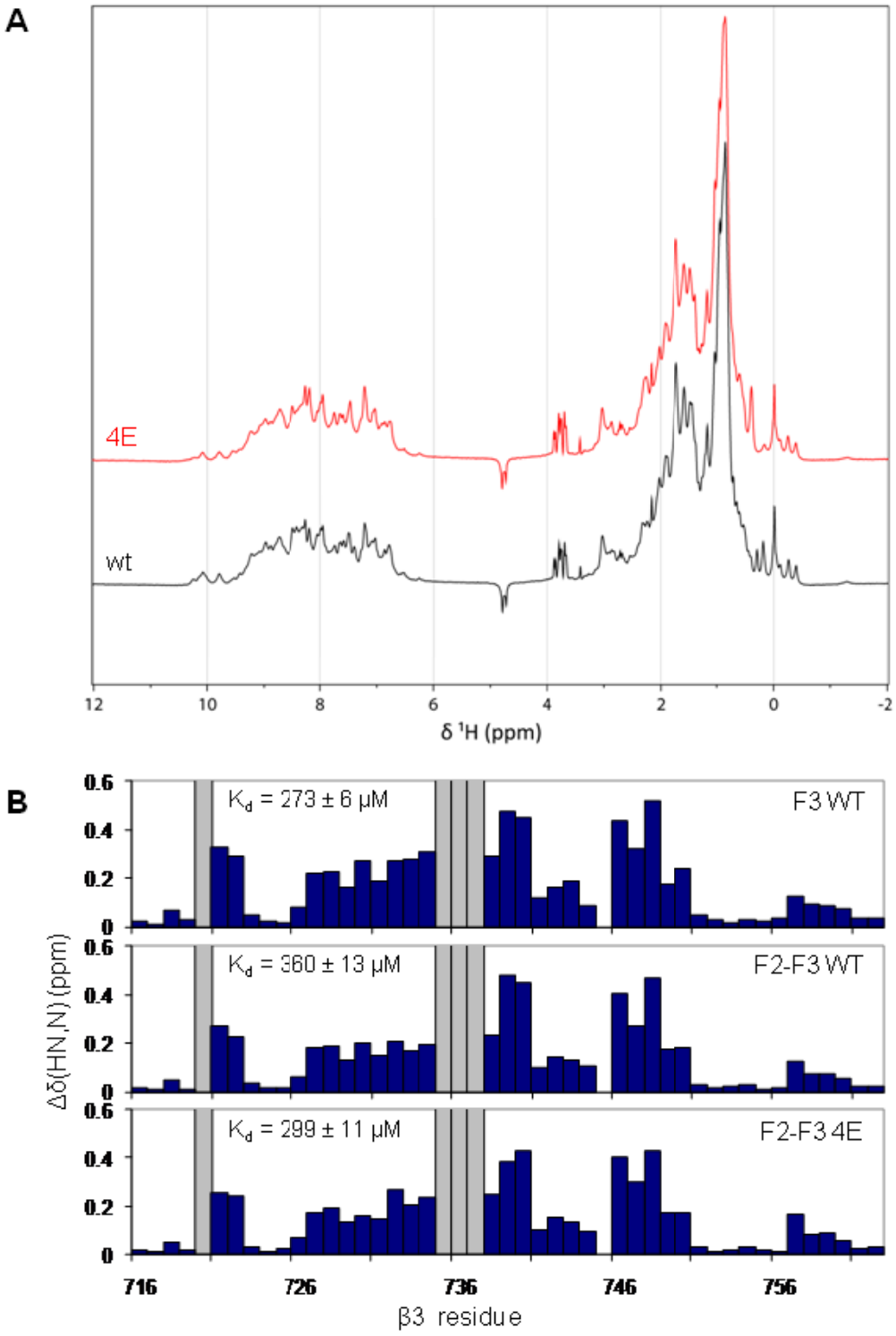

Figure 3.9 Talin F2 mutants do not affect talin integrity or integrin binding. (A) 1D NMR spectra of 1 mM talin1 F2-F3 wild type (WT) and the 4E mutant in which K256, K272, K274, and R277 in F2 were substituted with glutamates. Both spectra are indicative of a folded protein and do not display major differences. (B) Chemical shift perturbation maps for 0.05 mM β3 titrated with 1 mM talin1 F3 WT, F2-F3 WT, and F2-F3 4E. K_d values for the interactions are shown. No major differences were observed between the different constructs.

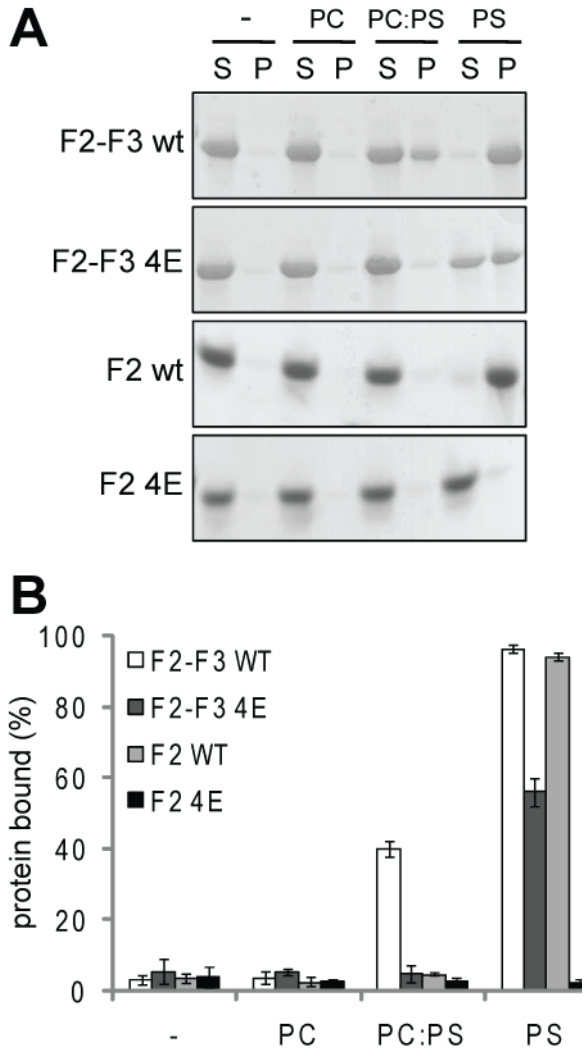

Figure 3.10 The talin F2 domain membrane orientation patch interacts with negatively-charged membrane phospholipids. Talin1 F2-F3 and F2 (0.15 mg/mL), either WT or 4E, were mixed with vesicles (0.5 mg/mL) consisting of phosphatidylcholine (PC), phosphatidylserine (PS), or a 4:1 ratio of PC:PS and then centrifuged. (A) Coomassie-stained gel of one representative experiment. Unbound protein was located in the supernatant (S) and bound protein in the pellet (P). (B) Graphical representation of the percentage of protein bound to lipid vesicles (average of three independent experiments ± standard error). These experiments were performed by Ben Goult (David Critchley's group, University of Leicester).

Table 3.4 K_d values for the interaction of talin1 F3 with the β3 integrin tail For wild type proteins and salt bridge-breaking mutants

	K_d (μM)*	ΔΔG (kJ/mol)†
WT	273 ± 6	-
β3 D723R	970 ± 26	3.1
talin1 K324D	800 ± 14	2.7

*K_d values are given in μM ± standard error.
†ΔG was calculated from K_d for each interaction, and ΔΔG was calculated by subtracting ΔG of that interaction from ΔG of the interaction involving the wild type tail (a positive value denotes a decrease in affinity)

significantly decreased this binding, although some residual binding was still detected. Similar results were achieved with the talin1 F2 domain, although binding was only detected in 100% PS vesicles, and the 4E mutation fully abrogated vesicle binding. Thus, we have identified a specific new talin/membrane interaction site that is essential for full integrin activation and is sensitive to the presence of negatively-charged moieties in the membrane.

3.2.3 Talin forms a key membrane-proximal salt bridge with the β integrin tail

The β1D/talin2 structure reveals a salt bridge between β1D D759 and talin2 K327 that caps the MP portion of the interaction (Fig. 3.4A, 3.5C). These two residues are conserved in other paralogues of talin and integrins (Fig. 3.1A, D723 in β3 and K324 in talin1). NMR experiments show that swapping the charge of these residues in the β3/talin1 pair (D/R in β3 and K/D in talin1) abrogates the MP interaction (Fig. 3.11A-C) and decreases the affinity of the overall interaction (Table 3.4). A similar effect was observed with the β1A/talin1 pair (Fig. 3.12). The effect of these mutations is virtually identical to that of a FF727/730AA mutation in the β3 membrane proximal helix, which also abrogates integrin activation (Wegener *et al.*, 2007) (Fig. 3.13).

This same β3 residue, D723, has previously been shown, by integrin activation assays (Hughes *et al.*, 1996), α/β TM association studies (Kim *et al.*, 2009), and NMR (Lau *et al.*, 2009), to stabilize the integrin inactive state by interacting with R995 in αIIb. Talin1 K324 would thus compete with αIIb R995 for a salt bridge with β3 D723, thereby weakening any αIIb R995-β3 D723 interaction (Fig. 3.14A). This hypothesis was tested in αIIbβ3-expressing CHO cells (experiments performed by Chungho Kim, Mark Ginsberg's group, University of San Diego). The addition of WT talin1 F0-F1-F2-F3 markedly increased integrin activation, but this increase was fully abrogated when talin1

K324D was introduced instead (Fig. 3.11D). β3 D723 thus constrains bidirectional integrin signalling via an interaction with αIIb R995 in the absence of talin, but also participates in the activation process via an interaction with talin1 K324.

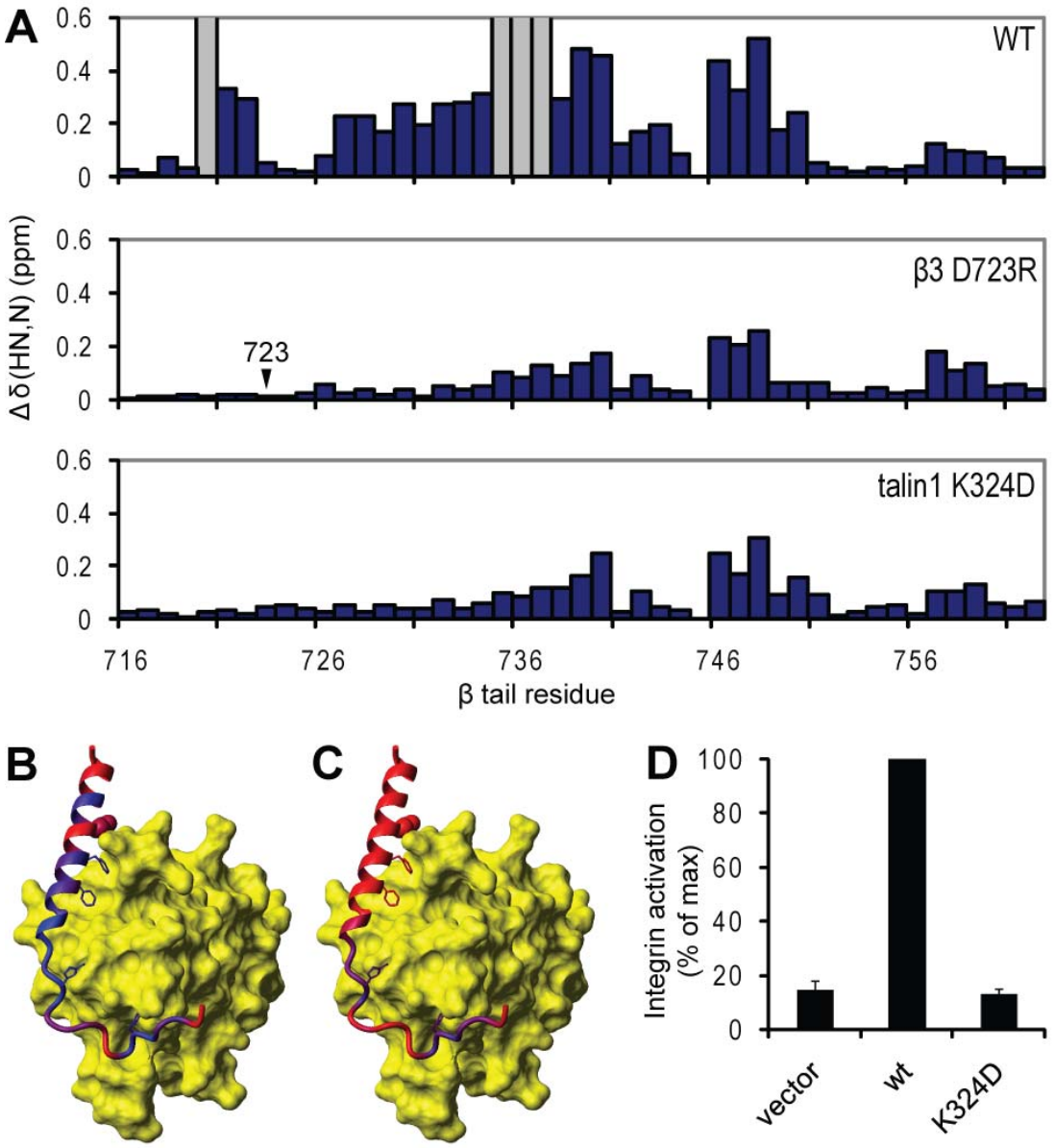

Figure 3.11 A key salt bridge between talin and the β integrin tail. (A) Weighted shift maps of perturbations observed in ^{1}H-^{15}N HSQC spectra of the β3 tail upon the addition of talin1 F3. Experiments were performed on β3 WT with talin1 WT, β3 D723R with talin1 WT, and β3 WT with talin1 K324D. Grey bars correspond to residues that could not be tracked due to exchange broadening. (B) Chemical shift perturbations in β3 upon binding to talin1 F3 WT domain mapped onto the β1D/talin2 structure (largest shifts in blue, smallest in red). (C) As in panel B but with β3 D723R. (D) As in Fig. 3.8A, but exploring the effect of talin1 F0-F1-F2-F3 WT or K324D on activation of αIIbβ3 expressed in CHO cells. The experiments in panel D were performed by Chungho Kim (Mark Ginsberg's group, University of California, San Diego).

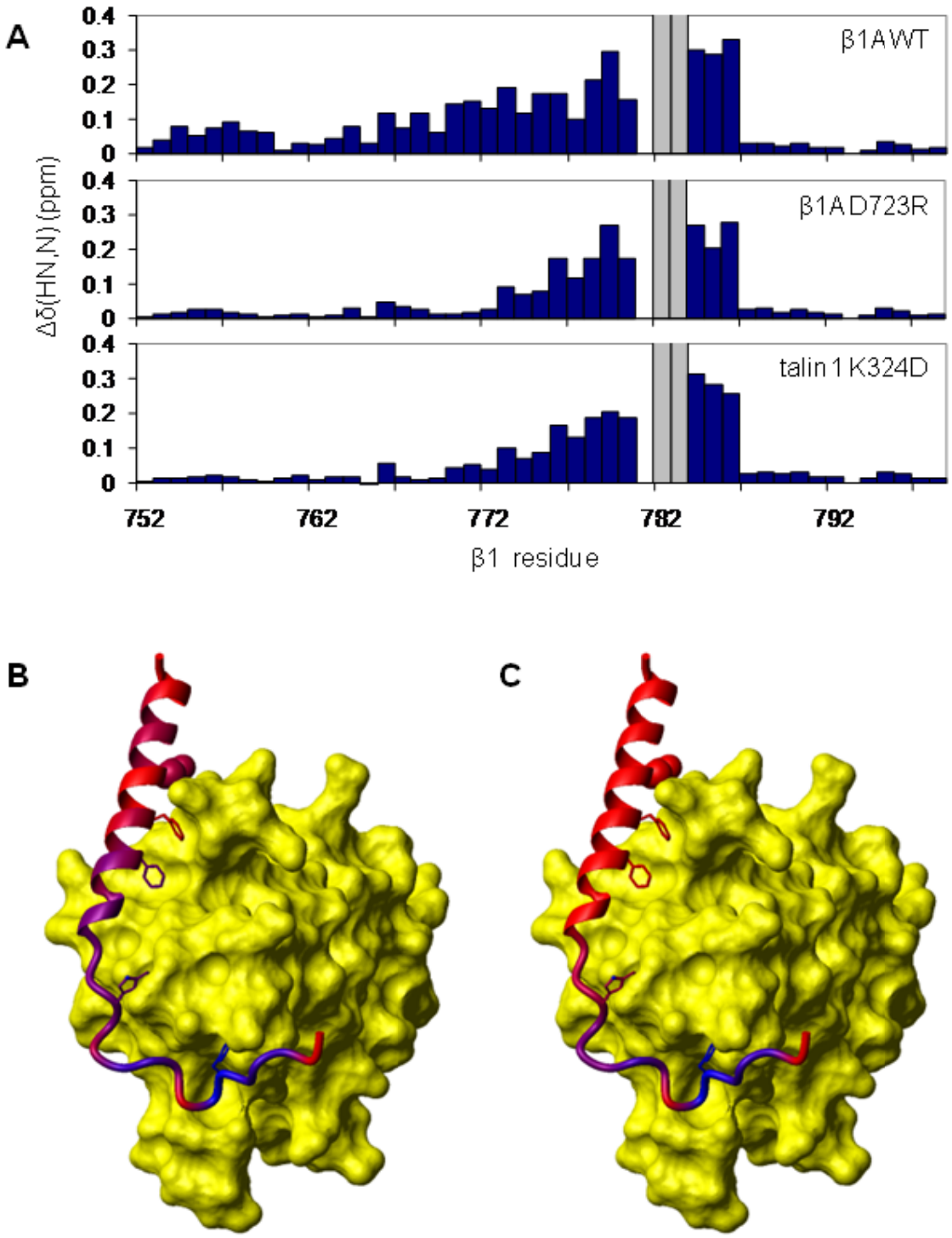

Figure 3.12 Disrupting the membrane-proximal salt bridge between β1A and talin1. (A) Weighted shift maps of perturbations observed in ^{1}H-^{15}N HSQC spectra of the β1A tail upon the addition of talin1 F3. Experiments were performed on β1A WT with talin1 WT, β1A D759R with talin1 WT, and β1A WT with talin1 K324D. Grey bars correspond to residues that could not be tracked due to exchange broadening. (B) Chemical shift perturbations in β1A upon binding to talin1 F3 WT domain mapped onto the β1D/talin2 structure (largest shifts in blue, smallest in red). (C) As in panel B but with β1A D723R.

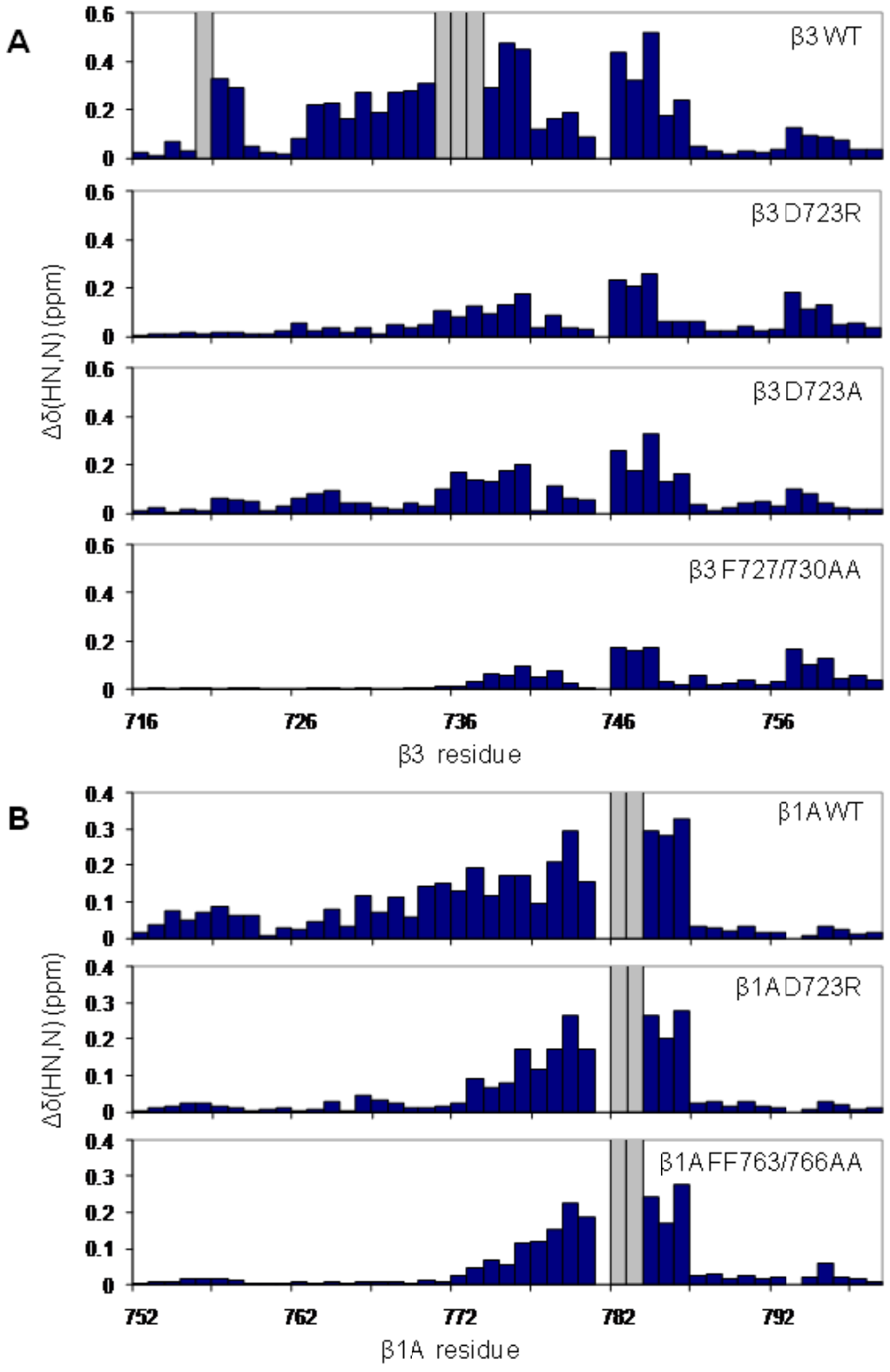

Figure 3.13 Mutations that abrogate talin binding to the membrane-proximal region of the β integrin tail. (A) Chemical shift perturbation maps for ^{15}N-labelled WT and mutant β3 tail (0.05 mM) titrated with 1 mM talin1 F3 domain. Mutants of β3 tested were D723R, D723A, and FF727/730AA. (B) As in panel A but with β1A WT, D723R and FF763/766AA.

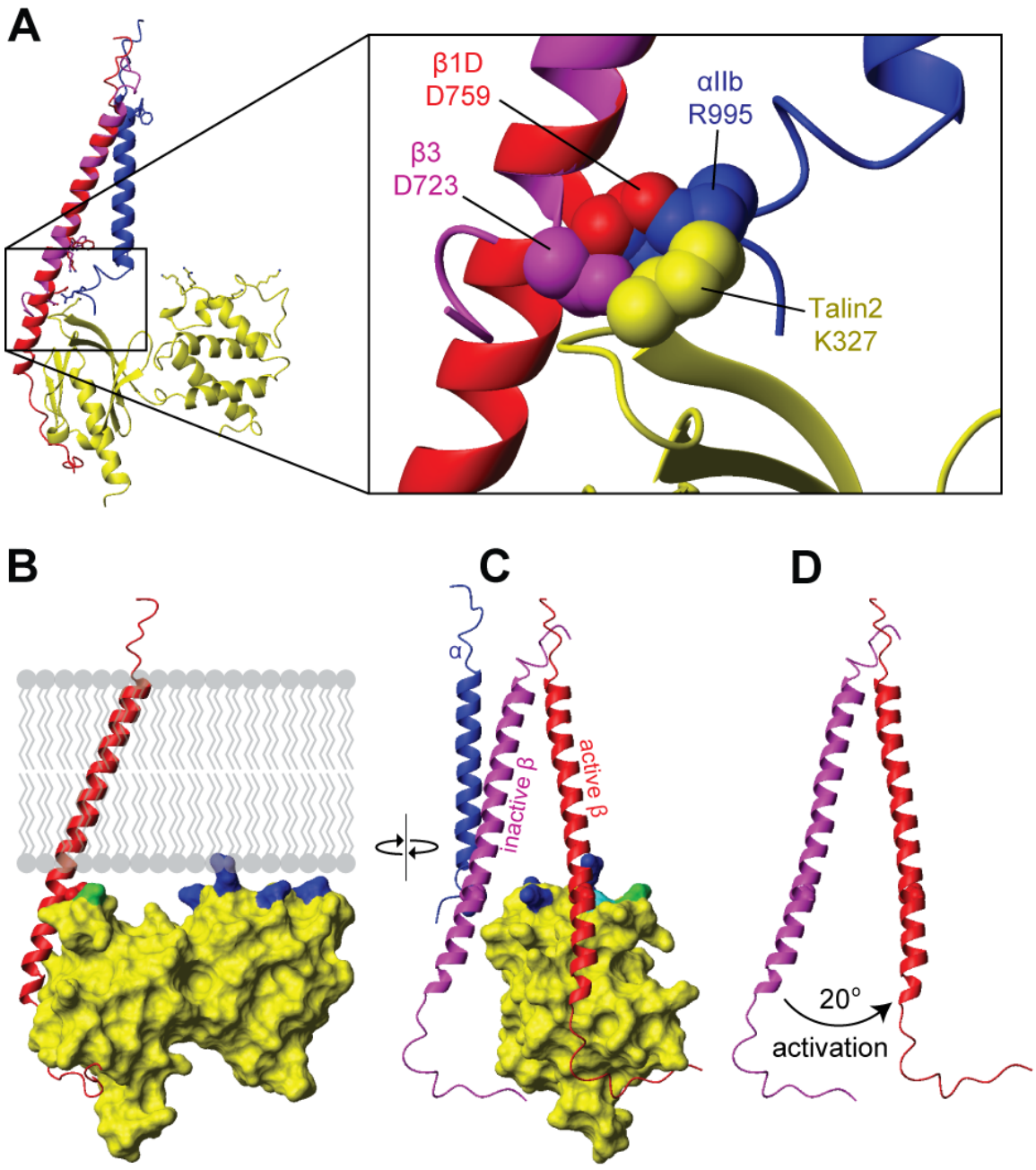

Figure 3.14 Disruption of the α/β integrin dimer by talin. (A) Overlay of the talin2/β1D structure (plus β3 TM) with the αIIbβ3 TM structure (PDB 2K9J) (Lau *et al.*, 2009). Talin is shown in yellow, αIIb in blue, β3/β1D bound to talin in red, and β3/β1D bound to αIIb in magenta. Inset shows inner membrane clasp competition. (B) The talin2/β1D structure (plus β3 TM) has been reoriented by 20° so that maximal contact is achieved between the membrane and the talin F2 membrane orientation patch (MOP). Membrane-targeting residues in F2 are highlighted in blue, and talin2 K325 (talin1 K322) in the F3 domain is highlighted in green. (C) The structure in panel B shown in an orthogonal "back" view. The inactive αIIbβ3 transmembrane domain complex has been added to illustrate the change in β tilt angle upon activation. The β3 TM structure has been extended into the cytoplasm by combining it with the β1D tail structure. Talin2 K327 (talin1 K324) is highlighted in cyan. (D) The same view as panel C, but with only the two β integrin tails shown to highlight the 20° change in tilt angle.

3.3 Discussion

By exploring a wide range of talin/integrin interactions, we identified a talin/integrin pair (talin2/β1D) that binds much more tightly than any previously studied pair and was more amenable to crystallization. The resulting crystal structure hinted at novel interactions between the talin F2 domain and the cell membrane and between the talin F3 domain and a MP aspartate residue in the β tail. We subsequently validated these interactions by additional biophysical methods and demonstrated their biological relevance through in-cell experiments. These findings can now be incorporated into a new comprehensive structural model of integrin activation by talin.

A recent NMR structure revealed that the αIIbβ3 integrin TM domains form a dimer of unique structure stabilized by two interactions: an outer membrane clasp that involves glycine-mediated TM helix packing and an inner membrane clasp that includes the D723/R995 salt bridge (Lau *et al.*, 2009). Another structure generated by disulfide-based distance restraints revealed a similar arrangement (Zhu *et al.*, 2009). An overlay of the talin2/β1D structure with the αIIbβ3 NMR structure reveals steric clashes between αIIb and talin2 located around the integrin inner membrane clasp (Fig. 3.14A). Thus, the breaking of the α/β salt bridge and its replacement with a β tail/talin salt bridge appears to be a key event in integrin activation. However, analysis of the talin2/β1D structure reveals that contact between the phospholipid headgroups of the membrane and the talin F2 MOP is better achieved if the tilt of the β TM domain changes by about 20° in a plane perpendicular to the plane of the membrane and to that of the initial β tilt (Fig. 3.14B-D). The α subunit would remain in a vertical orientation, constrained by tryptophan residues at each membrane interface (Lau *et al.*, 2008a; Yau *et al.*, 1998). The change in β TM orientation thus disrupts the precise packing of the β subunit against the α TM domain. This 20° reorientation also brings K325 in the talin2 F3 domain (K322 in talin1) adjacent

to the membrane, implying that the F2 MOP is a component of a larger membrane-interacting charged surface, spanning multiple domains of talin. This is consistent with a previous report showing that mutation of K322 in talin1 disrupts integrin activation (Wegener *et al.*, 2007); it could also explain why talin1 F2-F3 4E exhibits residual binding to membrane lipids (Fig. 3.10).

Our results are therefore consistent with a model of integrin activation in which membrane-based reorientation, together with the weakened electrostatic interaction at the α/β cytoplasmic face, results in tail separation (Fig. 3.15). Indeed, this explains why disruption of the αIIb R995-β3 D723 interaction is insufficient to activate integrins in the absence of talin binding (Tadokoro *et al.*, 2003; Wegener *et al.*, 2007) and is compatible with the observation that mutation of αIIb R995 or β3 D723 weakens, but does not eliminate, α/β TM association (Kim *et al.*, 2009; Lau *et al.*, 2009). The α/β TM domains interact only weakly (Kim *et al.*, 2009; Lau *et al.*, 2009), and the ability of talin to induce α/β TM separation was recently demonstrated directly (Kim *et al.*, 2009), thus adding plausibility to the mechanism of activation reported here.

The fact that the relevant talin and integrin residues are highly conserved implies that this mechanism of integrin activation is generalizable across different isoforms. The sequences of the MP regions of the β1 and β3 tails are remarkably similar (Fig. 3.1A), and previous studies have demonstrated that the D759A mutant in β1 increases integrin affinity for fibronectin (Millon-Fremillon *et al.*, 2008; Sakai *et al.*, 1998). Interestingly, mice with this knock-in mutation in β1 do not display a pronounced phenotype (Czuchra *et al.*, 2006). This could relate to the observation that whereas β3 integrins have more distinct “on” and “off” states, the activation of β1 integrins is more dynamically regulated, and β1 integrins exist in a more default “on” state (Hato *et al.*, 2008; Hynes, 2002). Thus, the combined effects of decreasing both α/β association and β/talin

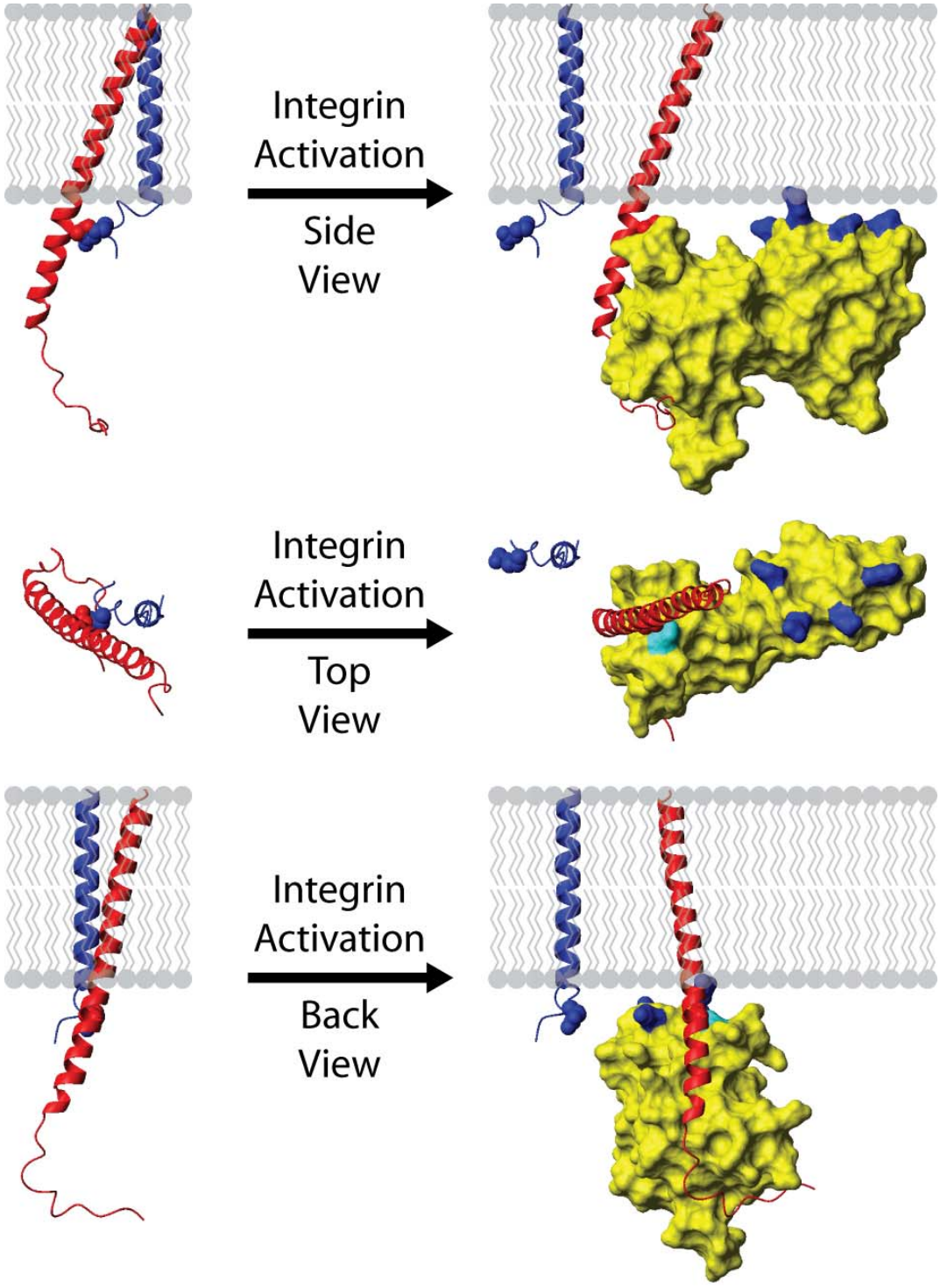

Figure 3.15 Model of integrin activation by talin, shown in three orientations. When talin binds to the β integrin tail it forms an extensive interface with the tail, including a membrane-proximal salt bridge, disrupting the salt bridge between the α and β subunits. To maximize contacts between the membrane and the positively-charged membrane orientation patch (MOP) on the talin F2 domain, the β integrin must be reoriented with respect to the membrane by approximately 20°. Through these actions talin causes α/β separation, inducing the active state in the extracellular region.

association by mutating D759 could compensate for one another in the case of β1 integrins. In contrast, the result of mutating D723 in β3 would be dominated by the effect of breaking its interaction with the α subunit. Regardless, experiments with a chimeric integrin containing the α5β1A cytoplasmic domains did reveal an essential role for the talin MOP in β1 integrin activation (Fig. 3.8C). Compared to activation of αIIbβ3, talin caused a smaller increase in activation of the chimeric α5β1A integrin—consistent with experiments reported on native α5β1A (Bouaouina *et al.*, 2008)—but the effect of mutating MOP residues was the same as in αIIbβ3, largely abrogating talin-induced integrin activation.

In summary, this high resolution structure of talin in complex with a full-length authentic integrin β cytoplasmic domain reveals that separation of the heterodimeric membrane-spanning helices is caused by the combined effects of talin-induced destabilization of the α/β inner membrane clasp and reorientation of the β TM domain. This model illustrates how localized membrane-specific protein interactions within the cell can lead to disruption of an interaction between TM helices in a large membrane-spanning receptor, effecting structural changes of great biological significance outside the cell.

3.4 References

Barsukov I.L., Prescot A., Bate N., Patel B., Floyd D.N., Bhanji N., Bagshaw C.R., Letinic K., Di Paolo G., De Camilli P., Roberts G.C., Critchley D.R. (2003) Phosphatidylinositol phosphate kinase type 1gamma and beta1-integrin cytoplasmic domain bind to the same region in the talin FERM domain. *J Biol Chem* **278:** 31202-31209

Belkin A.M., Zhidkova N.I., Balzac F., Altruda F., Tomatis D., Maier A., Tarone G., Koteliansky V.E., Burridge K. (1996) Beta 1D integrin displaces the beta 1A isoform in striated muscles: localization at junctional structures and signaling potential in nonmuscle cells. *J Cell Biol* **132:** 211-226

Bouaouina M., Lad Y., Calderwood D.A. (2008) The N-terminal domains of talin cooperate with the phosphotyrosine binding-like domain to activate beta1 and beta3 integrins. *J Biol Chem* **283:** 6118-6125

Calderwood D.A., Fujioka Y., de Pereda J.M., Garcia-Alvarez B., Nakamoto T., Margolis B., McGlade C.J., Liddington R.C., Ginsberg M.H. (2003) Integrin beta cytoplasmic domain interactions with

phosphotyrosine-binding domains: a structural prototype for diversity in integrin signaling. *Proc Natl Acad Sci U S A* **100:** 2272-2277

Conti F.J., Felder A., Monkley S., Schwander M., Wood M.R., Lieber R., Critchley D., Muller U. (2008) Progressive myopathy and defects in the maintenance of myotendinous junctions in mice that lack talin 1 in skeletal muscle. *Development* **135:** 2043-2053

Czuchra A., Meyer H., Legate K.R., Brakebusch C., Fassler R. (2006) Genetic analysis of beta1 integrin "activation motifs" in mice. *J Cell Biol* **174:** 889-899

de Pereda J.M., Wegener K.L., Santelli E., Bate N., Ginsberg M.H., Critchley D.R., Campbell I.D., Liddington R.C. (2005) Structural basis for phosphatidylinositol phosphate kinase type Igamma binding to talin at focal adhesions. *J Biol Chem* **280:** 8381-8386

Emsley P., Cowtan K. (2004) Coot: model-building tools for molecular graphics. *Acta Crystallogr D Biol Crystallogr* **60:** 2126-2132

Garcia-Alvarez B., de Pereda J.M., Calderwood D.A., Ulmer T.S., Critchley D., Campbell I.D., Ginsberg M.H., Liddington R.C. (2003) Structural determinants of integrin recognition by talin. *Mol Cell* **11:** 49-58

Han J., Lim C.J., Watanabe N., Soriani A., Ratnikov B., Calderwood D.A., Puzon-McLaughlin W., Lafuente E.M., Boussiotis V.A., Shattil S.J., Ginsberg M.H. (2006) Reconstructing and deconstructing agonist-induced activation of integrin alphaIIbbeta3. *Curr Biol* **16:** 1796-1806

Hato T., Yamanouchi J., Tamura T., Yakushijin Y., Sakai I., Yasukawa M. (2008) Cooperative role of the membrane-proximal and -distal residues of the integrin beta3 cytoplasmic domain in regulation of talin-mediated alpha IIb beta3 activation. *J Biol Chem* **283:** 5662-5668

Hughes P.E., Diaz-Gonzalez F., Leong L., Wu C., McDonald J.A., Shattil S.J., Ginsberg M.H. (1996) Breaking the integrin hinge. A defined structural constraint regulates integrin signaling. *J Biol Chem* **271:** 6571-6574

Hughes P.E., O'Toole T.E., Ylanne J., Shattil S.J., Ginsberg M.H. (1995) The conserved membrane-proximal region of an integrin cytoplasmic domain specifies ligand binding affinity. *J Biol Chem* **270:** 12411-12417

Hynes R.O. (2002) Integrins: bidirectional, allosteric signaling machines. *Cell* **110:** 673-687

Kim C., Lau T.L., Ulmer T.S., Ginsberg M.H. (2009) Interactions of platelet integrin alphaIIb and beta3 transmembrane domains in mammalian cell membranes and their role in integrin activation. *Blood* **113:** 4747-4753

Koradi R., Billeter M., Wuthrich K. (1996) MOLMOL: a program for display and analysis of macromolecular structures. *J Mol Graph* **14:** 51-55, 29-32

Larkin M.A., Blackshields G., Brown N.P., Chenna R., McGettigan P.A., McWilliam H., Valentin F., Wallace I.M., Wilm A., Lopez R., Thompson J.D., Gibson T.J., Higgins D.G. (2007) Clustal W and Clustal X version 2.0. *Bioinformatics* **23:** 2947-2948

Lau T.L., Dua V., Ulmer T.S. (2008a) Structure of the integrin alphaIIb transmembrane segment. *J Biol Chem* **283:** 16162-16168

Lau T.L., Kim C., Ginsberg M.H., Ulmer T.S. (2009) The structure of the integrin alphaIIbbeta3 transmembrane complex explains integrin transmembrane signalling. *EMBO J* **28:** 1351-1361

Lau T.L., Partridge A.W., Ginsberg M.H., Ulmer T.S. (2008b) Structure of the integrin beta3 transmembrane segment in phospholipid bicelles and detergent micelles. *Biochemistry* **47:** 4008-4016

Luo B.H., Carman C.V., Springer T.A. (2007) Structural basis of integrin regulation and signaling. *Annu Rev Immunol* **25:** 619-647

Millon-Fremillon A., Bouvard D., Grichine A., Manet-Dupe S., Block M.R., Albiges-Rizo C. (2008) Cell adaptive response to extracellular matrix density is controlled by ICAP-1-dependent beta1-integrin affinity. *J Cell Biol* **180:** 427-441

O'Toole T.E., Katagiri Y., Faull R.J., Peter K., Tamura R., Quaranta V., Loftus J.C., Shattil S.J., Ginsberg M.H. (1994) Integrin cytoplasmic domains mediate inside-out signal transduction. *J Cell Biol* **124:** 1047-1059

Sakai T., Zhang Q., Fassler R., Mosher D.F. (1998) Modulation of beta1A integrin functions by tyrosine residues in the beta1 cytoplasmic domain. *J Cell Biol* **141:** 527-538

Senetar M.A., Moncman C.L., McCann R.O. (2007) Talin2 is induced during striated muscle differentiation and is targeted to stable adhesion complexes in mature muscle. *Cell Motil Cytoskeleton* **64:** 157-173

Tadokoro S., Shattil S.J., Eto K., Tai V., Liddington R.C., de Pereda J.M., Ginsberg M.H., Calderwood D.A. (2003) Talin binding to integrin beta tails: a final common step in integrin activation. *Science* **302:** 103-106

Ulmer T.S., Calderwood D.A., Ginsberg M.H., Campbell I.D. (2003) Domain-specific interactions of talin with the membrane-proximal region of the integrin beta3 subunit. *Biochemistry* **42:** 8307-8312

Vinogradova O., Velyvis A., Velyviene A., Hu B., Haas T., Plow E., Qin J. (2002) A structural mechanism of integrin alpha(IIb)beta(3) "inside-out" activation as regulated by its cytoplasmic face. *Cell* **110:** 587-597

Wegener K.L., Partridge A.W., Han J., Pickford A.R., Liddington R.C., Ginsberg M.H., Campbell I.D. (2007) Structural basis of integrin activation by talin. *Cell* **128:** 171-182

Yau W.M., Wimley W.C., Gawrisch K., White S.H. (1998) The preference of tryptophan for membrane interfaces. *Biochemistry* **37:** 14713-14718

Zhu J., Luo B.H., Barth P., Schonbrun J., Baker D., Springer T.A. (2009) The structure of a receptor with two associating transmembrane domains on the cell surface: integrin alphaIIbbeta3. *Mol Cell* **34:** 234-249

CHAPTER IV: DIVERSITY IN INTEGRIN/TALIN INTERACTIONS

4.1 Introduction

Integrin adhesiveness for extracellular ligands can be activated from within the cell by a direct interaction between talin and the cytoplasmic tail of the β integrin subunit (Calderwood *et al.*, 2002; Tadokoro *et al.*, 2003; Wegener *et al.*, 2007). The F3 domain of talin binds to the membrane-distal (MD) portion of the integrin tail by a typical PTB domain/NPxY motif interaction (Calderwood *et al.*, 2003; Garcia-Alvarez *et al.*, 2003), but also interacts with the membrane-proximal (MP) helix of the integrin tail (Wegener *et al.*, 2007). This latter interaction endows talin with the unique ability to activate integrins. As demonstrated in Chapter III, the talin F3 domain disrupts a key salt bridge between the α and β integrin tails, and an interaction between the talin F2 domain and the cell membrane reorients the β subunit in order to further disrupt the α/β transmembrane (TM) complex. This causes separation of the integrin tails and TM domains, inducing a more open conformation in the extracellular domain with higher affinity for matrix ligands (Luo *et al.*, 2007).

Structural studies of integrin activation by talin to date have focused largely on the β3 integrin. The first insight into the interface between the β3 NPxY motif and the talin F3 domain emerged from a crystal structure of a short MD fragment of the β3 tail covalently tethered to the talin1 F2-F3 fragment (Garcia-Alvarez *et al.*, 2003). Further features of the interface between the β3 MP region and the talin1 F3 domain were provided by an NMR structure that employed a chimeric peptide of the β3 helix attached to a sequence from PIPK1γ that binds talin tightly (Wegener *et al.*, 2007). This focus on the β3 subunit in studies with talin follows a general trend in integrin structural biology. For example, atomic resolution structures exist for just two complete integrin

extracellular domains: αVβ3 (Xiong *et al.*, 2001; Xiong *et al.*, 2004; Xiong *et al.*, 2002) and αIIbβ3 (Zhu *et al.*, 2008). Likewise, structures of the β3 TM domain alone (Lau *et al.*, 2008) and in complex with αIIb (Lau *et al.*, 2009) are available, as are structures of the β3 cytoplasmic tail alone (Vinogradova *et al.*, 2004) and in complex with αIIb (Vinogradova *et al.*, 2002; Weljie *et al.*, 2002). Such structural data has not previously been available for any other integrin, although the structure of the β1D/talin2 presented in Chapter III has begun to address this imbalance. This is important, because the eight different β subunits (not including splice variants) expressed in mammals have non-redundant functions, including unique tissue distributions, ligand specificities, and α binding partners (Hynes, 2002).

The β1 integrin is widely expressed and plays key roles in a variety of biological process; knockout of this gene in mice is embryonic lethal (Fassler and Meyer, 1995). The β3 integrin, on the other hand, is of significance primarily in the blood and vasculature. Mice in which this gene has been knocked out exhibit a bleeding defect, due in part to the absence of αIIbβ3 in platelets, but are viable (Hodivala-Dilke *et al.*, 1999). Replacement of the β3 tail with that of β1 increases basal αIIbβ3 integrin activation levels (Hato *et al.*, 2008; O'Toole *et al.*, 1994), which is consistent with the general observation that the αIIbβ3 integrin exists in a default "off" state, and is only activated during thrombosis. In contrast, β1 integrins generally exist in a more active conformation, consistent with their role in adherent cells.

Another difference between β1 and β3 integrin activation has recently become apparent from the studies of Bouaouina *et al*., who found that the isolated talin1 F2-F3 domain pair was able to activate αIIbβ3 but not α5β1; activation of the latter integrin was only achieved in the presence of additional N-terminal portions of the talin head domain, particularly the talin F0 domain (Bouaouina *et al.*, 2008). The source of this difference

may be the MP region of the integrin tail, although the β1 and β3 tails are highly similar here (Fig. 4.1A). Only one of the differing residues in this region makes contact with talin in the β3-PIPK1γ/talin1 structure (Wegener *et al.*, 2007), and this residue (β3 R734, β1 K770) is a conservative substitution. Thus, current structural data does not explain the difference in talin-mediated activation between these two integrins.

An additional observation that remains unexplained is that the β1D integrin splice variant binds talin with higher affinity than β1A (see Chapter III), despite these isoforms only differing in the extreme C-terminal region of their cytoplasmic tails (Fig. 4.1A). β1D is expressed primarily in striated muscle cells (Belkin *et al.*, 1996) and is found in the myotendinous junction where it co-localizes with the talin2 isoform (Conti *et al.*, 2008), which is also highly expressed in striated muscle (Monkley *et al.*, 2001; Senetar *et al.*, 2007). In Chapter III, we show that β1D and talin2 bind more tightly than any previously reported integrin/talin complex, an observation consistent with their adhesive role in muscle. The sequence identity between β1A and β1D (and β3) (Fig. 4.1A) and between talin1 and talin2 (Fig. 4.1B) is high, and previous talin1/β3 structures do not explain this difference in affinity.

To explore these intriguing biological differences, we studied the interaction between talin and the cytoplasmic tails of different integrins using NMR, X-ray crystallography, isothermal titration calorimetry (ITC), and mutagenesis. This has revealed significant structural diversity in integrin/talin interactions, and has enabled us to offer novel explanations for some of the above biological observations.

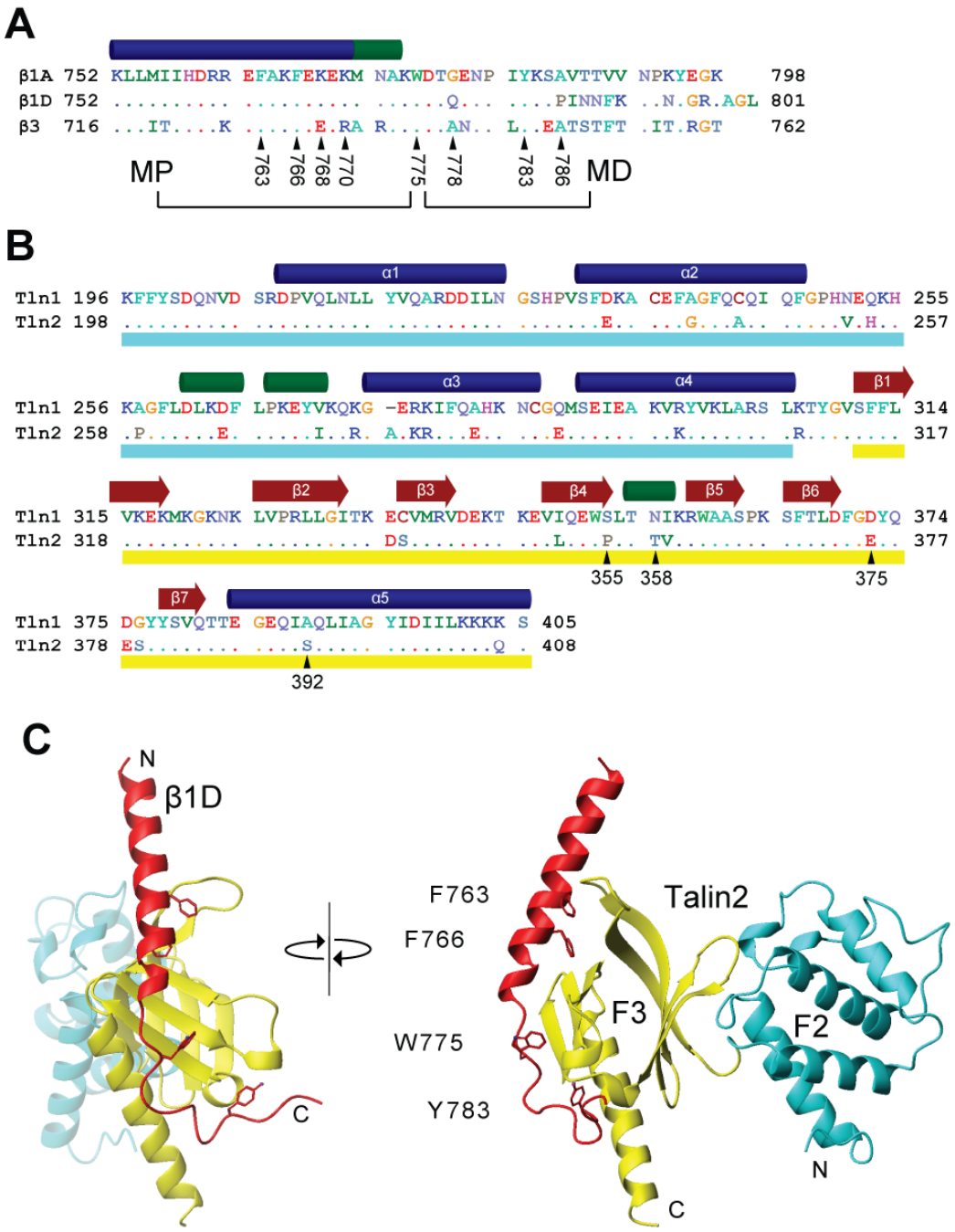

Figure 4.1 The structure of the integrin β1D tail bound to talin2 F2-F3. (A) Sequence of the cytoplasmic regions of the β1A, β1D, and β3 integrin tails. Residues in β1D and β3 that differ from β1A are highlighted, and residues of particular significance are noted. Secondary structure is based on the β1D/talin2 complex structure, with α helices denoted in blue and 3_{10} helices in green. Membrane-proximal (MP) and membrane-distal (MD) talin binding sites are noted. (B) Sequence of the F2-F3 domains of talin1 and talin2. Residues in talin2 that differ from talin1 are highlighted, and secondary structure was determined as in (A). The F2 domain is underlined in cyan and the F3 in yellow. (C) Crystal structure of talin2 F2-F3 bound to the β1D integrin tail, with significant β1D residues highlighted. All structure images were generated with MOLMOL (Koradi *et al.*, 1996) unless otherwise indicated.

4.2 Results

4.2.1 Diversity in integrin/talin interactions revealed by NMR

The NMR experiments presented in Chapter III using ^{15}N-labelled β1A, β1D, and β3 integrin cytoplasmic tails have revealed widely different affinities between these different integrins and the two isoforms of talin. In particular, the β1D/talin2 pair exhibits a much tighter affinity than any other WT integrin/talin pair (Table 4.1). As discussed in Chapter III, this unprecedentedly tight binding for an integrin/talin pair enabled crystallization of this complex, allowing the first structure of a fragment of talin (the F2-F3 domain pair) bound to an authentic full-length integrin tail to be solved (Fig. 4.1C).

The chemical shift perturbation maps produced in these NMR studies (Fig. 4.2, 4.3) also reveal striking differences in how talin1 and talin2 interact with different integrins. In particular, the F3 domains of both talin isoforms induce chemical shift perturbations of greater magnitude in the MP region of the β3 tail than they do in the β1 tails. Conversely, both talin isoforms induce larger perturbations in the MD region of β1 tails than in the β3 tail. Mutation of two phenylalanine residues in β3 (FF727/730AA) has previously been shown to inhibit activation of αIIbβ3 by disrupting the interaction of talin1 with the MP portion of the tail (Wegener *et al.*, 2007). Here, we show that this mutation abrogates the talin1-induced shift perturbations in the MP region of β3 (Fig. 4.4B) and decreases the affinity of the interaction by 5.0 kJ/mol (Table 4.1). The analogous mutation in β1A (FF763/766AA) also abrogates talin1-induced MP perturbations (Fig. 4.4A) but only decreases the affinity of the interaction by 2.4 kJ/mol (Table 4.1). Contributions to the MD portion of this interaction can be judged by mutating the tyrosine residue in the NPxY motif (Y747 in β3, Y783 in β1A). Mutation of this residue abrogates the MD perturbations and decreases the affinity of talin1 for both integrins (Fig. 4.4), although the effect is greater on β1A than on β3 by 1.9 kJ/mol (Table

Table 4.1 Affinity of β tail mutants for wild type talin F3 domains

Mutation	K_d (μM)*	ΔG (kJ/mol)†	ΔΔG (kJ/mol)‡	ΔΔG (%)§
β1A + Talin1				
WT	491 ± 10	-18.88 ± 0.05	-	-
FF763/766AA	1,280 ± 57	-16.50 ± 0.11	2.37	13
K768E	324 ± 7.7	-19.91 ± 0.06	-1.03	-5
K768E/K770R	253 ± 5.6	-20.52 ± 0.05	-1.64	-9
W775A	6,500 est.**	-12	6	34
E779N	767 ± 21	-17.77 ± 0.07	1.11	6
E779N/I782L	882 ± 23	-17.42 ± 0.06	1.45	8
I782L	556 ± 14	-18.57 ± 0.06	0.31	2
Y783A	5,000 est.	-13	6	30
S785E	494 ± 21	-18.86 ± 0.11	0.02	0
β1A + Talin2				
WT	652 ± 20	-18.18 ± 0.08	-	-
β1D + Talin1				
WT	95 ± 4.1	-22.95 ± 0.11	-	-
β1D + Talin2				
WT	36 ± 2.3	-25.36 ± 0.16	-	-
FF763/766AA	58 ± 2.9	-24.19 ± 0.12	1.17	5
W775A	258 ± 7.8	-20.47 ± 0.07	4.88	19
Y783A	3,700 est.	-14	11	45
S785E	71 ± 5.3	-23.66 ± 0.19	1.69	7
WT††	21.3 ± 0.5	-26.65 ± 0.06	-	-
(D776/T777/Q778)V††	0.017 ± 0.005	-44.3 ± 0.7	-17.6	-70
β3 + Talin1				
WT	273 ± 6.4	-20.33 ± 0.06	-	-
FF727/730AA	2,027 ± 73	-15.36 ± 0.09	4.97	24
E732K	538 ± 17	-18.65 ± 0.08	1.68	8
E732K/R734K	748 ± 27	-17.83 ± 0.09	2.50	12
R734K	374 ± 6.8	-19.55 ± 0.05	0.78	4
A735M	243 ± 4.2	-20.61 ± 0.04	-0.28	-1
R736N	279 ± 5.1	-20.27 ± 0.05	0.06	0
W739A	6,600 est.	-12	8	39
N743E/L746I	201 ± 5.4	-21.09 ± 0.07	-0.76	-4
Y747A	1,317 ± 36	-16.43 ± 0.07	3.90	19
β3 + Talin2				
WT	438 ± 15	-19.16 ± 0.09	-	-

* K_d values were determined by NMR unless otherwise noted and are given in μM ± standard error.
† ΔG is given for binding and calculated from K_d.
‡ ΔΔG (kJ/mol) is the ΔG value for the mutant integrin binding to talin, minus the ΔG value for the WT integrin binding to talin (a positive value denotes a decrease in affinity)
§ ΔΔG (%) is the percentage of binding energy lost (or gained) by the given mutation (a positive value denotes a decrease in affinity).
** Approximate K_d values were estimated by comparing magnitude of chemical shift perturbations to those in the WT titration, as described in Chapter II.
†† K_d value determined by ITC.

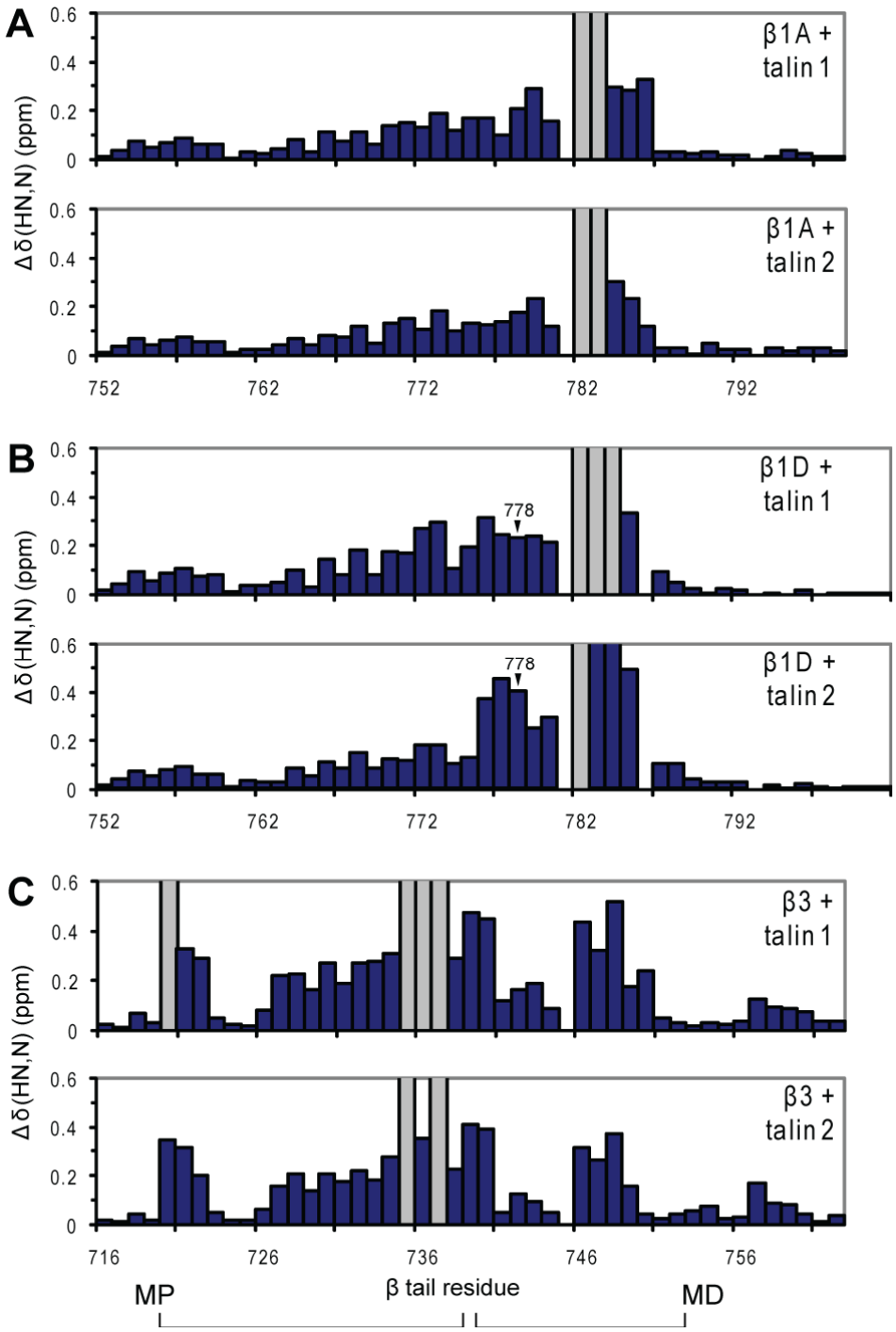

Figure 4.2 Diversity in integrin/talin interactions observed by NMR. Weighted chemical shift maps of perturbations observed in ^{1}H-^{15}N HSQC spectra of the β1A (A), β1D (B), and β3 (C) tail (50 μM) upon the addition of talin1 or talin2 F3 domain (1 mM). Membrane-proximal (MP) and membrane-distal (MD) binding sites are noted. The shift map for β1D with talin2 has been cropped, and the full map can be seen in Fig. 4.3. Most of the interactions studied here exist in the fast-intermediate chemical exchange regime, so resonances that experience a particularly large change in position upon binding are subject to extensive broadening and could not be tracked. These are denoted by grey bars in the chemical shift maps presented throughout this study. No other dynamic processes were observed in these studies that would contribute to broadening, so these grey bars can be read as being of similar or larger magnitude to the highest bars in these plots.

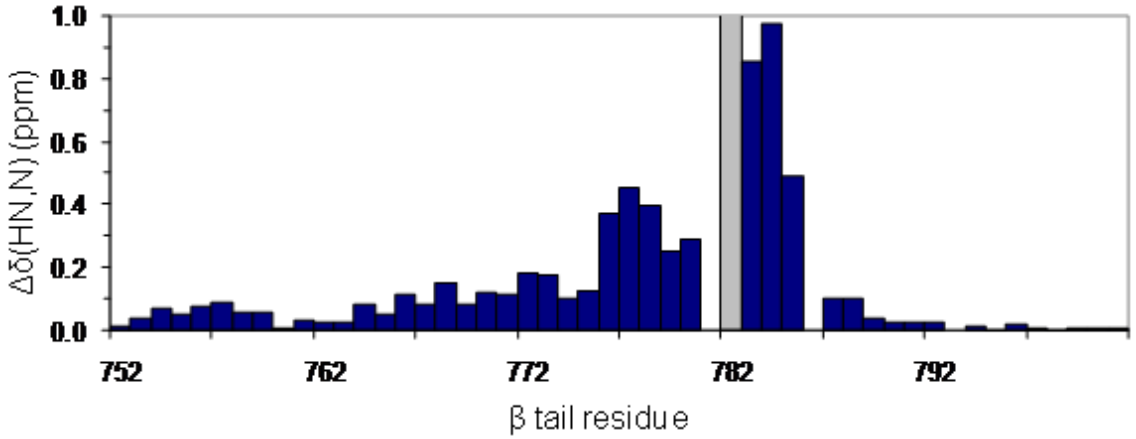

Figure 4.3 Interaction of the β1D integrin tail with the talin2 F3 domain. Weighted chemical shift map of perturbations observed in ^{1}H-^{15}N HSQC spectra of the β1D tail (50 μM) upon the addition of talin2 F3 domain (1 mM). The grey bar corresponds to a peak that could not be tracked due to exchange broadening. This is the full version of the shift map that was cropped in Fig. 4.2.

4.1). Thus, while the affinity of the talin1 F3 domain for β3 is largely derived from the MP region (24% of binding energy for β3 versus 13% for β1A), the MD portion is the greater contributor for β1A (30% for β1A, versus 19% for β3). This reliance on the NPxY motif was even more pronounced for β1D, where 45% of binding affinity was lost upon mutation of Y783. In all three of these cases, a large amount of binding energy also came from the tryptophan located between the MP and MD binding surfaces (W775 in β1, W739 in β3, Table 4.1).

4.2.2 Binding differences revealed by the structure of the β1D/talin2 complex

In Chapter III, we present the 2.2 Å resolution crystal structure of the full-length β1D integrin tail bound to the F2-F3 domains of talin2 (Fig. 4.1C). This structure reveals that the first 37 residues of the β1D tail (K752-N788) form a large elongated interface with the F3 domain of talin2, of about 1,300 $Å^2$ in area. The remaining 13 residues at the C-terminus remained unstructured and are not visible in the structure. The 22 most N-

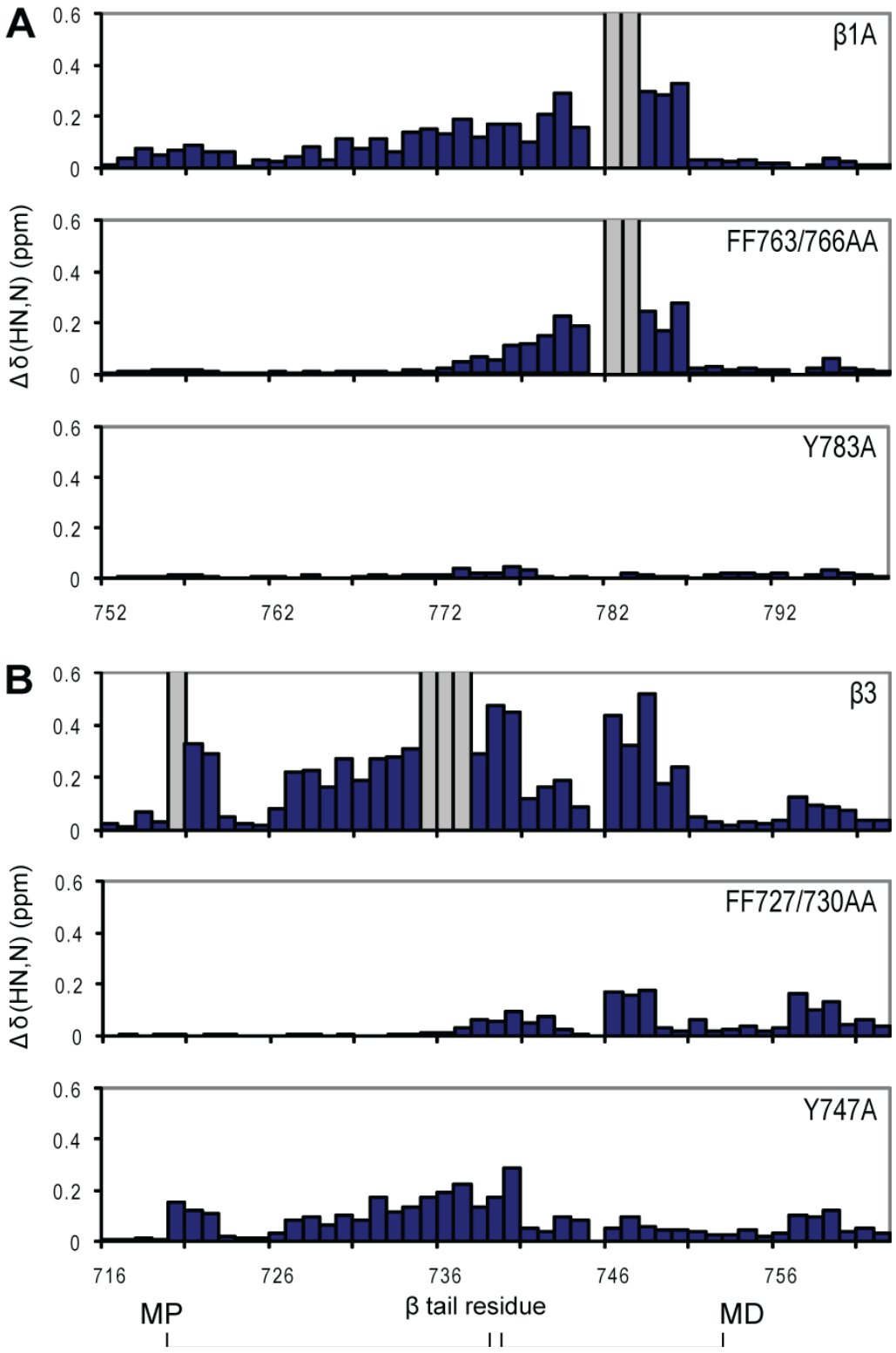

Figure 4.4 Mutations that specifically disrupt the membrane-proximal or membrane-distal portions of the integrin/talin interaction. Chemical shift maps of β1A (A) and β3 (B) tails were generated as in Fig. 4.2, but with mutants affecting either the membrane-proximal portion of the interaction (FF/AA) or the membrane-distal portion of the interaction (Y/A). Membrane-proximal (MP) and membrane-distal (MD) binding sites are noted.

terminal residues form a helix that, while similar to that observed for the MP portion of β3 in complex with talin1, is much better defined. This feature has allowed us to build a new model of integrin activation based on this structure, which is presented in Chapter III. The two talin2 domains are similar in structure to those observed for previous talin1 structures (Garcia-Alvarez *et al.*, 2003; Wegener *et al.*, 2007) (see Chapter III). Although strong electron density is observed for most of the β1D tail, from its N-terminus to P786 (followed by weaker density for the subsequent 2-3 residues), the intervening sequence between the MP helix and the NPxY motif (D776 to E779) is characterized by weaker electron density and multiple conformations in the two integrin peptides in the asymmetric unit (Fig. 4.5). This is likely due in part to nonphysiological crystallographic contacts in this region, which limit the structural insights that can be gleaned from this portion of the tail.

As well as the better defined N-terminal region of the β1D tail, the greatest differences observed between the β1D/talin2 structure and previous β3/talin1 structures lie in the MD portion of the integrin tail. An overlay of the MD region of the β1D structure with the analogous regions from β3 and two other NPxY-like peptides (layilin and PIPK1γ, Fig. 4.6A) bound to talin1 exposes pronounced structural differences in this region (Fig. 4.6B). Two observations are immediately apparent. Firstly, β1D and β3 exhibit strikingly different orientations in their NPxY motifs. Most notably, the orientation of the tyrosine side chain differs between these two peptides by about 90°. Secondly, a loop protrudes from the β1D structure between W775 and the NPxY motif. The sequence alignment of these four peptides shows that the two higher affinity (non-integrin) peptides have a two-residue-shorter linker sequence between the tryptophan residue and the NPxY motif. Although the MD portion of β1D otherwise aligns well to the structure of layilin, these two additional residues are accommodated in an extra loop.

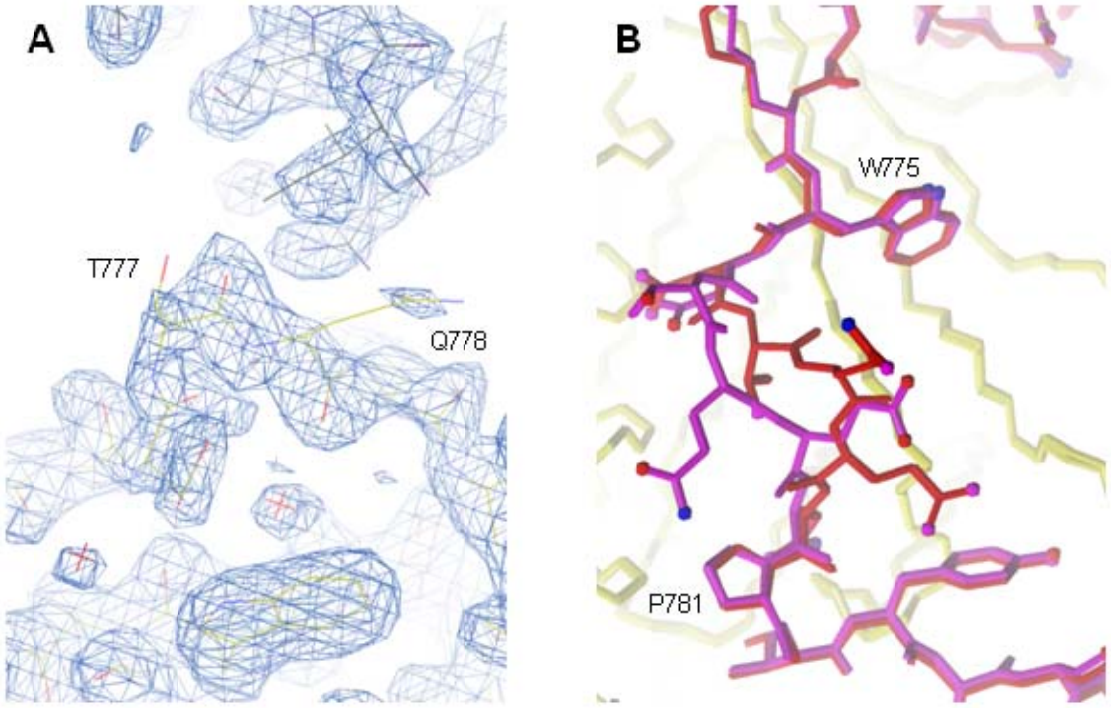

Figure 4.5 Indistinct linker in the β1D/talin2 crystal structure. (A) The linker region between β1D W775 and N780, showing indistinct electron density (sigma 1.0) and a non-physiological crystal contact with part of another integrin tail (in grey). This panel was generated in Coot (Emsley & Cowtan, 2004). (D) The two dimers in the asymmetric unit were superimposed upon one another, and the linker region is shown, illustrating differing conformations only in this region of the integrin tail.

The structure of β3, however, is significantly different, and these two extra residues are accommodated by the different orientation of the NPxY motif itself. In either case, these additional residues correlate with decreased affinity for talin.

To evaluate the role of these additional residues in modulating β1D binding affinity, we replaced them with the shorter sequence from layilin; i.e. β1D residues D776, T777 and Q778 were replaced with a single valine residue ((D776/T777/Q778)V). This dramatically increased the affinity of β1D for talin2 and pushed the kinetics of the interaction into the slow NMR exchange regime (Fig. 4.7). Because this interaction is too tight for accurate K_d determination by NMR, we further characterized it by isothermal titration calorimetry (ITC, Fig. 4.8), yielding a K_d value of 17 nM (ΔG = -44.3 kJ/mol,

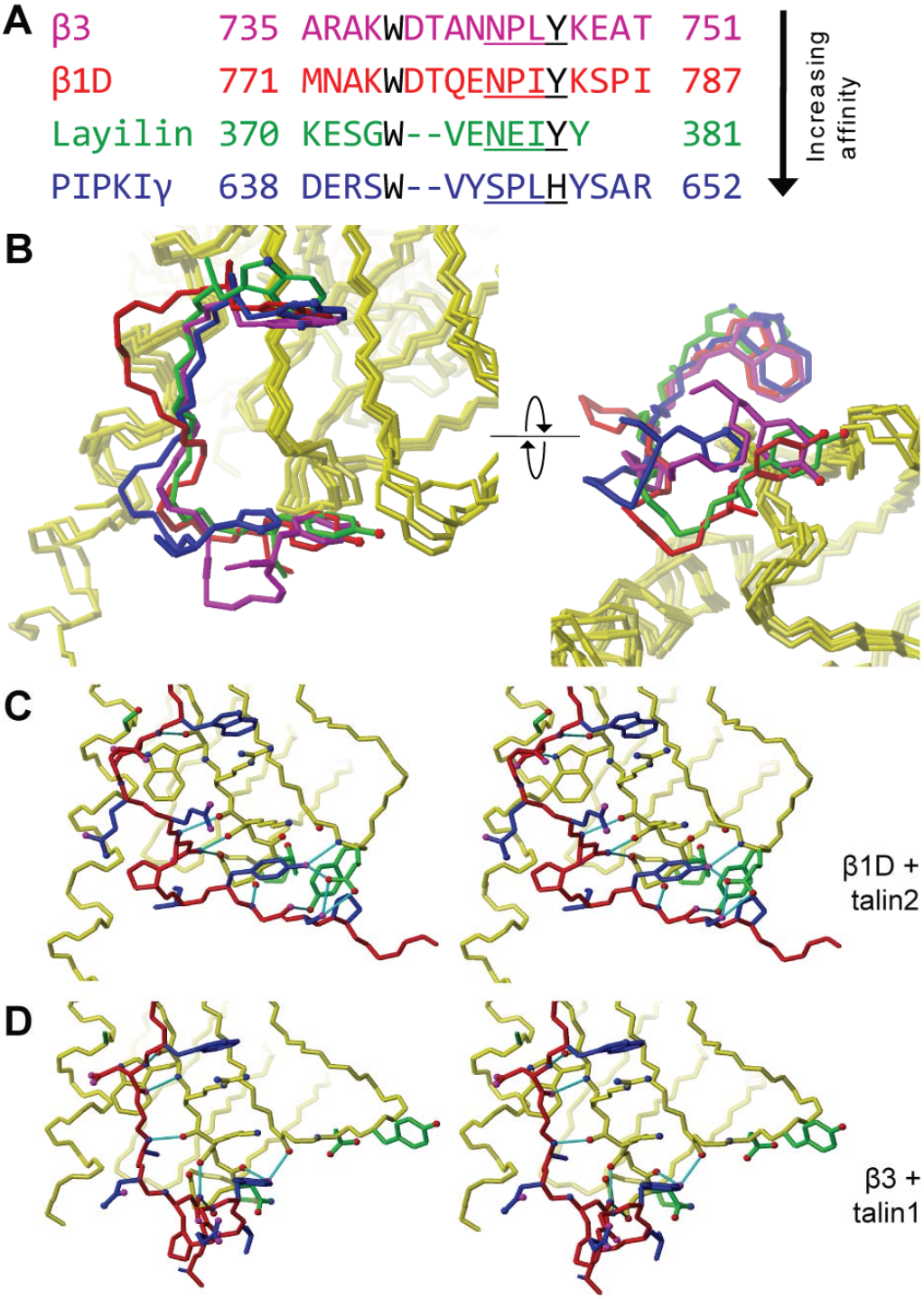

Figure 4.6 Diversity in NPxY motif binding to talin. Sequence (A) and structural (B) alignments of four structures of NPxY motifs bound to the talin F3 domain. The β1D integrin tail (red) is compared with β3 (magenta, PDB 1MK9) (Garcia-Alvarez *et al.*, 2003), layilin (green, PDB 2K00) (Wegener *et al.*, 2008), and PIPK1γ (blue, PDB 2H7E) (Wegener *et al.*, 2007). In each case, the backbone of the talin F3 domain was aligned to the talin F3 backbone in the talin2/β1D structure. The bottom panels, each shown in stereo, compare the NPxY region of the talin2/β1D structure (C) with that of the talin1/β3 structure (1MK9) (D). Talin is shown in yellow, the integrin tail in red. Intermolecular hydrogen bonds are highlighted in cyan. Residues that have been mutated in this study are shown in blue (integrin) or green (talin).

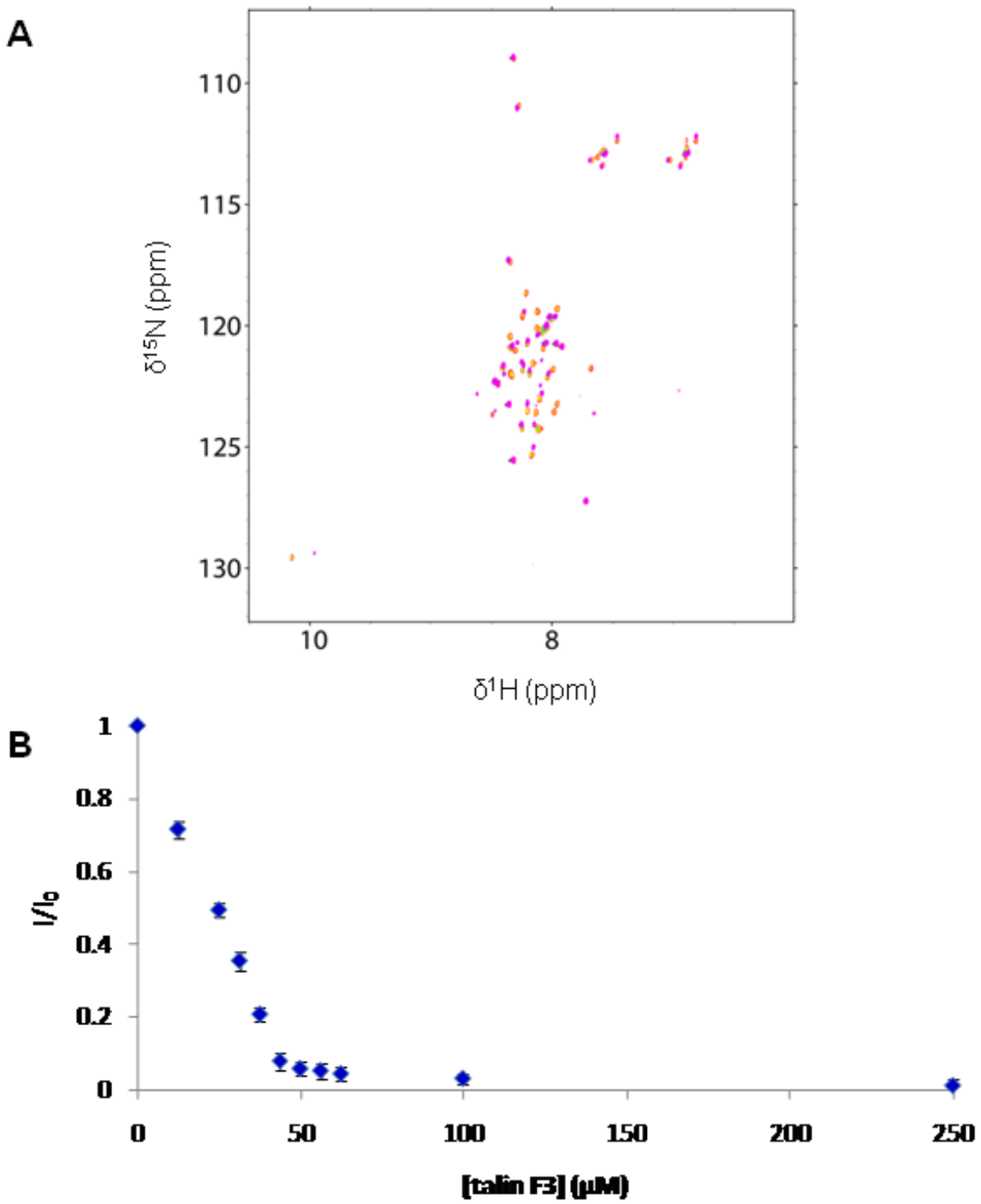

Figure 4.7 Tighter talin binding observed upon shortening of the β1D Linker Sequence. (A) ^{1}H-^{15}N HSQC spectra of 0.05 mM ^{15}N-labelled β1D tail with layilin-like linker shortening mutation with increasing concentrations of talin2 F3 domain: 0 mM (red), 0.0125 mM (tomato), 0.025 mM (orange), 0.03125 mM (yellow), 0.0375 mM (green), 0.04375 mM (cyan), 0.05 mM (light blue), 0.05625 mM (blue), 0.0625 mM (purple), 0.1 mM (maroon), 0.25 mM (magenta). (B) Binding curve used for K_d calculation. The intensity of each peak was recorded for each talin concentration, relative to the intensity with no talin added. Only peaks that began with appreciable signal/noise, were not overlapped, and corresponded to residues within the binding site were used. Each value shows the average of several peaks ± standard error.

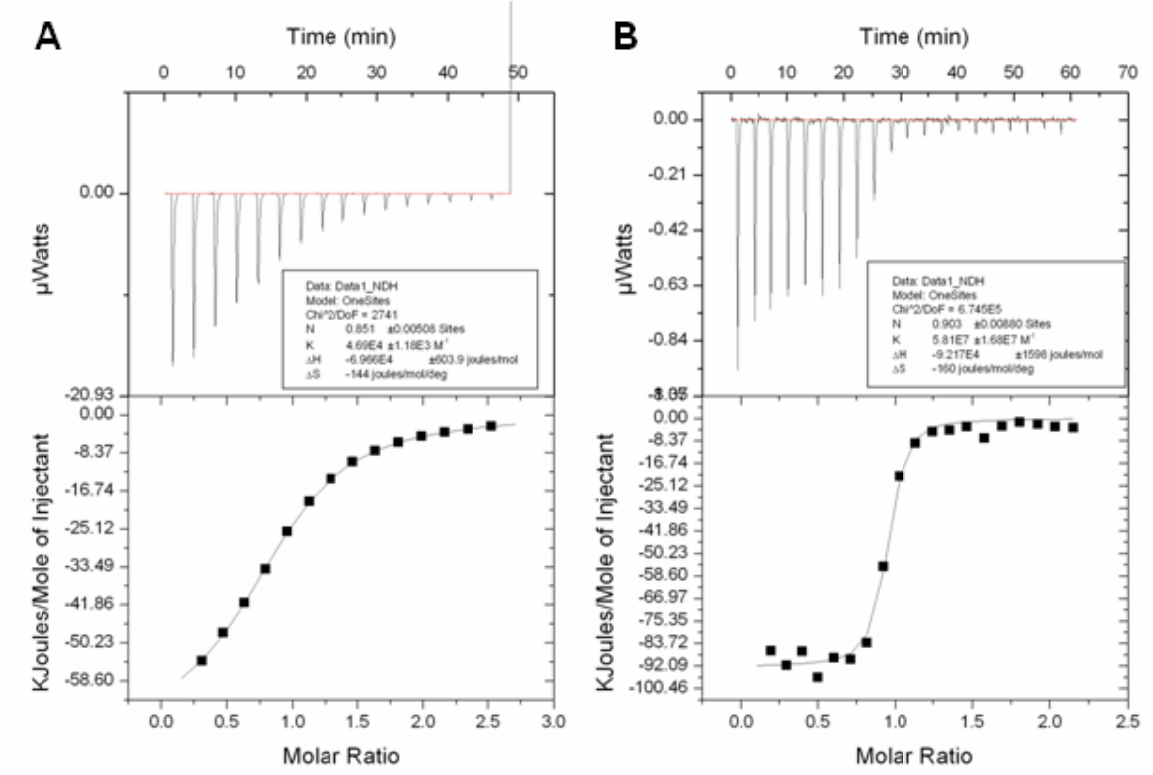

Figure 4.8 ITC analysis of the talin2/β1D interaction. ITC experiments were performed by titrating β1D tail with increasing amounts of talin2 F3 domain. (A) 149 µM β1D WT (200 µL) injected with 1.87 mM talin2 WT (16 x 2.5 µL). (B) 5 µM β1D (D776/T777/Q778)V (200 µL) injected with 50 µM talin2 WT (20 x 2.0 µL).

ΔH = -92.1 kJ/mol, and ΔS = -160 J/mol/K). Characterization of the talin2 interaction with the WT β1D peptide yielded a K_d value of 21.3 µM (ΔG = -26.7 kJ/mol, ΔH = -69.7 kJ/mol, and ΔS = -144 J/mol/K), comparable to the value determined by NMR (Table 4.1). The large increase in binding energy (17.6 kJ/mol) caused by the mutation can be fully attributed to a change in enthalpy. Each interaction exhibits a favourable negative enthalpy, but the affinity of the interaction is diminished by an unfavourable negative entropy. Thus, the presence of these extra residues in integrin tails appears to be a conserved mechanism to reduce the affinity of integrin/talin interactions, presumably to facilitate dynamic turnover of these complexes.

A more detailed comparison of the interaction of the MD portions of β1D and β3 with talin yields additional insights. In particular, this region of β1D has more

intermolecular hydrogen bonds with talin2 than are seen between β3 and talin1 (Fig. 4.6C&D). The residues involved in this hydrogen bonding network are largely conserved between β1A and β1D and between talin1 and talin2. However, many of these residues are also conserved in β3, so other sequence differences must orient β1 in a way that makes the formation of these hydrogen bonds favourable. The structure implies that one of these residues, β1 E779 (N743 in β3), is in a position to form a salt bridge with talin2 K360 (K357 in talin1, Fig. 4.9E), although electron density for this residue was weak due to it bordering the ill-defined linker region. The other residue that differs in the MD portion is I782, which forms extensive contacts with talin2. Mutagenesis studies suggest that the affinity of talin1 for the MD portion of β1A is 1.1 to 1.9 kJ/mol greater than that of β3. (These values are based on the difference in affinity between the two FF/AA mutants the difference in the decrease in affinity caused by the Y/A mutations.) Mutating these two residues in β1A to their β3 counterparts (i.e. β1A E779N/I782L) reduces the affinity of the β1A/talin1 interaction by 1.5 kJ/mol. Introducing the opposite mutations in β3 (N743E/L746I) increases its talin affinity for talin by 0.8 kJ/mol (Table 4.1). Thus, the difference in affinity displayed by these two integrins in the MD region is largely explained by these two residues. Lending weight to this idea is that, in this region, the chemical shift perturbations of β1A E779N/I782L upon binding talin resemble those of β3 WT; the shift map of this region in β3 N743E/L746I is also similar to that of β1A WT (Fig. 4.10). Thus, these residues appear to determine the structural mode of the NPxY/talin interaction.

Another major difference observed between the β1D/talin2 and β3/talin1 structures involves a tyrosine residue from the loop between strands 6 and 7 in the talin F3 domain (talin2 Y376, talin1 Y373). In the β1D/talin2 structure, this tyrosine residue is

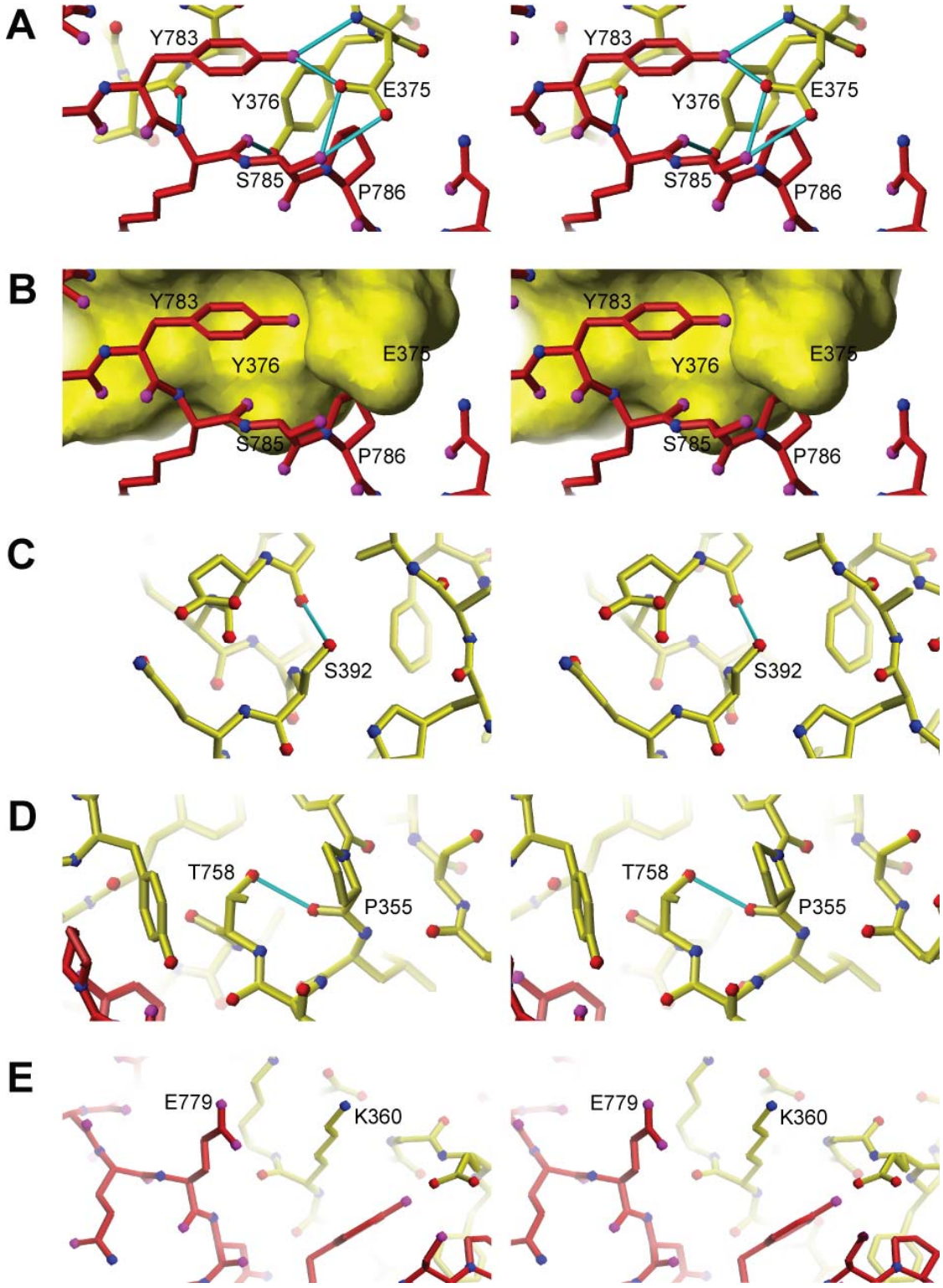

Figure 4.9 The structural basis of β1D/talin2 specificity. All views are shown in stereo. (A) The portion of the β1D/talin2 complex including β1D Y783, S785, and P786 and talin2 E375 and Y376. Talin2 is shown in yellow and β1D in red. Intermolecular hydrogen bonds are shown in cyan. (B) The same view as panel A, but with talin2 shown in space-filling form to illustrate the interface between talin2 Y376 and β1D P786. (C) Talin2 T358, shown forming a hydrogen bond from its side chain to the P355 backbone. (D) Talin2 S392, shown forming a hydrogen bond from its side chain to the G388 backbone. (E) The portion of the complex including β1D E779 and talin2 K360.

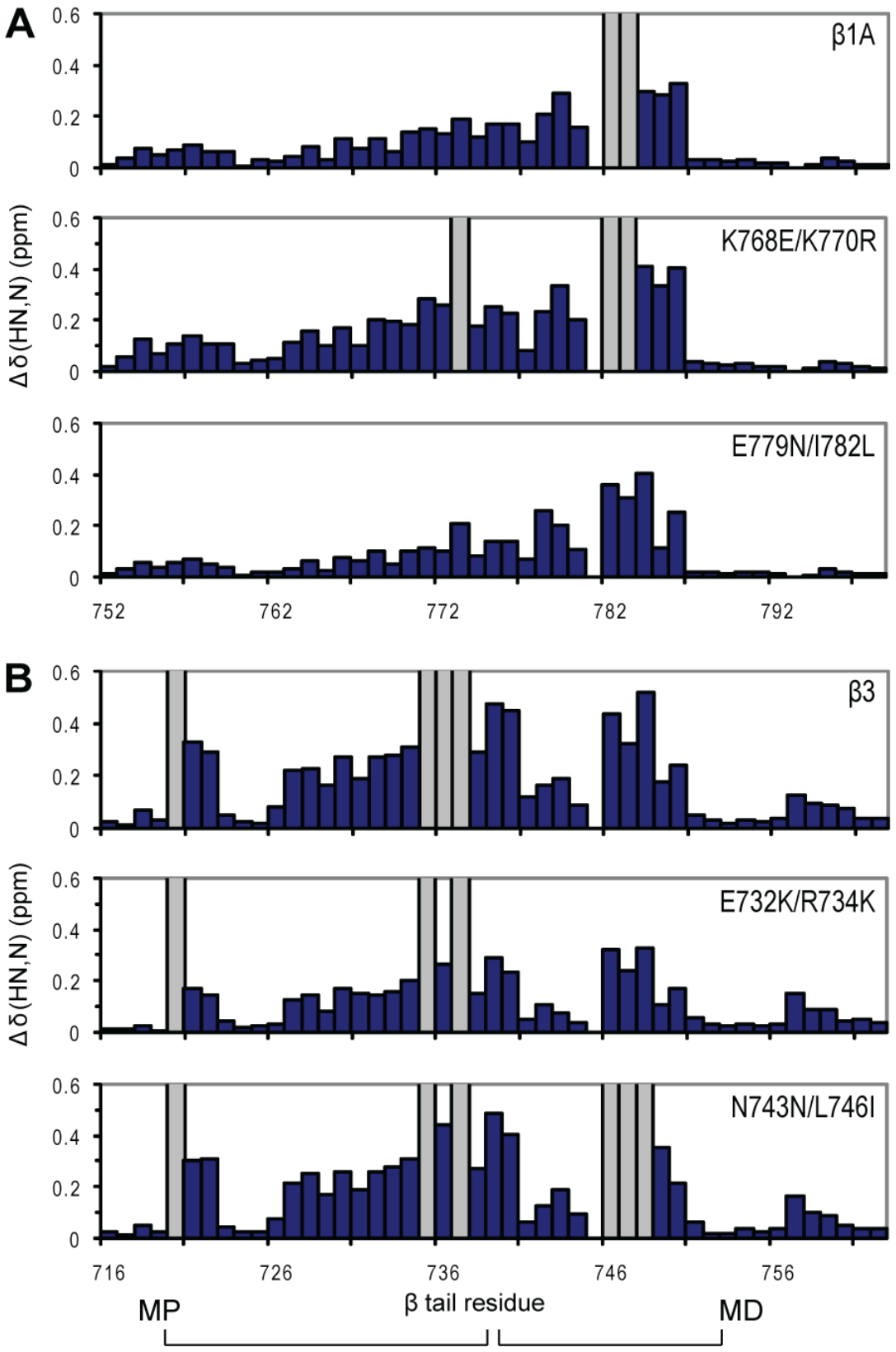

Figure 4.10 Mutations that switch the integrin/talin interaction between β1A-like and β3-like modes. Chemical shift maps of β1A (A) and β3 (B) tails were generated as in Fig. 4.2, but with mutants that made the β1A interaction with talin more β3-like (K768E/K770R in the MP portion, E779N/I782L in the MD portion) or made β3 more β1A-like (E732K/R734K in the MP portion, N743E/L746I in the MD portion).

sandwiched against β1D P786 (as discussed in the next section), and it participates in hydrogen bonding with the β1D backbone (Fig. 4.9A). However, in the β3/talin1 structure, this tyrosine residue and the loop it is located in do not make contact with β3 (Fig. 4.6C). The role of this tyrosine residue was tested by making a talin2 Y376A mutant. As predicted, the mutation had a significant effect on the affinity of the interaction of talin2 with β1D, a slightly smaller but still substantial effect on the interaction with β1A, and a smaller effect still on the interaction with β3 (Table 4.2). The greatly reduced effect of this mutation on the interaction with β3 compared to β1 integrins is consistent with the structural data. The above interaction also brings β1D S785 in position to hydrogen bond with talin2 E375 (as discussed in the following section), and mutation of this residue to the glutamate found in the β3 tail reduces the energy of β1D binding to talin2 by 1.7 kJ/mol (Table 4.1).

4.2.3 Mutual β1D/talin2 specificity explained

Both β1D and talin2 co-localise in the myotendinous junction (Belkin *et al.*, 1997; Conti *et al.*, 2008; Monkley *et al.*, 2001; Senetar *et al.*, 2007), and the tighter binding between these isoforms may allow the junction to withstand the forces exerted by muscle contraction. The cytoplasmic tails of β1A and β1D differ in two regions (Fig. 4.1A). At position 778, between the tryptophan residue and the first NPxY motif, β1A has a glycine and β1D a glutamine. The two tails then differ extensively in their C-termini, from position 786 onward. No significant conclusions can be drawn about the role of residue Q778 due to weak electron density in this region of the β1D/talin2 structure. However, NMR chemical shift mapping experiments reveal much larger perturbations in this region in the β1D/talin2 titration compared with the β1A/talin1, β1A/talin2, and β1D/talin1 titrations (Fig. 4.2). Consistent with this finding, site-directed mutagenesis and affinity

measurements reveal that position 778 explains about 35% of the difference in affinity between β1A and β1D for both talin isoforms (Table 4.3). Although the exact mechanism remains unclear, residue 778 does play a significant role in determining high β1D binding affinity for talin.

The structure does, on the other hand, quite clearly reveal the role of β1D P786 in contributing to this affinity. P786 packs against Y376 in talin2, forming a hydrophobic interface (Fig. 4.9B). This brings together two regions of the integrin tail and the talin2 F3 domain that then form an extensive hydrogen bonding network. This network includes β1D Y783 and S785, talin2 E375, and both backbones. Site-directed mutagenesis of

Table 4.2 Affinity of wild type β tails for talin2 F3 domain mutants

Mutation	K_d (μM)*	ΔG (kJ/mol)†	ΔΔG (kJ/mol)‡	ΔΔG (%)§	$\Delta\Delta G_{1\text{-}2}$ (%)**
β1A					
WT	652 ± 20	-18.18 ± 0.08	-	-	-
Y376A	3,600 est.††	-14	4	23	-
β1D					
WT	36 ± 2.3	-25.36 ± 0.16	-	-	-
P355S	51 ± 2.5	-24.50 ± 0.12	0.85	3	35
T358N	50 ± 2.6	-24.54 ± 0.13	0.82	3	34
E375D	63 ± 3.0	-23.98 ± 0.12	1.38	5	57
Y376A	698 ± 23	-18.01 ± 0.08	7.35	29	-
S392A	54 ± 2.7	-24.33 ± 0.12	1.03	4	43
Q407K	39 ± 2.0	-25.15 ± 0.13	0.21	1	9
β3					
WT	438 ± 15	-19.16 ± 0.09	-	-	-
Y376A	898 ± 26	-17.38 ± 0.07	1.78	9	-

* K_d values were determined by NMR and are given in μM ± standard error.
† ΔG is given for binding and calculated from K_d.
‡ ΔΔG (kJ/mol) is the ΔG value for the mutant integrin binding to talin, minus the ΔG value for the WT integrin binding to talin (a positive value denotes a decrease in affinity)
§ ΔΔG (%) is the percentage of binding energy lost (or gained) by the given mutation (a positive value denotes a decrease in affinity).
** $\Delta\Delta G_{1\text{-}2}$ (%) is the percentage of the difference in binding energy between talin1 and talin2 covered by the given mutation.
†† Approximate K_d values were estimated by comparing magnitude of chemical shift perturbations to those in the WT titration, as described in Chapter II.

Table 4.3 Affinity of β1A vs. β1D for talin F3 domains

Mutation	K_d (μM)*	ΔG (kJ/mol)†	$\Delta\Delta G_{AD}$ (kJ/mol)‡	$\Delta\Delta G_{AD}$ (%)§
Talin1				
Position 778				
β1A G778Q	312 ± 6.5	-20.00 ± 0.05	1.12	28
β1D Q778G	193 ± 5.2	-21.19 ± 0.07	1.76	43
Average			1.44	35
Position 786				
β1A A786P	243 ± 7.5	-20.62 ± 0.08	1.75	43
β1D P786A	269 ± 5.7	-20.37 ± 0.05	2.58	63
Average	-		2.16	53
Both Positions				
β1A G778Q/A786P	135 ± 5.3	-22.08 ± 0.10	3.20	79
β1D Q778G/P786A	388 ± 8.5	-19.46 ± 0.05	3.49	86
Average			3.34	82
β1A vs. β1D				
Actual difference			4.07	-
Talin2				
Position 778				
β1A G778Q	236 ± 5.4	-20.69 ± 0.06	2.52	35
β1D Q778G	97 ± 3.7	-22.90 ± 0.09	2.45	34
Average			2.48	35
Position 786				
β1A A786P	127 ± 6.2	-22.23 ± 0.12	4.05	56
β1D P786A	176 ± 4.7	-21.42 ± 0.07	3.94	55
Average			4.00	56
Both Positions				
β1A G778Q/A786P	57 ± 3.5	-24.19 ± 0.15	6.02	84
β1D Q778G/P786A	369 ± 7.4	-19.59 ± 0.05	5.77	80
Average			5.89	82
β1A vs. β1D				
Actual difference			7.18	-

* K_d values were determined by NMR and are given in μM, ± standard error.
† ΔG is given for binding and calculated from K_d.
‡ $\Delta\Delta G_{AD}$ (kJ/mol) gives the amount by which the free energy of binding is decreased when the β1D residue is mutated to the β1A residue (regardless of which integrin tail the mutation was made in). This value will always be positive.
§ $\Delta\Delta G_{AD}$ (%) is the percentage of the difference in binding energy between β1A and β1D covered by the given mutation.

P786, which is an alanine in β1A, reveal that it contributes about 53% of the difference between the tails for binding to talin1 and 56% of the difference for binding to talin2 (Table 4.3). Thus, P786 is the major contributor to high β1D binding affinity, but this

effect is additive, with Q778 and P786 combined explaining 82% of the difference in talin binding between the β1D and β1A integrin tails.

The difference in talin affinity between β1A and β1D is large and significant (4.07 kJ/mol for talin1 and 7.18 kJ/mol for talin2, Table 4.3, but there is also a smaller difference (2.41 kJ/mol) in binding energy between talin1 and talin2 for β1D (Table 4.1). Examination of the structure reveals that a likely candidate for the source of this difference is talin2 E375, which in talin1 is D372. Although these are two highly similar residues, E375 plays a key role in the interaction between talin2 and β1D, forming part of the extensive interaction between the region just C-terminal to the β1D NPxY motif and the S6-S7 loop in talin2, which includes the β1D P786/talin2 Y376 interaction (Fig. 4.9B). Shortening this glutamate side chain (by mutating it to an aspartate) could disrupt the optimal geometry of this interaction. Indeed, site-directed mutagenesis reveals that position 375 explains 57% of the difference in binding energy between talin1 and talin2 (Table 4.2). Two other nearby talin2-to-talin1 mutations (P355S and T358N) cause smaller effects. A mutation near the linker region of the β1D integrin tail (S392A) also had a significant effect (explaining 42.5% of the difference in affinity between talin1 and talin2), although it was not as large of an effect as E375D. Residues P355, T358, and S392 are involved in talin2-specific intramolecular hydrogen bonds near the β1D interaction site, and they likely stabilize the optimal geometry of talin2 for this interaction (Fig. 4.9C&D).

4.2.4 Entropic basis of membrane-proximal binding differences

One motivation for determining the structure of a β1 integrin tail bound to a talin F3 domain was to understand how differences in talin binding to the MP region of β1 and β3 integrins might relate to differences in integrin activation (Bouaouina *et al.*, 2008; Hato *et*

al., 2008). However, the structure the MP region of β1D bound to talin2 is similar to that of the MP region of β3 bound to talin1 (Fig. 4.11A,B). And, as is the case in the β3 structure, none of the residues that differ between the tails in this region make significant contact with talin, with the exception of β3 R734/β1 K770, which is a conservative substitution. However, a clue as to the biophysical basis of these binding differences has emerged from NMR-based backbone dynamics studies. Heteronuclear NOE experiments of free β3, β1A, and β1D tails reveal that while all three exhibit rapid nanosecond timescale dynamics throughout the tail, indicative of unstructured peptides, a region at the C-terminus of the MP helix of β3 is less flexible compared to the same region in β1A and β1D (Fig. 4.11C). Such a difference in dynamics could explain the observed differences in talin binding to the MP regions of these tails, in that by existing in a more rigid unbound state, there would be a decreased entropic cost for β3 binding to talin (compared to β1), thus increasing its affinity (Kriwacki *et al.*, 1996).

This observation was followed up to see if mutation of this region could make β3 behave like a β1 integrin, and vice versa. Four residues in this region differ between β3 and β1, so the following β3 mutants were constructed: E732K, R734K, A735M, R736N. While A735M and R736N have only minimal effects on β3 affinity for talin1, E732K and R734K cause more significant changes (Table 4.1). A double E732K/R734K mutation demonstrates that this effect is additive, decreasing talin1 binding affinity by 2.5 kJ/mol. The opposite mutation in β1A (K768E/K770R) caused a slightly smaller gain in binding affinity of 1.6 kJ/mol. Mutagenesis studies suggest that the affinity of talin1 for the MP portion of β3 is 2.6 to 3.3 kJ/mol higher for β1A. (This is based on the difference between the two tails in the decrease in affinity caused by the FF/AA mutations and the difference in affinity of talin1 for the two Y/A mutants.) Thus, these mutations reverse most, but not all, of the difference in binding affinity between the MP regions of the β1A and β3 tails.

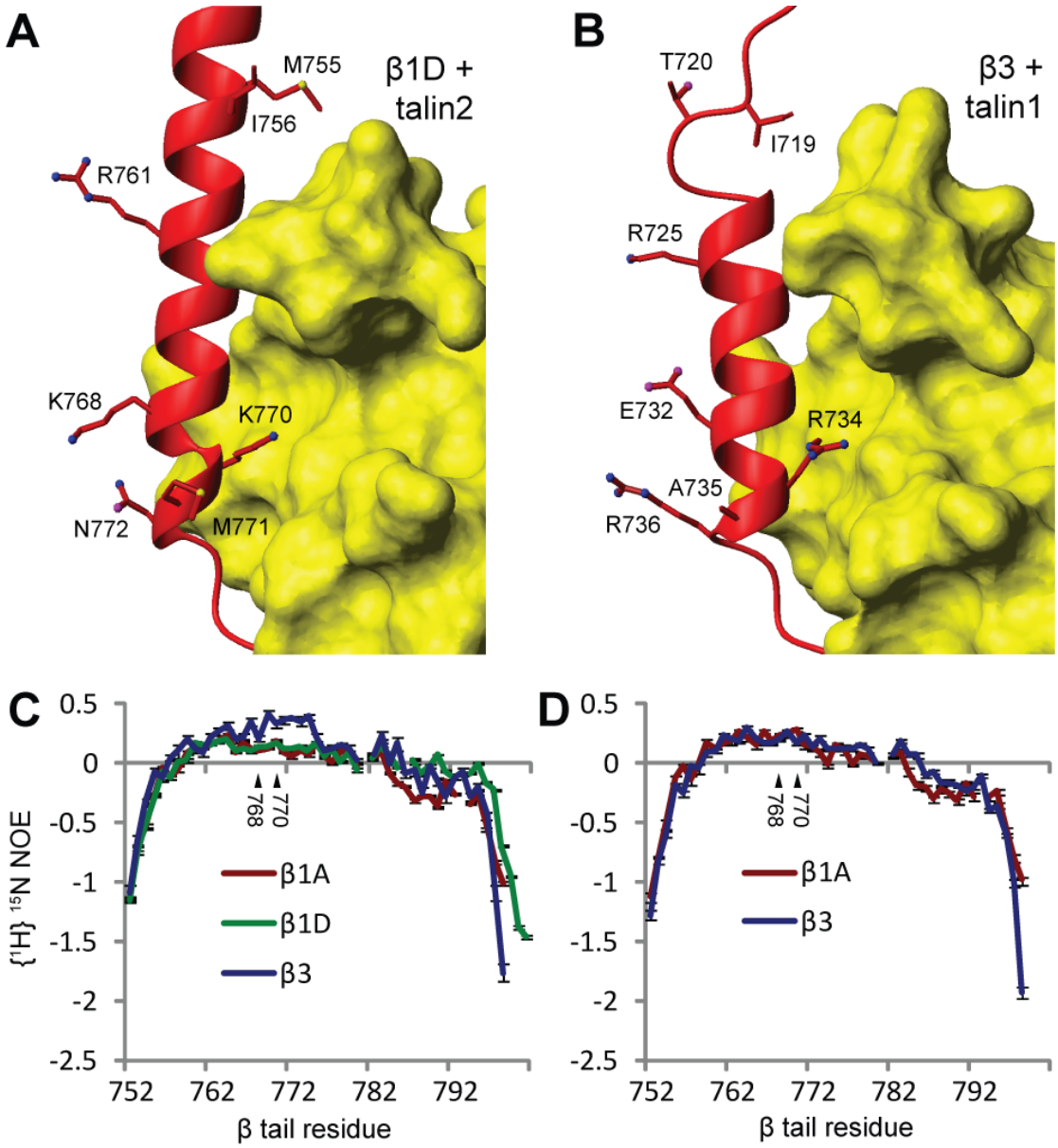

Figure 4.11 Backbone dynamics explain differences between β1 and β3 membrane-proximal interactions. Comparison of membrane-proximal regions of β1D (A) and β3 (B) bound to the talin F3 domain. The image of β3 comes from the β3/PIPK1γ chimera/talin1 F3 structure (PDB 2H7E) (Wegener *et al.*, 2007). Highlighted residues differ between β3 and β1 integrins. (C) Plot of the heteronuclear $\{^{1}H\}$-^{15}N NOE effect versus residue number for β1A, β1D, and β3 in the unbound state. Error bars were generated from spectral noise. (D) Heteronuclear $\{^{1}H\}$-^{15}N NOE plot for mutants that make β1A binding more β3-like (β1A K768E/K770R) or that make β3 binding more β1A-like (β3 E732K/R734K).

Consistent with this, the two mutant integrins exhibit fast timescale dynamics intermediate between those of the β3 and β1A WT tails (Fig. 4.11D).

4.3 Discussion

Integrin structural biology to date has focused largely on the β3 integrin. Now, our recently-solved crystal structure of the β1D/talin2 complex, together with our NMR-based system for performing experiments on a variety of full-length integrin tails, places us in a position to expand these results beyond β3. In doing so, we observe striking differences between integrins. These differences can be correlated with different biological activities, and they allow us to explain aspects of integrin signalling that have emerged from biological studies.

Through NMR studies, we have found that the β3 tail largely relies on a MP interaction for its binding affinity to talin. On the other hand, β1 relies more on the MD region. Whereas the MP binding difference appears to be an entropic effect, the MD difference is enthalpic, due to β1 integrins forming a more extensive hydrogen bonding network with talin in this region. The differences in the MD region are particularly striking, as the tyrosine side chains of the NPxY motifs of the different integrins are rotated by about 90° with respect to one another (Fig. 4.6). The structural consistency in the MP portion of this interaction between integrins hints at a largely conserved mechanism of activation between different integrins. The MD portion, however, where greater heterogeneity is observed, probably increases the affinity of this interaction but is not involved in orienting the integrin for activation.

The much tighter affinity of talin for the striated muscle-specific integrin β1D also stems from the MD region. Most of the difference in affinity between β1A and β1D is explained by β1D P786 (alanine in β1A), which provides a C-terminal cap to this

interaction. This residue forms an extensive hydrophobic interface with talin2 Y376 (Y373 in talin1), setting up more of this favourable β1 hydrogen bonding network with talin. The other major contributor to this increased β1D affinity is Q778 (glycine in β1A), and these two residues together explain 82% of the difference in affinity between β1A and β1D. Talin2 binds to β1D more tightly than talin1, although this is a relatively small difference (only 2.4 kJ/mol in ΔG, compared to the 4.1-7.2 kJ/mol difference in affinity between β1A and β1D). The difference between talin isoforms appears to stem from residues in talin2 that constrain the structure near the integrin binding site through intramolecular hydrogen bonds as well as the more optimal geometry allowed by a glutamate versus aspartate residue for one particular interaction (Fig. 4.9A). The β1D integrin exists in an environment where it is constantly exposed to relatively large forces, particularly in myotendinous junctions and costameres (Belkin *et al.*, 1996). Thus, the fact that this integrin forms tighter complexes with talin than any other studied integrin is consistent with its biological niche.

Bouaouina *et al*. found that the talin1 F2-F3 domain pair alone is able to activate αIIbβ3 but not α5β1 (Bouaouina *et al.*, 2008). We can offer an explanation for this observation from our finding that talin interacts with the β1 MP region weakly, compared with the interaction with this region in β3, due to differences in the intrinsic flexibility of the integrin tail and differing entropic costs upon binding talin. These MP interactions are essential for integrin activation (Wegener *et al.*, 2007). However, it is conceivable that β1 integrins may not require such a tight MP interaction in the cell, whether due to a weaker association between α and β1 TM domains or to other more complex factors. This could relate to the observation that mice with the knock-in β1 D759A mutation show no obvious defect (Czuchra *et al.*, 2006), despite this analogous residue in β3 (D723) having been shown to form a salt bridge with αIIb essential for stabilizing the integrin inactive

state (Lau *et al.*, 2009; Tadokoro *et al.*, 2003; Wegener *et al.*, 2007) as well as an alternative salt bridge with talin upon integrin activation (Chapter III). As this residue has been demonstrated in β3 to be only one of multiple factors (albeit the major one) contributing respectively to inactivation (Hughes *et al.*, 1996; Kim *et al.*, 2009; Lau *et al.*, 2009) and activation, a mechanism of β1 integrin activation in which this interaction plays a more subordinate role could be envisaged.

Beyond explaining previous observations and detailing differences between these integrins, these new results allow us to look critically at previous integrin/talin complex structures. In 2003, Garcia-Alvarez *et al*. reported a crystal structure of a short MD fragment of the β3 tail including the NPxY motif covalently tethered to the talin1 F2-F3 fragment (Garcia-Alvarez *et al.*, 2003). Wegener *et al*. reported a second structure in 2007, solved by NMR, which elucidated the interface between the F3 domain and the β3 MP helix by using a chimeric peptide of the β3 helix attached to a sequence from PIPK1γ that binds tightly to the talin NPxY binding pocket (Wegener *et al.*, 2007). As reported in Chapter III, the talin backbone of the β1D/talin2 structure follows the backbone in both of these structures closely, and with the exception of fraying of the N-terminus in the β3-PIPK1γ solution structure, the structures of the integrin MP regions are similar (see Chapter III). This is an expected outcome, given that there is high sequence identity between the β1 and β3 integrins in this region. However, this region in the β1D structure is better defined, and its orientation is slightly different from that of the β3 structure. Given that the structural determinants of talin binding to the MP region appear to be similar (with differing affinities explained by differences in intrinsic flexibility) the β1D structure may be a more realistic representation of what this region looks like in a biological setting, where the TM helix will tend to stabilise the MP helical character.

The fact that the structures of the MD regions of the β1A and β3 tails are so different could be due to real differences in structure or artefacts of the chimeric construct that Garcia-Alvarez *et al*. used to achieve the structure of the β3 MD region bound to talin1 (Garcia-Alvarez *et al.*, 2003). However, the NMR-based data (both affinity values and chemical shift maps from experiments with WT and mutant tails) are generally consistent with both the talin1 and talin2 structures. The only piece of data that hints at an artefact is that the talin2 Y376A mutation affects the interaction with β3, and this would not be predicted from the talin1 structure. This mutation only reduces the binding energy by 1.8 kJ/mol (compared with 4 kJ/mol for β1A and 7.6 kJ/mol for β1D, Table 4.2), which is small but still significant. This indicates that there is either a difference in β3 binding to talin1 and talin2 in this region, or, more likely, that because the C-terminus of the β3 tail was constrained in the talin1 structure, a weak interaction between the β3 tail and the analogous talin1 residue, Y373, was not observed although it may be biologically relevant.

Today it is well-accepted that protein dynamics play a key role in function, and this perspective has been informed largely by a wide array of robust NMR experiments that have been developed to probe protein dynamics on a variety of timescales (Kay, 1998, 2005; Wand, 2001). NMR-based relaxation methods have been developed to measure conformational entropy in proteins based on nanosecond timescale dynamics (Li et al., 1996; Yang and Kay, 1996; Yang et al., 1997), but these require collecting large data sets and subjecting them to extensive analysis. Here, we perform a series of experiments to show that differences in intrinsic backbone flexibility in integrin tails correlate with variations in affinity for talin. Although a more rigorous and in depth experimental and theoretical treatment would be necessary to make these results more quantitative, these findings still serve as an apt illustration of the role of protein dynamics

in function. NMR-based studies have shown that changes in conformational entropy during protein-protein interactions exert a significant effect on the overall ΔG of the process, affecting the affinity of the interaction (Frederick *et al.*, 2006; Frederick *et al.*, 2007). This effect is particularly pronounced when an intrinsically unstructured peptide is involved (Kriwacki *et al.*, 1996).

Based on the nanosecond timescale dynamics experiments presented here (Fig. 4.11), integrin cytoplasmic tails are intrinsically unstructured peptides, consistent with previously reported results on β3 (Li *et al.*, 2002; Ulmer *et al.*, 2001). As a major hub for protein-protein interactions (Liu *et al.*, 2000), this property of intrinsic disorder is a characteristic that integrin tails share with other hubs (Dunker *et al.*, 2005); it allows them to bind proteins with high specificity (favourable enthalpy) but with low affinity (because of the entropic cost of ordering the unstructured regions) and rapid kinetics (Kriwacki *et al.*, 1996). The ITC data presented here (Fig. 4.8) is also consistent with this idea. The importance of dynamics is highlighted by the fact that relatively small differences in disorder lead to significant differences in talin binding affinity between the MP regions of β1 and β3 integrins. Thus, intrinsic flexibility is one mechanism that integrins employ to maintain dynamic protein-protein interactions, but it is not the only one.

Integrins also exhibit a two-residue insert compared to other talin-binding NPxY-type peptides (Fig. 4.6). This insert considerably decreases the affinity of integrin tails for talin compared to these other peptides; the removal of these extra residues leads to a marked increase in affinity (Table 4.1) and greatly slows the kinetics of the interaction (Fig. 4.7). Thus, despite these extra residues and intrinsic flexibility being suboptimal for high talin binding affinity, it seems that biology has fine-tuned the integrin talin interaction to be relatively weak and highly transient. This is an important characteristic, since a process such as cell migration requires exquisitely fine modulation of integrin

affinity, and the integrin/talin interaction must be tight enough that activation is possible but not so tight that integrins remain constitutively active.

In summary, the data presented here indicate that significant structural diversity exists in how different integrins interact with talin and that these differences correlate with varying biological activities. Much previous work has focused specifically on the β3 integrin; in the future, however, it will be important to consider a more nuanced and heterogeneous picture of integrin activation. Despite these differences, the integrins share many characteristics in common, most notably intrinsic disorder in the C-terminus, which is key for fine-tuning cell adhesiveness.

4.4 References

Belkin, A.M., Retta, S.F., Pletjushkina, O.Y., Balzac, F., Silengo, L., Fassler, R., Koteliansky, V.E., Burridge, K., and Tarone, G. (1997). Muscle beta1D integrin reinforces the cytoskeleton-matrix link: modulation of integrin adhesive function by alternative splicing. J Cell Biol *139*, 1583-1595.

Belkin, A.M., Zhidkova, N.I., Balzac, F., Altruda, F., Tomatis, D., Maier, A., Tarone, G., Koteliansky, V.E., and Burridge, K. (1996). Beta 1D integrin displaces the beta 1A isoform in striated muscles: localization at junctional structures and signaling potential in nonmuscle cells. J Cell Biol *132*, 211-226.

Bouaouina, M., Lad, Y., and Calderwood, D.A. (2008). The N-terminal domains of talin cooperate with the phosphotyrosine binding-like domain to activate beta1 and beta3 integrins. J Biol Chem *283*, 6118-6125.

Calderwood, D.A., Fujioka, Y., de Pereda, J.M., Garcia-Alvarez, B., Nakamoto, T., Margolis, B., McGlade, C.J., Liddington, R.C., and Ginsberg, M.H. (2003). Integrin beta cytoplasmic domain interactions with phosphotyrosine-binding domains: a structural prototype for diversity in integrin signaling. Proc Natl Acad Sci U S A *100*, 2272-2277.

Calderwood, D.A., Yan, B., de Pereda, J.M., Alvarez, B.G., Fujioka, Y., Liddington, R.C., and Ginsberg, M.H. (2002). The phosphotyrosine binding-like domain of talin activates integrins. J Biol Chem *277*, 21749-21758.

Conti, F.J., Felder, A., Monkley, S., Schwander, M., Wood, M.R., Lieber, R., Critchley, D., and Muller, U. (2008). Progressive myopathy and defects in the maintenance of myotendinous junctions in mice that lack talin 1 in skeletal muscle. Development *135*, 2043-2053.

Czuchra, A., Meyer, H., Legate, K.R., Brakebusch, C., and Fassler, R. (2006). Genetic analysis of beta1 integrin "activation motifs" in mice. J Cell Biol *174*, 889-899.

Dunker, A.K., Cortese, M.S., Romero, P., Iakoucheva, L.M., and Uversky, V.N. (2005). Flexible nets. The roles of intrinsic disorder in protein interaction networks. FEBS J *272*, 5129-5148.

Fassler, R., and Meyer, M. (1995). Consequences of lack of beta 1 integrin gene expression in mice. Genes Dev *9*, 1896-1908.

Frederick, K.K., Kranz, J.K., and Wand, A.J. (2006). Characterization of the backbone and side chain dynamics of the CaM-CaMKIp complex reveals microscopic contributions to protein conformational entropy. Biochemistry *45*, 9841-9848.

Frederick, K.K., Marlow, M.S., Valentine, K.G., and Wand, A.J. (2007). Conformational entropy in molecular recognition by proteins. Nature *448*, 325-329.

Garcia-Alvarez, B., de Pereda, J.M., Calderwood, D.A., Ulmer, T.S., Critchley, D., Campbell, I.D., Ginsberg, M.H., and Liddington, R.C. (2003). Structural determinants of integrin recognition by talin. Mol Cell *11*, 49-58.

Hato, T., Yamanouchi, J., Tamura, T., Yakushijin, Y., Sakai, I., and Yasukawa, M. (2008). Cooperative role of the membrane-proximal and -distal residues of the integrin beta3 cytoplasmic domain in regulation of talin-mediated alpha IIb beta3 activation. J Biol Chem *283*, 5662-5668.

Hodivala-Dilke, K.M., McHugh, K.P., Tsakiris, D.A., Rayburn, H., Crowley, D., Ullman-Cullere, M., Ross, F.P., Coller, B.S., Teitelbaum, S., and Hynes, R.O. (1999). Beta3-integrin-deficient mice are a model for Glanzmann thrombasthenia showing placental defects and reduced survival. J Clin Invest *103*, 229-238.

Hughes, P.E., Diaz-Gonzalez, F., Leong, L., Wu, C., McDonald, J.A., Shattil, S.J., and Ginsberg, M.H. (1996). Breaking the integrin hinge. A defined structural constraint regulates integrin signaling. J Biol Chem *271*, 6571-6574.

Hynes, R.O. (2002). Integrins: bidirectional, allosteric signaling machines. Cell *110*, 673-687.

Kay, L.E. (1998). Protein dynamics from NMR. Nat Struct Biol *5 Suppl*, 513-517.

Kay, L.E. (2005). NMR studies of protein structure and dynamics. J Magn Reson *173*, 193-207.

Kim, C., Lau, T.L., Ulmer, T.S., and Ginsberg, M.H. (2009). Interactions of platelet integrin alphaIIb and beta3 transmembrane domains in mammalian cell membranes and their role in integrin activation. Blood *113*, 4747-4753.

Koradi, R., Billeter, M., and Wuthrich, K. (1996). MOLMOL: a program for display and analysis of macromolecular structures. J Mol Graph *14*, 51-55, 29-32.

Kriwacki, R.W., Hengst, L., Tennant, L., Reed, S.I., and Wright, P.E. (1996). Structural studies of p21Waf1/Cip1/Sdi1 in the free and Cdk2-bound state: conformational disorder mediates binding diversity. Proc Natl Acad Sci U S A *93*, 11504-11509.

Lau, T.L., Kim, C., Ginsberg, M.H., and Ulmer, T.S. (2009). The structure of the integrin alphaIIbbeta3 transmembrane complex explains integrin transmembrane signalling. EMBO J *28*, 1351-1361.

Lau, T.L., Partridge, A.W., Ginsberg, M.H., and Ulmer, T.S. (2008). Structure of the integrin beta3 transmembrane segment in phospholipid bicelles and detergent micelles. Biochemistry *47*, 4008-4016.

Li, R., Babu, C.R., Valentine, K., Lear, J.D., Wand, A.J., Bennett, J.S., and DeGrado, W.F. (2002). Characterization of the monomeric form of the transmembrane and cytoplasmic domains of the integrin beta 3 subunit by NMR spectroscopy. Biochemistry *41*, 15618-15624.

Li, Z., Raychaudhuri, S., and Wand, A.J. (1996). Insights into the local residual entropy of proteins provided by NMR relaxation. Protein Sci *5*, 2647-2650.

Liu, S., Calderwood, D.A., and Ginsberg, M.H. (2000). Integrin cytoplasmic domain-binding proteins. J Cell Sci *113 (Pt 20)*, 3563-3571.

Luo, B.H., Carman, C.V., and Springer, T.A. (2007). Structural basis of integrin regulation and signaling. Annu Rev Immunol *25*, 619-647.

Monkley, S.J., Pritchard, C.A., and Critchley, D.R. (2001). Analysis of the mammalian talin2 gene TLN2. Biochem Biophys Res Commun *286*, 880-885.

O'Toole, T.E., Katagiri, Y., Faull, R.J., Peter, K., Tamura, R., Quaranta, V., Loftus, J.C., Shattil, S.J., and Ginsberg, M.H. (1994). Integrin cytoplasmic domains mediate inside-out signal transduction. J Cell Biol *124*, 1047-1059.

Senetar, M.A., Moncman, C.L., and McCann, R.O. (2007). Talin2 is induced during striated muscle differentiation and is targeted to stable adhesion complexes in mature muscle. Cell Motil Cytoskeleton *64*, 157-173.

Tadokoro, S., Shattil, S.J., Eto, K., Tai, V., Liddington, R.C., de Pereda, J.M., Ginsberg, M.H., and Calderwood, D.A. (2003). Talin binding to integrin beta tails: a final common step in integrin activation. Science *302*, 103-106.

Ulmer, T.S., Yaspan, B., Ginsberg, M.H., and Campbell, I.D. (2001). NMR analysis of structure and dynamics of the cytosolic tails of integrin alpha IIb beta 3 in aqueous solution. Biochemistry *40*, 7498-7508.

Vinogradova, O., Vaynberg, J., Kong, X., Haas, T.A., Plow, E.F., and Qin, J. (2004). Membrane-mediated structural transitions at the cytoplasmic face during integrin activation. Proc Natl Acad Sci U S A *101*, 4094-4099.

Vinogradova, O., Velyvis, A., Velyviene, A., Hu, B., Haas, T., Plow, E., and Qin, J. (2002). A structural mechanism of integrin alpha(IIb)beta(3) "inside-out" activation as regulated by its cytoplasmic face. Cell *110*, 587-597.

Wand, A.J. (2001). Dynamic activation of protein function: a view emerging from NMR spectroscopy. Nat Struct Biol *8*, 926-931.

Wegener, K.L., Basran, J., Bagshaw, C.R., Campbell, I.D., Roberts, G.C., Critchley, D.R., and Barsukov, I.L. (2008). Structural basis for the interaction between the cytoplasmic domain of the hyaluronate receptor layilin and the talin F3 subdomain. J Mol Biol *382*, 112-126.

Wegener, K.L., Partridge, A.W., Han, J., Pickford, A.R., Liddington, R.C., Ginsberg, M.H., and Campbell, I.D. (2007). Structural basis of integrin activation by talin. Cell *128*, 171-182.

Weljie, A.M., Hwang, P.M., and Vogel, H.J. (2002). Solution structures of the cytoplasmic tail complex from platelet integrin alpha IIb- and beta 3-subunits. Proc Natl Acad Sci U S A *99*, 5878-5883.

Xiong, J.P., Stehle, T., Diefenbach, B., Zhang, R., Dunker, R., Scott, D.L., Joachimiak, A., Goodman, S.L., and Arnaout, M.A. (2001). Crystal structure of the extracellular segment of integrin alpha Vbeta3. Science *294*, 339-345.

Xiong, J.P., Stehle, T., Goodman, S.L., and Arnaout, M.A. (2004). A novel adaptation of the integrin PSI domain revealed from its crystal structure. J Biol Chem *279*, 40252-40254.

Xiong, J.P., Stehle, T., Zhang, R., Joachimiak, A., Frech, M., Goodman, S.L., and Arnaout, M.A. (2002). Crystal structure of the extracellular segment of integrin alpha Vbeta3 in complex with an Arg-Gly-Asp ligand. Science *296*, 151-155.

Yang, D., and Kay, L.E. (1996). Contributions to conformational entropy arising from bond vector fluctuations measured from NMR-derived order parameters: application to protein folding. J Mol Biol *263*, 369-382.

Yang, D., Mok, Y.K., Forman-Kay, J.D., Farrow, N.A., and Kay, L.E. (1997). Contributions to protein entropy and heat capacity from bond vector motions measured by NMR spin relaxation. J Mol Biol *272*, 790-804.

Zhu, J., Luo, B.H., Xiao, T., Zhang, C., Nishida, N., and Springer, T.A. (2008). Structure of a complete integrin ectodomain in a physiologic resting state and activation and deactivation by applied forces. Mol Cell *32*, 849-861.

CHAPTER V: INTEGRIN TYROSINE PHOSPHORYLATION

5.1 Introduction

The different β integrins found in mammals occupy unique biological niches (Hynes, 2002) and show significant diversity in their protein-protein interactions. Of the six β integrins tails that display a high level of sequence homology to one another (β1, β2, β3, β5, β6, and β7), all contain two NPxY or NPxY-like motifs—a near membrane-distal (nMD) site and a far membrane-distal (fMD) site—that bind to phosphotyrosine-binding (PTB) domains (including the talin F3 domain) (Calderwood *et al.*, 2003) and are potential phosphorylation sites. In the β2 tail, however, both tyrosine residues are substituted with phenylalanine, and in the β7 tail, this substitution occurs in the fMD site. Uniquely, the β7 tail also exhibits two additional membrane-proximal (MP) tyrosine phosphorylation sites that are not part of an NPxY motif (Krissansen *et al.*, 2006).

This chapter explores three of these integrins: β3, β1A (the most common splice variant of β1), and β7 (Fig. 5.1A). Previous studies on integrin tyrosine phosphorylation have generally focused on two of these: β3 and β1. When the β1 integrin was first isolated and sequenced, a potential tyrosine phosphorylation site was proposed (Tamkun *et al.*, 1986), and an early study observed β1 tyrosine phosphorylation in response to transformation of cells with viral Src (v-Src) (Hirst *et al.*, 1986); this was followed by the direct demonstration of tyrosine phosphorylation of β1 by v-Src *in vitro* (Tapley *et al.*, 1989). These studies used a viral protein, but it was later shown that αIIbβ3 is tyrosine-phosphorylated in response to platelet activation, and that cellular Src (c-Src) and related tyrosine kinases phosphorylate β3 *in vitro* (Law *et al.*, 1996). Studies suggest that β1 interacts with various Src family kinases and that these kinases are activated by integrin engagement with the extracellular matrix (Arias-Salgado *et al.*, 2003; Arias-Salgado *et*

al., 2005; Hood *et al.*, 2003; Huveneers *et al.*, 2008; Klinghoffer *et al.*, 1999; Lowell, 2004; Miller *et al.*, 1999; Ulanova *et al.*, 2005). There is also evidence for a direct and constitutive interaction between β3 and c-Src (Shattil, 2005).

Various studies have demonstrated that tyrosine phosphorylation of β1 influences integrin localization and activity, as well as cell morphology. An early study showed that transformation of cells with Rous sarcoma virus—which expresses v-Src—leads to β1 integrins adopting a more diffuse distribution on the cell surface, rather than being localized in focal contacts. Transformed cells also display rounding, decreased fibronectin matrix assembly, and decreased cell migration (Hirst *et al.*, 1986). Another study found that while unphosphorylated β1 integrins localize to focal contacts, phosphorylated integrins localize to podosomes (Johansson *et al.*, 1994).

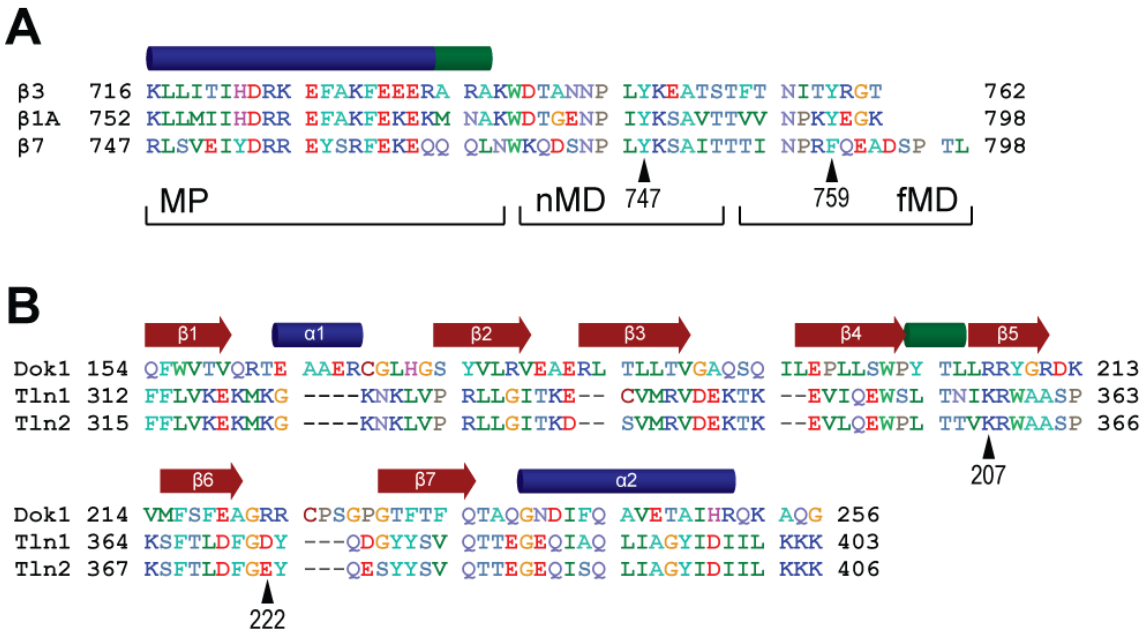

Figure 5.1 Integrin tail and PTB domain sequence alignments. (A) Sequences of the cytoplasmic regions of the β3, β1A, and β7 integrin tails. The two NPxY motif tyrosine residues are highlighted, with β3 numbering. The membrane-proximal (MP), near membrane-distal (nMD), and far membrane-distal (fMD) regions are denoted. Secondary structure is based on the structure of the β1D/talin2 complex, with α helices denoted in blue and 3_{10} helices in green. (B) Sequences of the PTB domains of Dok1, talin1, and talin2 aligned by secondary structure, with secondary structure elements from the Dok1 PTB domain structure (PDB 2V76) (Oxley *et al.*, 2008) shown. Notable residues are highlighted with Dok1 numbering.

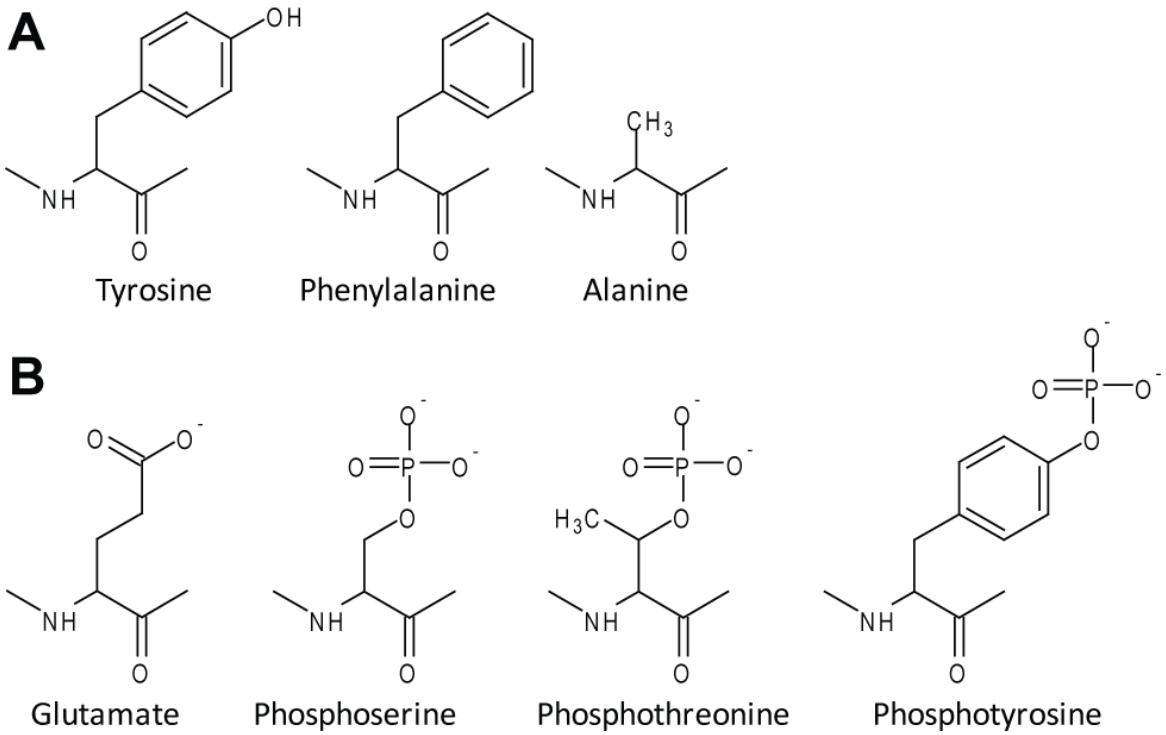

Figure 5.2 Mutations for studying phosphorylation. (A) The structures of tyrosine and two amino acids that a tyrosine residue is often substituted with in functional studies: phenylalanine and alanine. Phenylalanine is identical to tyrosine, with the exception of the absence of the phosphorylatable hydroxyl group. Thus, a phenylalanine mutation is often used to make the residue non-phosphorylatable. Alanine, on the other hand, lacks the aromatic ring present in tyrosine and phenylalanine, so a mutation to alanine effectively removes the tyrosine side chain. (B) The structures of glutamate, phosphoserine, phosphothreonine, and phosphotyrosine. A comparison of these structures reveals why glutamate is often used to mimic phosphoserine or phosphothreonine. The negative charge in glutamate is centred about the carboxyl carbon atom, which is located three bonds from Cα. Analogously, the phosphorous atom—around which the negative charge is centred in phosphoserine and phosphothreonine—is also located three bonds away from Cα. In phosphotyrosine, however, this negative centre is located seven bonds away from Cα, and these two residues display few other structural similarities—indicating that there is not a sound structural basis for the use of glutamate as a phosphotyrosine-mimicking substitution.

Further insight has come from studies using non-phosphorylatable integrins with Y-to-F mutations (Fig. 5.2A). A Y783F mutation in the β1 nMD site reverses the effects of v-Src (Sakai *et al.*, 2001). Fibroblasts expressing β1 Y783F, Y795F, or YY783/795FF display impaired directed cell migration but increased fibronectin binding (Sakai *et al.*, 1998), and YY783/795FF also causes slowed cell spreading and decreased focal adhesion

kinase activation (Wennerberg *et al.*, 2000). In β3, the nMD mutation Y747F disrupts adhesion and clot retraction in hematopoietic cells (Blystone *et al.*, 1997). More tellingly, mice with the knock-in double YY747/759FF mutation in β3 display a severe bleeding defect (Law *et al.*, 1999), although, surprisingly, mice with the analogous β1 knock-in mutation show no significant phenotype (Chen *et al.*, 2006; Czuchra *et al.*, 2006).

The role of tyrosine phosphorylation in outside-in β3 signalling is relatively well-established (Blystone *et al.*, 1997; Butler & Blystone, 2005; Chandhoke *et al.*, 2004; Cowan *et al.*, 2000; Gao *et al.*, 2005; Jenkins *et al.*, 1998; Kirk *et al.*, 2000; Law *et al.*, 1999; Prasad *et al.*, 2003; Xi *et al.*, 2006). The role in inside-out integrin activation is less clear, but various lines of evidence indicate that phosphorylation negatively regulates activation. Most significantly, tyrosine phosphorylation of αVβ3 decreases the affinity of live cells for fibronectin (Datta *et al.*, 2002), and phosphorylation of β1 decreases its affinity for fibronectin *in vitro* (Tapley *et al.*, 1989).

Dok1 is a signalling protein with a PTB domain capable of binding integrins (Calderwood *et al.*, 2003). Dok1 negatively regulates β3 integrin activation (Wegener *et al.*, 2007), an observation initially difficult to explain due to the very weak interaction observed between these proteins. We subsequently reported that tyrosine phosphorylation greatly increases Dok1 affinity for short β3 peptides while slightly decreasing talin1 affinity, observations that led to an initial structural explanation for this phenomenon (Fig. 5.3) (Oxley *et al.*, 2008). However, these findings did not clarify the specific roles of the different NPxY motifs or indicate whether this mechanism could be generalized across different integrins. Here, we explore the phosphorylation dependence of the talin1 and Dok1 interactions with full-length β3, β1A, and β7 tails. We show that tyrosine phosphorylation is a common mechanism for regulating the affinity of these proteins for integrin tails, and the crystal structure of a talin/β1 complex presented in Chapter III

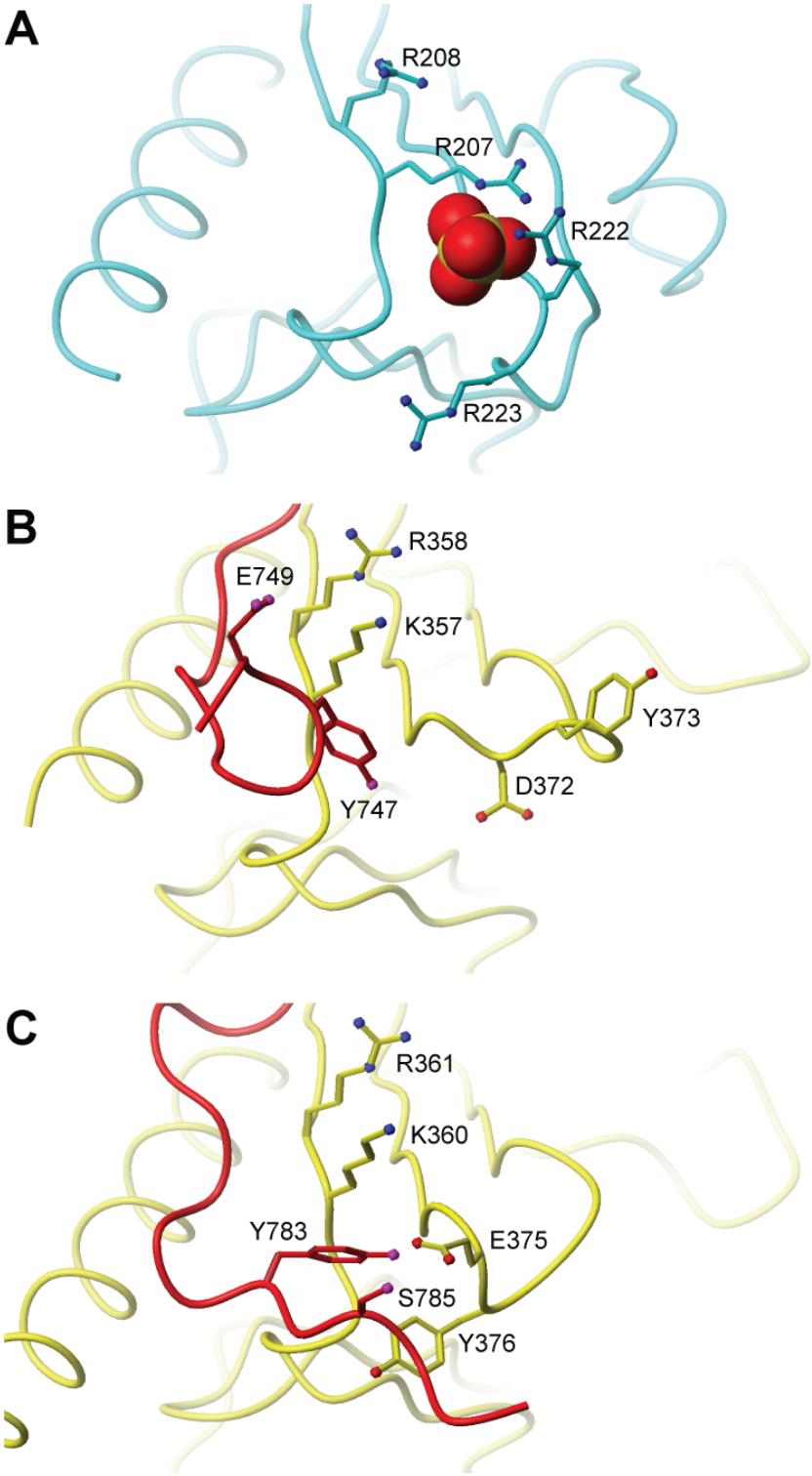

Figure 5.3 The structural basis of Dok1 specificity for phosphorylated integrin tails. (A) Detail of the Dok1 PTB domain structure (PDB 2V76) (Oxley *et al.*, 2008) showing a sulphate anion located in the NPxY binding pocket. Key positively-charged residues are highlighted. (B) Detail of the NPxY motif of the β3 integrin tail bound to the talin1 F3 domain (PDB 1MK9) (Garcia-Alvarez *et al.*, 2003). (C) Detail of the NPxY motif of the β1D tail bound to the talin2 F3 domain (PDB 3G9W). The residues highlighted in panels B and C are analogous to those highlighted in the Dok1 structure in panel A. Molecular images were generated with MOLMOL (Koradi *et al.*, 1996).

allows us to explain subtle differences between different integrins. We also describe the structural basis of this phosphorylation state specificity in detail and generate a talin mutant that shows preferential binding for phosphorylated integrin tails.

5.2 Results

5.2.1 Production of tyrosine-phosphorylated integrin tails for NMR

Before the current study, structural work on integrin phosphorylation had involved short chemically-synthesized integrin tail fragment peptides (Oxley *et al.*, 2008). However, in Chapter II we present a robust system for studying integrin cytoplasmic protein-protein interactions by NMR using full-length ^{15}N-labelled integrin tails produced in *E. coli*. This system is cost-effective and versatile, but using such a system to produce tyrosine-phosphorylated peptides presents additional difficulties; modified residues can be incorporated directly during chemical peptide synthesis, but not in *E. coli*. Although glutamate can be introduced, by mutagenesis, to make an acceptable mimic for phosphoserine or phosphothreonine, phosphotyrosine has no natural analogue (Fig. 5.2B). Thus, the integrin tails would have to be phosphorylated directly.

Various methods were attempted to phosphorylate tyrosines in ^{15}N-labelled integrin tails, including *in vitro* phosphorylation with commercially-purchased c-Src (Upstate) (Fig. 5.4A) and *in vivo* phosphorylation with TKB1 cells (Stratagene) (Fig. 5.4B). Src had previously been used for *in vitro* phosphorylation of integrin tails (Kirk *et al.*, 2000; Law *et al.*, 1996), but not on a scale large enough for structural biology. Initial attempts at producing tyrosine-phosphorylated integrin tails used full-length c-Src from Upstate in a method similar to that described in Chapter II, but using much less Src. These trials revealed that c-Src will phosphorylate β3 and that the phosphorylated product can be separated from the unphosphorylated tail; but, the reaction is relatively inefficient.

For example, the total amount of integrin tail in the experiment shown in Fig. 5.4A would have been enough, roughly, for one NMR experiment. However, only a small fraction of the integrin was phosphorylated. Producing just this small amount required 1.5 units (2 μg) of Src (costing roughly 50 GBP). Due to the low efficiency of this reaction, producing just one NMR sample by this method would require several fold more material—and would cost several hundreds or even thousands of pounds. Despite this, these early attempts were successful in that they indicated that c-Src could phosphorylate both β1A and β3, and that it could phosphorylate β3 at both the nMD and fMD positions—as observed by autoradiography (Fig. 5.5). A second approach attempted was *in vivo* tyrosine phosphorylation in *E. coli*. For this purpose, TKB1 cells (Stratagene) were used, which express trp-inducible Elk, a promiscuous tyrosine kinase (Lhotak *et al.*, 1991). However, we observed that the induction of this tyrosine kinase was toxic to *E. coli*, as demonstrated by bacterial growth curves (Fig. 5.4B). Due to the toxicity of this tyrosine kinase to the bacteria, yields were low and not sufficient for NMR experiments.

However, we were eventually able to produce NMR-scale quantities of tyrosine-phosphorylated ^{15}N-labelled integrin tails by performing *in vitro* phosphorylation using Src kinase domain produced in house (Fig. 5.4C). To mitigate tyrosine kinase toxicity to bacteria, we produced the Src kinase domain in *E. coli* by coexpressing it with YopH phosphatase, as previously described by John Kuriyan's group (Seeliger *et al.*, 2005). By producing c-Src kinase domain and using it to phosphorylate integrin tails as described in Chapter II, we were able to produce sufficient quantities of integrin tails for NMR experiments. Experience indicates that the efficiency of this reaction is limited primarily by integrin solubility (i.e. efficiency approaches 100% when the entire population of the integrin tail remains in solution). In the example shown in Fig. 5.4C, roughly half of β3

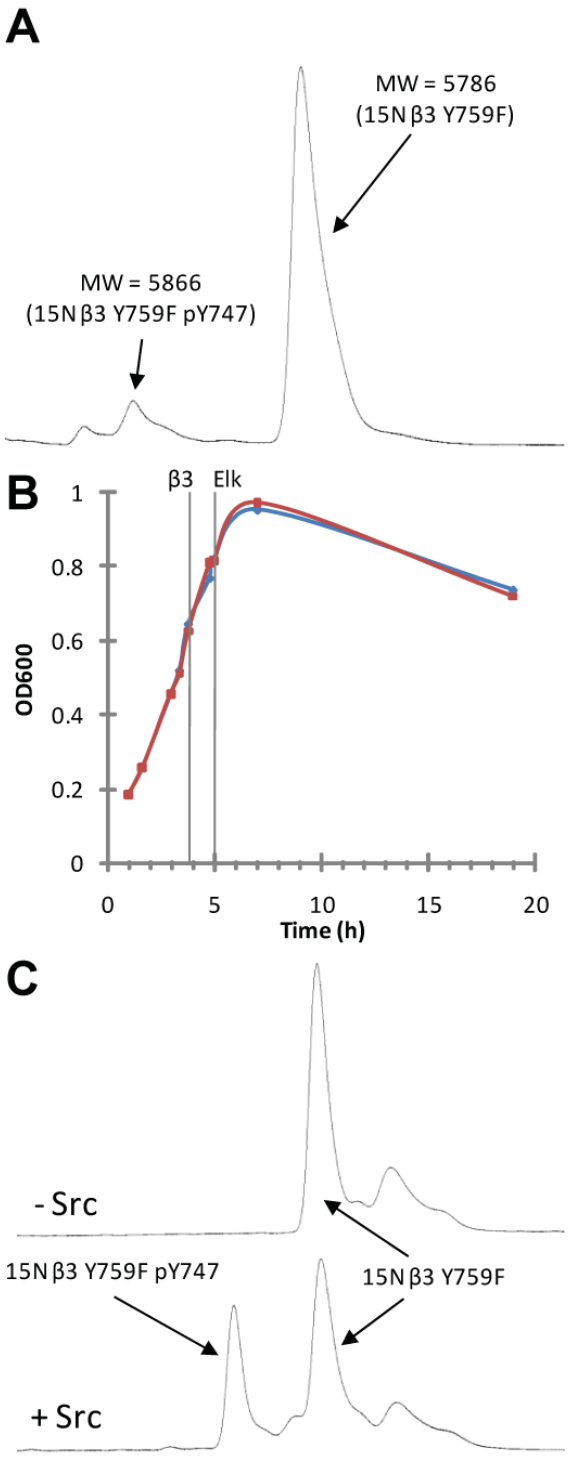

Figure 5.4 Unsuccessful and successful attempts at producing tyrosine-phosphorylated β3 integrin tails. (A) This panel shows an HPLC chromatograph of β3 Y759F after incubation with c-Src from Upstate, in an early attempt to produce phosphorylated integrin tails. Molecular weights were determined by mass spectrometry. This panel demonstrates that c-Src will phosphorylate β3 and that the phosphorylated product can be separated from the unphosphorylated tail; but, the reaction is relatively inefficient and produced insufficient quantities for NMR experiments. (B) A second approach attempted was *in vivo* tyrosine phosphorylation in *E. coli* using TKB1 cells (Stratagene). This panel shows two simultaneously acquired bacterial growth curves of *E. coli* TKB1 coexpressing GST-tagged β3 Y759F and the tyrosine kinase Elk. Note that bacterial growth is relatively unaffected by the induction of β3 but is significantly curtailed by the induction of Elk. (C) By producing c-Src kinase domain and using it to phosphorylate integrin tails as described in Chapter II, we were able to produce sufficient quantities of integrin tails for NMR experiments. This panel shows HPLC chromatographs of β3 Y759F after incubation with or without c-Src kinase domain. This experiment successfully produced NMR-scale quantities of phosphorylated integrin tail.

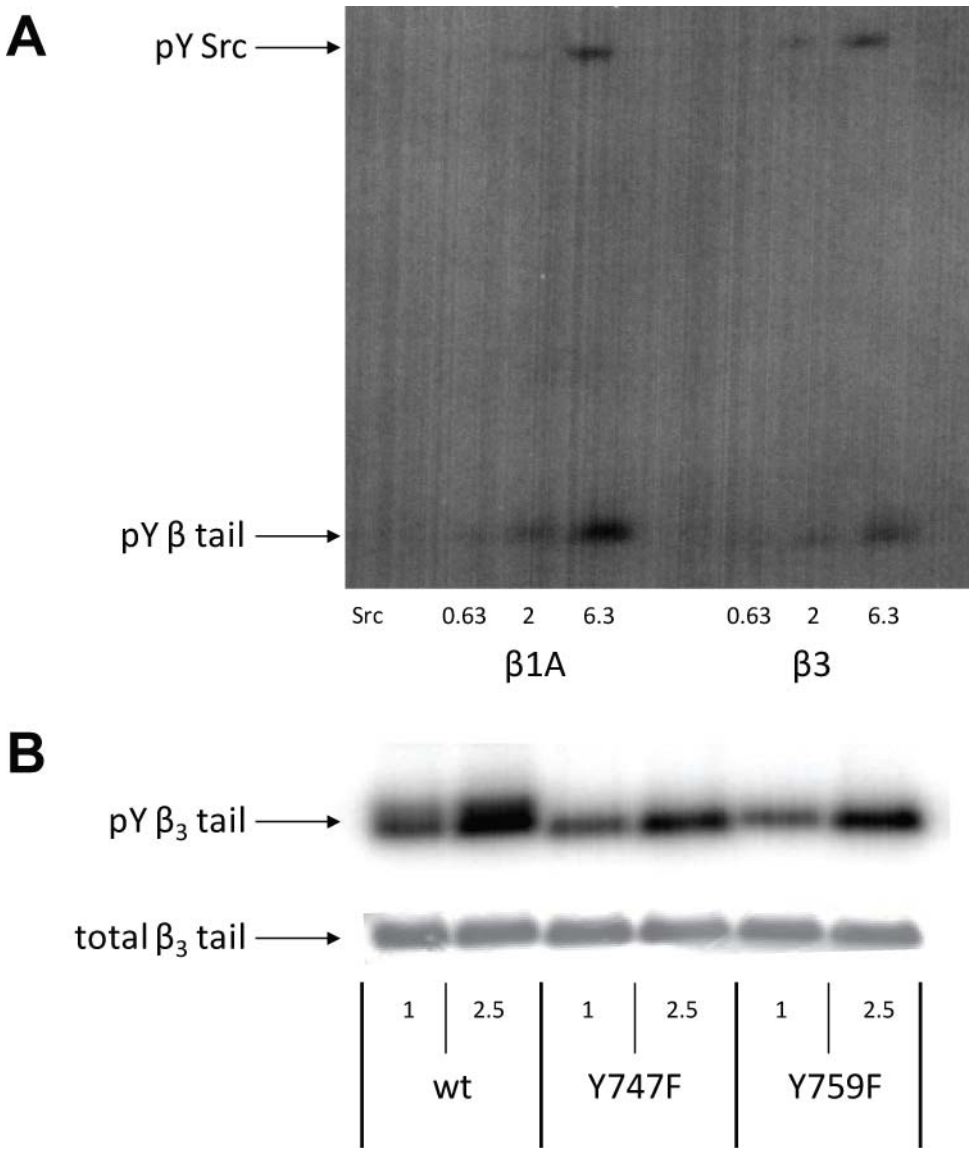

Figure 5.5 *In vitro* phosphorylation of β integrin tails observed by autoradiography. Autoradiographs of various β integrin tail constructs after phosphorylation in the presence of [γ-32P]ATP with full-length c-Src from Upstate. Samples underwent SDS-PAGE and were then visualized with a PhosphorImager. (A) β1A and β3 integrin tails were incubated with 0.00063, 0.002, or 0.0063 U/μL c-Src. Autophosphorylated c-Src can be observed near the top of the gel. These results indicate that c-Src is capable of phosphorylating both integrins. (B) β3 WT, Y747F, and Y759F were incubated with 0.001 or 0.0025 U/μL c-Src. The lower band is from a photo of the same gel stained with Coomassie blue in order to observe total protein. These results indicate that c-Src is capable of phosphorylating both the nMD and fMD sites in β3.

Y759F has been phosphorylated. This experiment produced NMR-scale quantities of phosphorylated integrin tail and only consumed a small fraction of the total c-Src kinase domain purified from 1 L of *E. coli* culture.

In order to phosphorylate specific tyrosine residues selectively, single and double Y-to-F mutants were made: β3 Y747F (for pY759) and Y759F (for pY747), β1A Y783F (for pY795) and Y795 (for pY783), and β7 YY753/758FF (for pY778). The β7 tail contains two MP tyrosine residues, but phosphorylation of just the nMD tyrosine residue was explored (the fMD site contains a natural Y-to-F substitution). All experiments on β7 tails presented in this chapter were performed by Massimiliano Memo, under my guidance. Tyrosine phosphorylation caused localized perturbations in the HSQC spectra of the integrin tails (Fig. 5.6). Phosphorylation of both β3 Y747F and Y759F was observed in this way, as was phosphorylation of β1A Y795F and β7 YY753/758FF. However, phosphorylation of β1A Y783F was not observed. When the phosphorylation reaction was performed on β1A wild type (WT), chemical shift perturbations were only observed near Y783, indicating that Y783, but not Y795, was phosphorylated in this system. Thus, for further studies, β1A pY783 was produced from WT peptides.

5.2.2 Tyrosine phosphorylation decreases integrin affinity for talin

Binding of proteins to integrin tails was assayed by observing chemical shift perturbations in integrin tail HSQC spectra. Upon the addition of the talin1 F3 domain to the β3, β1A, or β7 tail, significant perturbations were observed in the MP and nMD portions of the tail (Fig. 5.7). The MP perturbations were greatest in the β3 tail, but they were present in all tails tested. The affinities of these interactions were quantified, giving K_d values that ranged from 142 μM for β7 to 273 μM for β3 to 491 μM for β1A (Table

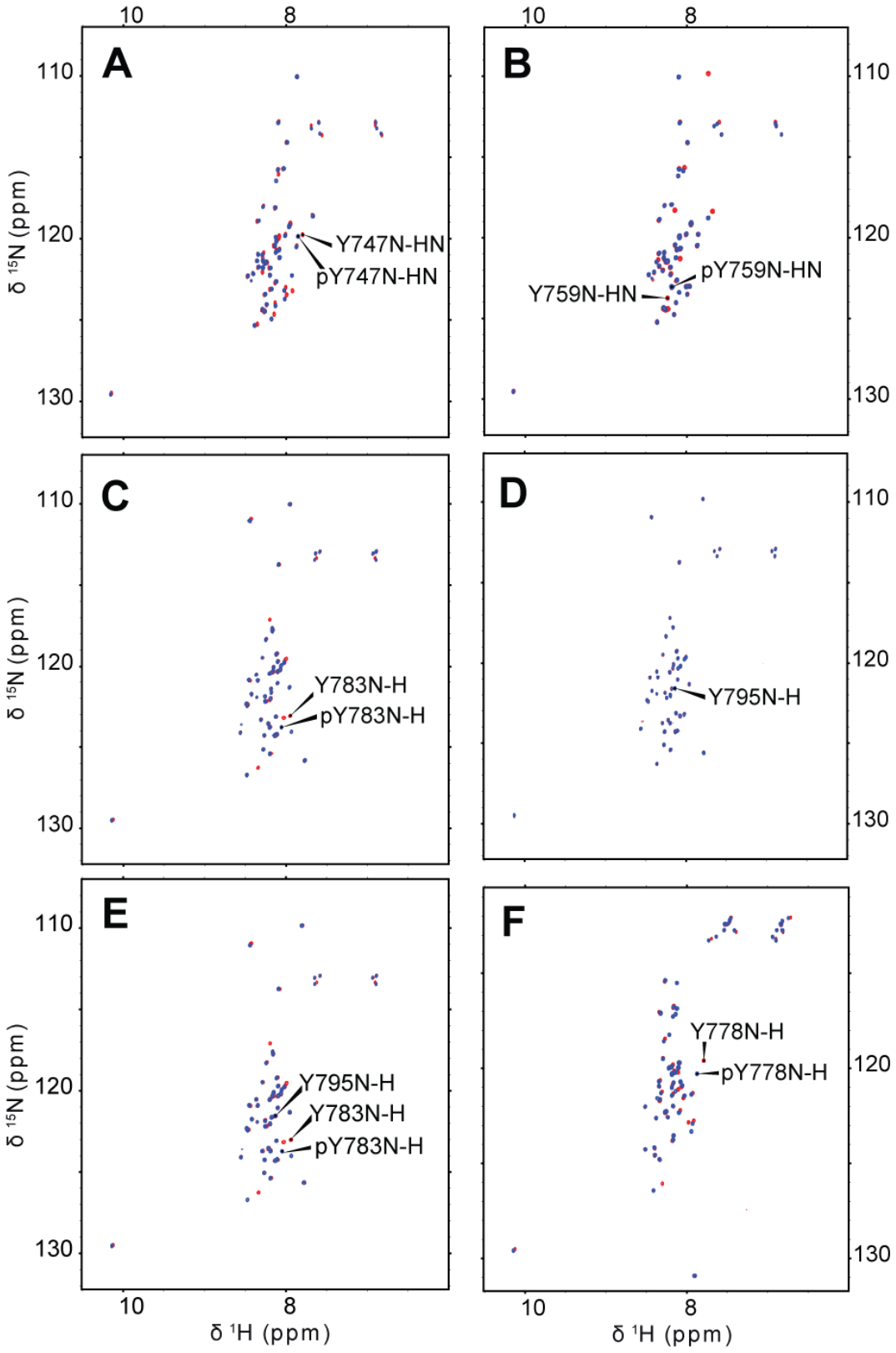

Figure 5.6 Phosphorylation of integrin tails. HSQC spectra of integrin tails before (red) and after (blue) the tyrosine phosphorylation reaction. Phosphorylated residues are indicated. (A) β3 Y759F. (B) β3 Y747F. (C) β1A Y795F. (D) β1A Y783F. (E) β1A WT. (F) β7 YY753/758FF. Experiments on β7 tails were performed by Massimiliano Memo, under my guidance.

5.1). Smaller shifts were also observed in the fMD portion of the β3 integrin tail (and to a lesser extent in the β1A tail), but these perturbations are likely due to a weak competing integrin/talin interaction, with a K_d of several mM for the fMD portion.

The introduction of Y-to-F mutations employed for specific phosphorylation in β3 and β7 has negligible effects on talin affinity in these integrins. The greatest effect was seen with Y747F in β3, which increases the K_d to 366 μM (Table 5.1). Such a decrease in affinity upon a mutation in the talin binding site is not surprising, and it is notable that this effect is very small compared to the much greater changes in affinity observed elsewhere in this study.

Tyrosine phosphorylation of the nMD NPxY motif decreases the magnitude of chemical shift perturbations observed upon talin binding (Fig. 5.7) and decreases the affinity of these interactions substantially. This effect is most pronounced in β7 (a loss of 5.3 kJ/mol in binding energy), less so in β1A (4.0 kJ/mol), and least in β3 (3.2 kJ/mol) (Table 5.1). Phosphorylation of the fMD NPxY motif in β3 abrogated chemical shift perturbations upon talin binding in that region, but had little effect on the much tighter interaction with the MP and nMD regions or the overall affinity (Table 5.1).

5.2.3 Tyrosine phosphorylation increases integrin affinity for Dok1

Unlike the talin1 F3 domain, the PTB domain of Dok1 only causes small perturbations in the HSQC spectra of unphosphorylated integrin tails. Such perturbations are localized to the nMD region of β3 and the fMD regions of β1A and β7 (Fig. 5.8). However, these interactions are so weak (K_d greater than several mM) that it is unlikely that any of these interactions are physiologically relevant (Table 5.2). It is of note that although the K_d value for β3 (12.6 mM) is only an estimate, as described in Chapter II, it agrees well with the 14.3 mM value reported previously for a short fragment of β3 (Oxley *et al.*, 2008).

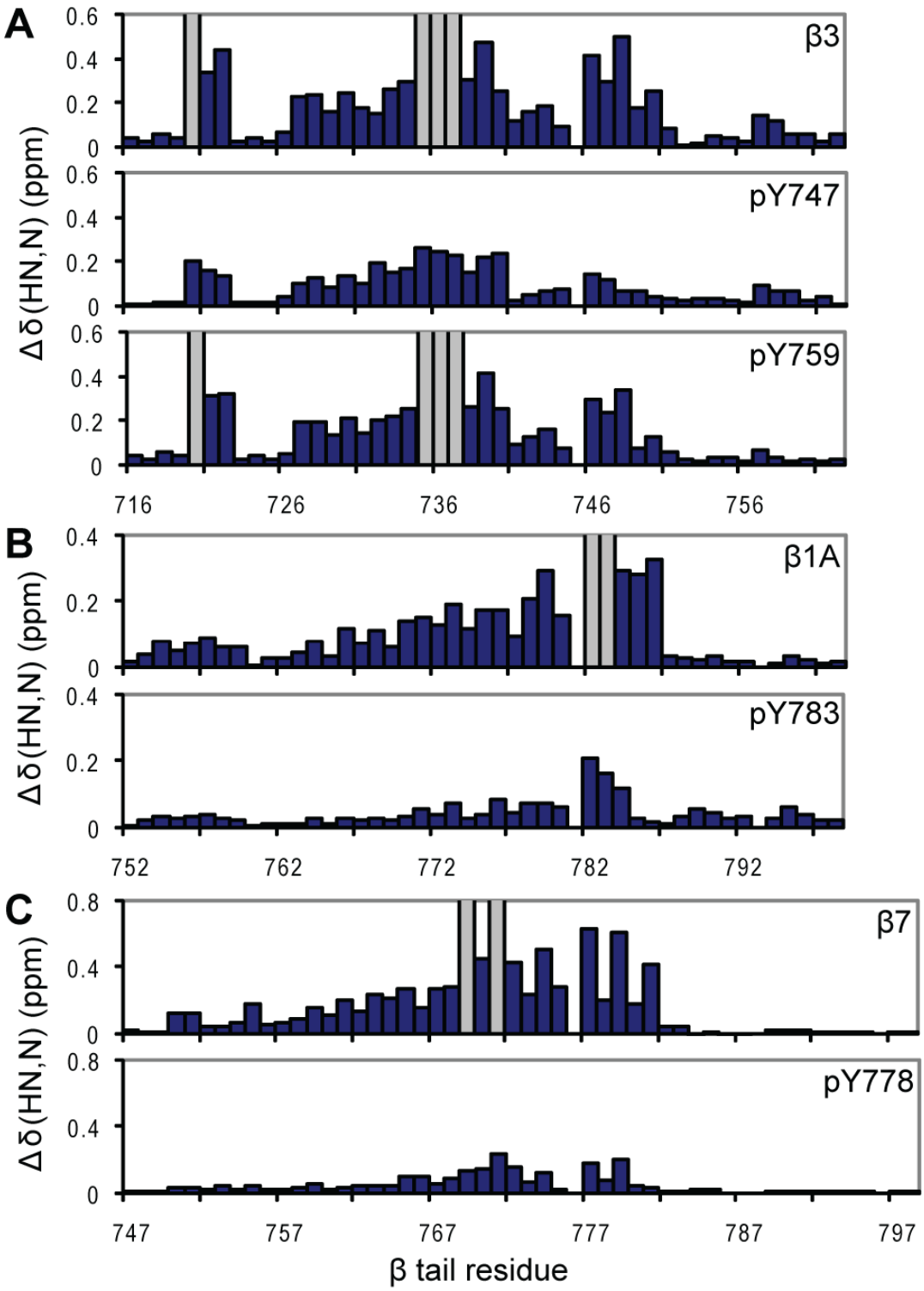

Figure 5.7 Effect of tyrosine phosphorylation on the integrin/talin interaction. Weighted chemical shift maps of perturbations observed in ^{1}H-^{15}N HSQC spectra of the β3 (A), β1A (B), and β7 (C) tails (50 μM) upon the addition of talin1 F3 domain (1 mM). Interaction studies were performed on unphosphorylated integrin tails and tails phosphorylated at the nMD site (β3, β1A, and β7) and at the fMD site (β3). Grey bars correspond to residues that could not be tracked due to exchange broadening. Note that the y-axis scale differs between panels. Experiments on β7 tails were performed by Massimiliano Memo, under my guidance.

Table 5.1 Effect of tyrosine phosphorylation on the affinity of integrin/talin interactions

Mutation	K_d (μM)*	ΔG (kJ/mol)†	$\Delta\Delta G_{pY}$ (kJ/mol)‡
β3			
WT	273 ± 6.4	-20.33 ± 0.06	-
Y759F	286 ± 4.6	-20.22 ± 0.04	-
Y759F pY747	1032 ± 27	-17.04 ± 0.07	3.18
Y747F	366 ± 6.4	-19.61 ± 0.04	-
Y747F pY759	386 ± 15	-19.48 ± 0.10	0.13
β1A			
WT	491 ± 10	-18.88 ± 0.05	-
pY783	2,500 est.§	-14.8	4.0
β7			
WT	142 ± 3.0	-21.95 ± 0.05	-
YY753/758FF	145 ± 4.3	-21.89 ± 0.07	-
YY753/758FF pY778	1,217 ± 62	-16.63 ± 0.13	5.26

* K_d values are given ± standard error.
† ΔG is given for binding and calculated from K_d.
‡ $\Delta\Delta G_{pY}$ is the ΔG value for the phosphorylated integrin binding to talin1, minus the ΔG value for the unphosphorylated integrin binding to talin1 (a positive value denotes a decrease in affinity upon phosphorylation).
§ Approximate K_d values were estimated by comparing the magnitude of chemical shift perturbations to those in a relevant titration, as described in Chapter II.

Table 5.2 Effect of tyrosine phosphorylation on the affinity of integrin/Dok1 interactions

Mutation	K_d (μM)*	ΔG (kJ/mol)†	$\Delta\Delta G_{pY}$ (kJ/mol)‡
β3			
WT	12,600 est.§	-10.8	-
Y759F pY747	8.4 ± 0.66	-28.97 ± 0.19	-18.1
Y747F pY759	226 ± 7.7	-20.80 ± 0.08	-10.0
β1A			
WT	N/A **		
pY783	78.7 ± 2.4	-23.41 ± 0.07	
β7			
WT	N/A **		
YY753/758FF pY778	36.8 ± 1.4	-25.30 ± 0.09	

* K_d values are given ± standard error.
† ΔG is given for binding and calculated from K_d.
‡ $\Delta\Delta G_{pY}$ is the ΔG value for the phosphorylated integrin binding to Dok1, minus the ΔG value for the unphosphorylated integrin binding to Dok1 (a negative value denotes an increase in affinity upon phosphorylation)
§ Approximate K_d values were estimated by comparing the magnitude of chemical shift perturbations to those in a relevant titration, as described in chapter II.
** No detectable binding to the applicable binding site.

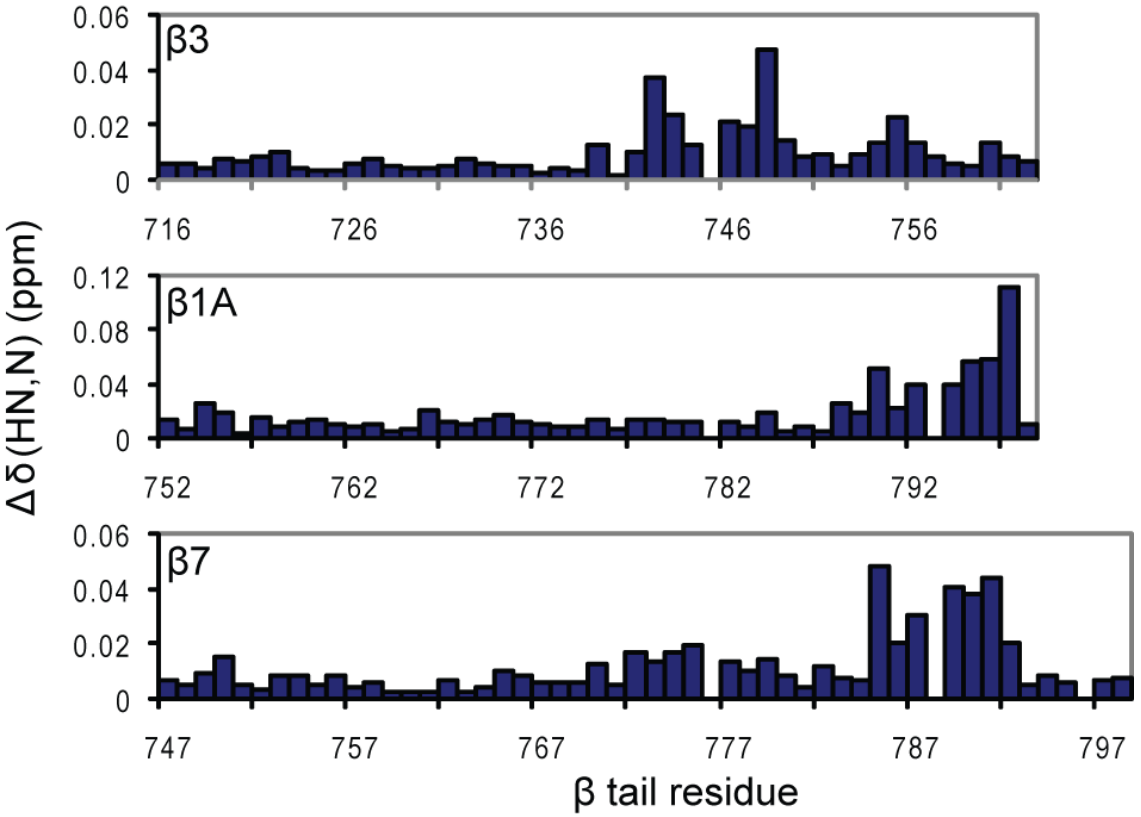

Figure 5.8 Chemical shift perturbations observed in unphosphorylated integrin tails upon addition of Dok1 PTB domain. Weighted chemical shift maps of perturbations observed in ^{1}H-^{15}N HSQC spectra of unphosphorylated β3, β1A, and β7 tails (50 μM) upon the addition of Dok1 PTB domain (1 mM). Note that the y-axis scale differs between graphs. Experiments on β7 tails were performed by Massimiliano Memo, under my guidance.

Upon phosphorylation, the affinities of these interactions increase substantially. For phosphorylation in the nMD regions, K_d values range from 8.4 μM for β3 to 36.8 μM for β1A to 78.7 μM for β7 (Table 5.2, Fig. 5.9). Phosphorylation of β3 Y759 also increases Dok1 affinity to a K_d of 226 μM. In each case, the interaction as observed by NMR was localized to residues near the site of phosphorylation (Fig. 5.10). No MP perturbations were observed in β3 or β1A, and only minor MP perturbations in β7. Tyrosine phosphorylation thus greatly increases the affinity of Dok1 for integrin tails (adding 18 kJ/mol of binding energy to the interaction in the case of β3 pY747), making

the interaction tight enough to be physiologically relevant (and significantly tighter than the competing talin/integrin interaction).

Experiments were also conducted on a β3 Y747E mutant. Glutamate is occasionally reported as a phosphotyrosine mimic, despite very little chemical similarity to phosphotyrosine (Fig. 5.2B). The chemical shift perturbation pattern of this mutant upon interaction with Dok1 closely resembled that of β3 Y747A (Fig. 5.11B). In both cases, the interaction with the nMD NPxY region was abrogated. This stands in stark contrast to the significant increase in chemical shift perturbations observed upon phosphorylation of Y747; this strongly suggests that glutamate is an unwise choice as a phosphotyrosine mimic.

5.2.4 The positively-charged Dok1 NPxY binding pocket

When Oxley *et al*. solved the crystal structure of the human Dok1 PTB domain (PDB 2V76) (Oxley *et al.*, 2008), a sulphate anion was observed in the NPxY binding pocket, surrounded by a collection of positively-charged residues: R207, R208, R222, and R223, with R207 and R222 making the most direct contact (Fig. 5.3A). We hypothesized that these positively-charged residues explained the higher affinity of Dok1 for phosphorylated β3. Residues R207 and R208 correspond to positively charged residues in talin, but R222 and R223 do not (Fig. 5.1B). Residue R223 corresponds to Y373 in talin1 and Y376 in talin2—a residue that plays a significant role in binding integrins, particularly β1 integrins (Chapter IV). Interestingly, however, R222 corresponds to a negatively charged residue (D372 in talin1, E375 in talin2, Fig. 5.1B). R222 was thus chosen as a particularly suitable candidate for exploring Dok1 specificity for phosphorylated integrin tails.

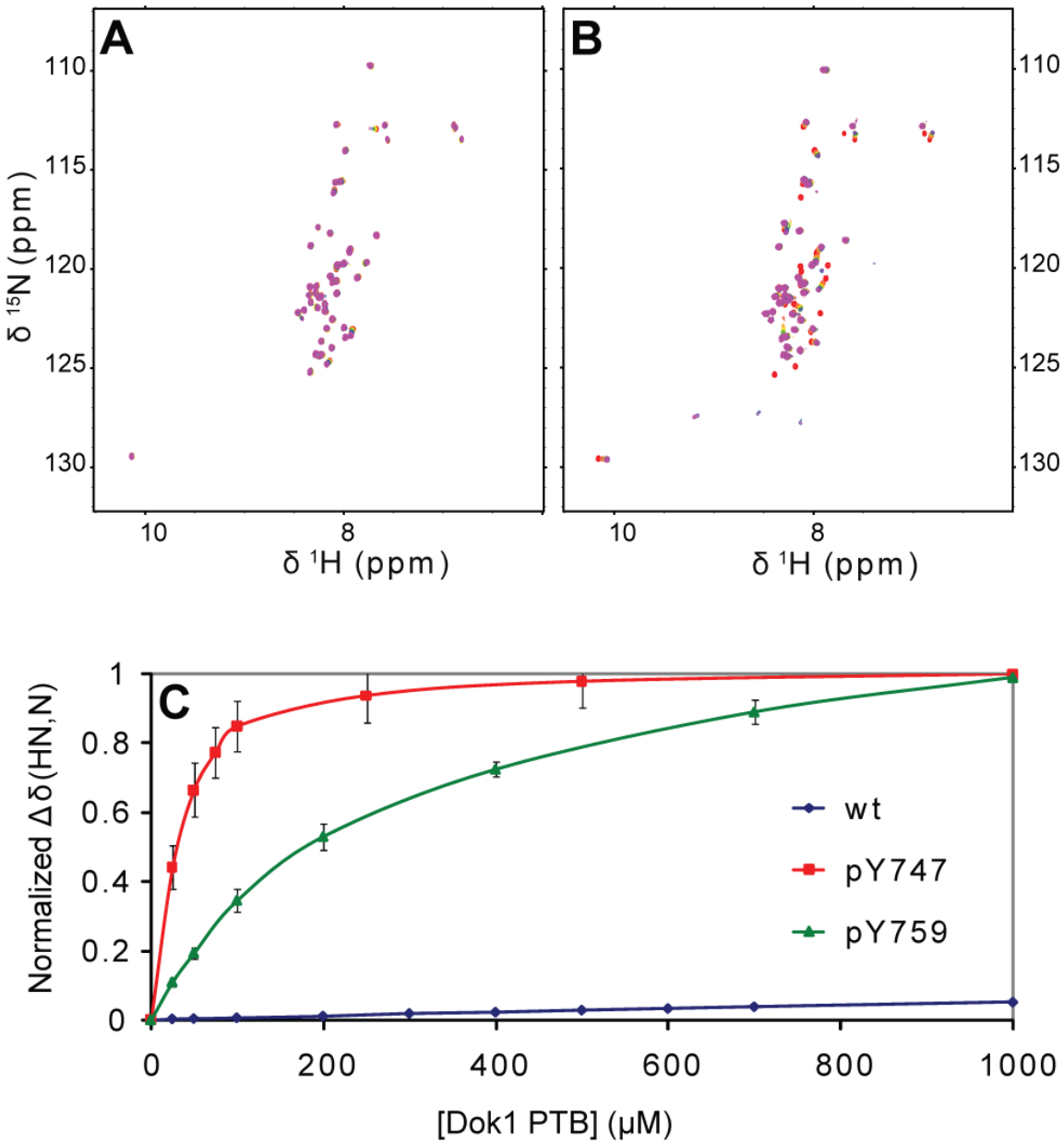

Figure 5.9 Chemical shift perturbation experiments with integrin tails. (A) ^{1}H-^{15}N HSQC spectra of 0.05 mM ^{15}N-labelled β3 tail with increasing concentrations of Dok1 PTB domain: 0 mM (red), 0.2 mM (yellow), 0.4 mM (green), 0.6 mM (blue), 1 mM (magenta). (B) ^{1}H-^{15}N HSQC spectra of 0.05 mM ^{15}N-labelled β3 tail Y759F pY747 with increasing concentrations of Dok1 PTB domain: 0 mM (red), 0.025 mM (tomato), 0.05 mM (orange), 0.075 mM (yellow), 0.1 mM (green), 0.25 mM (blue), 0.5 mM (purple), 1 mM (magenta). A few peaks broaden out due to intermediate exchange, but these can still be traced when the contour levels are taken lower. (C) Binding curves used for K_d calculation. Peaks were tracked through HSQC spectra of ^{15}N-labelled β3 tail acquired with increasing concentrations of Dok1 PTB domain. For each trackable peak, the change in chemical shift was normalized to the change at 1 mM Dok1, adjusted based on the maximal perturbation observed in that titration. Note that while K_d values were determined by fitting several curves simultaneously, for clarity each value plotted here shows the average of several peaks ± standard error.

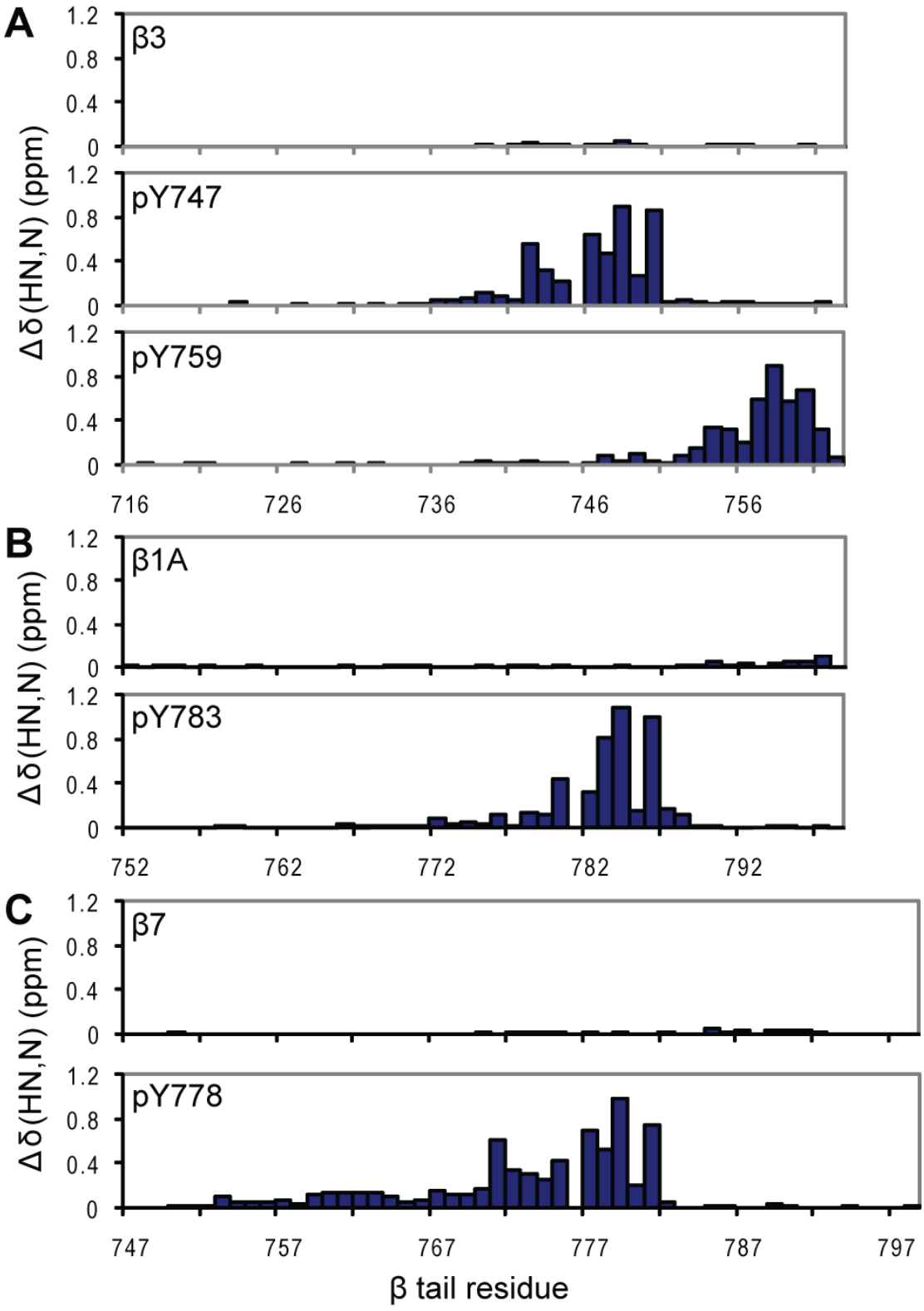

Figure 5.10 Effect of tyrosine phosphorylation on the integrin/Dok1 interaction. Weighted chemical shift maps of perturbations observed in ^{1}H-^{15}N HSQC spectra of the β3 (A), β1A (B), and β7 (C) tails (50 μM) upon the addition of Dok1 PTB domain (1 mM). Interaction studies were performed on unphosphorylated integrin tails and tails phosphorylated at the nMD site (β3, β1A, and β7) and at the fMD site (β3). Experiments on β7 tails were performed by Massimiliano Memo, under my guidance.

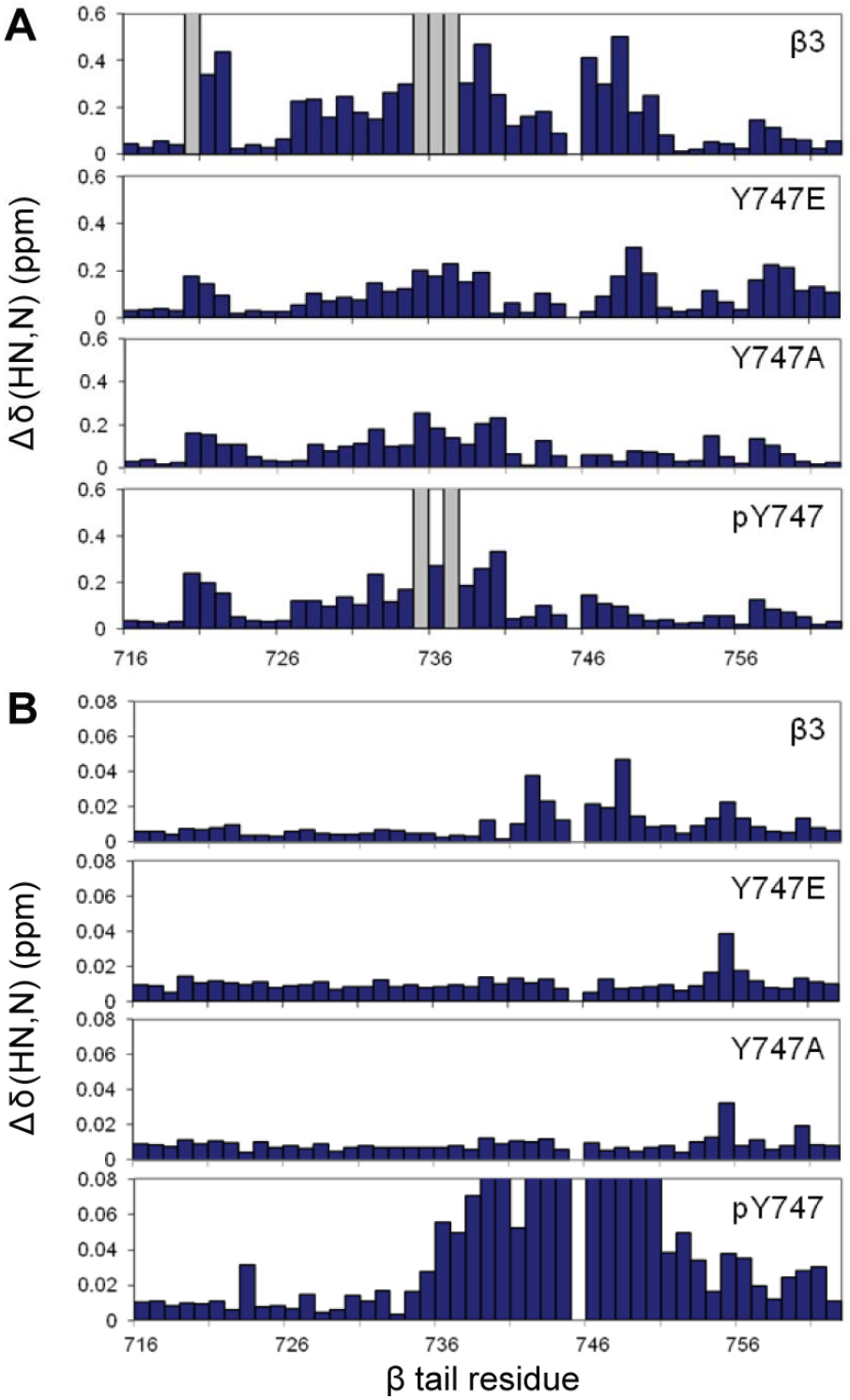

Figure 5.11 Glutamate does not mimic phosphotyrosine. Weighted chemical shift maps of perturbations observed in ^{1}H-^{15}N HSQC spectra of the β3 tail WT, Y747E, Y747A, and Y759F pY747 (50 μM) upon the addition of 1 mM talin1 F3 domain (A) or 1 mM Dok1 PTB domain (B). Grey bars correspond to residues that could not be tracked due to exchange broadening. Note that the y-axis scale differs between panels. Also, note that while all three mutations/modifications have a similar effect on the interaction with talin1, the shift map of Dok1 interacting with the Y747E mutant looks most similar to that involving the Y747A mutant and does not resemble in any way the shift map involving the phosphorylated integrin. The full perturbation map for the titration of β3 Y759F pY747 with Dok1 can be seen in Fig. 5.10.

Introduction of the mutation R222A into Dok1 greatly reduces the affinity of Dok1 for phosphorylated β3 integrin tail by 9.6 kJ/mol, from a K_d of 8.4 μM to 398 μM (Table 5.3). This mutation also affects the interaction of Dok1 with unphosphorylated β3 tail, but to a much lesser degree, decreasing the binding energy by only 1.0 kJ/mol. Introduction of the double mutation RR207/208AA also greatly decreases Dok1 affinity for integrins in a manner that is phosphorylation-specific, causing a 14.2 kJ/mol loss of binding energy to phosphorylated β3, but just a 2.0 kJ/mol loss of binding energy to unphosphorylated β3. Together, these three residues thus dominate the 18.1 kJ/mol difference in binding energy of Dok1 to phosphorylated versus unphosphorylated β3.

5.2.5 Engineering talin to bind preferentially to phosphorylated integrin tails

As discussed above, Dok1 R222 has a reversed charge in talin (D372 in talin1, E375 in talin2) and is a key residue for determining Dok1 specificity for phosphorylated integrins. Consistent with this, introduction of the mutation D372R in talin1 substantially increases its binding affinity for integrin tails phosphorylated at the nMD site: 33.1 μM for β3 pY747 and 128 μM for β1A pY783 (Table 5.4). For β3, this marks an increase of 8.5 kJ/mol in binding energy compared to talin1 WT. For β1A, this is an increase of 7.4 kJ/mol. Interestingly, this mutation also affects talin1 binding to unphosphorylated integrin tails in different ways, although to a lesser degree. Talin1 D372R binds more tightly to unphosphorylated β3 than does talin1 WT (86 μM vs. 273 μM) but binds more weakly to unphosphorylated β1A than talin1 WT (793 μM vs. 491 μM). These differences can be explained on the basis of the structural information on the talin2/β1D complex presented in Chapter III and the follow-up studies presented in Chapter IV, as detailed later in the Discussion (Fig. 5.3). We note that these differences could influence the biological activity of this mutant.

Table 5.3 Disrupting Dok1 binding to phosphorylated β integrin tails

Mutation	K_d (μM)*	ΔG (kJ/mol)†	$\Delta\Delta G_{mut}$ (kJ/mol)‡	$\Delta\Delta G_{mut}$ (%)§
β3 WT				
Dok1 WT	12,600 est.**	-10.8	-	-
Dok1 RR207/208AA	27,700 est.	-8.9	2.0	18
Dok1 R222A	18,600 est.	-9.9	1.0	9
β3 Y749F pY747				
Dok1 WT	8.4 ± 0.66	-28.97 ± 0.19	-	-
Dok1 RR207/208AA	2,601 ± 180	-14.75 ± 0.17	14.22	49
Dok1 R222A	398 ± 18	-19.40 ± 0.11	9.57	33

* K_d values are given ± standard error.
† ΔG is given for binding and calculated from K_d.
‡ $\Delta\Delta G_{mut}$ (kJ/mol) is the ΔG value for the integrin binding to mutant Dok1, minus the ΔG value for the binding to WT Dok1 (a positive value denotes a decrease in affinity upon mutation)
§ $\Delta\Delta G_{mut}$ (%) is the percentage of binding energy lost by the given mutation (a positive value denotes a decrease in affinity).
** Approximate K_d values were estimated by comparing the magnitude of chemical shift perturbations to those in a relevant titration, as described in Chapter II.

Table 5.4 Engineering talin1 to preferentially bind to phosphorylated integrin tails

Mutation	K_d (μM)*	ΔG (kJ/mol)†	$\Delta\Delta G_{DR}$ (kJ/mol)‡	$\Delta\Delta G_{pY}$ (kJ/mol)§
β3 + talin1 F3 D372R				
WT	86 ± 3.3	-23.18 ± 0.09	-2.85	-
Y759F pY747	33.1 ± 1.6	-25.56 ± 0.12	-8.52	-2.38
β1A + talin1 F3 D372R				
WT	793 ± 24	-17.69 ± 0.07	1.19	-
pY783	128 ± 5.1	-22.21 ± 0.10	-7.4	-4.52

* K_d values are given ± standard error.
† ΔG is given for binding and calculated from K_d.
‡ $\Delta\Delta G_{DR}$ is the ΔG value for integrin binding to talin1 D372R, minus the ΔG value for binding to talin1 WT (a negative value denotes an increase in affinity upon mutation).
§ $\Delta\Delta G_{pY}$ is the ΔG value for the phosphorylated integrin binding to talin1, minus the ΔG value for the unphosphorylated integrin binding to talin1 (a negative value denotes an increase in affinity upon phosphorylation).

5.2.6 Talin D372R localizes to phosphorylated integrins in live cells

Due to its dramatic effect on talin binding to phosphorylated integrins, we hypothesized that the talin1 D372R mutation would affect talin activity *in vivo*. To investigate this, we examined talin localization to focal adhesions. These experiments on live cells were performed by Jacob Haling (Mark Ginsberg's group, University of California San Diego). We transiently expressed GFP-talin1 WT or D372R in SYF MEFs (deficient for the tyrosine kinases Src, Yes, and Fyn), which were then plated on fibronectin (an extracellular ligand for α5β1) and stained for the focal adhesion marker vinculin. Talin1 D372R was abundantly expressed (Fig. 5.12D), but was not seen at the sites of focal adhesions, whereas talin1 WT co-localized with vinculin and was therefore present in focal adhesions (Fig. 5.12A). Focal adhesions were also more prominent in cells expressing talin1 WT compared to those expressing talin1 D372R.

In SYF MEFs stably reconstituted with c-Src (SYF + Src), talin1 WT was also targeted to focal adhesions, but these adhesions were less prominent than in cases where c-Src was absent (Fig. 5.12B). However, talin1 D372R in SYF + Src MEFs was targeted to focal adhesions, and these were more prominent than those observed in SYF MEFs expressing talin1 D372R or SYF + Src MEFs expressing talin1 WT. To confirm the levels of phosphorylation in SYF MEFs and SYF + Src MEFs, fixed cells were stained with an anti-phosphotyrosine antibody (pY100), and an anti-paxillin antibody to mark focal adhesions (Fig. 5.12C). Greater phosphorylation was observed in the focal adhesions of SYF + Src MEFs when compared to SYF MEFs. In agreement with our structural model, these data suggest that talin1 D372R is capable of competing with endogenous talin for integrin binding only when integrins are tyrosine phosphorylated. Furthermore, tyrosine phosphorylation appears to affect cell morphology in a manner that is reversed by the D372R mutation.

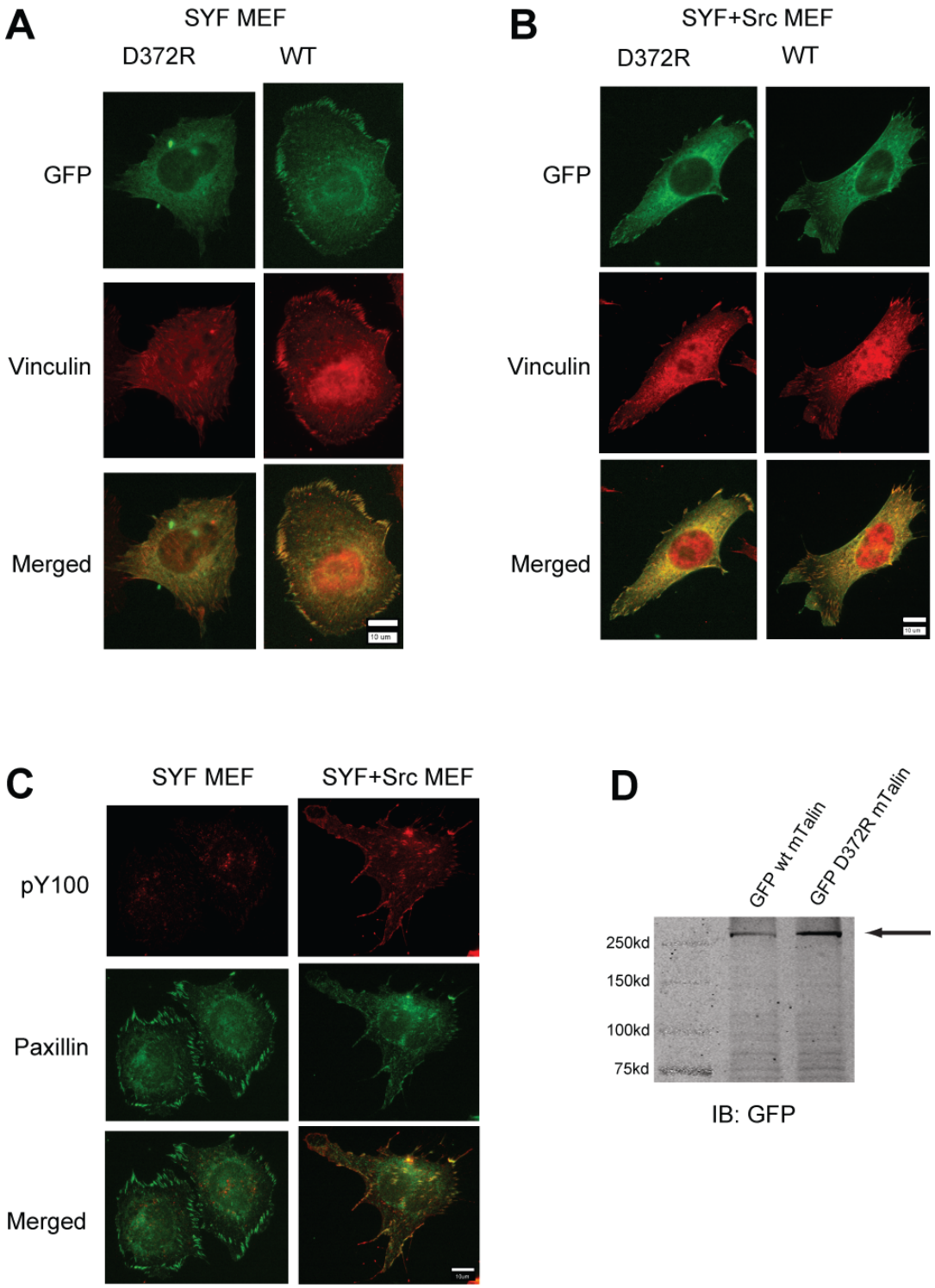

Figure 5.12 Talin D372R preferentially localizes to focal adhesions that are tyrosine-phosphorylated. SYF MEFs (A) and SYF + Src MEFs (B) transiently expressing GFP-Talin1 wild type (WT) or D372R were allowed to adhere to fibronectin-coated coverslips and stained to visualize vinculin. Depicted are the localization of talin (green) and vinculin (red). (C) SYF MEFs and SYF + Src MEFs were stained to visualize phosphotyrosine (pY100, red) and paxillin (green). (D) SYF cells expressing GFP-Talin1 WT and GFP-Talin1 D372R were lysed and analyzed by Western blotting to confirm comparable expression of D372R and WT talin1. These experiments were performed by Jacob Haling (Mark Ginsberg's group, University of California San Diego).

5.3 Discussion

Here we have demonstrated that key interactions involving the β3, β1A, and β7 integrin tails are similarly affected by tyrosine phosphorylation. Phosphorylation at the nMD site in each tail decreases its affinity for talin; in contrast, phosphorylation greatly increases the affinity for Dok1 (by 18.1 kJ/mol in the case of β3). The interaction of Dok1 is localized to the NPxY region of the integrin tail, even when the affinity is relatively high (8.4 μM for β3 pY747). Talin, on the other hand, also binds to the MP region, a unique interaction that is essential for integrin activation (Wegener *et al.*, 2007). Thus, tyrosine phosphorylation acts to decrease integrin activation both by decreasing talin affinity and by increasing the affinity of competing proteins incapable of activating the integrin. This is consistent with our previous report that tyrosine phosphorylation of β3 decreases affinity for talin1 while increasing affinity for Dok1 (Oxley *et al.*, 2008), and with an earlier report that phosphorylation of β1 decreases affinity for talin (Tapley *et al.*, 1989). The latter study was performed by gel filtration, so our current report is the first detailed analysis of tyrosine phosphorylation across different integrins using structural biological methods.

By performing these studies on intact full-length integrin tails, we have been able to show definitively where these interactions are localized within the cytoplasmic tails, and we can look at the effect of independently phosphorylating different tyrosine residues within the same peptide. In β3, we could phosphorylate both Y747 and Y759; in either case, the interaction with Dok1 was localized just to the site of phosphorylation. Whereas phosphorylation at Y747 disrupted the interaction with talin, phosphorylation at Y759 did not. Thus, the role of phosphorylation at this fMD site is probably not related to integrin activation; the integrin tail is very flexible in this region (Ulmer *et al.*, 2001), and binding of Dok1 there would not necessarily compete with talin binding.

Chemical shift perturbation maps of the interaction of β3 and β1A with talin are presented in Chapter III and IV, and this chapter expands these results by presenting the shift map for β7, a lymphocyte-specific integrin (Shaw & Brenner, 1995). While showing some subtle differences in the interaction of talin with β3 and β1A, the interactions observed with β7 are broadly similar in that they consists of both MP and nMD interactions. In fact, the chemical shift perturbation map appears intermediate between those of β3 and β1A. In studying talin binding, use of full-length peptides is particularly important given the large interaction surface. For example, in our previous study, we reported the K_d of the interaction between talin and a short β3 peptide to be 3.49 mM (unphosphorylated) and 6.53 mM (phosphorylated) (Oxley *et al.*, 2008). The values for the full-length β3 peptide reported here are, respectively, 0.273 mM and 1.03 mM. With respect to Dok1, which engages a more limited interaction surface, the values are more comparable.

These experiments could only be carried out on phosphorylated integrin tails, as a suitable phosphomimetic mutation does not exist for studying tyrosine phosphorylation. In fact, we show here that mutating Y747 in β3 to glutamate has the same effect as mutating that residue to alanine, which effectively abrogates protein-protein interactions in that region. (Fig. 5.11). This is observed for interactions with Dok1 and talin1, but in the case of Dok1, phosphorylation of Y747 strongly enhances binding—demonstrating that in this system at least, glutamate does not mimic phosphotyrosine. Any use of glutamate as a phosphotyrosine mimic should therefore be extensively validated—at the very least by comparing it to the effect of an alanine substitution. The results of a rudimentary search through the recent literature suggest that this is not common practice, and recent studies that did compare a “phosphomimetic” Y-to-E mutant with a Y-to-A mutant found that the two different mutations had the same effect on the system under

study (Hussain *et al.*, 2007; Potter *et al.*, 2005), meaning that the observed effects cannot necessarily be interpreted as being phosphorylation specific.

Here we show that mutation of positively-charged residues in the NPxY-binding pocket of Dok1 (Fig. 5.3A) (Oxley *et al.*, 2008) disrupts Dok1 binding to the β3 integrin tail in a phosphorylation-specific manner. It has previously been reported that the mutation of two of these residues to alanine (RR207/208AA) decreased Dok1 binding to β3 and disrupted Dok1 signalling (Ling *et al.*, 2005). We can now explain this observation in terms of interference with the positively-charged structural pocket necessary for specific binding of phosphorylated integrins. The analogous residues in talin1 and talin2, however, are also positively charged, so this does not explain why Dok1 binds specifically to phosphorylated integrins while talin does not. Another residue in the Dok1 NPxY-binding pocket, R222, is oppositely charged in talin1 (D372) and talin2 (E375). Mutation of this residue in Dok1 to alanine significantly decreases the affinity of the interaction with the β3 integrin in a phosphorylation dependent manner.

We hypothesized that this understanding of the structural basis of the phosphorylation dependence of Dok1 could be used to engineer a talin variant that would bind specifically to phosphorylated integrins. Indeed, this effect was observed for talin1 D372R binding to β3 and β1A. This mutation increased talin affinity for phosphorylated β3 by 8.5 kJ/mol and β1A by 7.4 kJ/mol. Interestingly, this mutant had differing effects on the interaction with unphosphorylated integrins: it increased talin1 affinity for unphosphorylated β3 by 2.9 kJ/mol but decreased affinity for β1A by 1.2 kJ/mol. An examination of the structures of β3 and β1D in complex with talin (Fig. 5.3) explains this difference. In the β3/talin1 structure (PDB 1MK9) (Garcia-Alvarez *et al.*, 2003), the portion of the tail C-terminal to Y747 does not make extensive contacts with talin. However, this region contains a negatively-charged glutamate residue (749) that could

make favourable electrostatic contacts with the mutant D372R residue. Alternatively, β1A has an uncharged serine residue in this position. In the β1D/talin2 structure, this residue hydrogen bonds with talin2 E375. In the similar β1A/talin1 complex this mutation would disrupt such an interaction if present and would not be expected to make the interaction more favourable as is the case for β3.

We tested some aspects of our structural model by observing the behaviour of talin1 WT and D372R in live cells. In MEFs that do not express Src or related kinases, talin1 WT localizes to focal adhesions, but talin1 D372R does not. As these experiments were carried out using fibronectin, and α5β1 is the primary fibronectin receptor in MEFs (Hodivala-Dilke *et al.*, 1999), this effect correlates with the decreased affinity observed between the mutant talin and unphosphorylated β1A integrins. When c-Src is introduced into these cells, both talin1 WT and D372R co-localize with phosphorylated integrins at focal adhesions. Thus, the effects observed in *in vitro* binding experiments translate into observable effects in live cells. Interestingly, tyrosine phosphorylation correlates with reduced focal adhesion formation in the presence of talin1 WT but not talin1 D372R. Thus, these results provide additional evidence that integrin tyrosine phosphorylation downregulates integrin activation by inhibiting talin binding.

Phosphorylation of the nMD tyrosine residue has been shown in to modulate inside-out integrin activation in β3 (Datta *et al.*, 2002) and in β1 (Tapley *et al.*, 1989). In β3, phosphorylation of both nMD Y747 (Blystone *et al.*, 1997; Butler & Blystone, 2005; Chandhoke *et al.*, 2004; Gao *et al.*, 2005; Law *et al.*, 1999) and fMD Y759 (Cowan *et al.*, 2000; Kirk *et al.*, 2000; Xi *et al.*, 2006) have been associated with outside-in signalling β3. This is consistent with a report that the nMD region of β3 in general is associated with both inside-out and outside-in signalling, while the fMD portion only engages in outside-in signalling (Zou *et al.*, 2007). This makes sense from a structural standpoint, in that

talin only interacts tightly with the nMD NPxY. In β1, studies point to a role for phosphorylation at nMD Y783 in signalling in both directions. Evidence of a role for Y795 is less good, but also exists (Sakai *et al.*, 1998; Wennerberg *et al.*, 2000). However, under the conditions used in this study, c-Src did not phosphorylate this residue, so a different kinase may be involved *in vivo*. Interestingly, in β7, this fMD residue is a non-phosphorylatable phenylalanine.

Despite the substantial evidence for a role for tyrosine phosphorylation in β1 integrin signalling, mice with the β1 YY783/795FF knock-in mutation do not display any apparent developmental abnormalities (Chen *et al.*, 2006; Czuchra *et al.*, 2006). The β3 YY747/759FF mouse, however, displays a severe phenotype (Law *et al.*, 1999). β1 tyrosine phosphorylation is central to the pathological effect of v-Src on cells (Hirst *et al.*, 1986; Johansson *et al.*, 1994; Sakai *et al.*, 2001), but given that these residues are highly conserved across different integrins and across different species, it is unlikely that such conservation would exist if the residue only participated in pathological conditions. In the case of β3, at least, mutation of either NPxY tyrosine to phenylalanine has little effect on the interaction with talin1, so it is reasonable to hypothesize that these residues are conserved as tyrosine because of a role for phosphorylation—although the side chains of unphosphorylated β1D Y783 and β3 Y747 also participate in intermolecular hydrogen bonds in complex with talin (see Chapter IV). The β1 YY783/795FF mutation affects cell behaviour in tissue culture conditions (Sakai *et al.*, 1998; Wennerberg *et al.*, 2000), so the lack of a phenotype in the β1 YY783/795FF may be the result of compensation by other integrins. On the other hand, the more extreme effect of tyrosine phosphorylation on Dok1 binding to β3 correlates with the more definitive biological role observed for tyrosine phosphorylation in that integrin.

From the current study, and from the bulk of structural and biological data on the topic, integrin tyrosine phosphorylation appears to be involved in a wide variety of integrin signalling processes, particularly in β3, but in other integrins as well. We demonstrate here a conserved structural mechanism in β3, β1A, and β7 integrins for regulation of integrin activation by nMD tyrosine phosphorylation. We have tested our predictions by engineering a talin mutant that is specific for phosphorylated integrins, and we have shown that this influences talin localization in live cells. Given that the literature on integrin tyrosine phosphorylation is substantial but sometimes ambiguous, our results add weight to the idea that tyrosine phosphorylation plays a significant role in integrin signalling.

5.4 References

Arias-Salgado E.G., Lizano S., Sarkar S., Brugge J.S., Ginsberg M.H., Shattil S.J. (2003) Src kinase activation by direct interaction with the integrin beta cytoplasmic domain. *Proc Natl Acad Sci U S A* **100:** 13298-13302

Arias-Salgado E.G., Lizano S., Shattil S.J., Ginsberg M.H. (2005) Specification of the direction of adhesive signaling by the integrin beta cytoplasmic domain. *J Biol Chem* **280:** 29699-29707

Blystone S.D., Williams M.P., Slater S.E., Brown E.J. (1997) Requirement of integrin beta3 tyrosine 747 for beta3 tyrosine phosphorylation and regulation of alphavbeta3 avidity. *J Biol Chem* **272:** 28757-28761

Butler B., Blystone S.D. (2005) Tyrosine phosphorylation of beta3 integrin provides a binding site for Pyk2. *J Biol Chem* **280:** 14556-14562

Calderwood D.A., Fujioka Y., de Pereda J.M., Garcia-Alvarez B., Nakamoto T., Margolis B., McGlade C.J., Liddington R.C., Ginsberg M.H. (2003) Integrin beta cytoplasmic domain interactions with phosphotyrosine-binding domains: a structural prototype for diversity in integrin signaling. *Proc Natl Acad Sci U S A* **100:** 2272-2277

Chandhoke S.K., Williams M., Schaefer E., Zorn L., Blystone S.D. (2004) Beta 3 integrin phosphorylation is essential for Arp3 organization into leukocyte alpha V beta 3-vitronectin adhesion contacts. *J Cell Sci* **117:** 1431-1441

Chen H., Zou Z., Sarratt K.L., Zhou D., Zhang M., Sebzda E., Hammer D.A., Kahn M.L. (2006) In vivo beta1 integrin function requires phosphorylation-independent regulation by cytoplasmic tyrosines. *Genes Dev* **20:** 927-932

Cowan K.J., Law D.A., Phillips D.R. (2000) Identification of shc as the primary protein binding to the tyrosine-phosphorylated beta 3 subunit of alpha IIbbeta 3 during outside-in integrin platelet signaling. *J Biol Chem* **275:** 36423-36429

Czuchra A., Meyer H., Legate K.R., Brakebusch C., Fassler R. (2006) Genetic analysis of {beta}1 integrin "activation motifs" in mice. *J Cell Biol* **174:** 889-899

Datta A., Huber F., Boettiger D. (2002) Phosphorylation of beta3 integrin controls ligand binding strength. *J Biol Chem* **277:** 3943-3949

Gao C., Schaefer E., Lakkis M., Blystone S.D. (2005) Beta3 tyrosine phosphorylation and alphavbeta3-mediated adhesion are required for Vav1 association and Rho activation in leukocytes. *J Biol Chem* **280:** 15422-15429

Garcia-Alvarez B., de Pereda J.M., Calderwood D.A., Ulmer T.S., Critchley D., Campbell I.D., Ginsberg M.H., Liddington R.C. (2003) Structural determinants of integrin recognition by talin. *Mol Cell* **11:** 49-58

Hirst R., Horwitz A., Buck C., Rohrschneider L. (1986) Phosphorylation of the fibronectin receptor complex in cells transformed by oncogenes that encode tyrosine kinases. *Proc Natl Acad Sci U S A* **83:** 6470-6474

Hodivala-Dilke K.M., McHugh K.P., Tsakiris D.A., Rayburn H., Crowley D., Ullman-Cullere M., Ross F.P., Coller B.S., Teitelbaum S., Hynes R.O. (1999) Beta3-integrin-deficient mice are a model for Glanzmann thrombasthenia showing placental defects and reduced survival. *J Clin Invest* **103:** 229-238

Hood J.D., Frausto R., Kiosses W.B., Schwartz M.A., Cheresh D.A. (2003) Differential alphav integrin-mediated Ras-ERK signaling during two pathways of angiogenesis. *J Cell Biol* **162:** 933-943

Hussain A., Cao D., Peng J. (2007) Identification of conserved tyrosine residues important for gibberellin sensitivity of Arabidopsis RGL2 protein. *Planta* **226:** 475-483

Huveneers S., Arslan S., van de Water B., Sonnenberg A., Danen E.H. (2008) Integrins uncouple Src-induced morphological and oncogenic transformation. *J Biol Chem* **283:** 13243-13251

Hynes R.O. (2002) Integrins: bidirectional, allosteric signaling machines. *Cell* **110:** 673-687

Jenkins A.L., Nannizzi-Alaimo L., Silver D., Sellers J.R., Ginsberg M.H., Law D.A., Phillips D.R. (1998) Tyrosine phosphorylation of the beta3 cytoplasmic domain mediates integrin-cytoskeletal interactions. *J Biol Chem* **273:** 13878-13885

Johansson M.W., Larsson E., Luning B., Pasquale E.B., Ruoslahti E. (1994) Altered localization and cytoplasmic domain-binding properties of tyrosine-phosphorylated beta 1 integrin. *J Cell Biol* **126:** 1299-1309

Kirk R.I., Sanderson M.R., Lerea K.M. (2000) Threonine phosphorylation of the beta 3 integrin cytoplasmic tail, at a site recognized by PDK1 and Akt/PKB in vitro, regulates Shc binding. *J Biol Chem* **275:** 30901-30906

Klinghoffer R.A., Sachsenmaier C., Cooper J.A., Soriano P. (1999) Src family kinases are required for integrin but not PDGFR signal transduction. *EMBO J* **18:** 2459-2471

Koradi R., Billeter M., Wuthrich K. (1996) MOLMOL: a program for display and analysis of macromolecular structures. *J Mol Graph* **14:** 51-55, 29-32

Krissansen G.W., Singh J., Kanwar R.K., Chan Y.C., Leung E., Lehnert K.B., Kanwar J.R., Yang Y. (2006) A pseudosymmetric cell adhesion regulatory domain in the beta7 tail of the integrin alpha4beta7 that interacts with focal adhesion kinase and src. *Eur J Immunol* **36:** 2203-2214

Law D.A., DeGuzman F.R., Heiser P., Ministri-Madrid K., Killeen N., Phillips D.R. (1999) Integrin cytoplasmic tyrosine motif is required for outside-in alphaIIbbeta3 signalling and platelet function. *Nature* **401:** 808-811

Law D.A., Nannizzi-Alaimo L., Phillips D.R. (1996) Outside-in integrin signal transduction. Alpha IIb beta 3-(GP IIb IIIa) tyrosine phosphorylation induced by platelet aggregation. *J Biol Chem* **271:** 10811-10815

Lhotak V., Greer P., Letwin K., Pawson T. (1991) Characterization of elk, a brain-specific receptor tyrosine kinase. *Mol Cell Biol* **11:** 2496-2502

Ling Y., Maile L.A., Badley-Clarke J., Clemmons D.R. (2005) DOK1 mediates SHP-2 binding to the alphaVbeta3 integrin and thereby regulates insulin-like growth factor I signaling in cultured vascular smooth muscle cells. *J Biol Chem* **280:** 3151-3158

Lowell C.A. (2004) Src-family kinases: rheostats of immune cell signaling. *Mol Immunol* **41:** 631-643

Miller L.A., Hong J.J., Kinch M.S., Harrison M.L., Geahlen R.L. (1999) The engagement of beta1 integrins on promonocytic cells promotes phosphorylation of Syk and formation of a protein complex containing Lyn and beta1 integrin. *Eur J Immunol* **29:** 1426-1434

Oxley C.L., Anthis N.J., Lowe E.D., Vakonakis I., Campbell I.D., Wegener K.L. (2008) An integrin phosphorylation switch: the effect of beta3 integrin tail phosphorylation on Dok1 and talin binding. *J Biol Chem* **283:** 5420-5426

Potter M.D., Barbero S., Cheresh D.A. (2005) Tyrosine phosphorylation of VE-cadherin prevents binding of p120- and beta-catenin and maintains the cellular mesenchymal state. *J Biol Chem* **280:** 31906-31912

Prasad K.S., Andre P., He M., Bao M., Manganello J., Phillips D.R. (2003) Soluble CD40 ligand induces beta3 integrin tyrosine phosphorylation and triggers platelet activation by outside-in signaling. *Proc Natl Acad Sci U S A* **100:** 12367-12371

Sakai T., Jove R., Fassler R., Mosher D.F. (2001) Role of the cytoplasmic tyrosines of beta 1A integrins in transformation by v-src. *Proc Natl Acad Sci U S A* **98:** 3808-3813

Sakai T., Zhang Q., Fassler R., Mosher D.F. (1998) Modulation of beta1A integrin functions by tyrosine residues in the beta1 cytoplasmic domain. *J Cell Biol* **141:** 527-538

Seeliger M.A., Young M., Henderson M.N., Pellicena P., King D.S., Falick A.M., Kuriyan J. (2005) High yield bacterial expression of active c-Abl and c-Src tyrosine kinases. *Protein Sci* **14:** 3135-3139

Shattil S.J. (2005) Integrins and Src: dynamic duo of adhesion signaling. *Trends Cell Biol* **15:** 399-403

Shaw S.K., Brenner M.B. (1995) The beta 7 integrins in mucosal homing and retention. *Semin Immunol* **7:** 335-342

Tamkun J.W., DeSimone D.W., Fonda D., Patel R.S., Buck C., Horwitz A.F., Hynes R.O. (1986) Structure of integrin, a glycoprotein involved in the transmembrane linkage between fibronectin and actin. *Cell* **46:** 271-282

Tapley P., Horwitz A., Buck C., Duggan K., Rohrschneider L. (1989) Integrins isolated from Rous sarcoma virus-transformed chicken embryo fibroblasts. *Oncogene* **4:** 325-333

Ulanova M., Puttagunta L., Marcet-Palacios M., Duszyk M., Steinhoff U., Duta F., Kim M.K., Indik Z.K., Schreiber A.D., Befus A.D. (2005) Syk tyrosine kinase participates in beta1-integrin signaling and inflammatory responses in airway epithelial cells. *Am J Physiol Lung Cell Mol Physiol* **288:** L497-507

Ulmer T.S., Yaspan B., Ginsberg M.H., Campbell I.D. (2001) NMR analysis of structure and dynamics of the cytosolic tails of integrin alpha IIb beta 3 in aqueous solution. *Biochemistry* **40:** 7498-7508

Wegener K.L., Partridge A.W., Han J., Pickford A.R., Liddington R.C., Ginsberg M.H., Campbell I.D. (2007) Structural basis of integrin activation by talin. *Cell* **128:** 171-182

Wennerberg K., Armulik A., Sakai T., Karlsson M., Fassler R., Schaefer E.M., Mosher D.F., Johansson S. (2000) The cytoplasmic tyrosines of integrin subunit beta1 are involved in focal adhesion kinase activation. *Mol Cell Biol* **20:** 5758-5765

Xi X., Flevaris P., Stojanovic A., Chishti A., Phillips D.R., Lam S.C., Du X. (2006) Tyrosine phosphorylation of the integrin beta(3) subunit regulates beta(3) cleavage by calpain. *J Biol Chem* **281:** 29426-29430

Zou Z., Chen H., Schmaier A.A., Hynes R.O., Kahn M.L. (2007) Structure-function analysis reveals discrete beta3 integrin inside-out and outside-in signaling pathways in platelets. *Blood* **109:** 3284-3290

CHAPTER VI: CONCLUSION

6.1 Integrin Activation by Talin: Common Themes and Subtle Differences

Before the studies presented here, investigations of integrin activation had focused largely on β3 integrins—particularly structural and other studies on the mechanism of inside-out activation by talin. The NMR structure by Wegener *et al*. of a chimeric peptide that included the membrane-proximal (MP) region of the β3 cytoplasmic tail bound to the talin1 F3 domain offered particularly detailed insight into the structural basis of talin-induced integrin activation (Wegener *et al.*, 2007). However, our understanding of this process remained incomplete, especially with regard to the role of the membrane regions and how this process occurs in other integrins.

In order to address these shortcomings and to construct a more comprehensive model of integrin activation, we formulated a new approach. By producing a series of ^{15}N-labelled integrin cytoplasmic tail peptides in *E. coli*, we were able to explore the talin/integrin interaction in detail from the perspective of the integrin tail—primarily using the technique of NMR chemical shift perturbation mapping. Studies on the β1A, β1D, β3, and β7 integrin tails (wild type, mutant, and phosphorylated) revealed considerable diversity in both their affinity and their mode of interaction with talin F3 domains. High resolution structural studies of the integrin/talin complex had previously been hampered by the weak nature of this interaction. However, the identification of an integrin/talin pair that formed a particularly tight complex (β1D and talin2) allowed us to solve the first atomic resolution structure, by X-ray crystallography, of talin bound to a native integrin tail (with the added bonus that this was not the usual focus of attention, the β3 tail).

The structure of the β1D tail bound to the talin2 F2-F3 domain pair revealed novel features of the talin integrin complex that were not apparent from previous studies—due in part to the well-defined N-terminus of the integrin tail and the presence of the talin F2 domain in this structure. The structure exhibited a well-defined salt bridge between D759 in the β1D MP helix and K327 in the F3 domain of talin2. Additional NMR studies revealed that this salt bridge is essential for full engagement of talin with the MP region of the β1 and β3 integrin tails (involving D723 in β3 and K324 in talin1)—an interaction known to be important for integrin activation (Wegener *et al.*, 2007)—and whole cell measurements by our collaborators confirmed that this salt bridge is necessary for the activation of αIIbβ3. A comparison of the talin2/β1D structure with the recent structure of the αIIbβ3 TM complex (Lau *et al.*, 2009) demonstrated that this salt bridge disrupts an integrin α/β salt bridge (involving the same β integrin aspartate and R995 in αIIb) that helps maintain the integrin in the inactive state. However, earlier studies demonstrated that disruption of this α/β salt bridge is insufficient to activate the integrin in the absence of talin (Tadokoro *et al.*, 2003; Wegener *et al.*, 2007), indicating that the mechanism of integrin activation by talin is more complex.

Merging the β1D/talin2 structure with the structure of the β3 transmembrane (TM) domain in isolation (Lau *et al.*, 2008) gave a more complete picture of the talin/integrin activation complex—revealing a potential membrane interaction site involving a positively-charged patch on the talin F2 domain. Additional studies verified that this is a genuine membrane interaction site and that it is essential for full integrin activation. Further analysis revealed that this F2 patch may precisely orient the talin/β complex in order to fully disrupt the heterodimeric integrin TM complex. These results reveal key structural features that explain the ability of talin to mediate inside-out transmembrane signalling—a mechanism that appears to be conserved between different integrins.

A powerful motivation for undertaking an NMR-based approach in our studies is that beyond just providing K_d values, chemical shift perturbation studies also provide detailed information on protein-protein interaction sites from the same set of experiments. Our initial studies revealed marked heterogeneity in how different integrins interact with talin. Coupled with mutagenesis studies, we found that talin interacts only weakly with the membrane-distal (MD) region (including the NPxY motif) of the β3 tail compared to its interaction with β1A. This interaction is even tighter in β1D. The talin2/β1D crystal structure revealed that talin2 forms an extensive, heavily hydrogen-bonded interface with the MD portion of the β1D tail, something not observed in a previous structure of this region of β3 with talin1 (Garcia-Alvarez *et al.*, 2003)—thus explaining the higher affinity of talin for this region in β1 tails. In the talin2/β1D structure, a residue unique to β1D, P786, participates in a distinctive hydrophobic interface with talin2; this creates the exceptionally strong talin/integrin interaction that is necessary for these two striated muscle-specific isoforms to maintain persistent integrin activation and withstand the high forces they are exposed to in their biological environment (Belkin *et al.*, 1996). Thus, the MD portion of the integrin tail modulates integrin affinity for talin primarily by enthalpic means.

Through our studies, we also found that β3 displays a much tighter MP interaction with talin than β1A or β1D. It is plausible that this finding may explain the ability of talin to activate β3 but not β1 integrins by interaction with the F3 domain alone (Bouaouina *et al.*, 2008). However, such a difference in affinity is not explained by a comparison of integrin/talin structures. Instead, we found that while all of the integrin tails are largely unstructured, a key portion of the β3 tail is intrinsically less flexible than in β1. Thus, there is a decreased entropic cost for β3 to bind to talin compared to β1 integrins, increasing the affinity of the talin/β3 complex. Intrinsic flexibility is important for

integrin tails to act effectively as protein-protein interaction hubs, as the high entropic cost of forming structured complexes with other proteins makes such interactions weak and transient. Along these same lines, we found that integrins contain two extra residues in their talin binding sites compared to peptides that bind to talin more tightly. Removal of these residues greatly increases the affinity of β1D for talin2, as it removes what was otherwise an unfavourable distorted loop used by the integrin to accommodate these residues in the complex. Thus, these additional residues appear to be another mechanism that has evolved to allow greater dexterity in integrin/tail interactions.

In order to further understand how integrin activation is regulated *in vivo*, we studied the role of tyrosine phosphorylation in modulating these protein-protein interactions. Using our NMR-based approach, we found that tyrosine phosphorylation of β3, β1A, and β7 tails decreases their affinity for talin. We also found that Dok1—a protein known to have an inactivating effect on integrins (Wegener *et al.*, 2007)—only interacts weakly with unphosphorylated tails, but its affinity is greatly increased by integrin tyrosine phosphorylation. The Dok1 interaction remains restricted to the MD region, thus phosphorylation inhibits integrin activation by increasing the affinity of β integrin tails for a talin competitor that does not form activating MP interactions with the integrin. Key residues governing these specificities were identified by detailed structural analysis, and talin1 was engineered to bind preferentially to phosphorylated integrins by introducing the mutation D372R. As predicted, this mutation affects talin localization in live cells in an integrin phosphorylation-specific manner. Together, these results indicate that tyrosine phosphorylation is a common mechanism for regulating integrin activation, despite subtle differences in how these integrins interact with their binding proteins.

6.2 Future Outlook

Through the studies presented here, we have defined a structural model for integrin activation by talin, explored how it varies between different integrins, and described a mechanism by which activation is regulated within the cell. However, many avenues for future study remain. The most pressing issue will be to further extend our model of integrin activation—particularly by defining the exact nature of the change in the β integrin TM tilt angle induced by talin. One method of doing this would be to further characterize the interface between the talin F2 domain and the cell membrane by extending the approach undertaken in Chapter III. Other positively charged residues exist on the surface of the F2 domain, and it would be important to individually mutate a greater set of these to see if the membrane orientation patch (MOP) is more extensive than realised so far—as judged by the effect of specific mutations on integrin activation and vesicle cosedimentation assays. Such an approach could be undertaken using our current methodology.

A more powerful—but much more technically difficult—approach to further defining our model of activation would be to characterize the talin/integrin activation complex in more detail with advanced structural biological methods. Specifically, solid state NMR could be employed to define helical tilt angles with great precision (van der Wel *et al.*, 2002). Thus, experiments could be performed to determine the orientation of the β TM domain in the inactive state (when bound to the α subunit) and in the active state (when bound to talin). Such experiments would require the production of peptides encompassing both the TM and cytoplasmic portions of the β integrin—a feat that we have had some difficulty with in the past, but one that has been demonstrated before (Li *et al.*, 2002). Such experiments would also have to overcome the weak nature of the talin/integrin interaction, and this could be accomplished by constructing a “super

integrin" with exceptionally high talin affinity by deleting the two extra residues in the β tail linker region (as demonstrated in Chapter IV). Such an approach would also overcome the problem of the N-terminus of the β tail being unstructured in solution, despite this region being helical *in vivo*. Such a system could also open up the possibility of studying the integrin/talin/membrane complex by solution NMR, although due to the large size of such a complex, advanced NMR techniques using selective labelling and TROSY would have to be employed—and data acquisition and analysis would likely still be exceptionally difficult. If such a method proves unfeasible, preliminary experiments by Kate Wegener have indicated that the problem of N-terminal tail fraying at least might still be overcome by attaching an N-terminal helical sequence to the tail or performing experiments on the tails in detergent micelles.

Even using our current system of studying β integrin tails by NMR, more elaborate studies could be undertaken to understand the kinetic details of talin binding to the integrin. A variety of questions could be explored. How exactly does this unstructured peptide transition from the flexible free state to the more rigid bound state? Does this involve the simultaneous formation of the MP and MD interactions in a concerted process? Or, does this involve a sequence of semi-independent events? And, how do non-specific interactions between talin and the β tail contribute to binding efficiency? Answering these questions will require exploration of transient intermediates in the binding process; but, such lowly-populated states have traditionally been out of reach for structural biology. However, two recently developed NMR techniques, PRE (paramagnetic relaxation enhancement) (Clore, 2008) and relaxation dispersion (Korzhnev & Kay, 2008), make it possible to observe such invisible states, allowing the determination of kinetic, thermodynamic, and—in the case of PRE—detailed structural parameters. These two methods are somewhat complementary, as relaxation dispersion

can be employed on processes that take place on slow (millisecond) time scales, whereas PRE is effective on fast (microsecond or less) time scales. The integrin/talin system is well-suited to these studies; through selective mutagenesis we have designed peptides that vary widely in their affinity for talin (K_d values spanning five and a half orders of magnitude, from 17 nM to 6.6 mM) and in their exchange rates (from $k_{ex} << 50\ s^{-1}$ to $k_{ex} >> 1{,}000\ s^{-1}$), making a multi-technique strategy feasible. By undertaking these studies on the dynamics of a biologically relevant protein-protein interaction, one could produce results that would be of interest both for their biomedical significance and for the fundamental biophysical insight they yield into the general phenomenon of protein/peptide interactions.

These kinds of biophysical studies would offer additional insight into the common mechanism of integrin activation, but additional studies are also needed to further characterize how this process differs between integrins. In the work presented here, we have explored differences between three types of β subunits (β1, β3, and β7) and between two of their alternatively spliced isoforms (β1A and β1D). However, this study did not explore any of the five other β subunits found in mammals—nor did it explore any of the β subunits found in lower organisms. Given the large amount of diversity in talin/integrin interactions observed between the limited set of integrins explored in this study, the results of such further studies could be quite interesting. For example, it was recently reported that the β2 tail binds to talin exceptionally tightly (Bhunia *et al.*, 2009). This could be related to the β2 subunit having a one residue shorter linker than other β tails (making it intermediate in length between β tails and more tightly-binding layilin and PIPK1γ peptides; Fig. 1.1C, 4.6A). It is likely that many additional differences would be discovered by such broader studies, and it will be important to document these in order to build a more comprehensive and nuanced model of integrin activation.

Beyond the need to further define our model of integrin activation and expand it to other integrins, many other interesting future lines of investigation exist. Although we were able to explore one mechanism of regulating integrin activation in this study (tyrosine phosphorylation), many questions still exist regarding the details of how integrin adhesiveness is intricately regulated in time and space. Also, although kindlin has recently been identified as a co-activator of integrins (Harburger *et al.*, 2009; Ma *et al.*, 2008; Montanez *et al.*, 2008; Moser *et al.*, 2009; Moser *et al.*, 2008; Ussar *et al.*, 2008), we were not able to characterize its role structurally here due to difficulties in producing suitable fragments for NMR or crystallographic studies. If these problems could be overcome, however, the emerging picture of the talin/kindlin/integrin activation complex would be very interesting, as it is likely to involve an interaction between the talin F3 domain and the MP and near MD regions of the integrin tail, between the kindlin F3 domain and the far MD region of the tail, between the talin F2 domain and the membrane, between the kindlin PH domain and the membrane, and possibly between talin and kindlin. Finally, the studies presented here did not address the nature of the extracellular changes involved in integrin activation—and further investigations are still required to resolve the controversy between the switchblade and deadbolt models of activation. Despite the many remaining unanswered questions, the studies presented here have contributed to our understanding of integrin activation and shown it to be a unique, elegant, and multifaceted process.

6.3 References

Belkin A.M., Zhidkova N.I., Balzac F., Altruda F., Tomatis D., Maier A., Tarone G., Koteliansky V.E., Burridge K. (1996) Beta 1D integrin displaces the beta 1A isoform in striated muscles: localization at junctional structures and signaling potential in nonmuscle cells. *J Cell Biol* **132:** 211-226

Bhunia A., Tang X.Y., Mohanram H., Tan S.M., Bhattacharjya S. (2009) NMR solution conformations and interactions of integrin alphaLbeta2 cytoplasmic tails. *J Biol Chem* **284:** 3873-3884

Bouaouina M., Lad Y., Calderwood D.A. (2008) The N-terminal domains of talin cooperate with the phosphotyrosine binding-like domain to activate beta1 and beta3 integrins. *J Biol Chem* **283:** 6118-6125

Clore G.M. (2008) Visualizing lowly-populated regions of the free energy landscape of macromolecular complexes by paramagnetic relaxation enhancement. *Mol Biosyst* **4:** 1058-1069

Garcia-Alvarez B., de Pereda J.M., Calderwood D.A., Ulmer T.S., Critchley D., Campbell I.D., Ginsberg M.H., Liddington R.C. (2003) Structural determinants of integrin recognition by talin. *Mol Cell* **11:** 49-58

Harburger D.S., Bouaouina M., Calderwood D.A. (2009) Kindlin-1 and -2 directly bind the C-terminal region of beta integrin cytoplasmic tails and exert integrin-specific activation effects. *J Biol Chem* **284:** 11485-11497

Korzhnev D.M., Kay L.E. (2008) Probing invisible, low-populated States of protein molecules by relaxation dispersion NMR spectroscopy: an application to protein folding. *Acc Chem Res* **41:** 442-451

Lau T.L., Kim C., Ginsberg M.H., Ulmer T.S. (2009) The structure of the integrin alphaIIbbeta3 transmembrane complex explains integrin transmembrane signalling. *EMBO J* **28:** 1351-1361

Lau T.L., Partridge A.W., Ginsberg M.H., Ulmer T.S. (2008) Structure of the integrin beta3 transmembrane segment in phospholipid bicelles and detergent micelles. *Biochemistry* **47:** 4008-4016

Li R., Babu C.R., Valentine K., Lear J.D., Wand A.J., Bennett J.S., DeGrado W.F. (2002) Characterization of the monomeric form of the transmembrane and cytoplasmic domains of the integrin beta 3 subunit by NMR spectroscopy. *Biochemistry* **41:** 15618-15624

Ma Y.Q., Qin J., Wu C., Plow E.F. (2008) Kindlin-2 (Mig-2): a co-activator of beta3 integrins. *J Cell Biol* **181:** 439-446

Montanez E., Ussar S., Schifferer M., Bosl M., Zent R., Moser M., Fassler R. (2008) Kindlin-2 controls bidirectional signaling of integrins. *Genes Dev* **22:** 1325-1330

Moser M., Bauer M., Schmid S., Ruppert R., Schmidt S., Sixt M., Wang H.V., Sperandio M., Fassler R. (2009) Kindlin-3 is required for beta2 integrin-mediated leukocyte adhesion to endothelial cells. *Nat Med* **15:** 300-305

Moser M., Nieswandt B., Ussar S., Pozgajova M., Fassler R. (2008) Kindlin-3 is essential for integrin activation and platelet aggregation. *Nat Med* **14:** 325-330

Tadokoro S., Shattil S.J., Eto K., Tai V., Liddington R.C., de Pereda J.M., Ginsberg M.H., Calderwood D.A. (2003) Talin binding to integrin beta tails: a final common step in integrin activation. *Science* **302:** 103-106

Ussar S., Moser M., Widmaier M., Rognoni E., Harrer C., Genzel-Boroviczeny O., Fassler R. (2008) Loss of Kindlin-1 causes skin atrophy and lethal neonatal intestinal epithelial dysfunction. *PLoS Genet* **4:** e1000289

van der Wel P.C., Strandberg E., Killian J.A., Koeppe R.E., 2nd (2002) Geometry and intrinsic tilt of a tryptophan-anchored transmembrane alpha-helix determined by (2)H NMR. *Biophys J* **83:** 1479-1488

Wegener K.L., Partridge A.W., Han J., Pickford A.R., Liddington R.C., Ginsberg M.H., Campbell I.D. (2007) Structural basis of integrin activation by talin. *Cell* **128:** 171-182